Visible Light-Induced Reductive Photoredox Catalysis in Organic Synthesis

Dissertation

Zur Erlangung des Doktorgrades der Naturwissenschaften
(Dr. rer. nat)
an der Fakultät für Chemie und Pharmazie
der Universität Regensburg

vorgelegt von

Tamal Ghosh

aus

West Bengal (Indien)

2016

The experimental part of this work was carried out between September 2012 and June 2016 under the supervision of Prof. Dr. Burkhard König at the Institute of Organic Chemistry, University of Regensburg.

The Ph.D. thesis was submitted on:	28.07.2016
The colloquium took place on:	02.09.2016

Board of examiners:	PD Dr. Sabine Amslinger	(chair)
	Prof. Dr. Burkhard König	(1st referee)
	Prof. Dr. David Díaz Díaz	(2nd referee)
	Prof. Dr. Arno Pfitzner	(examiner)

Dedicated

to

My Family

"It always seems impossible until it's done."

– Nelson Mandela

Table of Contents

Chapter 1

1 Useful Tools in Photoredox Catalysis and Some Applications

1.1 Introduction

The formation of carbon-carbon or carbon-heteroatom bonds in molecular scaffolds is an important task addressed by catalysis.[1] Transition metal catalyzed cross coupling methodologies allow access to that for the syntheses of natural products,[2] drugs[3] and biologically important compounds.[4] Having said that, the toxicity and high cost of the catalyst, specific ligands, additives and elevated temperature remain the drawbacks of this well-established method.[5] Visible light photoredox catalysis has therefore caught considerable attention in the past decades[6-10] and has become an attractive alternative because photocatalytic reactions can be carried out at very mild experimental conditions (room temperature and visible light). This can be very beneficial when the reactants or products are heat sensitive or explosive. As photocatalytic reactions are mainly performed at room temperature, intermediates may be formed which are not accessible at thermal conditions, providing better mechanistic insight for different reaction pathways.[11]

Typically, organic molecules do not absorb in the visible region, therefore a colored photocatalyst is used, which is excited absorbing visible light. The excited photocatalyst can then either accept an electron from a donor returning to the ground state in reduced form (reductive quenching cycle, **Fig. 1a**) or donate an electron to an acceptor returning to the ground state in the oxidized form (oxidative quenching cycle, **Fig. 1b**).[7]

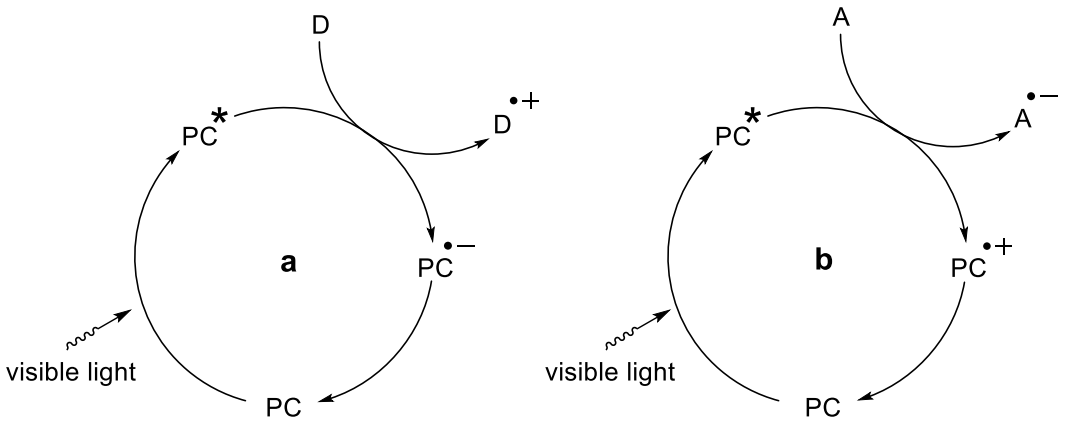

Fig. 1: Typical reductive (**a**) and oxidative (**b**) quenching cycle of a photocatalyst.

1.2 Feasibility of photo-induced electron transfer processes

Reductive/oxidative quenching of the photoexcited state of a photocatalyst (PC) is controlled by the reduction potential of the donor(D)/acceptor(A) and the excited photocatalyst.[12] In the reductive quenching cycle, for the efficient electron transfer from D to PC^*, the reduction potential of $D^{\bullet+}$ should be lower than that of the PC^* [$E^0(D^{\bullet+}/D) < E^0(PC^*/PC^{\bullet-})$]‡. Similarly, in the oxidative quenching cycle, for the efficient electron transfer from PC^* to A, the reduction potential of $PC^{\bullet+}$ should be lower than the reduction potential of A [$E^0(PC^{\bullet+}/PC^*) < E^0(A/A^{\bullet-})$]§. However, electron transfer reactions in solution can occur even if it is thermodynamically unfavorable,[13] *i.e.* the electron transfer from D to A is possible even when $E^0(D^{\bullet+}/D) > E^0(A/A^{\bullet-})$. Such reactions, which are opposite to the standard potential gradient,[14-15] occur when the thermodynamically unfavorable electron transfer equilibrium (see, **Scheme 1**, **Eq. 1**) is followed by a very fast and irreversible reaction step (see, **Scheme 1**, **Eq. 2**). A report by Cano-Yelo and Deronzier in 1984 showed[16] that RuL_3^{3+} [$E^0(RuL_3^{3+}/ RuL_3^{2+}) = + 1.59$ V vs SCE] is able to oxidize 4-methylbenzylalcohol [$E^0(Alc^{\bullet+}/Alc) = + 1.89$ V vs SCE] to the corresponding aldehyde in 35% yield using aryldiazonium salt as the sacrificial oxidant, even though the electron transfer from 4-methylbenzylalcohol to RuL_3^{3+} is endothermic by 300 mV potential difference.

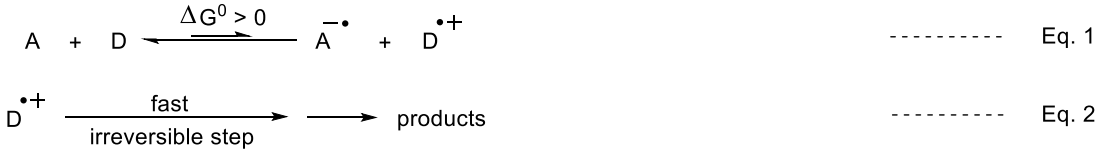

Scheme 1: Thermodynamically unfavorable photo-induced electron transfer.

In 1986, Stekhan *et. al.* reported[17] that this kind of reactions can be carried out up to a potential difference of 0.6 V, which was again supported by a review[18] from Little *et. al.* in 2013, where it was mentioned for an inner-sphere electron transfer this value can be up to 2 V whereas for an outer-sphere electron transfer the value is around 0.5 V. Photo-induced electron transfer mainly occurs *via* an outer-sphere mechanism, inner-sphere

‡ $E^0(Bu_3N^{\bullet+}/Bu_3N) = + 0.72$ V vs SCE < $E^0(Ru(bpy)_3^{2+*}/ Ru(bpy)_3^{+}) = + 0.77$ V vs SCE; therefore, Bu_3N can reductively quench the excited state of $Ru(bpy)_3^{2+}$.

§ $E^0(Ru(bpy)_3^{3+}/ Ru(bpy)_3^{2+*}) = – 0.81$ V vs SCE < $E^0(MV^{2+}/ MV^{\bullet+}) = – 0.4$ V vs SCE; therefore, dimethyl viologen (MV^{2+}) can oxidize the excited state of $Ru(bpy)_3^{2+}$.

mechanism is much less probable as the photocatalyst is coordinatively saturated and it cannot form additional bonds for an inner-sphere electron transfer.[19-20]

1.3 Simplified calculation of excited state reduction potential of a photocatalyst

In principle, a photoexcited state of a photocatalyst is much more potent reducing/oxidizing agent than its ground state. The photoexcited state is a stronger reductant, because the electron in its HOMO is excited to an even higher energy state. At the same time, it can be a stronger oxidant because upon excitation one of its lower energy state becomes singly occupied, which is fully occupied in the ground state. As mentioned before, the oxidation/reduction of a photo-excited state is governed by the reduction potentials of the excited state of the photocatalyst and the quencher. Reduction potentials of an excited state cannot be measured; but it can be calculated in two ways. One method estimates the redox potential from a comparison of the rates of excited-state electron transfer to a series of stable compounds whose ground state redox potentials are known.[21-22] The second and the most common one[23-24] is a rough estimation which can be written in a simplified way as below:

$$E^0(PC^{\bullet+}/PC^*) = E^0(PC^{\bullet+}/PC) - E_{00} \quad \text{……. Eq. 3}$$

$$E^0(PC^*/PC^{\bullet-}) = E^0(PC/PC^{\bullet-}) + E_{00} \quad \text{……. Eq. 4}$$

where E_{00} is the photoexcitation energy (0-0 transition, energy gap between the zeroth vibrational levels of the ground and excited states) of the photocatalyst (PC). As described before, the photoexcited state of a photocatalyst is a stronger reductant/oxidant than its ground state, can also be explained from the above equations (eq. 3 and 4). From the eq. 3, we can say that the magnitude of $E^0(PC^{\bullet+}/PC^*)$ should be less than $E^0(PC^{\bullet+}/PC)$, which indicates that the excited state can donate an electron to an acceptor much more easily than the ground state. Likewise, from the eq. 4, $E^0(PC^*/PC^{\bullet-})$ must be more positive than $E^0(PC/PC^{\bullet-})$, suggesting that the excited state can accept an electron from a donor more easily than its ground state.[23] Estimation of the excited state redox potential of $Ru(bpy)_3^{2+}$ is shown as an example in **Fig. 2**.

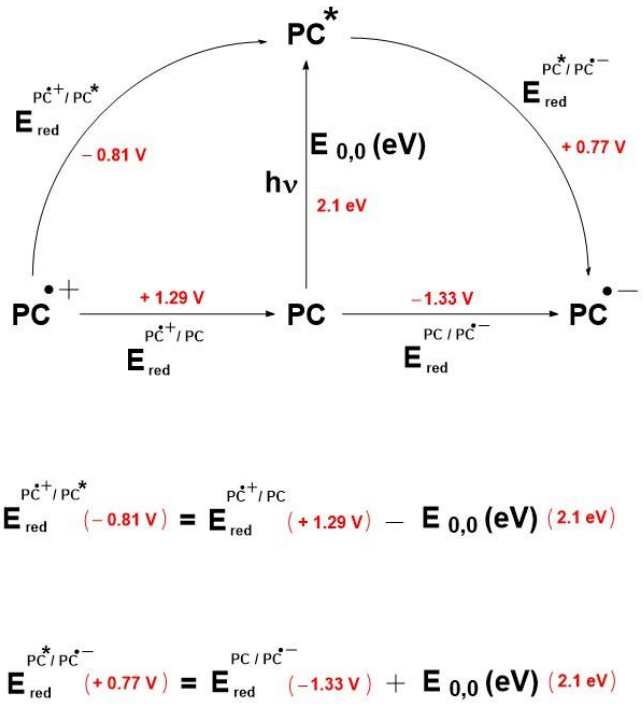

Fig. 2: Exemplary simplified calculation of excited state reduction potential of $Ru(bpy)_3^{2+}$ (PC in the figure), all the redox potentials are against SCE in MeCN.[21]

1.4 Extension of aryl radical precursors to aryl halides and its challenges

One of the key intermediates for the photocatalytic C-H arylation are aryl radicals.[25] Very commonly used aryl radical precursors in photoredox catalysis are aryl diazonium salts.[9] Other substrates, which were used for photocatalytic C-H arylation are diaryliodonium salts,[26-29] triarylsulfonium salts[30] and aryl sulphonyl chlorides.[31-33] Most of these starting materials are not bench-stable and some of them are stored in low temperature, not commercially available and have a tendency to hydrolyze. Aryl halides are the most convenient aryl radical precursors, which are readily available and stable; but the challenge here is the high negative reduction potentials of aryl halides, which hinder the initial electron transfer step as compared to other aryl radical precursors. Most of the aryl halides have reduction potentials of –1.8 V vs SCE or more, which is not accessible by any commonly used photocatalysts [*e.g.* Eosin Y,[9] $Ru(bpy)_3^{2+}$,[7] $Cu(dap)_2^{+}$,[34] $Ir(ppy)_3$[7]] *via* normal reductive/oxidative quenching cycles. There have been reports where aryl radicals

were generated from aryl halides using UV light[35] and strong bases such as potassium *tert*-butoxide,[36] following a radical chain mechanism.[37-38] Combination of a photocatalyst and strong base (*e.g.* potassium *tert*-butoxide) to generate aryl radicals from aryl halides were shown.[39] Stephenson[40] and Lee[41] used Ir-complexes as the photocatalyst and visible light for the reduction of aryl halides; but, those are limited to aryl iodides. Therefore, a novel concept was introduced, namely consecutive photoinduced electron transfer (conPET)[42] which can overcome the limitation of reaching high reduction potentials of aryl halides, including aryl chlorides. This concept includes a reductive quenching photocatalytic cycle, where the *in situ* generated radical anion of the photocatalyst, which is colored and stable under nitrogen atmosphere, can be excited again. By doing that, we simply accumulate the energy of two photons in a single molecule, which provides enough redox power which can overcome the barrier of high redox potentials of most of the aryl halides (**Fig. 3**).

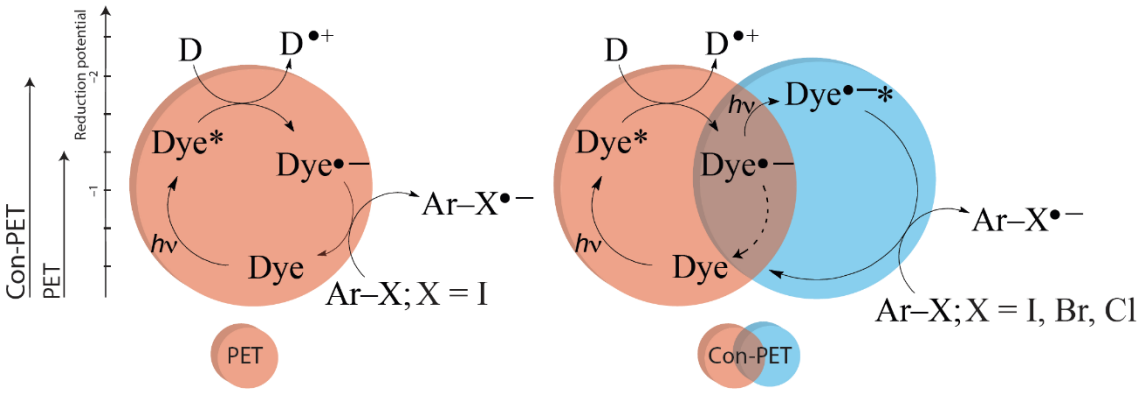

Fig. 3: Single photoinduced electron transfer (left) *vs* consecutive photoinduced electron transfer (conPET, right) processes.

Perylene diimides (PDIs) are a class of organic dyes, which can form colored and stable radical anions[43] in nitrogen atmosphere upon irradiation with visible light in the presence of a sacrificial electron donor (*e.g.* triethylamine). This radical anion ($PDI^{\bullet-}$) can be excited again with visible light, upon which, it gains enough redox power to reduce aryl halides and the generated aryl radicals from aryl halides were used for C-H arylation reactions.[42] The detail studies of this chemistry will be discussed in **Chapter 2**.

1.5 Reductive proflavine photocatalysis for synthetic reductions

Flavin has been used a lot for synthetic oxidations.[44-46] Attempts to react the reduced flavin with an electron acceptor other than molecular oxygen was not successful. Also, reductive flavin photocatalysis using different mediators for synthetic reductions, remains ineffective (discussed in detail in **Chapter 5**). Proflavine is an acridinium, dye which can be reduced upon photoinduced electron transfer (PET).[47] Hence, we wanted to examine the possibility of using proflavine for photocatalytic reduction reactions. Park and Nam[48] have shown that reduced proflavine can be reoxidized back using [Cp*Rh(III)(bpy)Cl]Cl. They successfully used this methodology for regeneration of NADH from NAD^+ produced by enzymatic synthesis of L-glutamate.

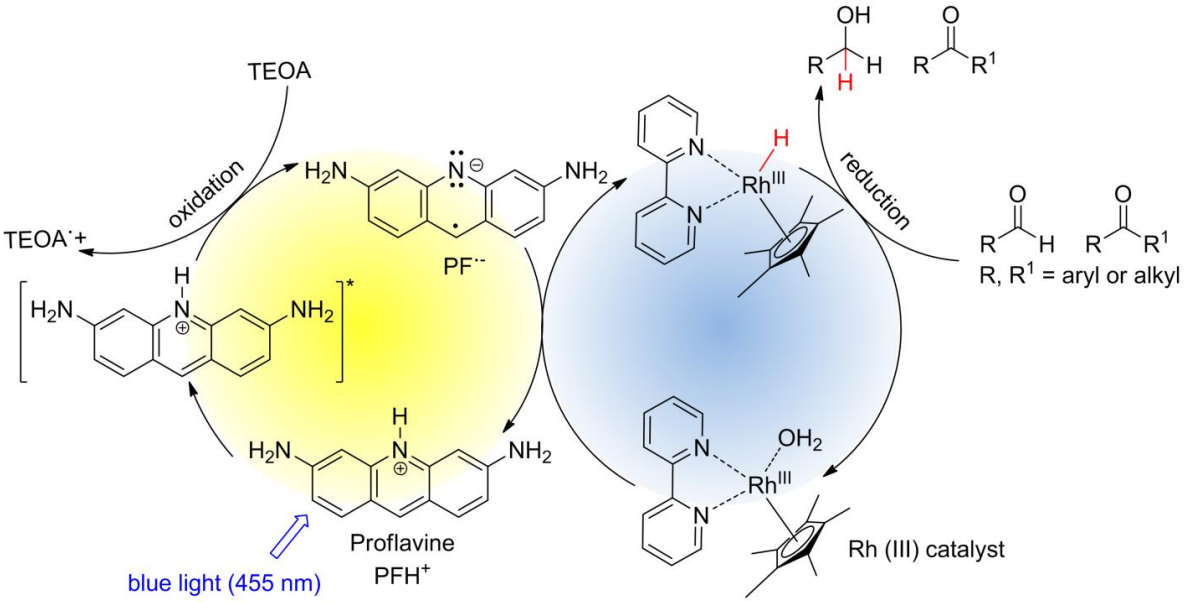

Fig. 4: Selective aldehyde reduction by Rh(III)–H photochemically regenerated by PFH^+.

We have modified the system for synthetic purpose by changing the amount of triethanolamine from 1000 equiv. to 2 equiv. and achieved excellent selectivity for the synthetic reduction of aldehydes over ketones (**Fig. 4**).[49] The detail chemistry of this chemoselective reductions with excellent substrate scope and a vast mechanistic study of this rhodium-proflavine system will be discussed in **Chapter 3**.

1.6 By-products of photochemically oxidized amines for further chemistry

In photocatalytic reductive quenching cycle, a sacrificial electron donor is used to quench the excited photocatalyst forming the radical anion.[7] The most commonly used reductive quenchers are amines. Amines after photochemical oxidation typically decompose and not being used for further chemistry.[50-51] Both in the conPET[42] and rhodium-proflavine systems[49] we have used amines as electron donors, as those systems proceed *via* a reductive quenching cycles and the chemistry after oxidation of those amines were not in our interest. So, our next aim was to avoid the waste of these oxidized amines and use it for synthetic transformations.

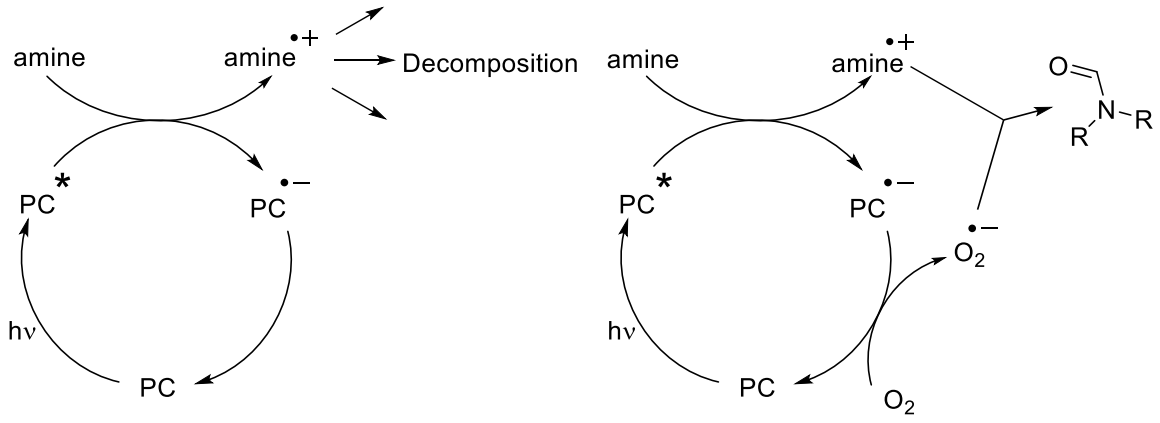

Fig 5: Oxidized amine decomposition in reductive quenching cycle (left) *vs* utilization of oxidized amines in combination with *in situ* formed superoxide radical anion to form *N*-formamides (right).

We have used amines in a reductive quenching photocatalytic cycle in the presence of air and we found that amines are transformed to *N*-formamides *in situ* without any additional formylating agent or C_1 building block source. The additional carbon source in *N*-formamides will be discussed in detail in **Chapter 4** with examples.

1.7 References

[1] I. Nakamura, Y. Yamamoto, *Chem. Rev.* **2004**, *104*, 2127-2198.

[2] Y. Qiu, S. Gao, *Nat. Prod. Rep.* **2016**, *33*, 562-581.

[3] M. Baumann, I. R. Baxendale, *Beilstein J. Org. Chem.* **2013**, *9*, 2265-2319.

[4] B. Yu, H. Xing, D.-Q. Yu, H.-M. Liu, *Beilstein J. Org. Chem.* **2016**, *12*, 1000-1039.

[5] L. Ackermann, *"Modern Arylation Methods"*, 1st ed.; Wiley-VCH Verlag GmbH & Co. KGaA19 MAY 2009.

[6] S. Fukuzumi, K. Ohkubo, *Org. Biomol. Chem.* **2014**, *12*, 6059-6071.

[7] C. K. Prier, D. A. Rankic, D. W. MacMillan, *Chem. Rev.* **2013**, *113*, 5322-5363.

[8] M. D. Kärkäs, J. A. Porco, C. R. J. Stephenson, *Chem. Rev.* **2016**, DOI: 10.1021/acs.chemrev.1025b00760.

[9] D. P. Hari, B. König, *Angew. Chem. Int. Ed.* **2013**, *52*, 4734-4743.

[10] N. A. Romero, D. A. Nicewicz, *Chem. Rev.* **2016**, DOI: 10.1021/acs.chemrev.1026b00057.

[11] H. Hennig, R. Billing, *Coord. Chem. Rev.* **1993**, *125*, 89-100.

[12] D. Rehm, A. Weller, *Isr. J. Chem.* **1970**, *8*, 259-271.

[13] N.-t. Zhang, C.-c. Zeng, C. M. Lam, R. K. Gbur, R. D. Little, *J. Org. Chem.* **2013**, *78*, 2104-2110.

[14] V. G. Mairanovsky, *Angew. Chem. Int. Ed.* **1976**, *15*, 281-292.

[15] W. Schmidt, E. Steckhan, *J. Electroanal. Chem.* **1978**, *89*, 215-220.

[16] H. Cano-Yelo, A. Deronzier, *Tetrahedron Lett.* **1984**, *25*, 5517-5520.

[17] E. Steckhan, *Angew. Chem. Int. Ed.* **1986**, *25*, 683-701.

[18] R. Francke, R. D. Little, *Chem. Soc. Rev.* **2014**, *43*, 2492-2521.

[19] L. M. Torres, A. F. Gil, L. Galicia, I. González, *J. Chem. Educ.* **1996**, *73*, 808.

[20] J. K. Kochi, *Angew. Chem. Int. Ed.* **1988**, *27*, 1227-1266.

[21] C. R. Bock, J. A. Connor, A. R. Gutierrez, T. J. Meyer, D. G. Whitten, B. P. Sullivan, J. K. Nagle, *J. Am. Chem. Soc.* **1979**, *101*, 4815-4824.

[22] R. Ballardini, G. Varani, M. T. Indelli, F. Scandola, V. Balzani, *J. Am. Chem. Soc.* **1978**, *100*, 7219-7223.

[23] G. J. Kavarnos, *"Fundamentals of Photoinduced Electron Transfer"*, VCH Publishers, Inc., **1993**.

[24] W. E. Jones, M. A. Fox, *J. Phys. Chem.* **1994**, *98*, 5095-5099.

[25] A. M. Rosa, A. M. Lobo, P. S. Branco, P. Sundaresan, *Tetrahedron* **1997**, *53*, 285-298.

[26] Y. X. Liu, D. Xue, J. D. Wang, C. J. Zhao, Q. Z. Zou, C. Wang, J. L. Xiao, *Synlett* **2013**, *24*, 507-513.

[27] M. Tobisu, T. Furukawa, N. Chatani, *Chem. Lett.* **2013**, *42*, 1203-1205.

[28] A. Baralle, L. Fensterbank, J.-P. Goddard, C. Ollivier, *Chem. Eur. J.* **2013**, *19*, 10809-10813.

[29] G. Fumagalli, S. Boyd, M. F. Greaney, *Org. Lett.* **2013**, *15*, 4398-4401.

[30] S. Donck, A. Baroudi, L. Fensterbank, J.-P. Goddard, C. Ollivier, *Adv. Synth. Catal.* **2013**, *355*, 1477-1482.

[31] P. Natarajan, A. Bala, S. K. Mehta, K. K. Bhasin, *Tetrahedron* **2016**, *72*, 2521-2526.

[32] G.-B. Deng, Z.-Q. Wang, J.-D. Xia, P.-C. Qian, R.-J. Song, M. Hu, L.-B. Gong, J.-H. Li, *Angew. Chem. Int. Ed.* **2013**, *52*, 1535-1538.

[33] L. Gu, C. Jin, J. Liu, H. Ding, B. Fan, *Chem. Commun.* **2014**, *50*, 4643-4645.

[34] M. Pirtsch, S. Paria, T. Matsuno, H. Isobe, O. Reiser, *Chem. Eur. J.* **2012**, *18*, 7336-7340.

[35] E. Cahard, F. Schoenebeck, J. Garnier, S. P. Y. Cutulic, S. Zhou, J. A. Murphy, *Angew. Chem. Int. Ed.* **2012**, *51*, 3673-3676.

[36] R. Rossi, M. Lessi, C. Manzini, G. Marianetti, F. Bellina, *Adv. Synth. Catal.* **2015**, *357*, 3777-3814.

[37] S. Zhou, E. Doni, G. M. Anderson, R. G. Kane, S. W. MacDougall, V. M. Ironmonger, T. Tuttle, J. A. Murphy, *J. Am. Chem. Soc.* **2014**, *136*, 17818-17826.

[38] A. Studer, D. P. Curran, *Angew. Chem. Int. Ed.* **2011**, *50*, 5018-5022.

[39] Y. Cheng, X. Gu, P. Li, *Org. Lett.* **2013**, *15*, 2664-2667.

[40] J. D. Nguyen, E. M. D'Amato, J. M. R. Narayanam, C. R. J. Stephenson, *Nat. Chem.* **2012**, *4*, 854-859.

[41] H. Kim, C. Lee, *Angew. Chem. Int. Ed.* **2012**, *51*, 12303-12306.

[42] I. Ghosh, T. Ghosh, J. I. Bardagi, B. König, *Science* **2014**, *346*, 725-728.

[43] D. Gosztola, M. P. Niemczyk, W. Svec, A. S. Lukas, M. R. Wasielewski, *J. Phys. Chem. A* **2000**, *104*, 6545-6551.

[44] R. Lechner, S. Kummel, B. König, *Photochem. Photobiol. Sci.* **2010**, *9*, 1367-1377.

[45] H. Schmaderer, P. Hilgers, R. Lechner, B. König, *Adv. Synth. Catal.* **2009**, *351*, 163-174.

[46] R. Lechner, B. König, *Synthesis* **2010**, *2010*, 1712-1718.

[47] B. Chakraborty, S. Basu, *Chem. Phys. Lett.* **2009**, *477*, 382-387.

[48] D. H. Nam, C. B. Park, *ChemBioChem* **2012**, *13*, 1278-1282.

[49] T. Ghosh, T. Slanina, B. König, *Chem. Sci.* **2015**, *6*, 2027-2034.

[50] Y.-Q. Zou, J.-R. Chen, X.-P. Liu, L.-Q. Lu, R. L. Davis, K. A. Jørgensen, W.-J. Xiao, *Angew. Chem. Int. Ed.* **2012**, *51*, 784-788.

[51] C. K. Mann, K. K. Barnes, *"Electrochemical Reactions in Nonaqueous Systems"*, Marcel Dekker, New York, N.Y., **1970**.

Chapter 2

2 Reduction of Aryl Halides by Consecutive Visible Light-Induced Electron Transfer Processes

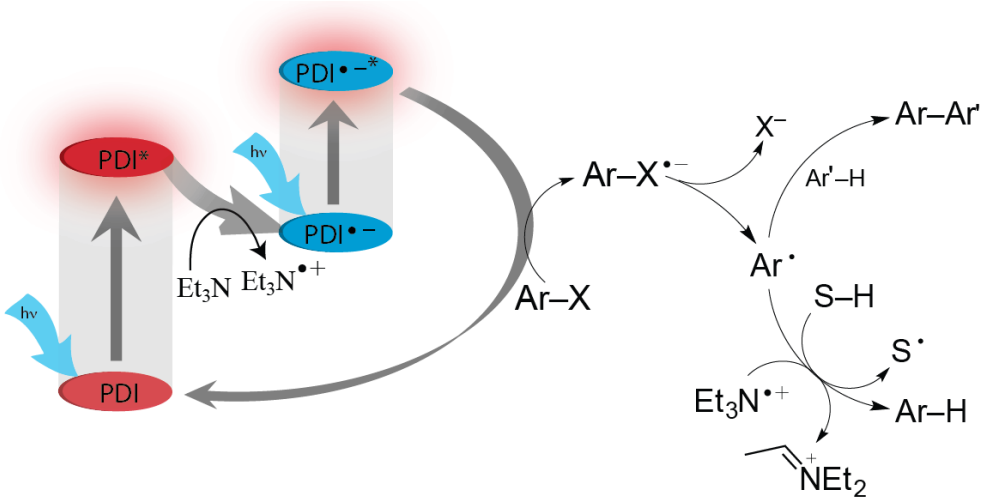

Biological photosynthesis uses the energy of several visible light photons for the challenging oxidation of water, whereas chemical photocatalysis typically involves only single-photon excitation. Perylene bisimide is reduced by visible light photoinduced electron transfer (PET) to its stable and colored radical anion. We report here that subsequent excitation of the radical anion accumulates sufficient energy for the reduction of stable aryl chlorides giving aryl radicals, which were trapped by hydrogen atom donors or used in carbon-carbon bond formation. This consecutive PET (conPET) overcomes the current energetic limitation of visible light photoredox catalysis and allows the photocatalytic conversion of less reactive chemical bonds in organic synthesis.

This chapter has been published:
I. Ghosh, T. Ghosh, J. I. Bardagi, B. König, *Science* **2014**, *346*, 725-728.

TG and JIB did the GC calibrations. TG optimized the reaction conditions and performed all the reactions (except, entry 2 and 10 in Fig. 3). IG performed all the spectroscopic measurements and wrote the manuscript. BK supervised the project and is corresponding author.

2.1 Introduction

Visible light provides sufficient energy to promote challenging chemical reactions. Biological photosynthesis as the omnipresent example uses a visible portion of the solar spectrum to separate charges by electron transfer, providing the energy for water oxidation. This transformation (water to oxygen, protons, and electrons) requires the cumulative absorption of four photons.[1] In the past decades visible light mediated chemical photoredox catalysis has emerged into a conceptually related valuable method for organic synthesis.[2-4] Here, single photon excitation of dye molecules, such as redox active coordination compounds (e.g. $Ru(bpy)_3^{2+}$ or $Ir(ppy)_3$),[3][5] conjugated organics (*e.g.* eosin Y),[6] or inorganic semiconductors (e.g. CdS)[7] mediates photoinduced electron or energy transfer process to substrates.

A recent application is the generation of highly reactive aryl radicals, which are useful arylating reagents in synthesis, by photoinduced electron transfer (PET) from photoredox catalysts to suitable precursors followed by bond scission.[8-9] However, the choice of aryl radical precursors is currently limited to electron poor arenes, such as diazonium[6][10] or iodonium[11] salts or in a few cases aryl iodides[9][12] with weakly bound leaving groups, due to the accessible reducing power of typical visible light photoredox catalysts.[13-14] Two mechanistic scenarios for the aryl radical generation can be considered: (i) oxidative quenching of the excited photoredox catalyst by the aryl radical precursor, which must be exergonic or, if the lifetime of the excited state is long and the subsequent bond cleavage fast and irreversible, at least thermo neutral;[15] (ii) oxidation of the photoreduced catalyst in its ground state (**Fig. 5**, left), which can be slightly endergonic. The energy conferred by visible light excitation for subsequent reduction chemistry is limited by the energy of a single absorbed photon. The energy of blue photons (440 nm) of 270 KJ/mol or 2.8 eV defines a maximum theoretical energy threshold between the donor (i.e. photocatalyst) and acceptor (i.e. substrate). In addition, part of the accessible energy is always lost due to intersystem crossing and reorganization of the excited states of the photocatalysts by non-radiative pathways. In the case of Ru complexes this loss is ~ 0.6 eV.[3] As a consequence, the available energy of typical photocatalysts just reaches the reduction potential (E^o) of aryl iodides[9] defining the current synthetic scope of photoredox catalysis.

Herein, we report a practical approach to overcome the limitations of visible light mediated chemical photocatalysis by using the energies of two photons in one catalytic cycle.[16]

Photocatalytic alkylation or arylation reactions as reported by MacMillan,[3][17] Stephenson,[18] Yoon,[2] and others[6] employ a typical PET process (**Fig. 5**, left). The excited dye becomes a stronger oxidant (and reductant) and is converted into its radical anion, which activates substituted benzyl bromides,[3][19] alpha bromo carbonyl compounds,[20] aryl iodides,[9][12] diazonium[6] and iodonium[11] salts. However, compounds that are less reactive (e.g. aryl bromides and chlorides)[21-23] due to a more negative reduction potential, higher carbon-halide bond dissociation energy and a different, stepwise cleavage mechanism[23] are not accessible by this process using typical photocatalysts and more importantly visible light. Our approach is inspired by the Z-scheme of biological photosynthesis, which has already been used in water photooxidation,[24] but surprisingly, has not yet been applied in organic synthesis. The energy of a second visible light excitation can be added to the process if the radical anion of the dye is reasonably stable in the ground state, colored, and thus can be excited again by visible light (**Fig. 5**, right).

2.2 Results and discussion

Perylene diimides, a class of fluorescent dye molecules that have been used as pigments, colorants, photoreceptors, and more recently as electronic materials because of their unique combination of thermal- and photo-stability and optical and redox properties,[25] fulfill the requirements of such bio-mimetic organic dye based catalytic system. Among different perylene diimides *N*,*N*-bis(2,6-diisopropylphenyl)perylene-3,4,9,10-bis(dicarboximide) **(PDI**, see **Fig. 1** for chemical structure) was selected due to its better solubility in DMF and DMSO (solvents used in this study, see below). Upon irradiation with blue light (455 nm) in the presence of triethylamine (Et_3N) as electron donor, **PDI** forms a colored radical anion **PDI**$^{\bullet-}$ (see **Fig. 1** and **Fig. 7–9** in the experimental section) that can be again excited by visible light.[26] In the absence of oxygen the radical anion is very stable. Spectroscopic investigations confirmed that electron transfer from Et_3N to **PDI** requires photoexcitation (**Fig. 1** and **Fig. 8**).[27]

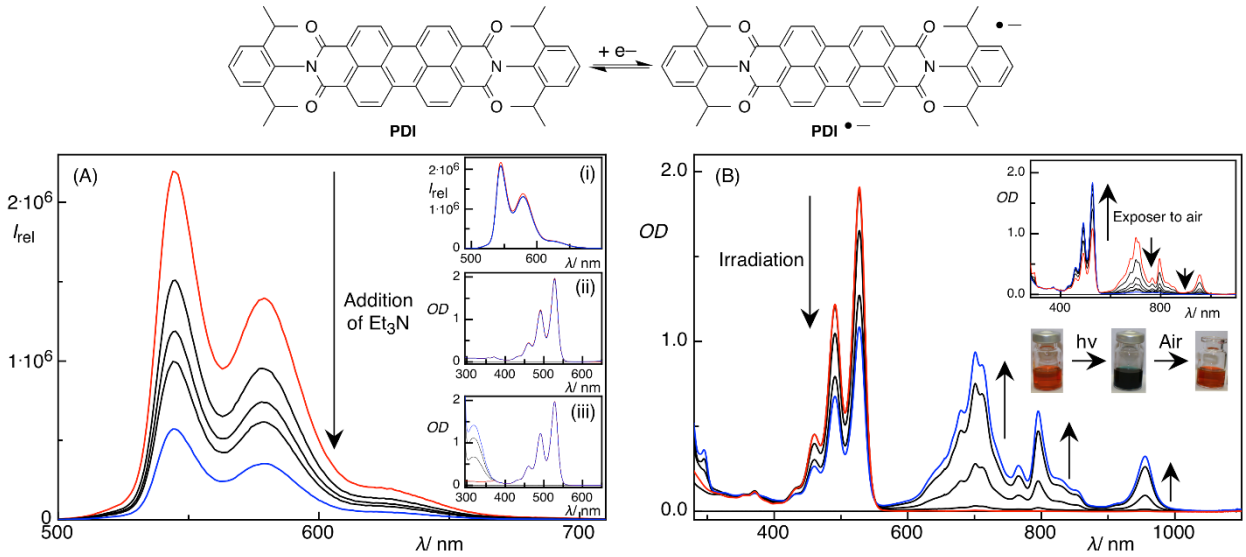

Fig. 1: Chemical structure of the photocatalyst PDI, one electron reduction of PDI to its radical anion, and effects of Et_3N and 4′-bromoacetophenone on its photophysical properties. (A) Changes in the fluorescence spectra (in this case intensity; λ_{Ex} = 455 nm) of **PDI** upon successive addition of Et_3N in DMF. In the insets, changes in the fluorescence spectra of **PDI** upon addition of (i) 4′-bromoacetophenone, and changes in the absorption spectra of **PDI** upon addition of (ii) Et_3N, and (iii) 4′-bromoacetophenone are shown. (B) Formation of the **PDI** radical anion (**PDI**$^{\bullet-}$) upon photoexcitation (λ_{Ex} = 455 nm) of **PDI** in the presence of Et_3N. In the inset, regeneration of neutral **PDI** from **PDI**$^{\bullet-}$ upon exposure to air is shown (see also **Fig. 9** in the experimental section).

A synthetic application of this catalytic system is the photoreduction of aryl halides, including aryl chlorides, using visible light irradiation. The reaction conditions were optimized by irradiating a mixture of 4′-bromoacetophenone, **PDI** (5 mol%), and Et_3N with blue light (455 nm) (see Table 1). In DMSO as solvent the reduction product acetophenone was obtained in 4h with 47% photoreduction yield (entry 16, Table 1). Continuous irradiation of the reaction mixture for 8h gave 69% yield. Use of DMF as solvent gave comparable or slightly better yields (see entry 10 in **Fig. 2** and Table 1) in shorter reaction time of 4h. Control experiments confirmed that **PDI**, electron donor, and light irradiation are necessary for the photoreduction reaction to occur (entry 1–6 in Table 1).

Using the optimized conditions the reaction scope was explored with a range of substituted aryl bromides giving the corresponding reduction products in good to nearly quantitative yields (**Fig. 2**). The reduction potentials of NMe_2 and OMe substituted aryl bromides are

too high to be reached employing these photoreduction conditions, whereas *p*-nitro-substituted aryl bromides have such a low fragmentation rate[22] that back electron transfer becomes dominant. The photoreduction reactions could also be performed under sunlight (entry 10 in **Fig. 2**) or with 530 nm LEDs as the absorption spectrum of **PDI** spans a broad portion of the visible spectrum (see **Fig. 7** in the experimental section). Substituted aryl iodides having slightly lower reduction potentials than aryl bromides[22] gave comparable photoreduction yields (see entries 1–6 in **Fig. 2**). Notably, an aryl–iodine bond was chemoselectively reduced in the presence of a bromine substituent (entry 6 in **Fig. 2**).

A commercially available catalyst, *N*,*N*′-bis(3-pentyl)perylene-3,4,9,10-bis(dicarboximide) (for the chemical structure, see **Fig. 6**), gave similar yields when the reaction mixtures were irradiated for 8h (see entry 14 and 15 in Table 1). The slightly slower reaction rate is attributed to its poorer solubility.

Based on the reduction potential of **PDI**/**PDI**$^{\bullet-}$ (–0.37 V *vs* SCE) and the E_{0-0} transition energy of **PDI**$^{\bullet-}$, we estimated a reducing power of the excited state **PDI**$^{\bullet-*}$ according to the Rehm-Weller equation[28] that reaches or exceeds the reduction potentials of substituted aryl chlorides.[26][29] This class of compounds, although easily accessible and relatively inexpensive, has not been considered in visible light photocatalysis, because of their low reactivity due to high reduction potentials, high carbon–chlorine bond energies, and a stepwise fragmentation mechanism. To the best of our knowledge, the reduction of aryl chlorides has only been achieved using strong bases ,[30-31] such as potassium tert-butoxide, or nucleophiles under UV ($\lambda_{Ex} \leq 350$ nm) irradiation ($S_{RN}1$)[32] and in the presence of an excess of highly reactive neutral organic reducing agents, such as N^2,N^2,N^{12},N^{12}-tetramethyl-7,8-dihydro-6H-dipyrido[1,4]diazepine-2,12-diamine (for the chemical structure, see **Fig. 6**) and UV-A (365 nm) irradiation as introduced by Murphy.[21] The conPET process generates the strong reducing **PDI**$^{\bullet-*}$ *in situ* by two subsequent visible light excitations starting from air stable **PDI**. This avoids the use of highly air and moisture sensitive donor molecules, which require strict inert reaction conditions, UV-A irradiation, and strongly basic conditions that are incompatible with many functional groups. Aryl chlorides bearing electron withdrawing groups gave the corresponding reduction products with good to excellent yields in photocatalytic conditions (entry 13–17 in **Fig. 2**) that require only mixing of substrates, **PDI**, Et_3N, and irradiation with visible light.

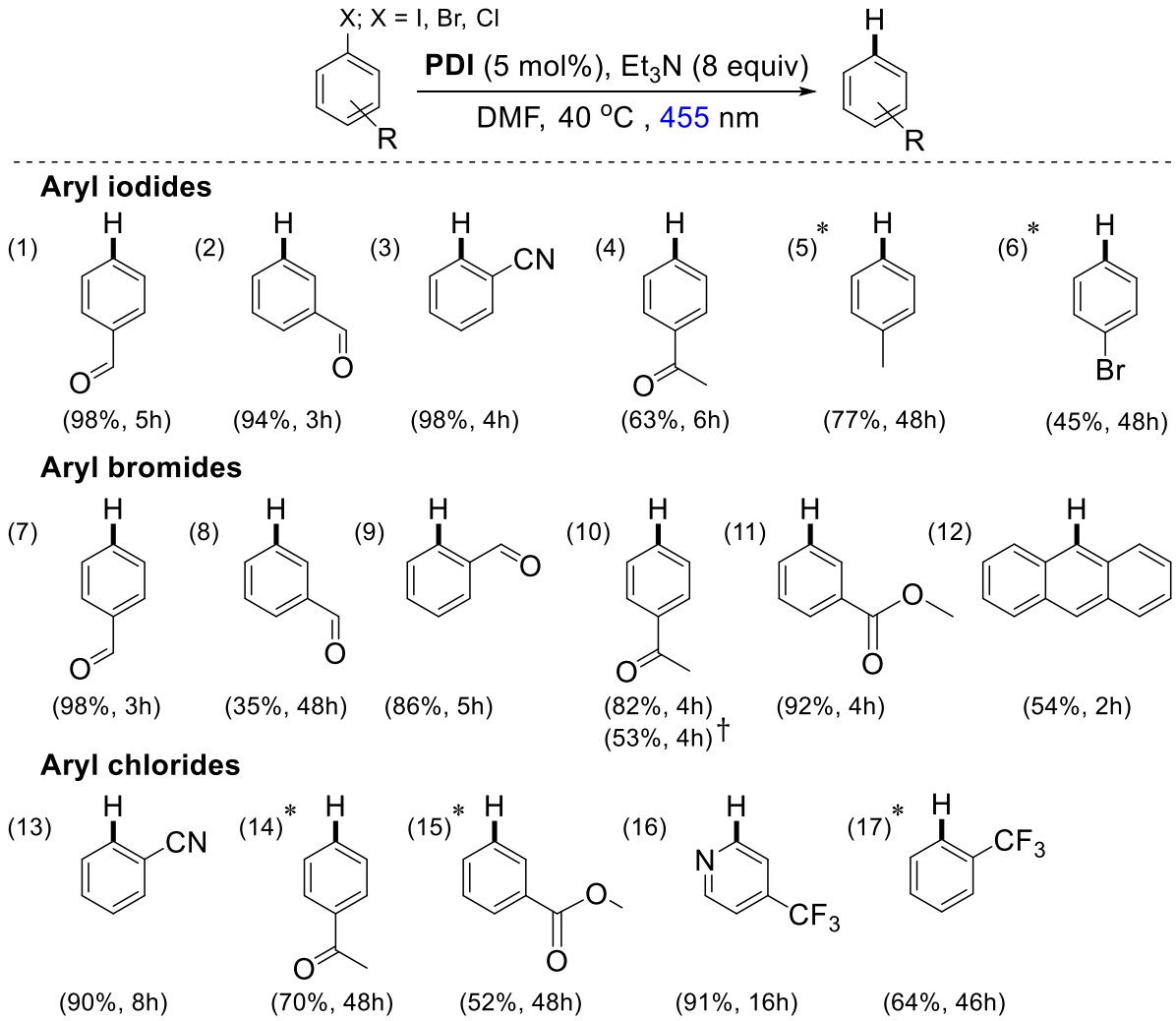

Yields (Error ca. 5 %) were calculated from GC measurements using internal standards.
*10 mol% catalyst and 16 equiv of Et_3N were employed. †Photoreduction performed in sunlight

Fig. 2: Photoreduction of aryl halides. Yields (%) and reaction times (h) are given.

Next, we applied the aryl radical intermediates for C–C bond forming arylation reactions. Challenge in this case is competition from fast hydrogen abstraction of the aryl radical from the solvent and the radical cation of Et_3N (see below).[33] We therefore selected as the reaction partner *N*-heterocyclic pyrroles, which were found to have high reaction rates in the addition of radicals. Substantial amounts of the expected arylation product were indeed obtained irradiating aryl halides in the presence of *N*-methylpyrrole and catalytic amounts of **PDI**. The reduction product is a minor byproduct, but dominates when furan or thiophene are used as reaction partner. Changing the solvent from DMF, which favors the reduction product, to DMSO improved the yields significantly. Isolated yields of functionalized *N*-methylpyrrole derivatives obtained from different substituted aryl halides are depicted in **Fig. 3**. As in the photoreduction reaction (see above), the C–H arylation reaction with *N*-

methylpyrrole could also be performed with *N,N′*-bis(3-pentyl)perylene-3,4,9,10-bis(dicarboximide) (entry 6 in **Fig. 3**). The reaction scope was extended to other pyrrole derivatives affording arylated products in good to excellent yields (**Fig. 3**).

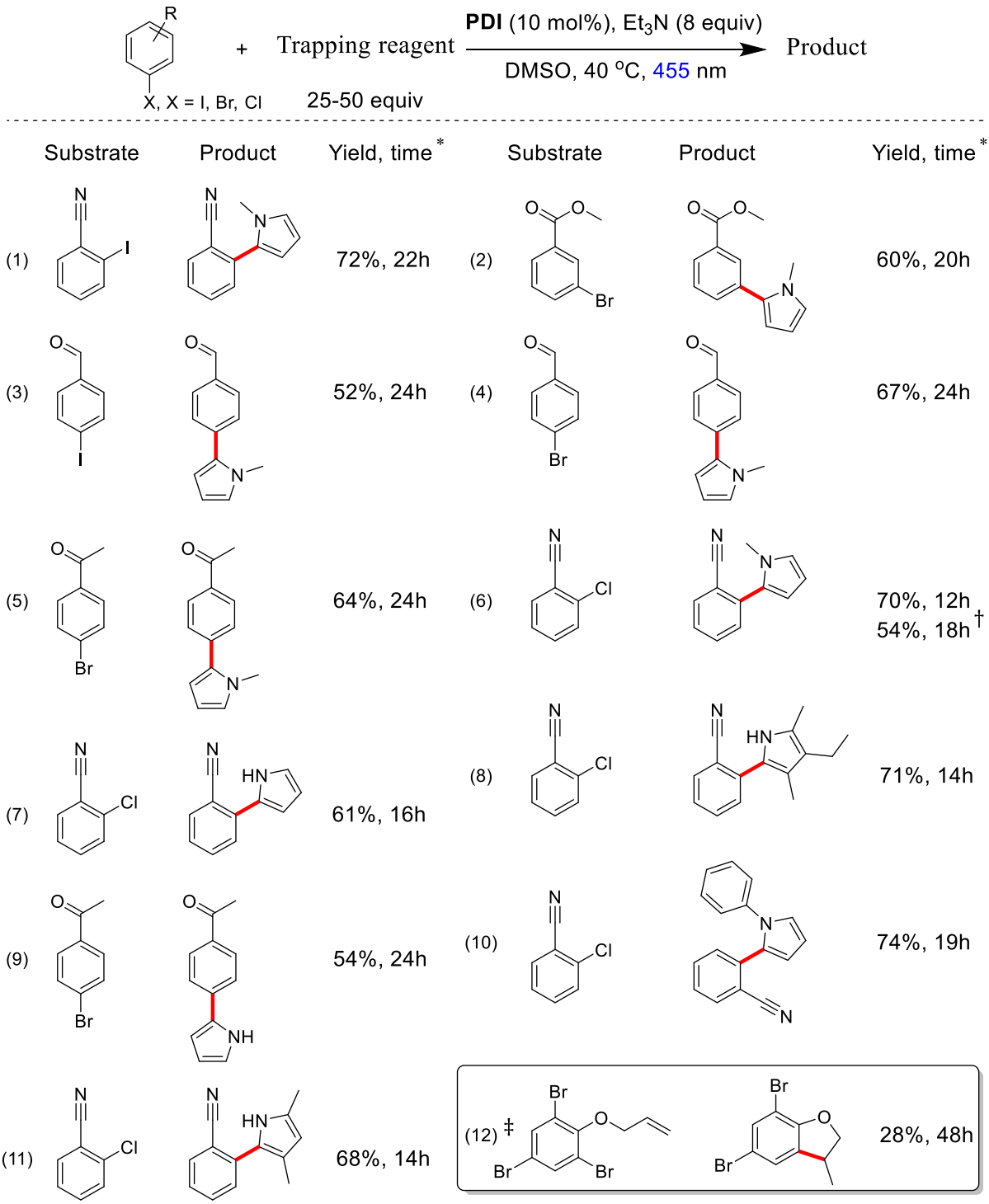

Fig. 3: C–H aromatic substitution reactions of aryl halides with substituted pyrroles and intramolecular addition to an alkene.

The photoreduction of aryl halides appears to proceed *via* a radical mechanism[23]34] as evidenced by the conversion of 2-(allyloxy)-1,3,5-tribromobenzene to the 5-*exo* cyclization product 5,7-dibromo-3-methyl-2,3-dihydrobenzofuran (entry 12, **Fig. 3**), which implies a radical intermediate.[12]34] Furthermore, the reduction reaction of 4′-bromoacetophenone in the presence of 2,2,6,6-tetramethylpiperidinoxyl (TEMPO) gave the expected TEMPO adduct (see experimental section). The formation of a **PDI** dianion, which could be formed via two electron reduction,[35] was not detected under the reaction conditions (compare **Fig-1(B)** and **Fig. 8** with **Fig. 7**; **Fig. 7** shows the absorption spectrum of the electrochemically generated **PDI** dianion). The photoreduction of 4′-bromoacetophenone was insignificant in air, preventing the formation of the **PDI** radical anion (entry 6 Table 1 and **Fig. 1(B) and 9**). In the absence of light no reduction product is obtained: 4′-bromoacetophenone added to a photochemically generated **PDI** radical anion (by photo-irradiating the mixture of **PDI** and Et_3N) and kept in the dark for 4h was not converted (entry 9 and 11 in Table 1). When the reaction mixture was then illuminated with 455 nm light, acetophenone was obtained in yields comparable to the normal photoreduction protocol. Reduction of 4′-bromoacetophenone also did not occur when the substrate was added to a chemically generated (using $(Et_4N)_2S_2O_4$ as chemical reductant of **PDI**) radical anion (see entry 10 in table 1). Degradation products of the catalyst formed during the course of the reaction may still contribute to substrate conversion as only the perylene core is required (c.f. **PDI** and *N*,*N*′-bis(3-pentyl)perylene-3,4,9,10-bis(dicarboximide): The substituents in the amide nitrogens of perylene have almost no influence on the photophysical properties and are mainly introduced to increase the solubility of perylene diimides).[25]

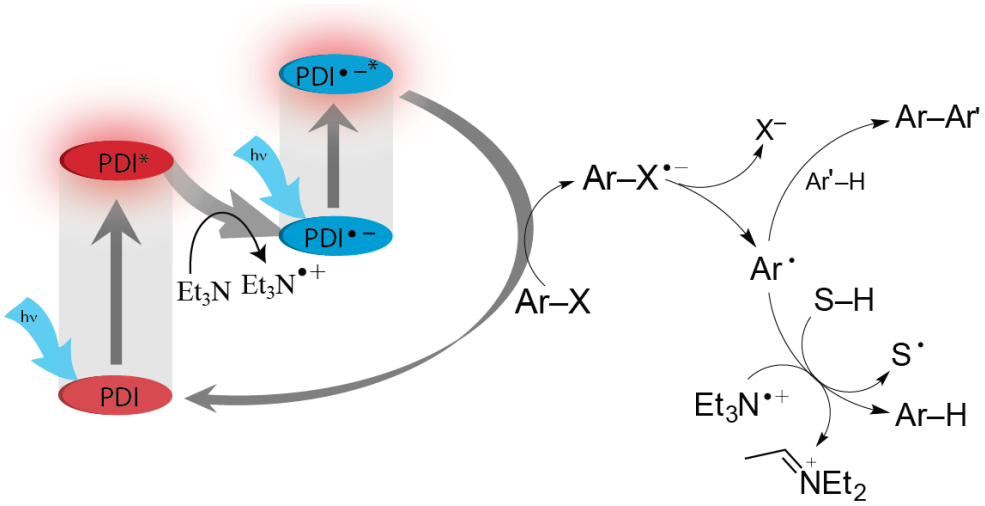

Fig. 4: Proposed catalytic mechanism.

All experiments support the proposed catalytic cycle shown in **Fig. 4**. Excited **PDI*** is reductively quenched by Et_3N to give $\mathbf{PDI}^{\bullet-}$ and the radical cation of triethylamine ($Et_3N^{\bullet+}$).[27] Upon the second excitation $\mathbf{PDI}^{\bullet-*}$ reduces the substrate yielding the aryl radical precursor ($ArX^{\bullet-}$) and regenerating the neutral **PDI**. Fragmentation of $ArX^{\bullet-}$ yields the aryl radical, which abstracts a hydrogen atom from either $Et_3N^{\bullet+}$ or solvents (SH) to yield the reduction products, or reacts with unsaturated compounds yielding C–C coupling products. GC–MS analysis of the crude product mixture confirmed the formation of diethylamine and hydrogen atom abstraction reduction reactions in D_7-DMF gave deuterated products (see experimental section).

2.3 Conclusion

Two consecutive photoinduced electron transfer (conPET) steps using perylene diimide dyes accumulate the energy from two visible light excitations. The process is a minimalistic chemical model of the Z scheme in biological photosynthesis and extends the scope of visible light photocatalysis to aryl chlorides. Highly reactive aryl radicals are obtained from stable, and in the case of aryl chlorides, inexpensive bulk chemicals, under very mild and metal free reaction conditions.

2.4 Experimental section

2.4.1 Materials and methods

Aryl halides were commercially available and used without further purification unless otherwise stated. *N*,*N*′-Bis(3-pentyl)perylene-3,4,9,10-bis(dicarboximide) was purchased from Sigma-Aldrich and used without further purification. *N*,*N*-Bis(2,6-diisopropyl-phenyl)perylene-3,4,9,10-bis(dicarboximide) (**PDI**) was prepared according to a literature procedure.[29] Spectroscopic grade DMF and DMSO were dried with 3 Å molecular sieves according to a reported procedure.[36]

Thin-layer chromatography was performed using silica gel plates 60 F254: Visualization was accomplished with short wavelength UV light (254 nm). Standard flash chromatography was performed on an Isolera™ Spektra Systems automated with high

performance flash purification system using silica gel of particle size 40−63 μm or a reverse column (specification: Biotage SNAP KP-C18-HS-12g). Preparative high-pressure liquid chromatography (HPLC) was performed using a C18 reverse column and water/acetonitrile mixtures with a UV detector. ^{1}H and ^{13}C NMR spectra were recorded on Bruker Avance spectrometers (300 MHz and 75 MHz or 400 MHz and 101 MHz) in $CDCl_3$ and DMSO-d_6 solution with internal solvent signal as reference (7.26 and 77.0, 2.50 and 39.4 respectively). Proton NMR data are reported as follows: chemical shift (ppm), multiplicity (s = singlet, d = doublet, t = triplet, q = quartet, quint = quintet, sext = sextet, hept = heptet, dd = doublet of doublets, ddd = doublet of doublets of doublets, td = triplet of doublets, qd = quartet of doublets, m = multiplet, br. s. = broad singlet), coupling constants (Hz) and numbers of protons. Data for ^{13}C NMR are reported in terms of chemical shift and no special nomenclature is used for equivalent carbons. High resolution mass spectra (HRMS) were obtained from the central analytic mass spectrometry facilities of the Faculty of Chemistry and Pharmacy, Regensburg University and are reported according to the IUPAC recommendations 2013. Gas chromatography (GC) and gas chromatography coupled to low resolution mass spectrometry (GC–MS) analysis were performed using a capillary column (length: 30 m; diam. 0.25 mm; film: 0.25 μ) using He gas as carrier. GC was equipped with an FID detector. GC–MS was performed on 5975 MSD single quadruple detector. Reduction products were identified by comparing with authentic samples (GC/FID and GC–MS). Quantification of reduction products was performed by GC/FID analysis using internal standards. UV–Vis and fluorescence measurements were performed with Varian Cary 50 UV/Vis spectrophotometer and FluoroMax-4 spectrofluorometer, respectively. Electrochemical studies were carried out under argon atmosphere. The measurements were performed in dimethylformamide (DMF) containing 0.1 M tetra-*n*-butylammonium tetrafluoroborate using ferrocene/ferrocenium (Fc/Fc^{+}) as an internal reference. A glassy carbon electrode (working electrode), platinum wire counter electrode, and Ag quasi-reference electrode were employed. Spectroelectrochemical studies were carried out in an optically transparent thin layer electrochemical cell (OTTLE). Photoreduction and C–H arylation reactions were performed with 455 nm LEDs (OSRAM Oslon SSL 80 royal-blue LEDs (λ = 455 nm (± 15 nm), 3.5 V, 700 mA).

Synthesis of *N*,*N*-bis(2,6-diisopropylphenyl)perylene-3,4,9,10-bis(dicarboximide) (**PDI**):

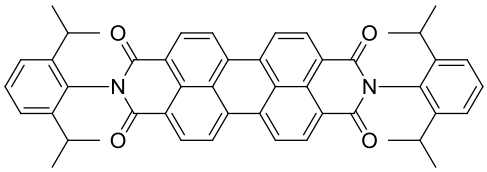

PDI was synthesized according to the literature procedure.[29] To a dry Schlenk flask, equipped with a stirring bar, 1 g (2.55 mmol) of 3,4,9,10-perylenetetracarboxydianhydride, 2.0 mL (10.6 mmol) of 2,6-diisopropylaniline and 7.5 g of imidazole were added. The reaction mixture was heated to 190 ºC under N_2 and after 24h the reaction mixture was cooled to room temperature and diluted with 50 mL of EtOH and 60 mL of 2 M HCl. This mixture was stirred for 3 h, filtered and washed with EtOH/HCl and EtOH/water mixtures. The solid was purified by silica column chromatography using petrol ether/dichloromethane (1:1 to dichloromethane only) as eluents yielding **PDI** (895 mg, 49% isolated yield) as a red solid.

^{1}H NMR (400 MHz, $CDCl_3$) δ 8.80 (d, J = 8.0 Hz, 4H), 8.75 (d, J = 8.1 Hz, 4H), 7.55 – 7.47 (m, 2H), 7.36 (d, J = 7.8 Hz, 4H), 2.76 (hept, J = 6.7 Hz, 4H), 1.19 (d, J = 6.8 Hz, 24H).

^{13}C NMR (101 MHz, $CDCl_3$) δ 163.5, 145.7, 135.1, 132.1, 130.5, 130.2, 129.7, 129.2, 124.1, 123.5, 123.4, 29.2, 24.0.

E^o in DMF vs Fc/Fc^+: E^o (**PDI**$^{\bullet-}$/**PDI**) = –0.88 V, E^o (**PDI**$^{2-}$/**PDI**$^{\bullet-}$) = –1.18 V.

General procedure for the photoreduction of aryl halides:

In a 5 mL snap vial with magnetic stirring bar the respective aryl halide (0.05 mmol, 1 equiv) and **PDI** (0.0025 mmol, 0.05 equiv) were dissolved in dry DMF/DMSO (total volume of the solution 3 mL) and the resulting mixture was degassed (× 2) *via* a syringe needle. Et_3N (0.40 mmol, 8 equiv) was added under N_2 and the reaction mixture was irradiated through the plane bottom side of the snap vial using a 455 nm LED. The reaction progress was monitored by GC analysis. Photoreduction yields were calculated from GC measurements using internal standards.

Hydrogen abstraction of aryl radicals from solvents (in this case DMF) was confirmed by performing the photoreduction reaction of 4′-bromoacetophenone in DMF-d_7. A significantly higher amount of the deuterated product was observed in the GC–MS analysis

when the photoreduction reaction was performed in DMF-d_7 compared to non-deuterated DMF as solvent.

The presence of diethylamine in the reaction mixture, resulting from the proposed hydrogen abstraction of aryl radicals from the triethylamine radical cation, was confirmed by GC–MS analysis.

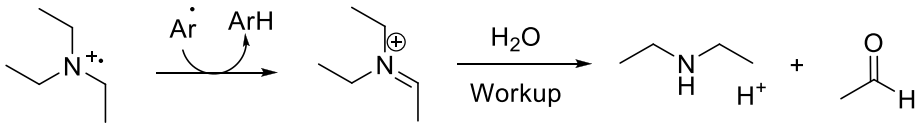

General procedure for C–H arylation reactions:

In a 5 mL snap vial with magnetic stirring bar the aryl halide (0.1 mmol, 1 equiv) and **PDI** (0.01 mmol, 0.1 equiv) were dissolved in dry DMSO (total volume of the solution 3 mL), and the resulting mixture was degassed by syringe needle. Et_3N (0.40 mmol, 8 equiv) and the corresponding pyrrole (2.5 mmol or 5.0 mmol) (except for the intramolecular reaction) were added under N_2 and the reaction mixture was irradiated through the plane bottom side of the snap vial using a 455 nm LED. The reaction progress was monitored by GC analysis. For work up, the reaction mixture was transferred into a separating funnel and 10 mL of distilled water and 2 mL of brine were added. The resulting mixture was extracted with ethyl acetate (3 × 10 mL). The combined organic layers were dried over $MgSO_4$, filtered and concentrated in vacuum. Purification of the crude product was achieved by flash column chromatography using petrol ether/ethyl acetate and water/acetonitrile as eluents on silica gel and reverse phase column, respectively.

HRMS analysis of the TEMPO adduct:

A solution of 4′-bromoacetophenone in DMSO with 10 mol% **PDI**, 8 equivalents Et_3N, and 1 equivalent TEMPO was irradiated with a 455 nm LED at 40 ºC. The reaction mixture was analyzed by HRMS, which shows the exact molecular ion indicating the formation of the proposed TEMPO adduct to the aryl radical intermediate.

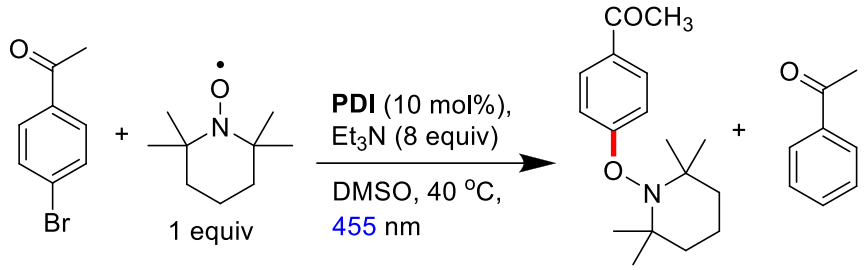

HRMS: calculated for $[M+H]^+$ $C_{17}H_{26}NO_2^+$ 276.1964; found 276.1959.

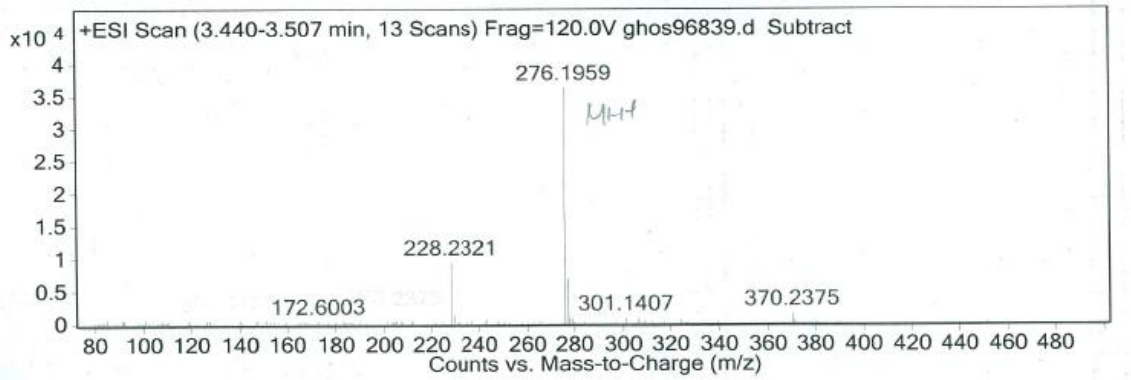

2.4.2 Characterization of C–H arylated products

2-(1-Methyl-1*H*-pyrrol-2-yl)benzonitrile:[37]

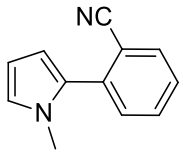

The compound was prepared according to the general procedure using 13.6 mg of 2-chlorobenzonitrile, 7.2 mg of **PDI**, 222 μL of *N*-methylpyrrole, and 112 μL of triethylamine. The crude product was purified using chromatography on silica gel.

^{1}H NMR (300 MHz, $CDCl_3$): δ 7.74 (dd, J = 7.7, 0.9 Hz, 1H), 7.66 – 7.56 (m, 1H), 7.48 – 7.36 (m, 2H), 6.84 – 6.75 (m, 1H), 6.41 (dd, J = 3.7, 1.7 Hz, 1H), 6.25 (dd, J = 3.7, 2.7 Hz, 1H), 3.62 (s, 3H).

^{13}C NMR (75 MHz, $CDCl_3$): δ 135.8, 132.5, 131.3, 129.8, 128.9, 126.4, 123.8, 117.6, 111.8, 110.4, 107.3, 33.8.

4-(1-Methyl-1*H*-pyrrol-2-yl)benzaldehyde:

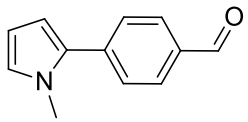

The compound was prepared according to the general procedure using 23.0 mg of 4-iodobenzaldehyde, 7.0 mg of **PDI**, 444 μL of *N*-methylpyrrole, and 112 μL of triethylamine. The crude product was purified using chromatography on silica gel.

^{1}H NMR (300 MHz, DMSO-d_6): δ 10.00 (s, 1H), 7.92 (d, J = 8.2 Hz, 2H), 7.69 (d, J = 8.3 Hz, 2H), 6.96 (t, J = 2.1 Hz, 1H), 6.40 (dd, J = 3.7, 1.8 Hz, 1H), 6.19 – 6.06 (m, 1H), 3.74 (s, 3H).

^{13}C NMR (75 MHz, DMSO-d_6): δ 192.3, 138.6, 133.6, 132.1, 129.7, 127.5, 126.5, 110.6, 107.9, 35.4.

HRMS: calculated for $[M+H]^+$ $C_{12}H_{12}NO^+$ 186.0919; found 186.0915.

4-(1-Methyl-1*H*-pyrrol-2-yl)acetophenone:

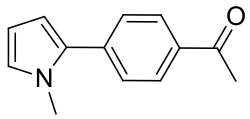

The compound was prepared according to the general procedure using 19.8 mg of 4-bromoacetophenone, 7.0 mg of **PDI**, 444 μL of *N*-methylpyrrole, and 112 μL of triethylamine. The crude product was purified using chromatography on silica gel.

^{1}H NMR (300 MHz, $CDCl_3$): δ 8.09 – 7.88 (m, 2H), 7.61 – 7.42 (m, 2H), 6.85 – 6.71 (m, 1H), 6.36 (dd, J = 3.7, 1.8 Hz, 1H), 6.24 (dd, J = 3.6, 2.7 Hz, 1H), 3.73 (s, 3H), 2.63 (s, 3H).

^{13}C NMR (75 MHz, $CDCl_3$): δ 197.6, 137.9, 134.9, 133.4, 128.6, 128.0, 125.4, 110.2, 108.4, 35.5, 26.6.

HRMS: calculated for M^+ $C_{13}H_{13}NO^+$ 199.0997; found 199.0997.

Methyl 3-(1-methyl-1*H*-pyrrol-2-yl)benzoate:

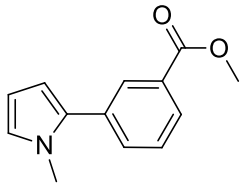

The compound was prepared according to the general procedure using 21.1 mg of methyl 3-bromobenzoate, 7.3 mg of **PDI**, 444 μL of *N*-methylpyrrole, and 112 μL of triethylamine. The crude product was purified using chromatography on silica gel.

^{1}H NMR (300 MHz, DMSO-d_6) δ 7.96 (t, J = 1.6 Hz, 1H), 7.87 (dt, J = 7.6, 1.1 Hz, 1H), 7.79 – 7.68 (m, 1H), 7.56 (t, J = 7.7 Hz, 1H), 6.94 – 6.83 (m, 1H), 6.25 (dd, J = 3.6, 1.8 Hz, 1H), 6.14 – 6.04 (m, 1H), 3.87 (s, 3H), 3.66 (s, 3H).

^{13}C NMR (75 MHz, DMSO-d_6) δ 166.0, 133.3, 132.3, 132.1, 129.9, 128.9, 128.1, 126.9, 124.9, 109.0, 107.5, 52.1, 34.8.

HRMS: calculated for $[M+H]^+$ $C_{13}H_{14}NO_2^+$ 216.1025; found 216.1016.

2-(1*H*-Pyrrol-2-yl)benzonitrile:[38]

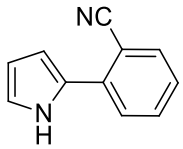

The compound was prepared according to the general procedure using 13.8 mg of 2-chlorobenzonitrile, 7.3 mg of **PDI**, 175 μL of pyrrole and 112 μL of triethylamine. The crude product was purified using reverse phase chromatography.

^{1}H NMR (300 MHz, DMSO-d_6) δ 11.53 (s, 1H), 7.82 (d, *J* = 7.6 Hz, 1H), 7.75 – 7.66 (m, 2H), 7.35 (ddd, *J* = 7.9, 5.7, 2.9 Hz, 1H), 7.01 (td, *J* = 2.7, 1.5 Hz, 1H), 6.84 (ddd, *J* = 3.8, 2.7, 1.4 Hz, 1H), 6.23 (dt, *J* = 3.6, 2.5 Hz, 1H).

^{13}C NMR (75 MHz, DMSO-d_6) δ 135.5, 134.3, 133.3, 127.2, 126.3, 126.0, 121.2, 119.4, 109.5, 109.4, 106.3.

HRMS: calculated for $[M+H]^+$ $C_{11}H_9N_2^+$ 169.0766; found 169.0764.

4-(1*H*-Pyrrol-2-yl)acetophenone:[39]

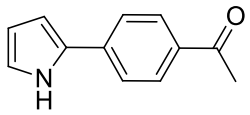

The compound was prepared according to the general procedure using 19.9 mg of 4´-bromoacetophenone, 7.1 mg of **PDI**, 350 μL of pyrrole, and 112 μL of triethylamine. The crude product was purified using reverse phase chromatography.

^{1}H NMR (300 MHz, DMSO-d_6) δ 11.54 (s, 1H), 7.97 – 7.88 (m, 2H), 7.80 – 7.69 (m, 2H), 6.96 (dd, J = 4.1, 2.6 Hz, 1H), 6.72 (ddd, J = 3.7, 2.6, 1.5 Hz, 1H), 6.17 (dt, J = 3.5, 2.4 Hz, 1H), 2.55 (s, 3H).

^{13}C NMR (75 MHz, DMSO-d_6) δ 196.8, 137.1, 133.3, 129.9, 128.9, 122.7, 121.0, 109.7, 107.9, 26.4.

HRMS: calculated for $[M+H]^+$ $C_{12}H_{12}NO^+$ 186.0919; found 186.0915.

2-(3,5-Dimethyl-1*H*-pyrrol-2-yl)benzonitrile:

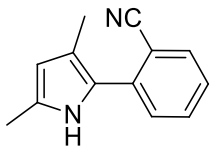

The compound was prepared according to the general procedure using 13.8 mg of 2-chlorobenzonitrile, 7.1 mg of **PDI**, 337 µL 2,4-dimethylpyrrole and 112 µL of triethylamine. The crude product was purified using chromatography on silica gel.

^{1}H NMR (300 MHz, DMSO-d_6): δ 10.76 (s, 1H), 7.83 (dd, J = 7.8, 0.9 Hz, 1H), 7.69 (td, J = 7.8, 1.4 Hz, 1H), 7.52 – 7.35 (m, 2H), 5.74 (d, J = 2.2 Hz, 1H), 2.19 (s, 3H), 2.00 (s, 3H).

^{13}C NMR (75 MHz, DMSO-d_6): δ 137.1, 133.3, 132.7, 130.0, 128.9, 126.4, 123.2, 118.9, 117.7, 110.0, 109.2, 12.6, 12.3.

HRMS: calculated for $[M+H]^+$ $C_{13}H_{13}N_2^+$ 197.1079; found 197.1076.

2-(4-Ethyl-3,5-dimethyl-1*H*-pyrrol-2-yl)benzonitrile:

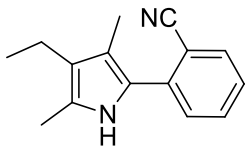

The compound was prepared according to the general procedure using 13.9 mg of 2-chlorobenzonitrile, 7.3 mg of **PDI**, 336 µL 3-ethyl-2,4-dimethylpyrrole and 112 µL of triethylamine. The crude product was purified by chromatography on silica gel.

^{1}H NMR (300 MHz, DMSO-d_6): δ 10.58 (s, 1H), 7.82 (dd, J = 7.8, 1.2 Hz, 1H), 7.67 (td, J = 7.7, 1.4 Hz, 1H), 7.44 (d, J = 7.9 Hz, 1H), 7.39 (td, J = 7.6, 1.1 Hz, 1H), 2.35 (q, J = 7.5 Hz, 2H), 2.16 (s, 3H), 1.96 (s, 3H), 1.03 (t, J = 7.5 Hz, 3H).

^{13}C NMR (75 MHz, DMSO-d_6): δ 137.3, 133.3, 132.6, 129.9, 126.2, 125.3, 122.3, 120.9, 119.0, 116.4, 109.8, 17.1, 15.5, 10.7, 10.6.

HRMS: calculated for $[M+H]^+$ $C_{15}H_{17}N_2^+$ 225.1392; found 225.1385.

2-(1-Phenyl-1*H*-pyrrol-2-yl)benzonitrile:

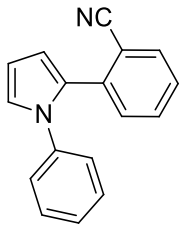

The compound was prepared according to the general procedure using 13.5 mg of 2-chlorobenzonitrile, 7.0 mg of **PDI**, 355 mg of 1-phenyl-1*H*-pyrrole and 112 μL of triethylamine. The crude product was purified by chromatography on silica gel.

^{1}H NMR (400 MHz, DMSO-d_6) δ 7.89 – 7.83 (m, 1H), 7.58 (td, J = 7.7, 1.3 Hz, 1H), 7.46 (td, J = 7.6, 1.1 Hz, 1H), 7.44 – 7.37 (m, 2H), 7.37 – 7.26 (m, 2H), 7.22 – 7.12 (m, 3H), 6.64 (dd, J = 3.6, 1.7 Hz, 1H), 6.48 – 6.43 (m, 1H).

^{13}C NMR (101 MHz, DMSO-d_6) δ 139.1, 135.9, 133.4, 132.6, 130.8, 129.1, 128.5, 127.6, 126.7, 125.4, 125.0, 118.2, 113.3, 111.1, 109.5.

HRMS: calculated for $[M+H]^+$ $C_{17}H_{13}N_2^+$ 245.1079; found 245.1077.

5,7-Dibromo-3-methyl-2,3-dihydrobenzofuran

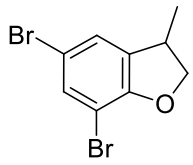

The compound was prepared according to the general procedure using 37.0 mg of 2-allyloxy-1,3,5-tribromobenzene, 7.1 mg of **PDI**, and 112 μL of triethylamine. The reaction was performed in DMF. The crude product was purified by chromatography on silica gel and preparative HPLC.

^{1}H NMR (300 MHz, $CDCl_3$) δ 7.41 (dd, *J* = 1.9, 0.7 Hz, 1H), 7.17 (dd, *J* = 1.9, 1.1 Hz, 1H), 4.78 (t, *J* = 9.0 Hz, 1H), 4.19 (dd, *J* = 8.8, 7.5 Hz, 1H), 3.73 – 3.53 (m, 1H), 1.33 (d, *J* = 6.9 Hz, 3H).

^{13}C NMR (75 MHz, $CDCl_3$) δ 156.4, 135.5, 133.1, 126.1, 112.5, 103.6, 79.2, 37.6, 19.3.

HRMS: calculated for M^+ $C_9H_8Br_2O$ 289.8942; found 289.8932.

2.4.3 Figs. 5 to 9 and Table 1

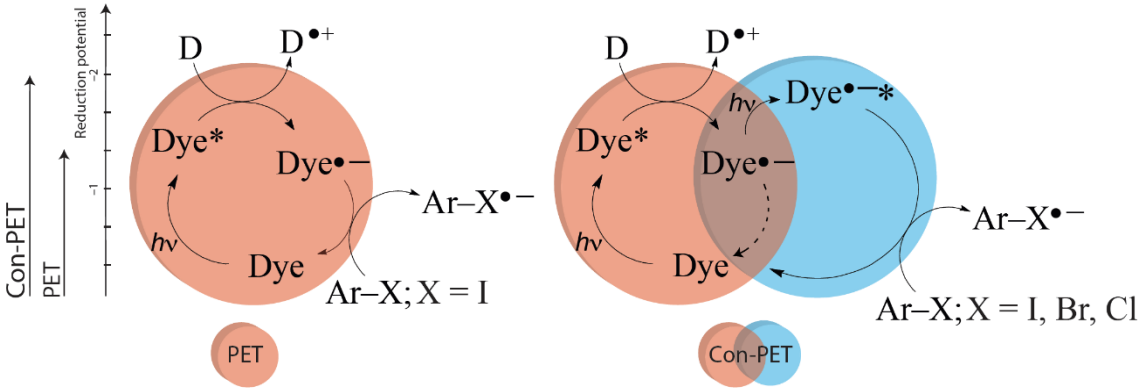

Fig. 5: Schematic representation of catalytic cycles involving one (left) and two (right) photoexcitation events, respectively.

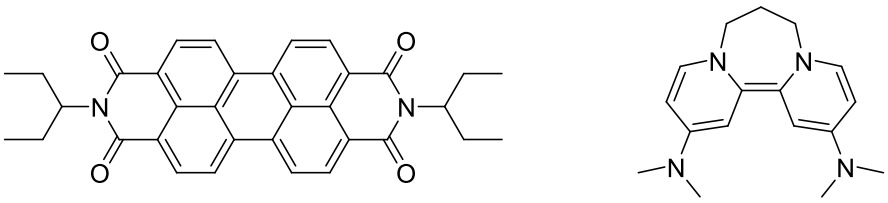

Fig. 6: Chemical structure of *N*,*N*′-bis(3-pentyl)perylene-3,4,9,10-bis(dicarboximide) (left) and N^2,N^2,N^{12},N^{12}-tetramethyl-7,8-dihydro-6*H*-dipyrido[1,2-*a*:2',1'-*c*][1,4]diazepine-2,12-diamine (right).

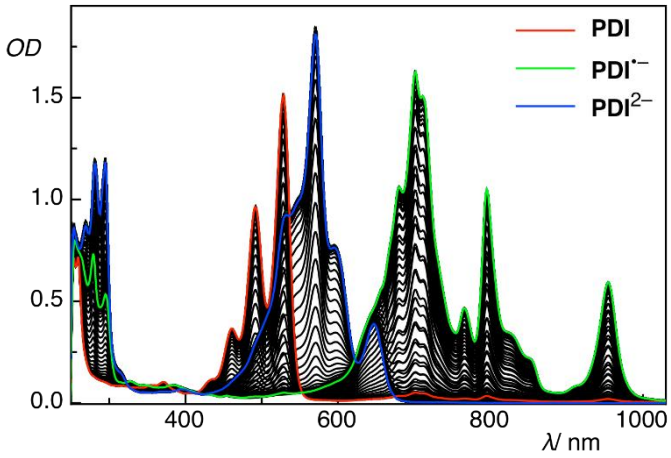

Fig. 7: Spectroelectrochemical analysis of PDI in DMF.

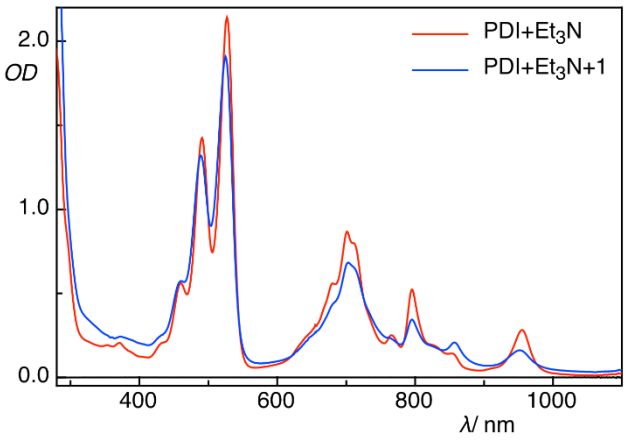

Fig. 8: Formation of the PDI radical anion upon photoexcitation (λ_{Ex} = 455 nm) in the presence of Et_3N and in the reaction mixture. An aliquot of the reaction mixture (after a few minutes of irradiation (λ_{Ex} = 455 nm); 1: 4′-bromoacetophenone) was diluted in DMF under nitrogen to record the absorption spectra.

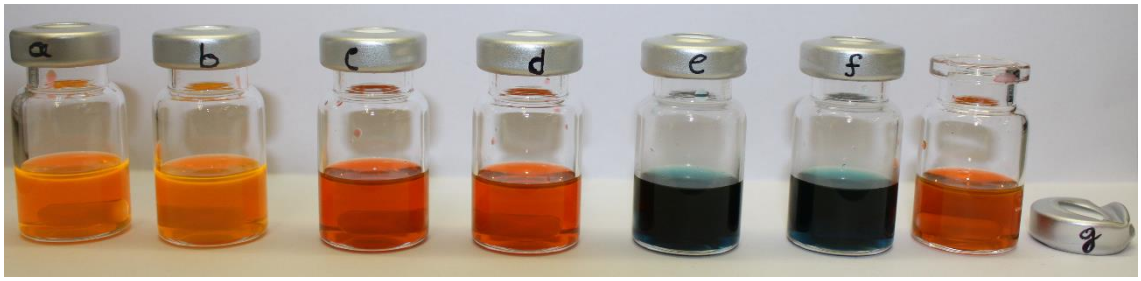

Fig. 9: Photographs of (a) PDI, (b) PDI in the presence of 4′-bromoacetophenone, (c) PDI in the presence of Et_3N, (d) PDI in the presence of 4′-bromoacetophenone and Et_3N, (e) mixture of PDI and Et_3N after ca. 2 minutes of photoirradiation (λ_{Ex} = 455 nm), (f) mixture of PDI, 4′-bromoacetophenone, and Et_3N after ca. 2 minutes of photoirradiation (λ_{Ex} = 455 nm), (g) mixture of PDI and Et_3N was photoirradiated for ca. 2 minutes and then exposed to air (for ca. 30 minutes). All solutions are under nitrogen atmosphere (for g, photoirradiation was performed under nitrogen).

Table 1: Control experiments and optimization of photoreduction reaction condition

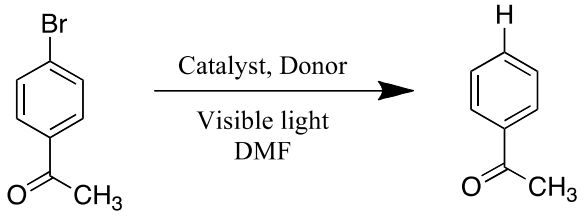

Entry	Catalyst/ mol %	Donor (equiv)	Reaction condition*	Time/ h	Yield/ %†
		Control experiments			
1	5	Et_3N (8)	DMF, 40 °C, 455 nm, N_2	4	82
2	5	Et_3N (8)	DMF, 40 °C, Dark, N_2	4	0‡
3	–	–	DMF, 40 °C, 455 nm, N_2	4	0‡
4	5	–	DMF, 40 °C, 455 nm, N_2	4	ca. 14
5	–	Et_3N (8)	DMF, 40 °C, 455 nm, N_2	4	0‡
6	5	Et_3N (8)	DMF, 40 °C, 455 nm, Air	4	ca. 5
7§	5	Et_3N (8)	DMF, 40 °C, 455 nm, N_2	2	54
8 ‖	5	Et_3N (8)	DMF, 40 °C, 455 nm, N_2	4	70
9¶	5	Et_3N (8)	DMF, 40 °C, Dark, N_2	4	0‡
10	5	$(Et_4N)_2S_2O_4$	DMF, 40 °C, Dark, N_2	4	0‡
11¶	15	Et_3N (12)	DMF, 40 °C, Dark, N_2	4	0‡

Table 1 (cont.): Control experiments and optimization of photoreduction reaction condition

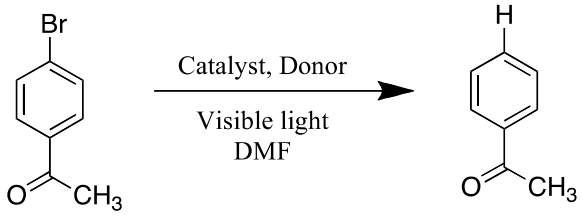

Entry	Catalyst/ mol %	Donor (equiv)	Reaction condition∗	Time/ h	Yield/ %†
Optimization of reaction condition					
12	5	Et_3N (2)	DMF, 40 °C, 455 nm, N_2	4	33
13	5	Et_3N (4)	DMF, 40 °C, 455 nm, N_2	4	43
14[#]	5	Et_3N (8)	DMF, 40 °C, 455 nm, N_2	4	38
15[#]	5	Et_3N (8)	DMF, 40 °C, 455 nm, N_2	8	78
16	5	Et_3N (8)	DMSO, 40 °C, 455 nm, N_2	4	47
17	5	Et_3N (8)	DMSO, 40 °C, 455 nm, N_2	8	69

∗The reaction was performed with 4′-bromoacetophenone; †From GC analysis with respect to an internal standard; ‡The yield, if any, is too low to quantify accurately; §The reaction was stopped after 2h and kept under dark; ||The radical anion of **PDI** was generated upon irradiation (λ_{Ex} = 455 nm) in the presence of Et_3N and then 4′-bromoacetophenone was added and irradiated continuously; ¶The radical anion of **PDI** was generated upon irradiation (λ_{Ex} = 455 nm) in the presence of Et_3N and then 4′-bromoacetophenone was added and kept under dark; #Reaction was performed with a commercially available catalyst: *N*,*N*′-bis(3-pentyl)perylene-3,4,9,10-bis(dicarboximide) (see **Fig. 6** for the chemical structure).

2.4.4 ^{1}H and ^{13}C NMR spectra of the isolated compounds

2-(1-Methyl-1*H*-pyrrol-2-yl)benzonitrile

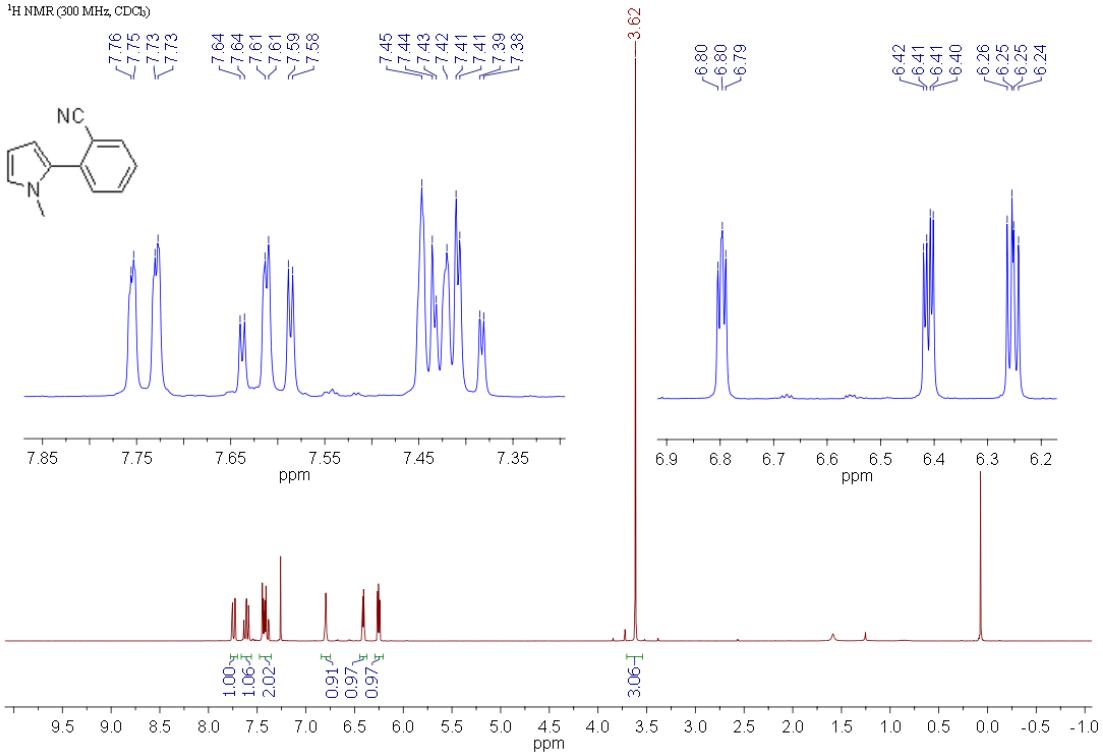

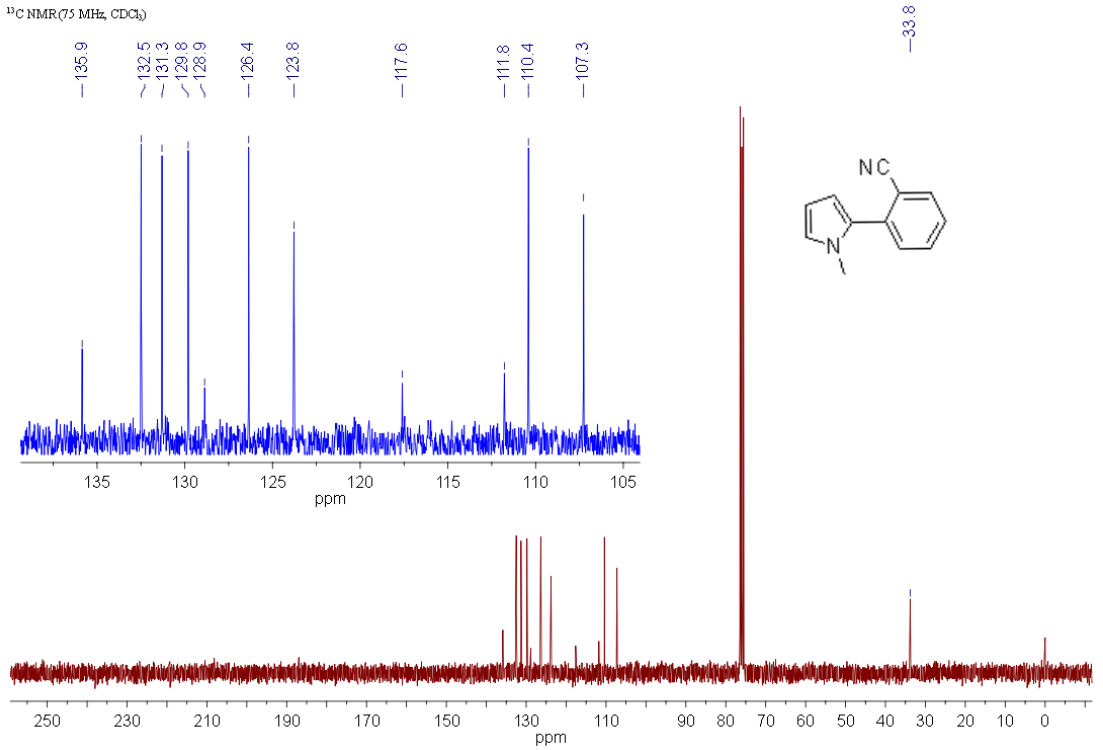

4-(1-Methyl-1*H*-pyrrol-2-yl)benzaldehyde

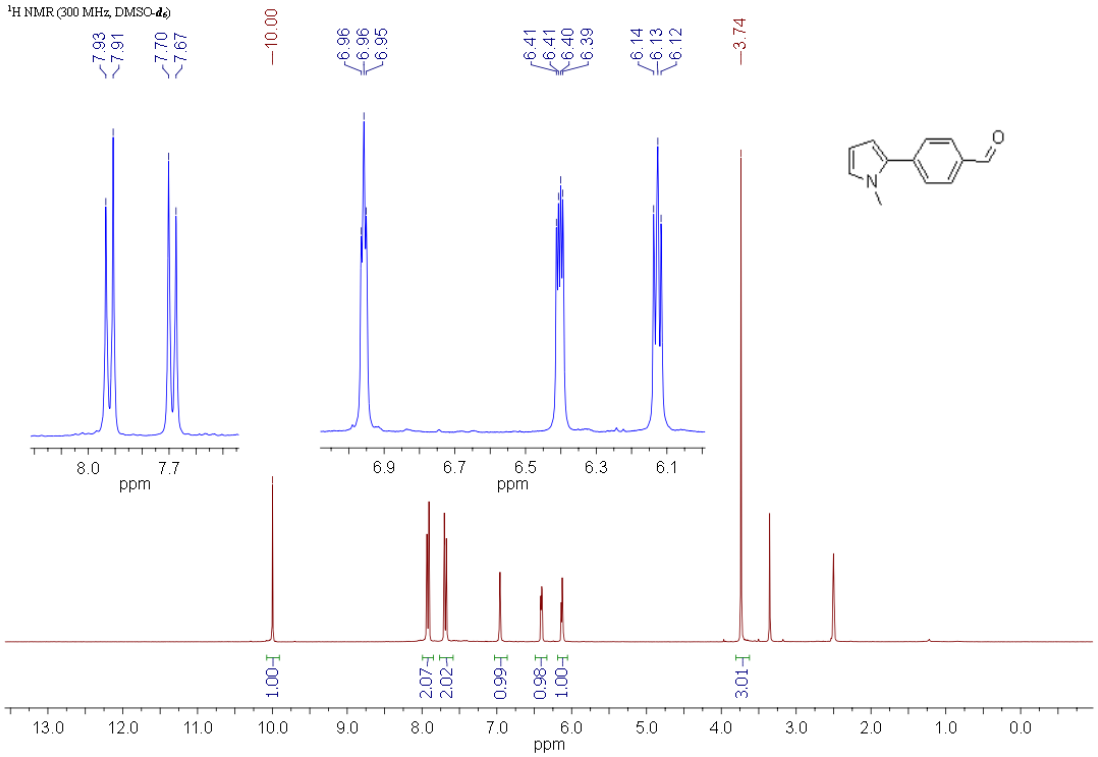

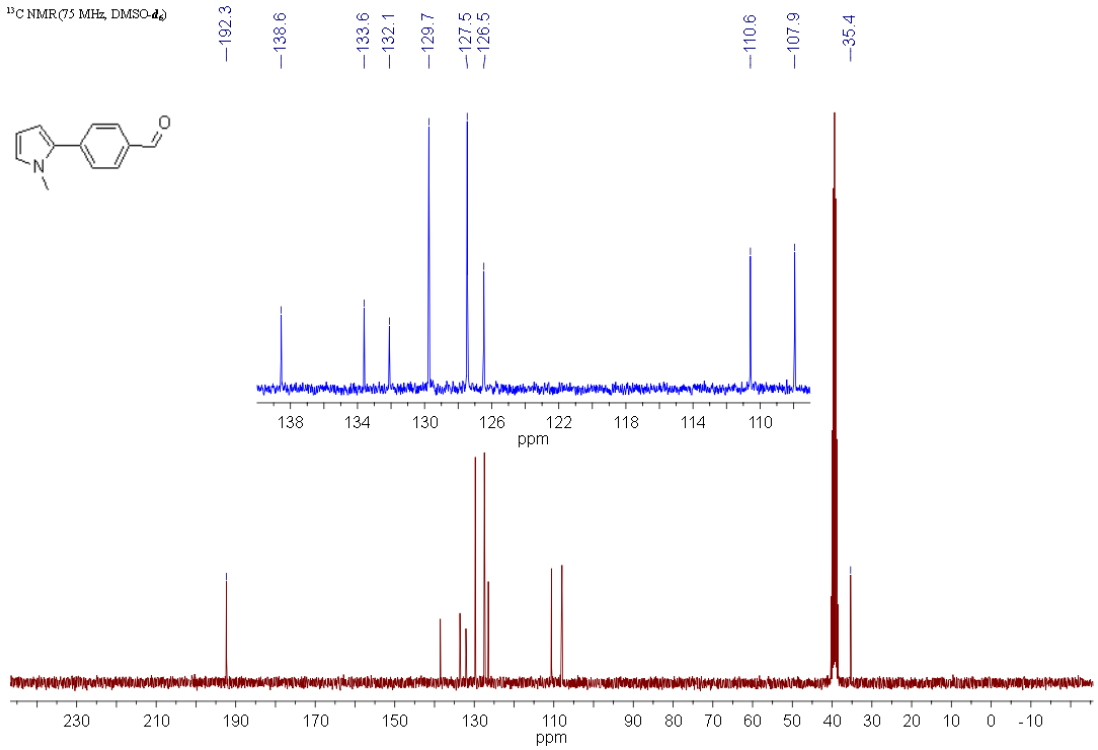

4-(1-Methyl-1*H*-pyrrol-2-yl)acetophenone

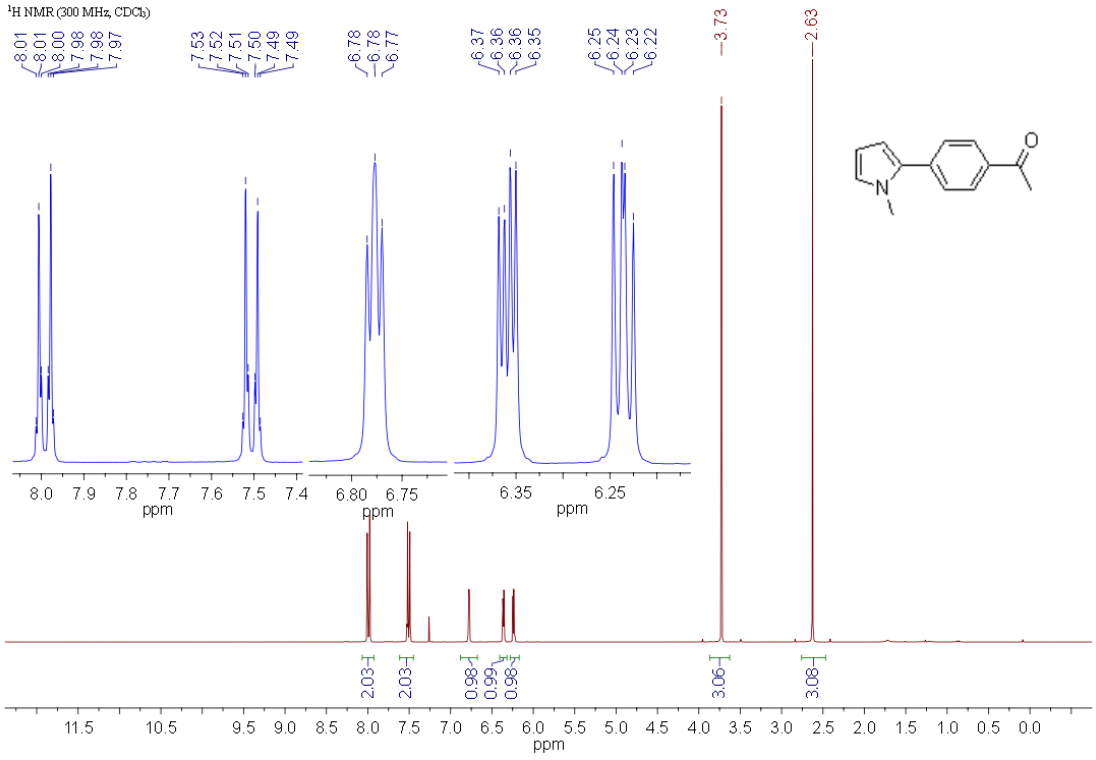

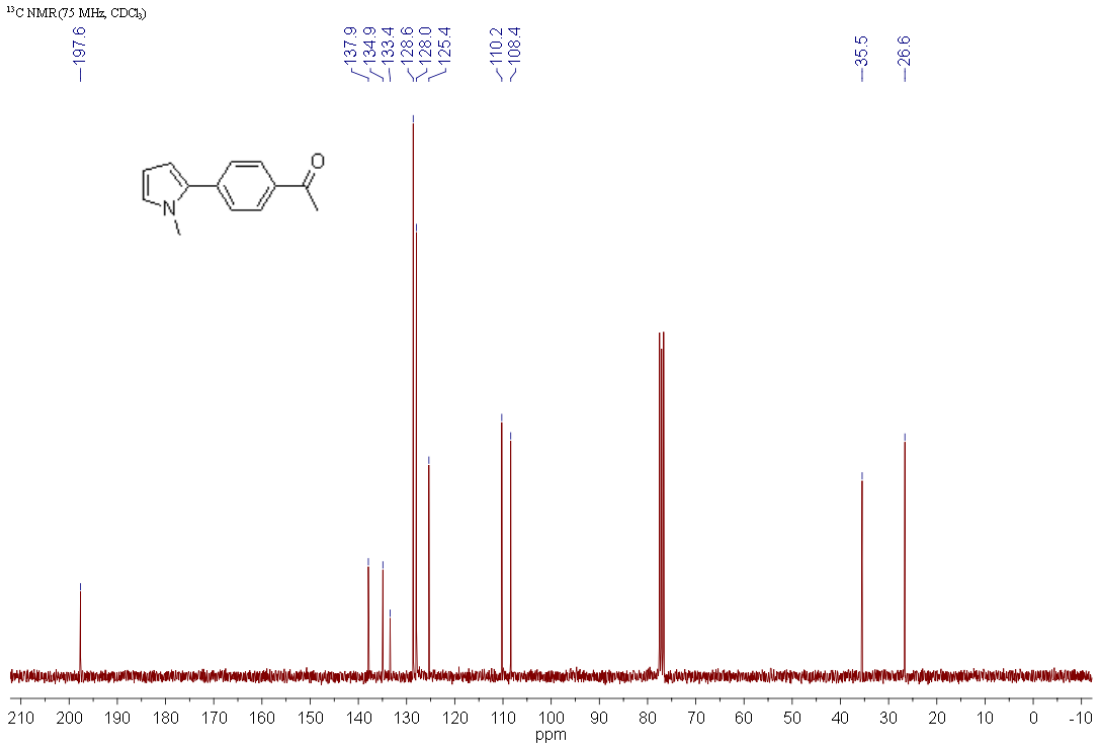

Methyl 3-(1-methyl-1*H*-pyrrol-2-yl)benzoate

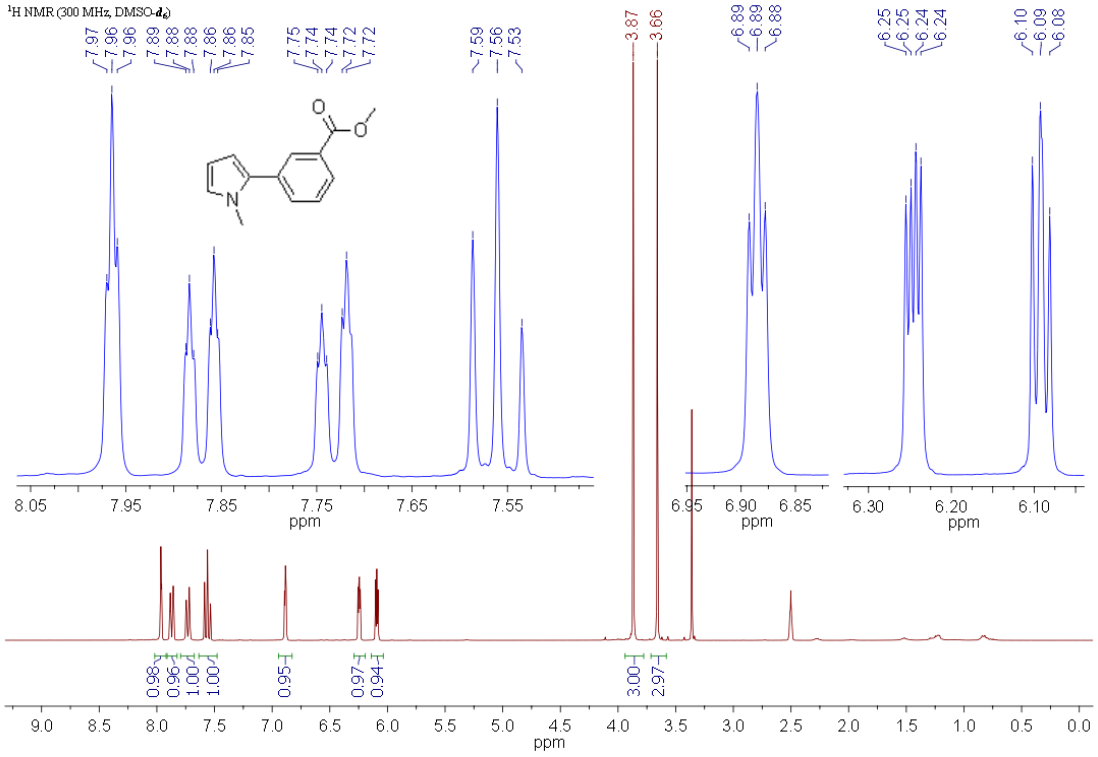

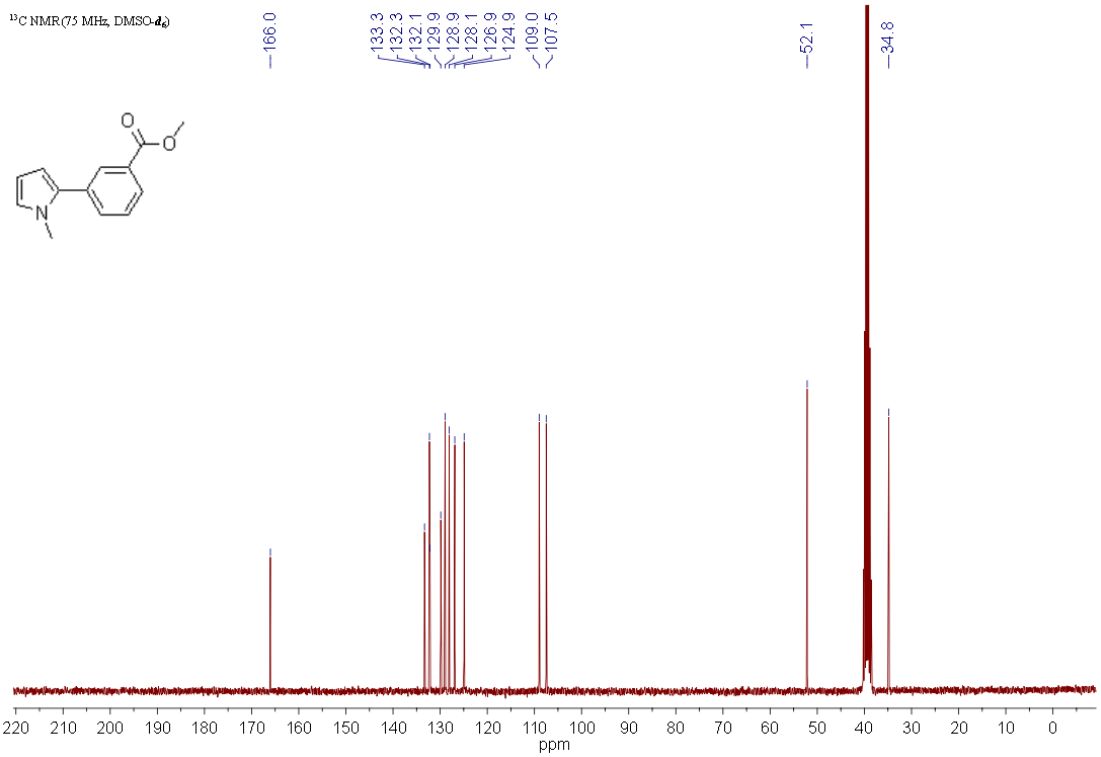

2-(1*H*-Pyrrol-2-yl)benzonitrile

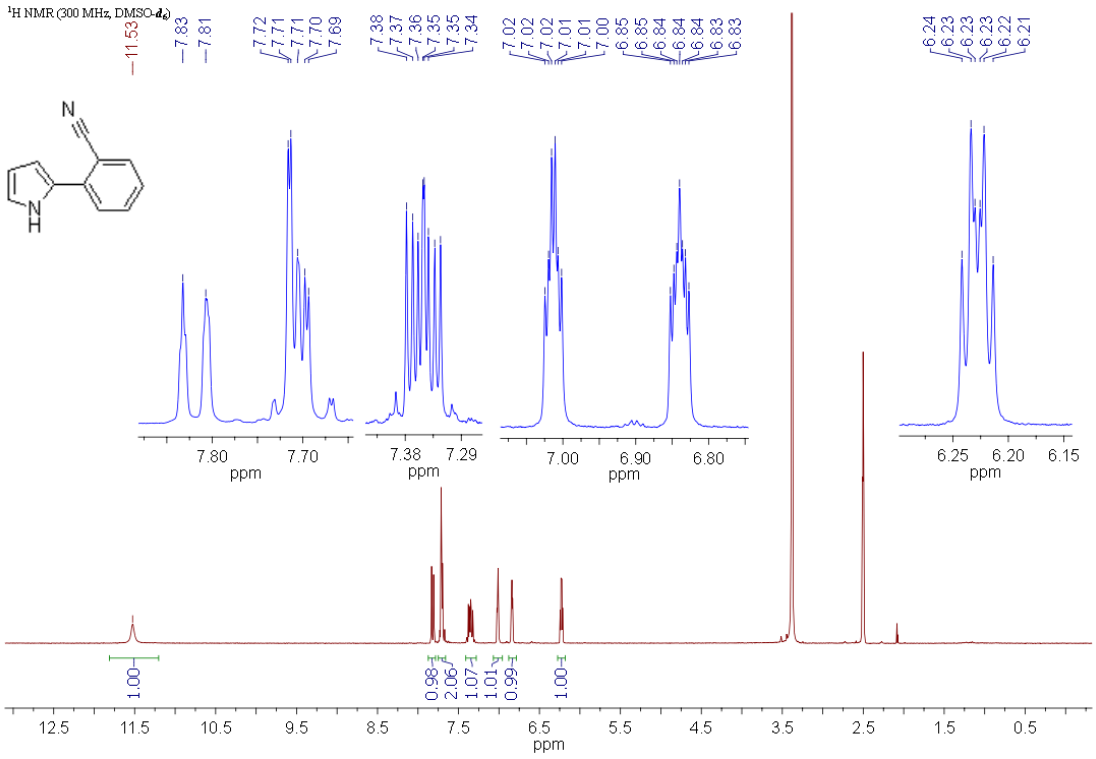

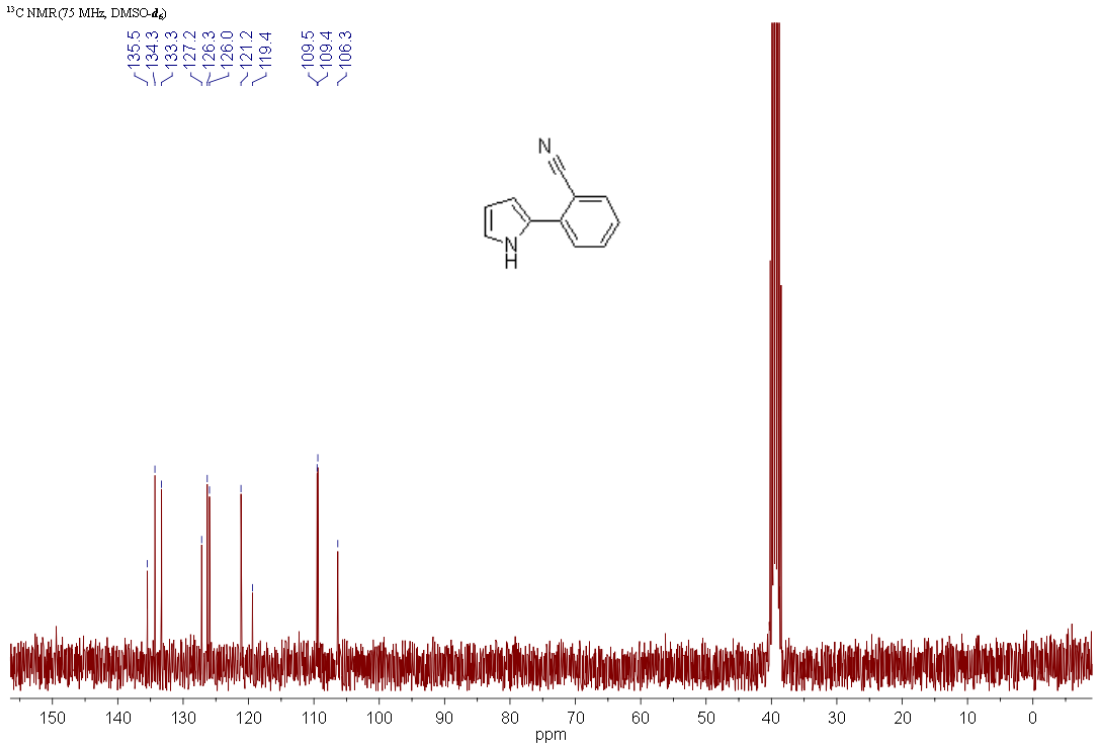

4-(1*H*-Pyrrol-2-yl)acetophenone

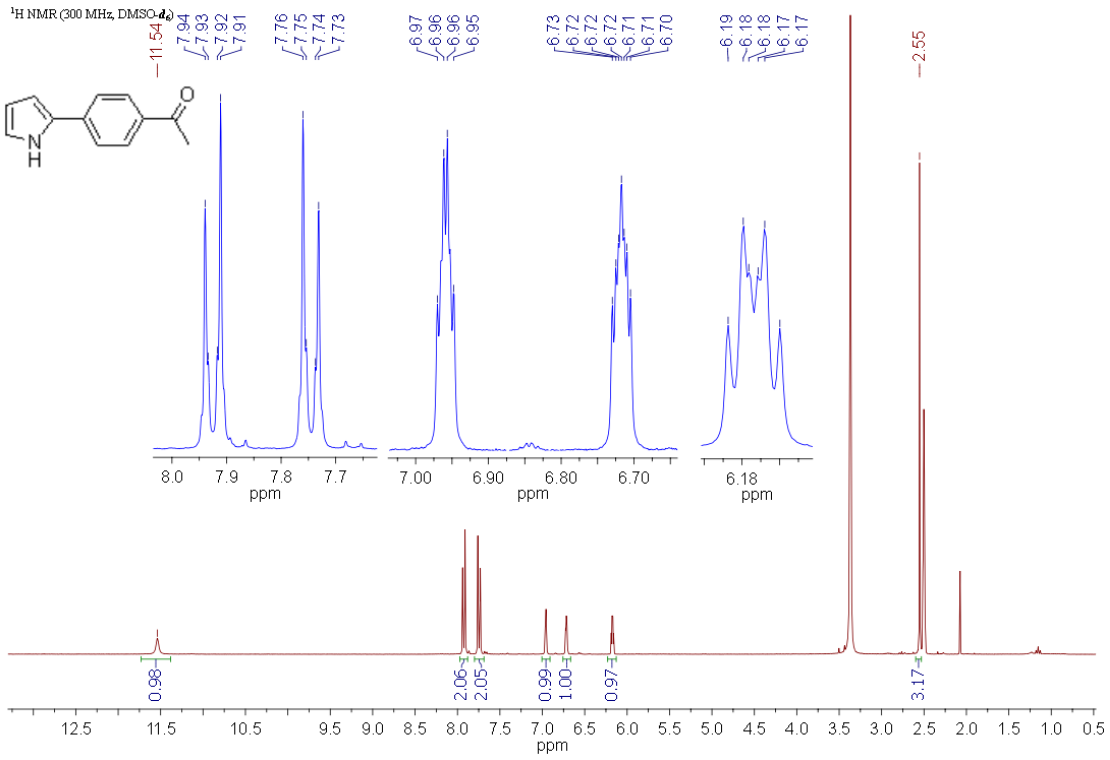

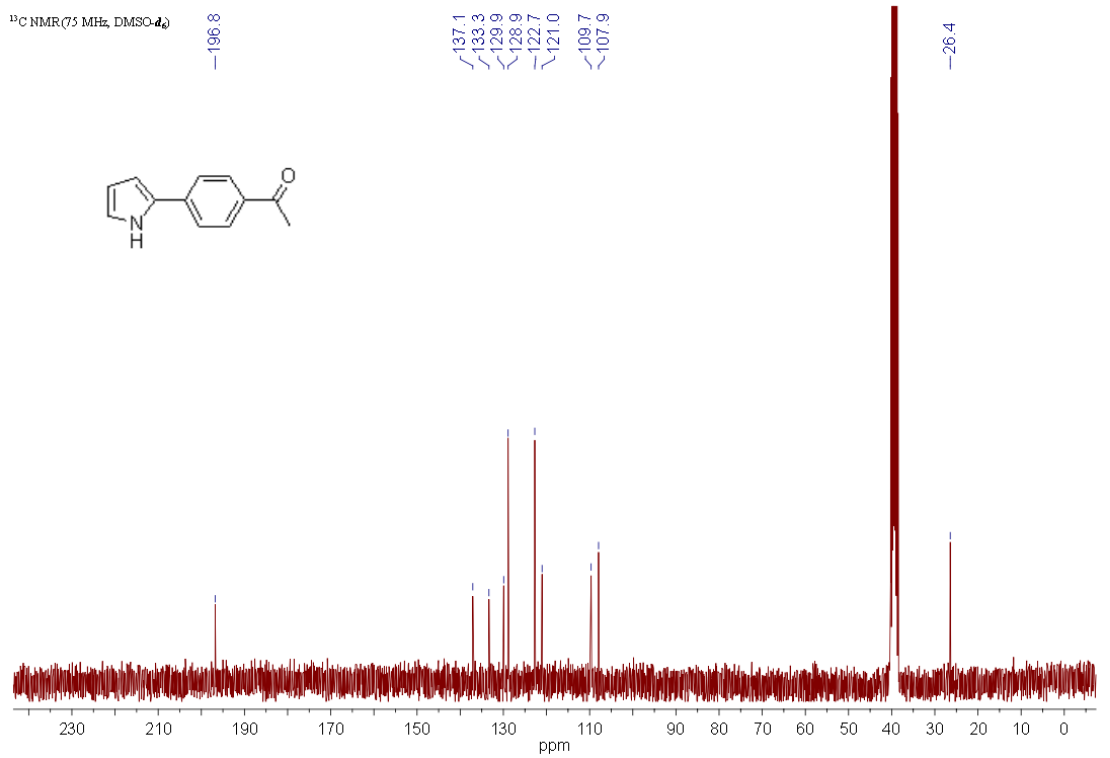

2-(3,5-Dimethyl-1*H*-pyrrol-2-yl)benzonitrile

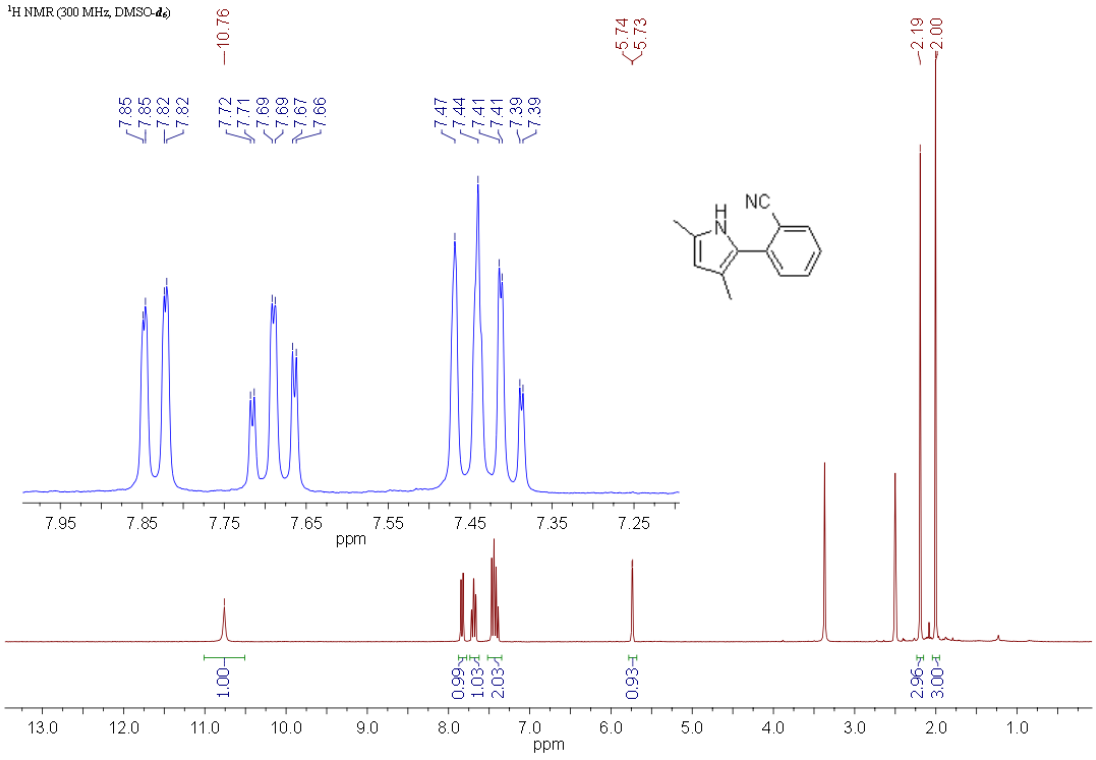

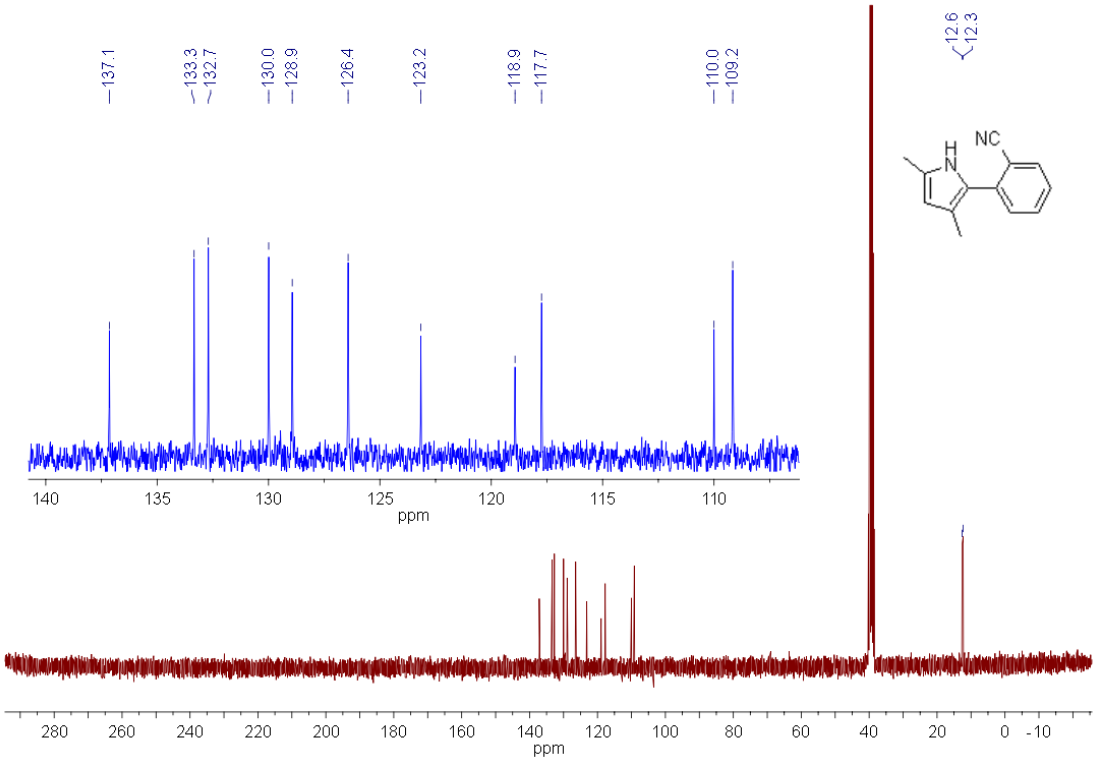

2-(4-Ethyl-3,5-dimethyl-1*H*-pyrrol-2-yl)benzonitrile

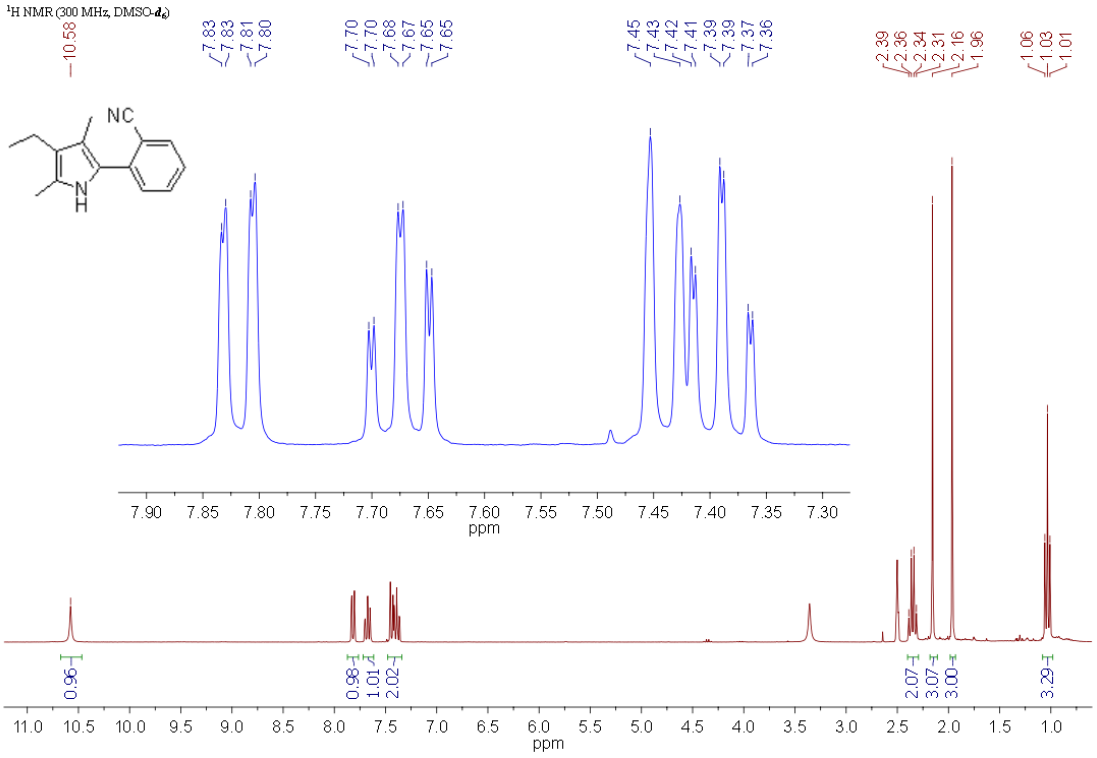

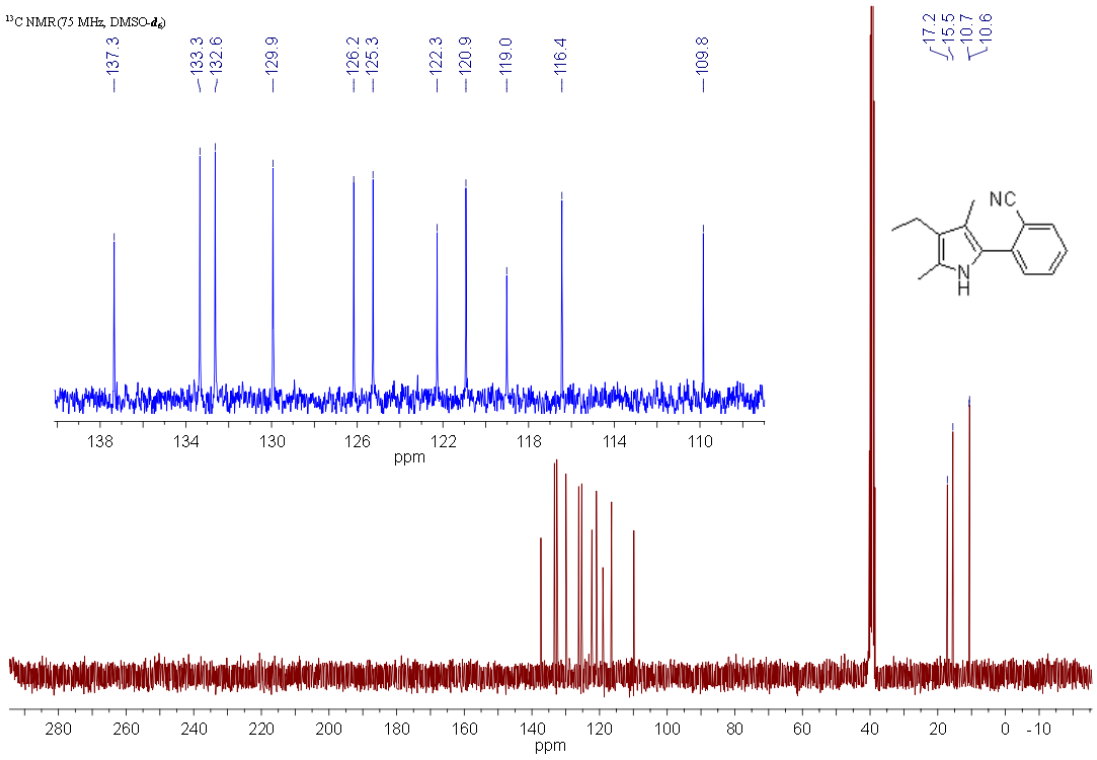

2-(1-Phenyl-1*H*-pyrrol-2-yl)benzonitrile

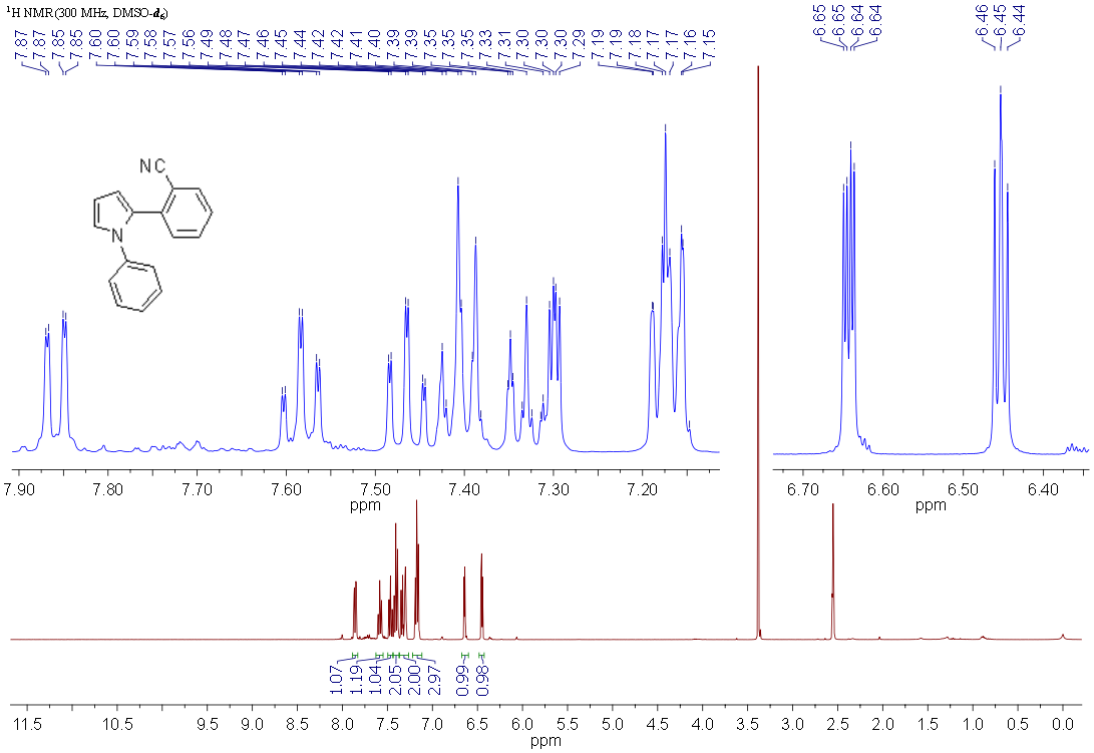

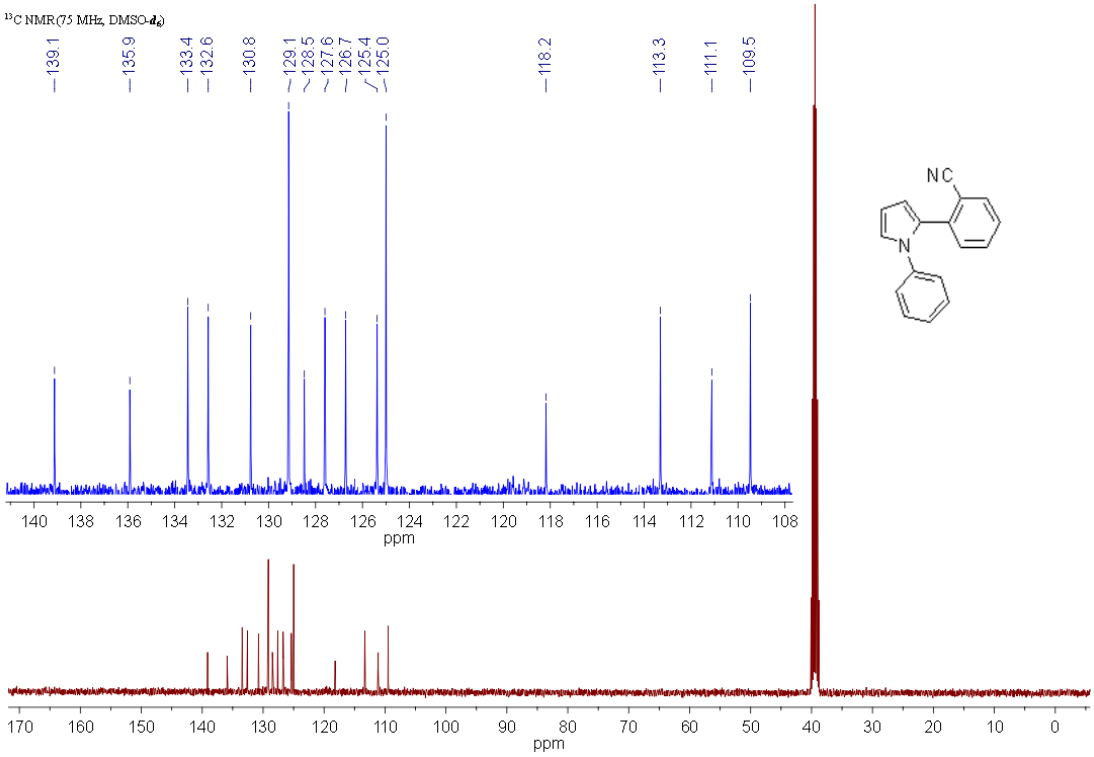

5,7-Dibromo-3-methyl-2,3-dihydrobenzofuran

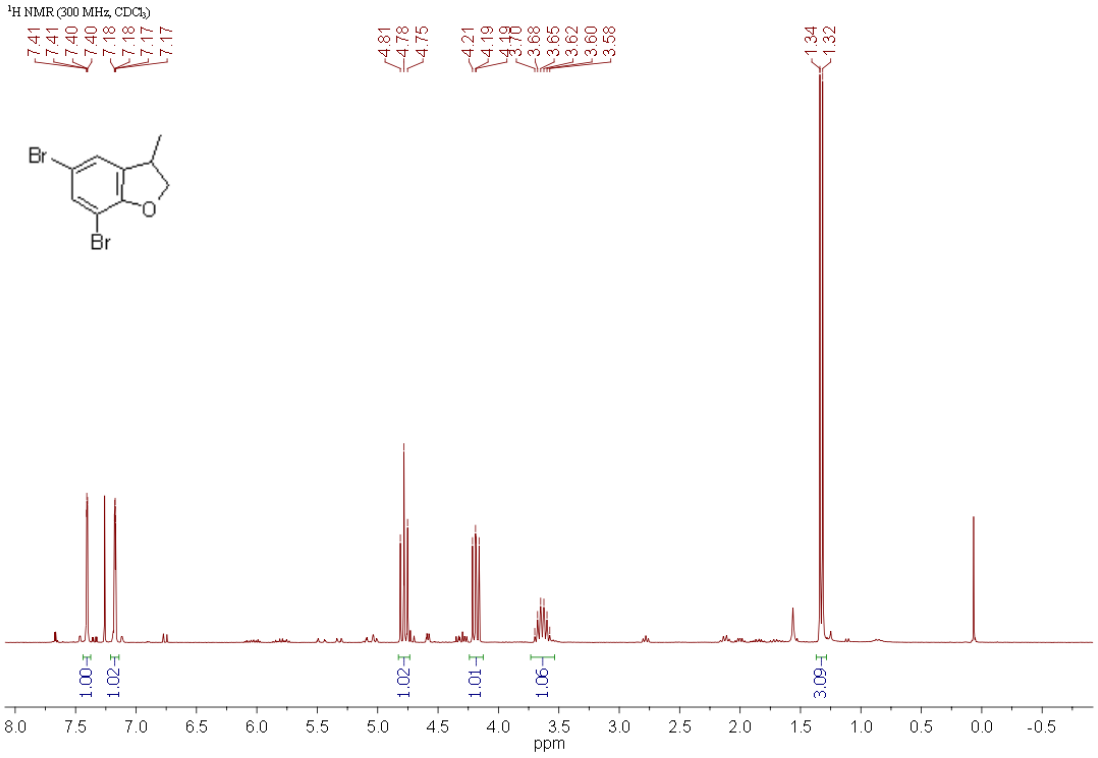

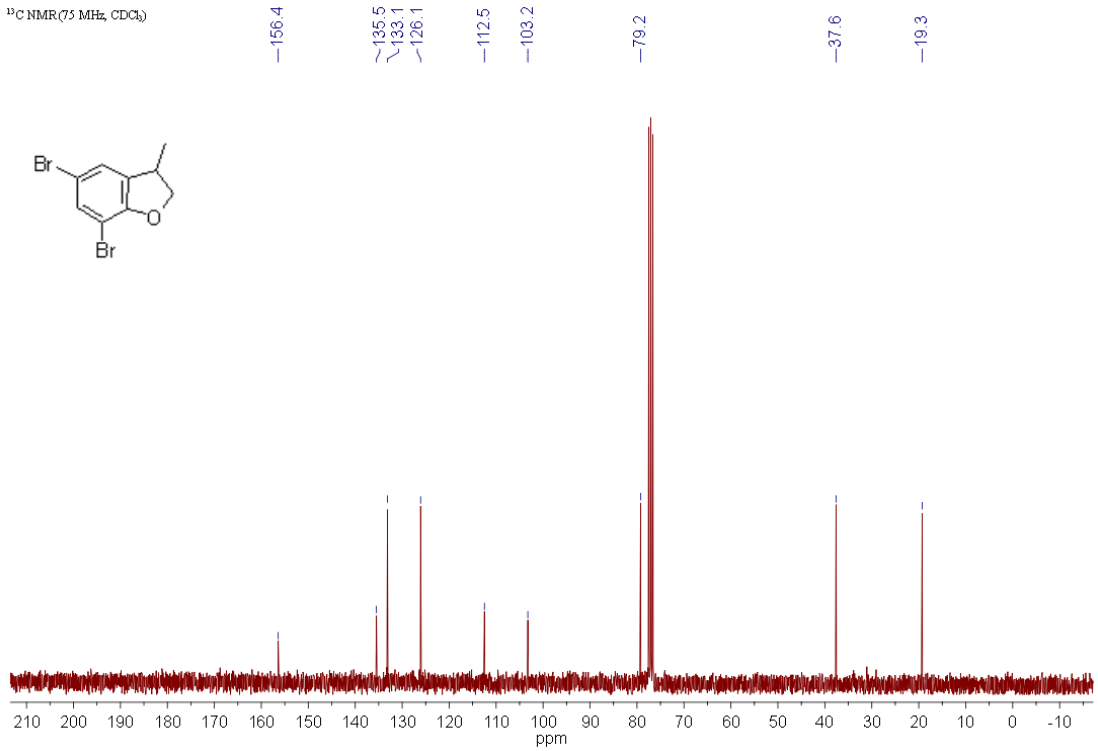

2.5 References and notes

[1] J. J. Concepcion, R. L. House, J. M. Papanikolas, T. J. Meyer, *Proc. Natl. Acad. Sci. U. S. A.* **2012**, *109*, 15560-15564.

[2] D. M. Schultz, T. P. Yoon, *Science* **2014**, *343*, 985-+.

[3] C. K. Prier, D. A. Rankic, D. W. C. MacMillan, *Chem. Rev.* **2013**, *113*, 5322-5363.

[4] J. Xuan, W. J. Xiao, *Angew. Chem. Int. Ed.* **2012**, *51*, 6828-6838.

[5] F. Teply, *Collect. Czech. Chem. Commun.* **2011**, *76*, 859-917.

[6] D. P. Hari, P. Schroll, B. König, *J. Am. Chem. Soc.* **2012**, *134*, 2958-2961.

[7] D. Ravelli, D. Dondi, M. Fagnoni, A. Albini, *Chem. Soc. Rev.* **2009**, *38*, 1999-2011.

[8] D. P. Hari, B. König, *Angew. Chem. Int. Ed.* **2013**, *52*, 4734-4743.

[9] J. D. Nguyen, E. M. D'Amato, J. M. R. Narayanam, C. R. J. Stephenson, *Nat. Chem.* **2012**, *4*, 854-859.

[10] D. P. Hari, T. Hering, B. König, *Angew. Chem. Int. Ed.* **2014**, *53*, 725-728.

[11] Y. X. Liu, D. Xue, J. D. Wang, C. J. Zhao, Q. Z. Zou, C. Wang, J. L. Xiao, *Synlett* **2013**, *24*, 507-513.

[12] H. Kim, C. Lee, *Angew. Chem. Int. Ed.* **2012**, *51*, 12303-12306.

[13] The excited state redox potential of fac-Ir(ppy)3 is estimated to be –1.73 vs SCE (see ref. 9). Some reports of metal complexes with even stronger reducing power in the excited state have been reported, but not applied to photoredox catalysis (see ref. 14).

[14] S. B. Harkins, J. C. Peters, *J. Am. Chem. Soc.* **2005**, *127*, 2030-2031.

[15] The Rehm Weller equation estimates the reduction potential of a photoredox catalyst in its excited state from the ground state redox potential and the $E_{0\text{-}0}$ transition energy (see ref. 28).

[16] For a recent example of two-step photoexcitation (Z-scheme) of heterogeneous semiconductor in water splitting see ref. 24.

[17] M. T. Pirnot, D. A. Rankic, D. B. C. Martin, D. W. C. MacMillan, *Science* **2013**, *339*, 1593-1596.

[18] L. Furst, B. S. Matsuura, J. M. R. Narayanam, J. W. Tucker, C. R. J. Stephenson, *Org. Lett.* **2010**, *12*, 3104-3107.

[19] J. M. R. Narayanam, J. W. Tucker, C. R. J. Stephenson, *J. Am. Chem. Soc.* **2009**, *131*, 8756-+.

[20] D. A. Nicewicz, D. W. C. MacMillan, *Science* **2008**, *322*, 77-80.

[21] E. Cahard, F. Schoenebeck, J. Garnier, S. P. Y. Cutulic, S. Z. Zhou, J. A. Murphy, *Angew. Chem. Int. Ed.* **2012**, *51*, 3673-3676.

[22] C. Costentin, M. Robert, J. M. Saveant, *J. Am. Chem. Soc.* **2004**, *126*, 16051-16057.

[23] L. Pause, M. Robert, J. M. Saveant, *J. Am. Chem. Soc.* **1999**, *121*, 7158-7159.

[24] Y. Sasaki, H. Kato, A. Kudo, *J. Am. Chem. Soc.* **2013**, *135*, 5441-5449.

[25] F. Wurthner, *Chem. Commun.* **2004**, 1564-1579.

[26] D. Gosztola, M. P. Niemczyk, W. Svec, A. S. Lukas, M. R. Wasielewski, *J. Phys. Chem. A* **2000**, *104*, 6545-6551.

[27] M. J. Tauber, R. F. Kelley, J. M. Giaimo, B. Rybtchinski, M. R. Wasielewski, *J. Am. Chem. Soc.* **2006**, *128*, 1782-1783.

[28] D. Rehm, A. Weller, *Isr. J. Chem.* **1970**, *8*, 259-271.

[29] C. Ramanan, A. L. Smeigh, J. E. Anthony, T. J. Marks, M. R. Wasielewski, *J. Am. Chem. Soc.* **2012**, *134*, 386-397.

[30] M. E. Buden, J. F. Guastavino, R. A. Rossi, *Org. Lett.* **2013**, *15*, 1174-1177.

[31] Y. N. Cheng, X. Y. Gu, P. X. Li, *Org. Lett.* **2013**, *15*, 2664-2667.

[32] R. A. Rossi, A. B. Pierini, A. B. Penenory, *Chem. Rev.* **2003**, *103*, 71-167.

[33] Z. Chami, M. Gareil, J. Pinson, J. M. Saveant, A. Thiebault, *J. Org. Chem.* **1991**, *56*, 586-595.

[34] M. Newcomb, in *Encyclopedia of Radicals in Chemistry, Biology and Materials* (Ed.: C. S. Chatgilialoglu, A.), John Wiley & Sons, Chichester, UK, **2012**.

[35] E. Shirman, A. Ustinov, N. Ben-Shitrit, H. Weissman, M. A. Iron, R. Cohen, B. Rybtchinski, *J. Phys. Chem. B* **2008**, *112*, 8855-8858.

[36] D. Bradley, G. Williams, M. Lawton, *J. Org. Chem.* **75**, 8351 (2010).

[37] D. T. Gryko, O. Vakuliuk, D. Gryko, B. Koszarna, *J. Org. Chem.* **74**, 9517 (2009).

[38] M. Aleskovic, N. Basaric, K. Mlinaric-Majerski, *J. Heterocycl. Chem.* **48**, 1329 (2011).

[39] G. Q. Li, S. Kiyomura, Y. Yamamoto, N. Miyaura, *Chem. Lett.* **40**, 702 (2011).

Chapter 3

3 Visible Light Photocatalytic Reduction of Aldehydes by Rh(III)–H: A Detailed Mechanistic Study

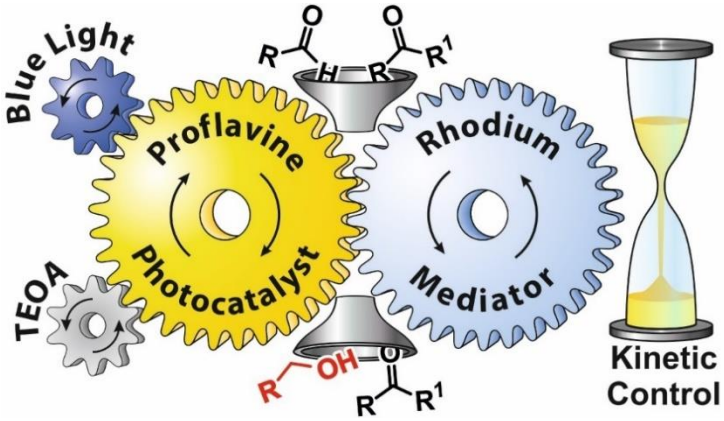

The chemoselective photoreduction of aldehydes in the presence of ketones was achieved using triethanolamine (TEOA) as sacrificial electron donor, proflavine (PF) as photocatalyst and [Cp*Rh(III)(bpy)Cl]Cl (Rh_{cat}) as mediator. The reducing agent, which reacts with the carbonyl group was found to be [Cp*Rh(III)(bpy)H]Cl (Rh(III)–H). Contrary to formate-based reduction, its slow photochemical *in situ* generation enables to kinetically distinguish aldehydes from ketones. The inherent reactivity difference of the carbonyl compounds is transferred by the method into synthetically useful reaction selectivities. The substrate scope is broad with excellent yields. A detailed study of the reaction mechanism reveals that the photoreduction of PF triplet and the subsequent reduction of Rh_{cat} leading to Rh(III)–H represents the major reaction pathway, which is highly oxygen sensitive. The oxidative quenching of the PF singlet state by Rh_{cat} is an alternative mechanism, which prevails in non-degassed systems.

This chapter has been published:
T. Ghosh, T. Slanina, B. König, *Chem. Sci.* **2015**, *6*, 2027-2034.

TG performed the GC calibrations, optimization of reaction conditions and the batch reactions. TS performed the flow reactions and all the mechanistic studies. TG and TS wrote the manuscript. BK supervised the project and is corresponding author.

3.1 Introduction

Aldehydes and ketones are similar in reactivity. The development of methods for the chemoselective reduction of aldehydes in the presence of ketones has therefore received considerable attention.[1-2] Employing $NaBH_4$ as reduction reagent, selectivity can be achieved only at very low temperatures (–78 °C)[3-4] or by using additives such as thiols,[5] metal salts,[6] resins,[7] PEG[8] or Na_2CO_3 in water.[9] Various modified borohydrides are known to allow chemoselective reduction of aldehydes in the presence of ketones. For example, tetraalkylammonium borohydride can reduce aldehydes in the presence of ketones to its corresponding alcohol, but with only low selectivity.[10] $Na(AcO)_3BH$[11] and *n*-$Bu_4N(AcO)_3BH$[12] were used to reduce aldehydes in the presence of ketones with a high selectivity, but rather harsh reduction conditions, such as reflux in benzene, are required. In recent past, chemists started to modify borohydrides[13] with sterically hindered substituents and different electron-withdrawing groups, which are then able to distinguish between the carbonyl groups of aldehydes and ketones. Most of these modified borohydrides require special reagents and methods to prepare. Moreover, in all these hydride reductions the reducing agent was used stoichiometrically. In 2006 Casey *et al.* introduced the catalytic chemoselective hydrogenation of aldehydes over ketones in non-polar solvent at elevated temperature, which was demonstrated with only one example: the reduction of benzaldehyde in the presence of acetophenone.[14] In 2012 McCulla *et al.* reported[15] photochemical chemoselectivity of aryl aldehydes in the presence of alkyl aldehydes and aryl ketones. They used a polymeric heterogeneous photocatalyst with a tail absorption (400–440 nm) in the visible part of the spectrum. However, by this method they were able to achieve only low conversion of starting materials with low overall yields of the corresponding alcohols for both neutral and electron rich aldehydes. Moreover, they often found benzoin condensation as a side reaction.

Herein, we report the chemoselective visible light induced photocatalytic hydride reduction of aldehydes in the presence of ketones. Our photocatalytic system offers, in comparison to previously published methods, a robust selectivity, which can differentiate aldehydes from ketones over a broad reactivity range. Park and Nam have introduced[16] a photocatalytic system using PF (3,6-diaminoacridine) as photocatalyst and Rh_{cat} as a mediator for the regeneration of NADH from NAD^+ produced by enzymatic synthesis of L-glutamate demonstrating an artificial photosynthetic approach. We modified the system

for synthetic purposes. The schematic mechanism is shown in Figure 1, upper part. PF is a well-known acridine dye studied in detail for its ability to bind with DNA.[17] It has also been used as a promising molecule for the photogeneration of hydrogen.[18] Rh_{cat} has been first described by Youinou and Ziessel in 1989.[19] Since then it has frequently been used as a hydride transferring agent for cofactor regeneration.[20] Unlike other hydrides, it exhibits an outstanding regioselectivity in the reduction of NAD^+.[21] It has also been used for the chemical reduction of both aldehydes and ketones by hydride transfer from formic acid.[22-23] We photochemically generate the same hydride reducing agent, Rh(III)–H as in the formate-based reduction. However, due to its slow *in situ* generation, we maintain a low concentration of Rh(III)–H in the reaction medium, which then kinetically distinguishes between aldehydes and ketones with a high selectivity (Figure 1, bottom).

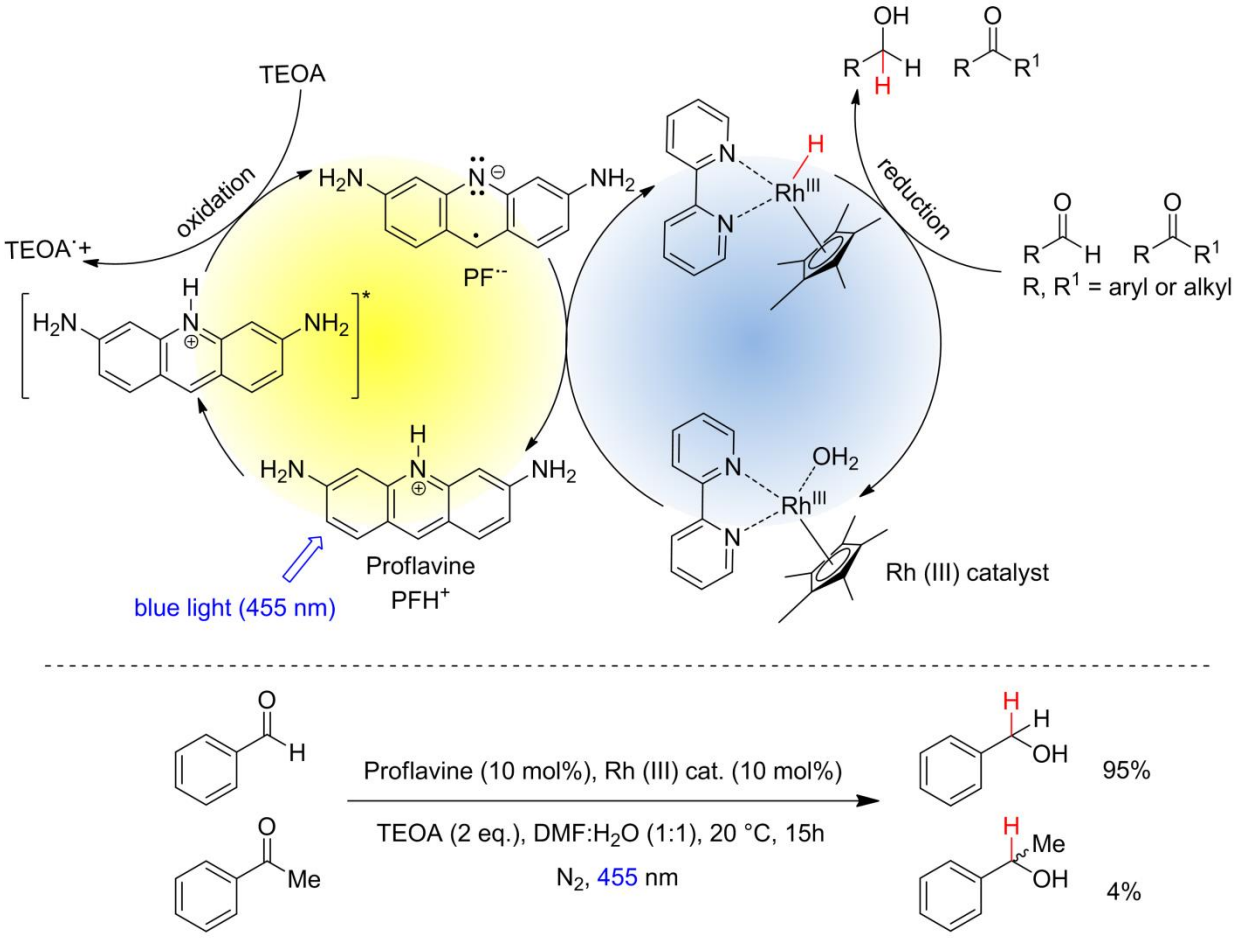

Figure 1: Top: Schematic representation of the photocatalytic cycle with mediator cycle involving PF as photocatalyst and [Cp*Rh(III)(bpy)Cl]Cl as mediator. Bottom: High chemoselectivity for benzaldehyde in the presence of acetophenone.

3.2 Results and discussion

3.2.1 Synthetic investigations

The reaction conditions were optimized using benzaldehyde as a substrate. The selected results are summarized in the Table 1. The yields were determined by GC/FID after 15 hours of irradiation at 455 nm. The reactions in anhydrous organic solvent (Table 1, entries 1,2) did not yield a significant amount of product as water is required as a proton source for generation of Rh(III)–H.[24] Both aqueous acetonitrile and DMF gave good yields and DMF/H_2O (1:1, v/v) was chosen for further studies as the aliphatic substrates dissolve better in the reaction medium. The yields of benzyl alcohol were highest in case of 10 mol % of both PF and Rh_{cat} (Table 1, entry 5). Using 5 mol % of both PF and Rh_{cat} we obtained a similar result for the benzaldehyde reduction (Table 1, entry 9), but we increased the catalysts loading to 10 mol % to accelerate the reduction rate of aliphatic substrates.

Table 1: Optimization of reaction conditions

Entry	Proflavine (mol%)	Rh_{cat} (mol%)	TEOA (eq.)	Solvent	Yield after 15 h (%)*
Optimization of reaction conditions					
1	10	10	2	Dry MeCN	<1
2	10	10	2	Dry DMF	7
3	10	10	2	DMF/H_2O (1:2)	83
4	10	10	2	DMF/H_2O (2:1)	61
5	**10**	**10**	**2**	**DMF/H_2O (1:1)**	**97**
6	10	10	2	MeCN/H_2O (1:1)	80
7	5	10	2	DMF/H_2O (1:1)	86
8	10	5	2	DMF/H_2O (1:1)	73
9	5	5	2	DMF/H_2O (1:1)	95
10	10	10	1	DMF/H_2O (1:1)	35
11	10	10	3	DMF/H_2O (1:1)	81

*****GC/FID determined yield of benzyl alcohol with appropriate internal standard.

To investigate the role of each component of the photocatalytic system we performed a series of control experiments. The results are summarized in Table 3. The data clearly show that each component is essential for the reaction progress. The reaction without degassing (Table 3, entry 6) yields about 30 % of the product. This has been further studied and will be discussed in the mechanistic part. Reactions in hydrogen atmosphere did not yield any product (Table 3, entries 7, 8) from which it is evident that no direct hydrogenation occurs. Various aromatic and aliphatic aldehydes and ketones were tested as substrates in our catalytic system (Table 2). For all substrates the optimized reaction conditions were used (Table 2, entry 5). The reaction rate could be accelerated by a factor of 5, without affecting the selectivity (Table 2, entries 1–3) using a flow reactor, which delivers the incident light more efficiently to the whole volume of the reaction mixture. Excellent yields were obtained for neutral, electron rich and electron poor aldehydes, whereas the corresponding ketones remained unreacted. Using an activated ketone as one reactant, we performed the reduction reactions varying the other reactant from electron-poor to electron-neutral to electron-rich aldehyde with notable selectivity (Table 2, entry 8-10). The selectivity was observed not only for a mixture of aldehyde and ketone, but also for a bifunctional molecule (Table 2, entry 11). Somewhat lower yield in entry 11 is caused by a side reaction leading to a pinacol-type product (detected by HPLC-MS, see Figure 50). In entry 12 a lower yield was obtained, because of decomposition of the substrate, which is not related to the photoreaction.

Table 2: Substrate scope

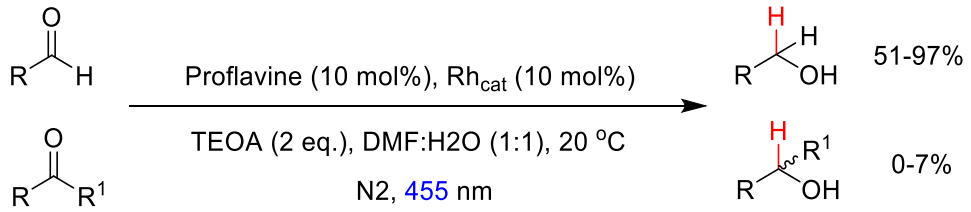

Entry	Substrate(s)	Reaction type	Time (h)	Yield(s)
1	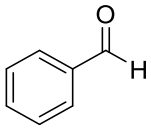	batch	15	97
		flow	3.5	91
2	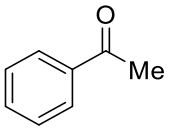	batch	15	7
		flow	3.5	4
3	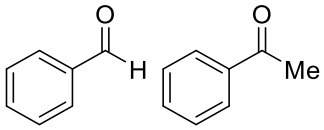	batch	15	95 (4)*
		flow	3.5	82 (<1)*
4	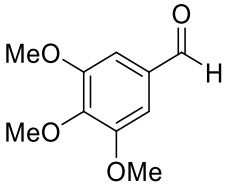	batch	25	95
5	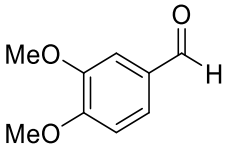	batch	25	83
6	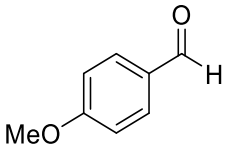	batch	32	84
7	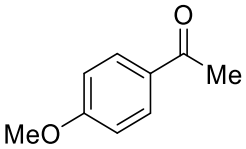	batch	32	3
8	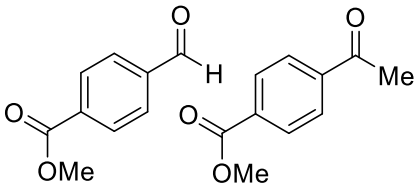	batch	18	76 (2)*

9	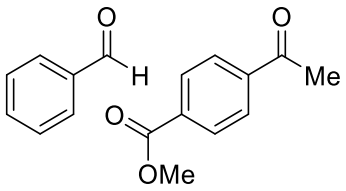	batch	16	91 (2)*
10	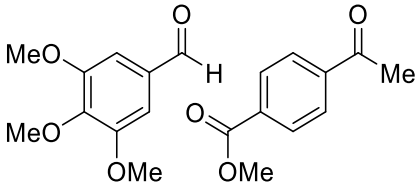	batch	25	93 (4)*
11	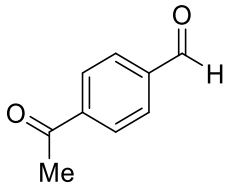	batch	16	51 (<1)**
12	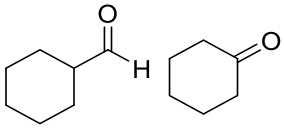	batch	42	56 (3)*

( )*Yields of ketone reductions; ( )**Yield of doubly reduced product.

The rate of reduction is partially dependent on the electron density of the aldehyde functionality. That indicates that the hydride transfer from Rh(III)–H to the carbonyl compound is the rate-determining step. The correlation of reaction yields, reduction potentials and Hammett's sigma values is shown in Figure 14. Generally, the photoreduction is slower for electron-rich aldehydes, but no clear trend was observed. Ketones are almost unreacted, which is mainly caused by steric effects. Rh_{cat} is sufficiently crowded to create selectivity even between similar substrates, which was demonstrated on various NAD^+ model compounds.[21]

The catalytic system also reduces imines (see Table 5). Dry DMSO was found to be the most suitable solvent and the addition of thiourea (1 eq.) accelerated the reaction significantly by hydrogen bond activation of the imine.[25]

The reaction selectivity was compared with known systems. Rh_{cat} has been recently used for chemical reductions of both aldehydes and ketones.[22-23] The selectivity is reported only marginally.[22] The reactions were accomplished in biphasic conditions without any phase transfer catalyst. The reduction was fast even with low catalyst loadings (~0.5 mol%). We therefore examined the selectivity of Rh(III)–H generated chemically using formate

aqueous buffer as a hydride source. The results are shown in Table 4). After 15 minutes the benzaldehyde is efficiently reduced, whereas the conversion of acetophenone is only 32 %. Contrary to the formate-based system our photocatalytic reduction is slower and the reaction can be easily stopped after the aldehyde is reduced and the ketone is almost intact. The aldehyde-ketone selectivity depends on the reaction conversion and therefore the ratio of reduction products is influenced by the reaction time. The kinetic of the reaction is described in more detail in the experimental section (Scheme 3, Figure 18).

3.2.2 Mechanistic investigations

The photophysical properties of PF have been studied in detail. In solution the dye is prone to dimerization (K_D = 500 M^{-1}) and its molar absorptivity is concentration dependent from $c \sim 10^{-4}$ M.[26] At physiological pH, PF is protonated at the central nitrogen atom *N*–10; PFH^+ (pK_a = 9.5)[27]. PFH^+ absorbs at 443 nm and has a strong fluorescence (λ_{fl} = 0.39, λ_{em} = 508 nm)[28] whereas the neutral form (PF) absorbs at 393 nm and exhibits no fluorescence[a] (see Figures 19 and 22). PFH^+ has interesting emission properties. It exhibits strong prompt fluorescence from the singlet state, $^1[PFH^+]^*$ (Figure 51), thermally dependent delayed E-type fluorescence (fl^E) originating from thermal repopulation of $^1[PFH^+]^*$ from $^3[PFH^+]^*$, concentration dependent delayed P-type fluorescence (fl^P) caused by triplet-triplet annihilation with energy transfer,[b] and light intensity dependent photoionization recombination delayed fluorescence (fl^{PIR}) which occurs after recombination of ion pair $[PFH^{\bullet}]^{2+}\cdots e^-$(solv) created by photoionization from $^1[PFH^+]^*$.[29] Phosphorescence from the triplet state is the most significant emission with maximum intensity at 570 nm till 197 K and is negligible above 253 K.[29]

Photoinduced electron transfer (PET) occurs between $^3[PFH^+]^*$ and an appropriate electron donor. The redox potential of $^3[PFH^+]^*$ can be estimated using the Rehm-Weller equation from the measured ground state redox potential (E_0 = –0.74 V vs SCE, Figure 12) and its triplet energy ($\lambda_{phosph.}$ = 570 nm ~ 2.17 eV) resulting in +1.44 V vs SCE.[c] Electron-rich compounds like amines can serve as electron donors for PET. TEOA (E_0 = +0.76 V vs

[a] PF is weakly fluorescent till pH = 11.5 which corresponds to the pK_a of the singlet excited state. Kalyanasundaram, K.; Dung, D. *J. Phys. Chem.* **1980**, *84*, 2551.
[b] $^3[PFH^+]^* + {}^3[PFH^+]^* \rightarrow {}^1[PFH^+]^* + {}^1[PFH^+]$
[c] This value corresponds well with the published potential (+1.36 V). Pileni, M. P.; Gratzel, M. *J. Phys. Chem.* **1980**, *84*, 2402.

SCE[d])[30] is easily[e] oxidized by $^3[PFH^+]^*$ creating $TEOA^{\cdot+}$ and a singly reduced proflavine radical ($PFH^{\cdot}$). The back electron transfer does not occur due to the fast deprotonation of $TEOA^{\cdot+}$.[31]

Interaction of PF with TEOA in aqueous media has been studied by measuring its fluorescence. Titration of PF solution (aq., $c = 5.0 \times 10^{-6}$ M) with TEOA or TEA resulted in a decrease in fluorescence intensity as observed by *Basu* et al.[32] This would indicate that TEOA is quenching the singlet excited state by PET and would be in contradiction with the well-established PET from PF triplet.[31] The UV spectra (Figure 21) indicate the formation of a new species with an absorption peak at 393 nm, which corresponds to PF formed by a simple acidobasic equilibrium, which is also supported by the UV pH titration (Figure 19) and fluorescence pH titration (Figure 2, upper part). The distribution of the respective acidobasic forms calculated from both pH and TEOA titration corresponds to each other (Figure 26). We did not observe the formation of $PFH^+\cdots$TEA ground-state complex as proposed by Basu *et al.*[32]

[d] E_0 = +0.80V vs Ag/AgCl

[e] $\Delta G° = -e \times (-0.76\text{ V} + 1.44\text{ V}) - 0.08\text{ eV} = -0.76\text{ eV} \sim -73.3\text{ kJ mol}^{-1}$, according to *J. Am. Chem. Soc.* **1999**, *121*, 1681–1687

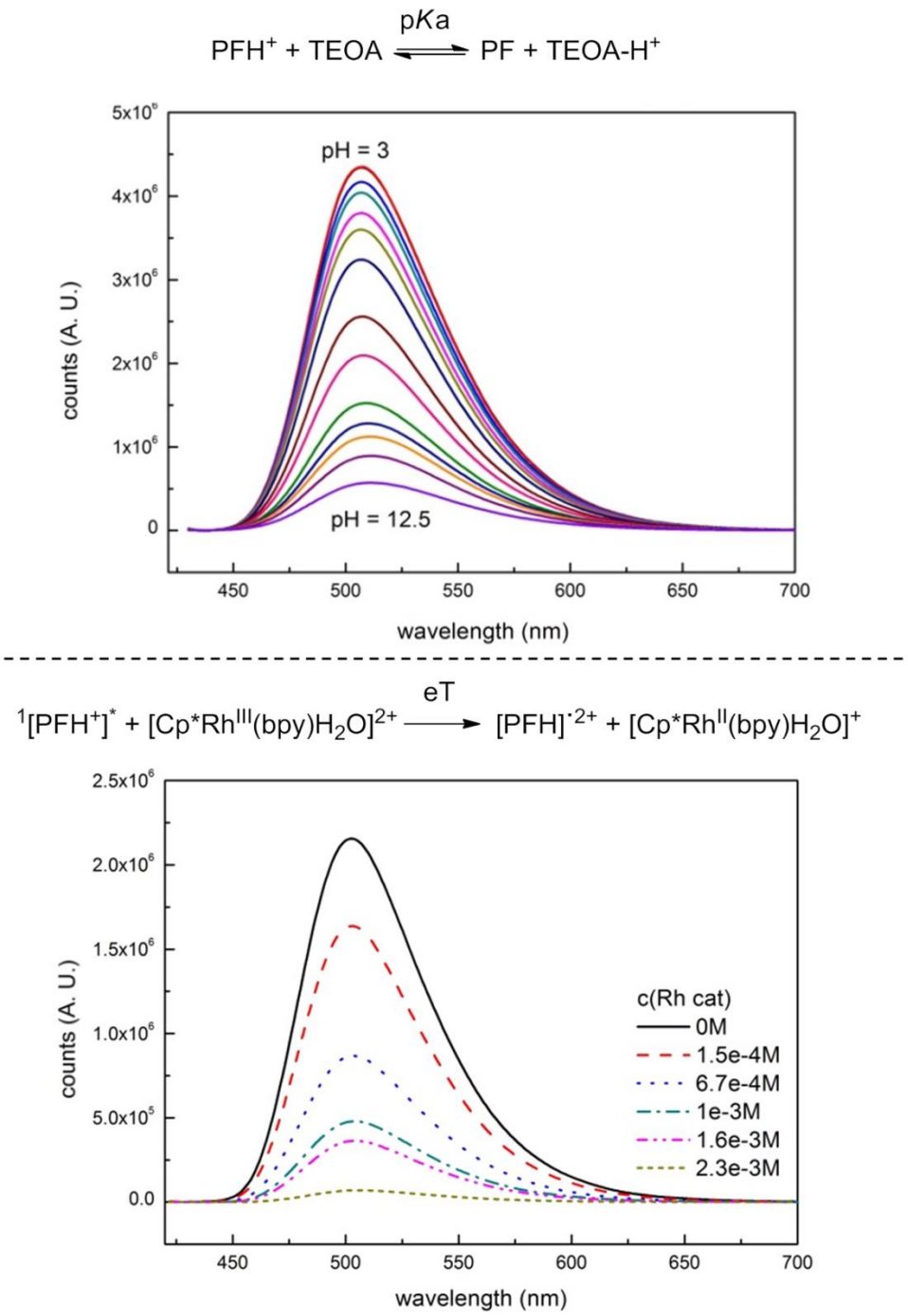

Figure 2: Fluorescence quenching of PF with TEOA (upper part) and Rh_{cat} (lower part).

Fluorescence quenching of PF with Rh_{cat} is shown in Figure 2, lower part. Unlike TEOA, the Rh catalyst does not interact with PF in the ground state. Fluorescence was quenched at relatively high concentrations.[f] The quenching constant was dependent on the excitation beam intensity. This indicates that Rh_{cat} is quenched by photoionized electrons, which are originally responsible for the photoionization recombination delayed fluorescence (fl^{PIR}).

[f] 300 eq. of Rh catalyst vs. PFH^+, Stern-Volmer quenching constant is (2260 ± 30) M^{-1}

The contribution of the photoionization recombination delayed fluorescence to the overall emission was determined by measuring the dependence of the relative fluorescence yield on the intensity of excitation light. The light intensity was kept below the saturation limit so that all of the excitation light was absorbed by the sample. Increasing intensity of the excitation light leads to a non-linear increase of the fluorescence intensity, which corresponds to the fl^{PIR} (Figure 28).

The properties of rhodium mediator were studied in detail. Rh_{cat} is a water-soluble air-stable d^6 metal complex, which undergoes a ligand exchange after its dissolution in water. The catalytic active form $[Cp^*Rh(III)(bpy)(H_2O)]Cl_2$ has its maximum absorption at 355 nm and a tail absorption in the visible region (λ_{tail} ~ 420 nm, Figure 31). Its absorption in the blue region (λ = 455 nm) is weak[g] and it does not interfere with PFH^+. The reducing species has been described as a metal hydride complex, Rh(III)–H. It was confirmed as a key intermediate in the formate-based reductive catalytic system generated by direct hydride transfer from $HCOO^-$.[33] It has also been proposed as a reducing agent in photocatalytic systems coupled with various dyes.[16]34-35] To identify Rh(III)–H in our reduction system we prepared Rh(III)–H independently from the reaction with formate ions. After dissolution of Rh_{cat} in formate buffer (2M; pH = 3.5) bubbles of CO_2 and H_2 were generated vigorously. The yellow solution turned blue and could be slowly re-oxidized back by O_2. A new absorption peak at 612 nm is observed (Figure 31) corresponding to the previously published spectra of Rh(III)–H (Figure 3). Due to the vigorous gas evolution we were not able to measure the NMR spectrum for structural characterization. EPR analysis showed that the hydride complex is diamagnetic, which corresponds to the previous findings. In the UV–vis spectrum of the typical reaction mixture without substrate (Figure 1) irradiated for 15 hours with 455 nm LED the shoulder at 612 nm corresponding to the Rh(III)–H was observed. After purging with air the peak vanished and the spectrum changed to the initial state before irradiation (Figure 3). This is a clear evidence for the presence of Rh(III)–H in the reaction mixture.

[g] measured molar absorptivities are: $\varepsilon^{455}(PFH^+) = 28600$; $\varepsilon^{455}(Rh^{III}cat) = 120$

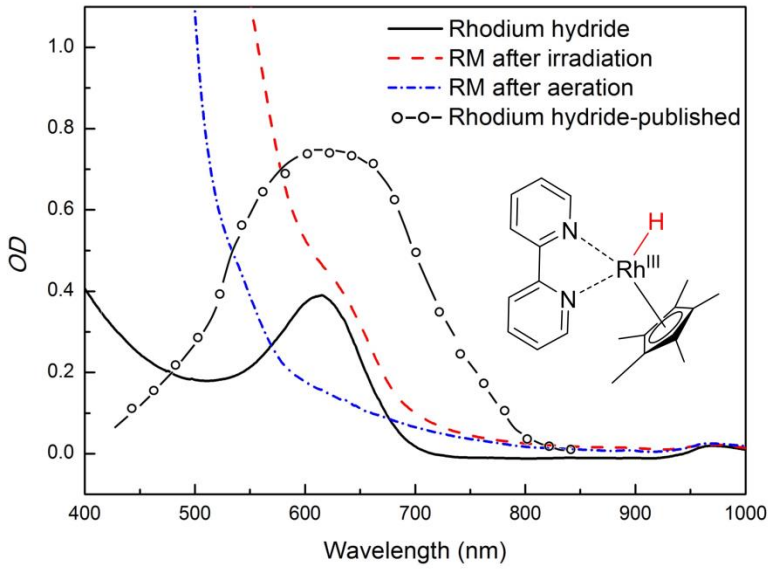

Figure 3: Spectroscopic evidence of presence of Rh(III)–H in the photocatalytic system (left side). Spectra of a typical reaction mixture after irradiation (dashed red line), after bubbling with air (dash – dotted blue line), of a prepared Rh(III)–H standard (solid black line), and a published[24] spectrum (open circles + dashed line; redrawn from the original) are shown.

Rh(III)–H is known to produce dihydrogen upon its protonation by the solvent.[24] We therefore examined if the hydrogen is produced in the catalytic system. We measured the composition of the gas phase above the typical reaction mixture after 15 hours of irradiation by head-space GC. Dihydrogen was present together with nitrogen used for degassing (Figure 15). We also examined if the presence of H_2 in the reaction mixture could be responsible for the course of the reaction. The typical reaction mixture without TEOA was purged with oxygen-free H_2 (Table 3, entries 7, 8) and was irradiated for 15 hr. No product formation was observed, which indicates that the decomposition of Rh(III)–H is an irreversible process and that carbonyls cannot be reduced by dihydrogen itself in the presence of the Rh catalyst.

To have a better insight into the mechanism we measured the kinetics of the evolution of H_2 using benzaldehyde or acetophenone as a substrate (benzaldehyde is being reduced by Rh(III)–H efficiently whereas acetophenone is not). The result is shown in Figure 16. In the photo-reduction of benzaldehyde the amount of H_2 produced is lower (approx. by the factor of 2) than when acetophenone is used. In the first case a fraction of Rh(III)–H (ca.

50%) is consumed for the reduction and the rest is decomposed by protonation.[h] In the case of the ketone, where no reduction was observed, the Rh(III)–H is solely decomposed to dihydrogen[i] This behavior corresponds to the side reaction kinetics shown in the Figure 18.

Based on the literature data and our experimental results we suggest the mechanism of the rhodium catalytic cycle depicted in the Figure 4. The aqueous solution of Rh_{cat} contains $[Cp^*Rh^{III}(bpy)H_2O]Cl_2$, formed after the ligand exchange of Cl^- to H_2O. This process is important for the catalytic activity making the central metal ion more accessible.[36] In the next step, the rhodium aqua-complex is reduced. In principle, two different mechanisms are possible: The one electron reduction[24] or a hydride transfer from a suitable hydrogen donor (*e.g.* $HCOO^-$)[36] have both been described in detail. The first mechanism applies for $PF^{\bullet -}$ generated by PET from $^3[PFH^+]^*$ and TEOA and subsequent deprotonation[j] (for pK_a values of PF species in various oxidation and excitation states see Figure 51). The deprotonation of PFH· to $PF^{\bullet -}$ is further proved by CV and spectroelectrochemistry (Figures 12 and 13). From the rate constants of dimerization and disproportionation[37] of $PF^{\bullet -}$ we can estimate the rate constant for electron transfer ($k_{red} \sim 5 \times 10^9$ s^{-1} M^{-1}, Figure 52). The photoreduction with solvated electrons generated by photo-ionization of PF occurs at a rate close to the diffusion limit.[37] The d^7 complex $[Cp^*Rh^{II}(bpy)H_2O]^+$ created after the one electron reduction is not stable and disproportionates fast ($k_{disp} = 3.7 \times 10^8$ s^{-1} M^{-1})[33] to a rhodium(I) complex. This d^8 complex, $[Cp^*Rh^{I}(bpy)]$, is then protonated[k] by a protic solvent to give Rh(III)–H. In case of a possible direct hydride transfer between $[Cp^*Rh^{III}(bpy)H_2O]Cl_2$ and PFH_2, Rh(III)–H is formed directly.

Rh(III)–H can either reduce the corresponding carbonyl (productive reaction) or can be protonated again to produce dihydrogen regenerating the catalyst.[l] In case of the hydride reduction the carbonyl group is reduced to an alkoxy ligand, which is easily hydrolyzed[22] giving the respective alcohol.

[h] These side reactions have similar rate constants.
[i] The ketone reduction does not efficiently compete with the decomposition.
[j] pK_a(PFH·) = 4.5; *J. Chem. Soc. Chem. Comm*. **1979**, 1137 - 1138
[k] $k_{prot} = 1.6 \times 10^6$ s^{-1} M^{-1}; Kölle, U.; Grätzel, M. *Angew. Chem.* **1987**, *99*, 572.
[l] Protonation: $k_{dec} = 1.8 \times 10^3$ s^{-1} M^{-1}; *Angew. Chem.* **1987**, *99*, 572; reduction: $k_{red} \sim 2 \times 10^3$ s^{-1} M^{-1}

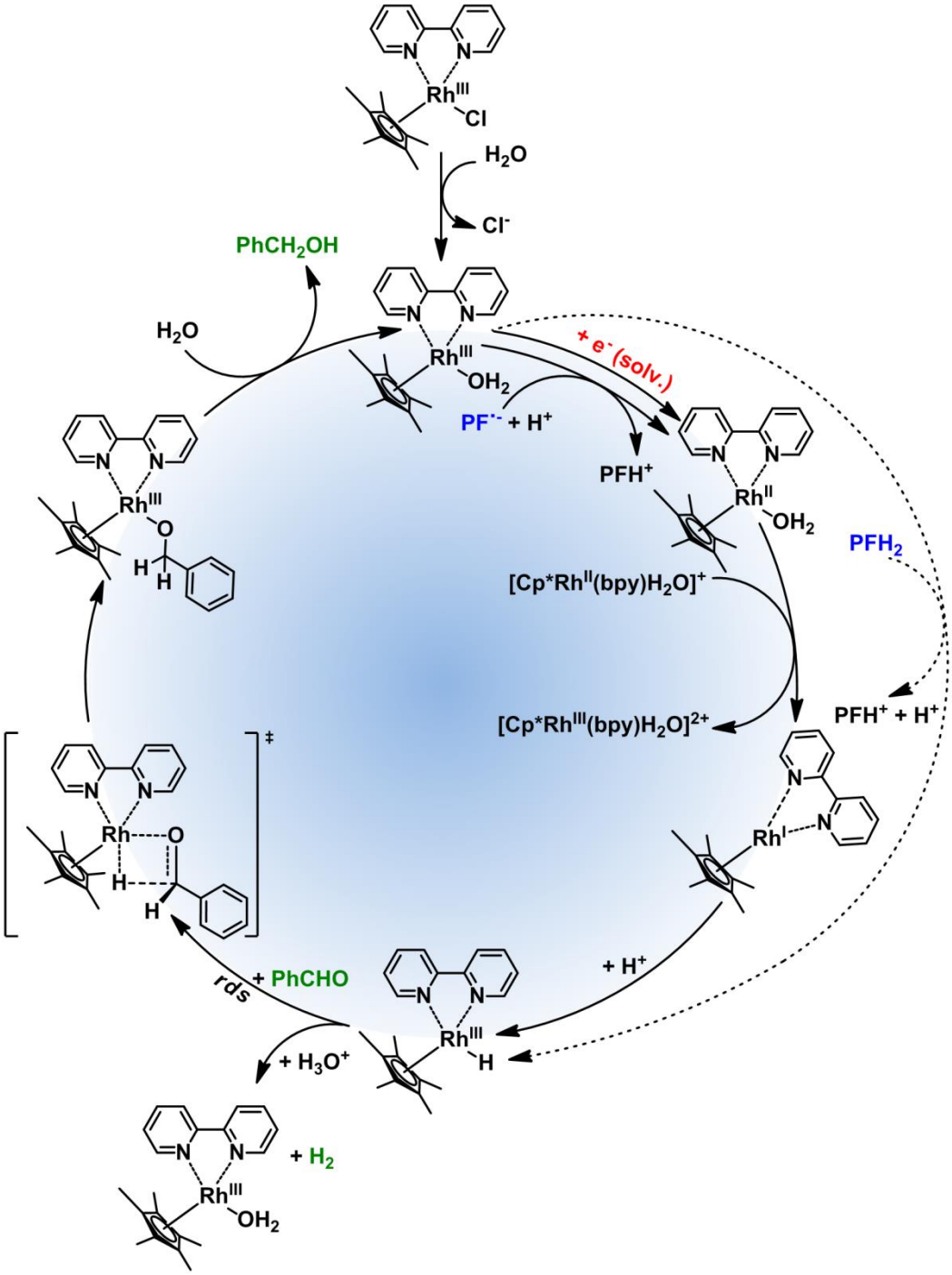

Figure 4: Proposed rhodium catalytic cycle, rds = rate determining step.

To investigate the fate of PF in the solution we examined the photoproducts formed from PF. The irradiation of degassed solutions of PF (c = 6.67 mmol) and TEOA (c = 133 mmol) provided a mixture of 2 photoproducts. The spectral characterization is provided in the experimental section (Figure 19 and 22). A product absorbing at 340 nm was assigned to "leuco PF" whereas the second product absorbing at 424 nm was assigned to "diacridine"

in accordance with published data.[38] The first product is only observed when irradiating a degassed sample, whereas the second product is oxygen insensitive. Therefore we assume that leuco PF is formed from PF•$^-$ (triplet reductive pathway) and diacridine is formed from PF•$^+$ (singlet ionization pathway).

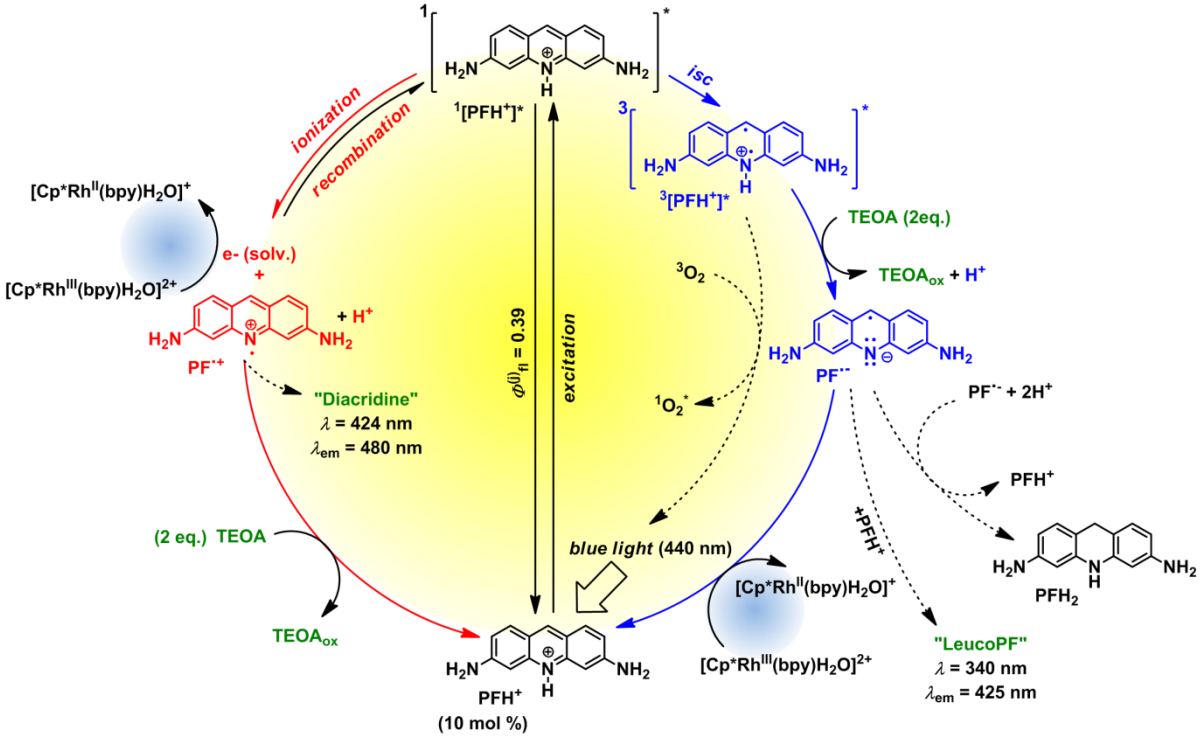

Figure 5: Proposed proflavine catalytic cycle.

Based on our mechanistic experiments and literature reports we propose the overall catalytic mechanism depicted in Figure 5. After absorption of a blue photon PFH$^+$ is excited to the first excited singlet state. Fluorescence (prompt and delayed) is a significant deactivation pathway with an overall quantum yield of 39%.[28] Intersystem crossing (isc) gives the triplet state which accepts an electron from TEOA. The radical PFH· is deprotonated to the radical anion PF•$^-$, which is then oxidized by Rh$_{cat}$ back to PFH$^+$. In the absence of the metal complex the radical anion forms leuco PF and disproportionates to PFH$_2$.[37] The reduced Rh$_{cat}$ reacts according to the catalytic cycle depicted in Figure 4.

The control experiment without degassing (Table 3, line 6) unexpectedly gave 30% of the product. As oxygen can efficiently quench both ^{3}[PFH$^+$]* and PF•$^-$ (for the rate constants see Figure 51), the product cannot be formed in this case through the triplet reductive pathway (Figure 5, right side). We propose that another, oxygen-insensitive, pathway is

present. PF is known for its photoionization from $^1[PFH^+]^{*m}$ after excitation.[31] Pileni and Gräzel[31] reported that the photoionization is a single-photon process, whereas Hussein and Goez examined the process in more detail and revealed that the photoionozation is caused by multiple photon process (*i. e.* absorption of the excited state).[39] The photoionization produces solvated electrons[40] which react[n] either with PFH^+ to form $PF^{\bullet -}$ or with[o] Rh_{cat} to form Rh(II) species.[37] Unlike the triplet pathway, the PET from the singlet state is obviously an outer-sphere process. The oxidized PF radical cation $[PF^{\bullet}]^+$ is than reduced back by TEOA present in the system[p]. These two parallel mechanisms (oxidative and reductive quenching) have been recently found in an iridium-based photocatalytic system.[41]

To further prove our mechanistic proposal, we performed a series of experiments using transient pump-probe spectroscopy (Figure 6; Figures 38 – 42). The solution of PF (c = 2.2 × 10^{-4} M) in DMF/water mixture exhibited a strong fluorescence negative peak directly after the excitation flash (Figure 38). After ~50 ns, when the fluorescence decays (the fluorescence lifetime was reported to be ~5 ns)[31] three peaks were observed at 550, 610 and 670 nm, respectively (Figure 6). This was assigned to the $^3[PFH^+]^*$. The lifetime of the PF triplet was approx. 2 μs in aerated solution. The triplet spectrum and lifetime corresponds to the previously published data.[40] The solution of PF and Rh_{cat} (c_{Rh} = 2.0 × 10^{-4} M) showed partially quenched fluorescence and the intensity of the PF triplet peak was significantly lowered (Figure 40). This finding corresponds to the Stern-Vollmer experiment discussed previously and indicates that Rh_{cat} partially quenches the excited singlet state, which also leads to a diminished triplet yield.

The transient spectra of the solution of PF and TEOA (c_{TEOA} = 25.8 × 10^{-3} M) exhibited a new peak with an absorption maximum at ~530 nm and with a lifetime of approx. 8 μs in aerated solution (Figure 39). The observed peak was oxygen-sensitive and corresponds to the $PF^{\bullet -}$,[40] confirming the PET from TEOA to $^3[PFH^+]^*$.

[m] and partially (10%) from $^3[PFH^+]^*$; *Chem. Phys. Lett.* **1980**, *69*, 61–65.
[n] k_{red} = 2.5 × 10^{10} s^{-1} M^{-1}; Solar, S.; Solar, W.; Getoff, N. *Z. Naturforsch.* **1982**, *37a*, 1077.
[o] k_{red} ~ 10^{10} s^{-1} M^{-1}; estimated value, based on: Solar, S.; Solar, W.; Getoff, N. *Z. Naturforsch.* **1982**, *37a*, 1077.
[p] redox potential of $[PFH^{\bullet}]^{2+}$ is E_0 = +1.07 V vs SCE, Figure 12. $\Delta G° = -e \times (-0.76\ V + 1.07\ V) - 0.08\ eV = -0.39\ eV \sim -37\ kJ\ mol^{-1}$

The transient spectrum of the solution of PF, TEOA and Rh_{cat} exhibited the absorption peak of $PF^{\bullet -}$ (Figure 41). The intensity of the peak was lower than in the case of PFH^+ and TEOA solution and its lifetime shortened to ~ 3 µs caused by the electron transfer from the $PF^{\bullet -}$ to Rh_{cat}.

Rh_{cat} itself does not exhibit any transient species and no product from PET with TEOA is detected. Unlike its iridium analogue, Rh(III)–H is not photoactive.[42]

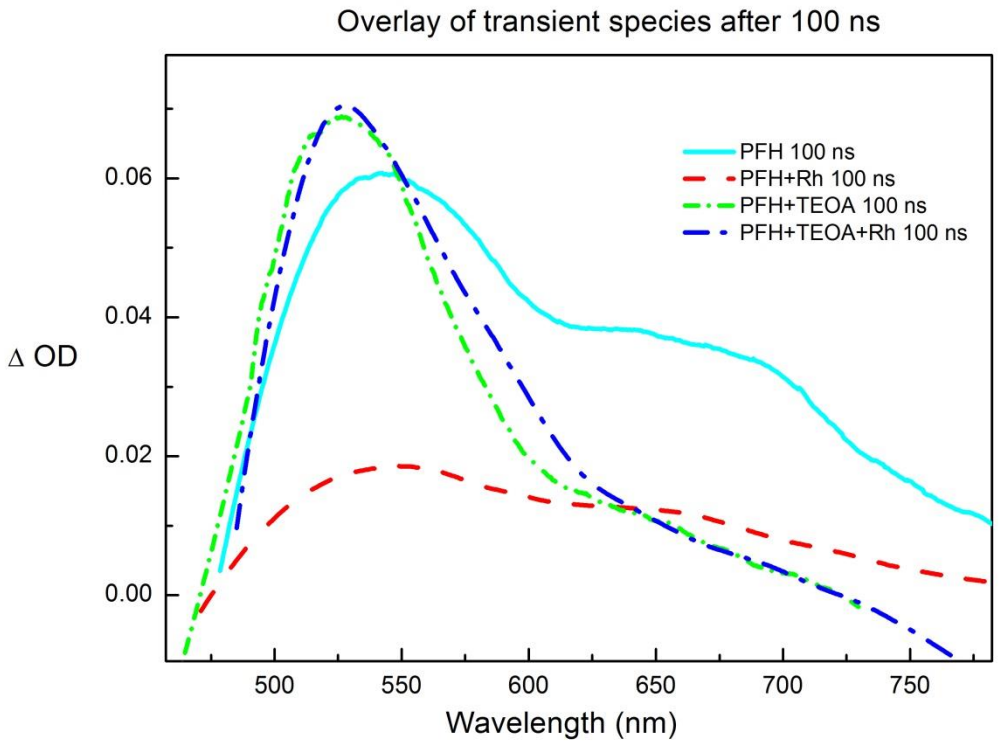

Figure 6: The overlay of the transient signal of proflavine (c = 2.24 × 10^{-4} M), TEOA (c = 2.58 × 10^{-2} M) and rhodium catalyst (c = 2.0 × 10^{-4} M) in DMF/water 1:1, bubbled with nitrogen, excitation wavelength λ_{ex} = 355 nm; time window 50 ns, 10 × accumulated, 100 ns after the pulse, smoothed; the single peak at ~530 nm corresponds to $PF^{\bullet -}$ and the peak at ~550 nm with a broad shoulder at ~670 nm corresponds to $^3[PFH^+]^*$

The quantum yield of the product formation was determined to be Φ = (0.14 ± 0.05) % at 455 nm measured at low light intensity ($P_{absorbed}$ = 9.3 mW, see SI for details). The low quantum yield is caused by loss of excitation by fluorescence (~39%),[28] low triplet yield (~10%),[29] disproportionation of the Rh^{II} species (two moles of $PF^{\bullet -}$ for one mole of Rh^I)[33] and partial Rh(III)–H decomposition (~50% of Rh(III)–H lost to H_2).

3.3 Conclusion

In summary, we have achieved selective photocatalytic reduction of aldehydes over ketones with a broad substrate scope employing *in situ* generated Rh(III)–H as the reduction reagent. Unlike in the case of formate based aqueous buffer system, the Rh(III)–H is formed slowly in the reaction medium and is therefore able to kinetically distinguish between aldehydes and ketones. The photoreduction proceeds both *via* photoinduced electron transfer from proflavine triplet and by oxidative quenching with Rh_{cat}. The former is oxygen sensitive and the latter is light intensity dependent. The light intensity influences directly the reaction mechanism and the reaction rate. A simple change of the light source (high-power LED vs. fluorescence light bulb) can affect both the product yield and the whole photocatalytic mechanism.

3.4 Experimental section

3.4.1 General methods and material

Proflavine (3,6-diaminoacridine hydrochloride, 95% dye content, catalogue number 131105-25G) was purchased from Sigma Aldrich. For all reactions and measurements proflavine was used in a form of hydrochloride. All other commercially available reagents and solvents were purchased and used without further purification.

Thin-layer chromatography was performed using silica gel plates 60 F254: Visualization was accomplished with short wavelength UV light (254 nm) and/or staining with appropriate stains (anisaldehyde, orthophosphomolybdic acid, $KMnO_4$).

Standard flash chromatography was performed on an Isolera™ Spektra Systems automated with high performance flash purification system using silica gel of particle size 40−63 μm. Macherey-Nagel silica gel 60 M (230-440 mesh) was used for column chromatography.
^{1}H and ^{13}C NMR spectra were recorded on Bruker Avance spectrometers (300 MHz and 75 MHz or 400 MHz and 101 MHz) in $CDCl_3$ solution with internal solvent signal as reference (7.26 and 77.0, respectively). Proton NMR data are reported as follows: chemical shift (ppm), multiplicity (s = singlet, d = doublet, t = triplet, q = quartet, dd = doublet of

doublets, ddd = doublet of doublets of doublets, td = triplet of doublets, m = multiplet, br. s. = broad singlet), coupling constants (Hz) and numbers of proton. Data for ^{13}C NMR are reported in terms of chemical shift and no special nomenclature is used for equivalent carbons.

Gas chromatography (GC) and gas chromatography coupled to low resolution mass spectrometry (GC-MS) analyses were performed using a capillary column (length: 30 m; diam. 0.25 mm; film: 0.25 µm) using He gas as carrier. GC was equipped with a FID detector. GC-MS was performed on 5975 MSD single quadruple detector. Reduction products were identified by comparing with authentic samples (GC/FID). Quantification of reduction products was performed by GC/FID analysis using internal standard. Head-space GC was performed on the Inficon Micro GC 3000 with a 3 Å mol sieve column, a thermal conductivity detector and Ar as carrier gas. The gas phase was taken directly from the sealed vial with the reaction mixture.

UV–Vis analyses were performed with Varian Cary 50 UV/Vis spectrophotometer and Agilent 8453 UV-Vis Spectrometer. Fluorescence measurements were performed with Horiba FluoroMax-4 fluorimeter. For UV and fluorescence measurements 10 mm Hellma fluorescence quartz cuvettes (117.100F-QS) with a screw cap with PTFE-coated silicon septum were used. The UV-Vis measurements with online irradiation were performed on a self-made apparatus using a fluorescence cuvette in a fluorescence cuvette holder, LED (Cree-XP, royal blue, 455 nm) placed perpendicular to the optical pathway of the Agilent 8453 UV-Vis Spectrometer (Figures 7 and 8). The whole system was stirred with a small magnetic PTFE stirring bar by a magnetic stirrer placed above the cuvette.

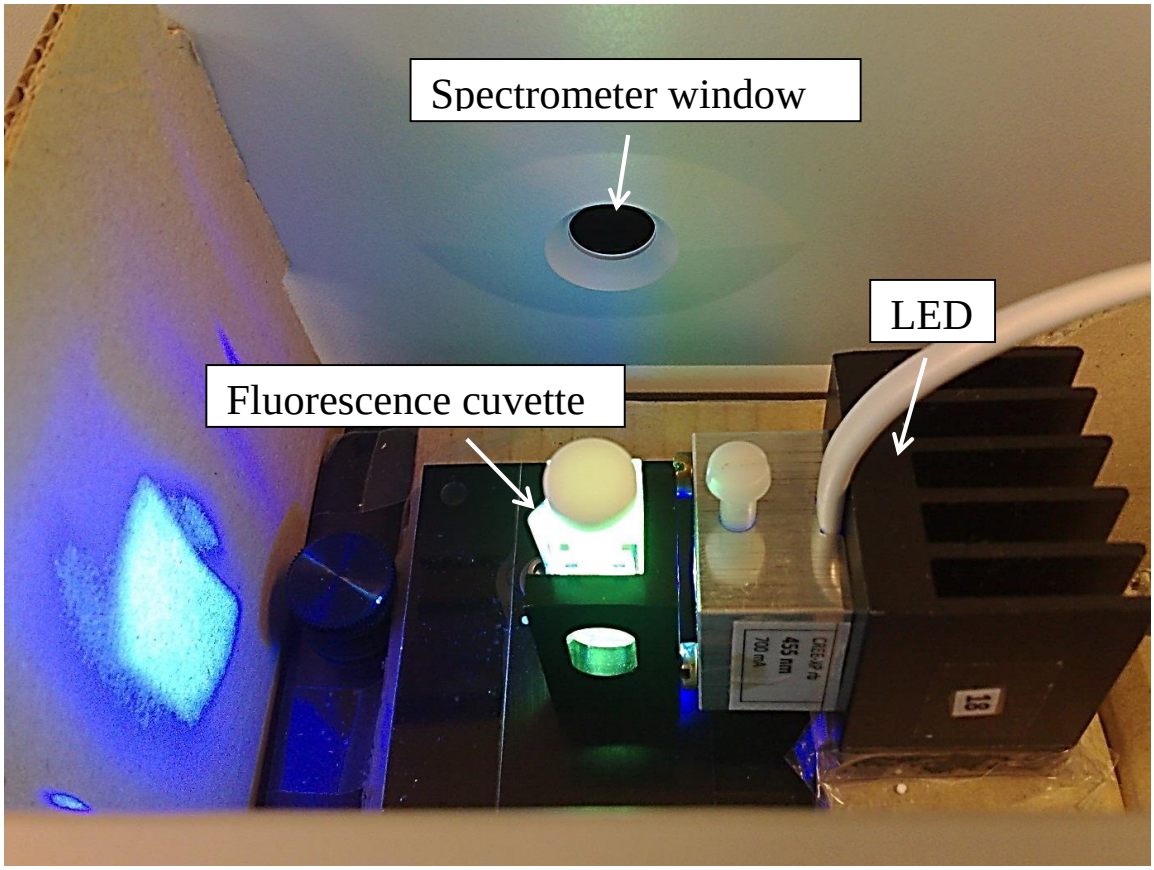

Figure 7: Setup for UV-Vis measurement with online irradiation.

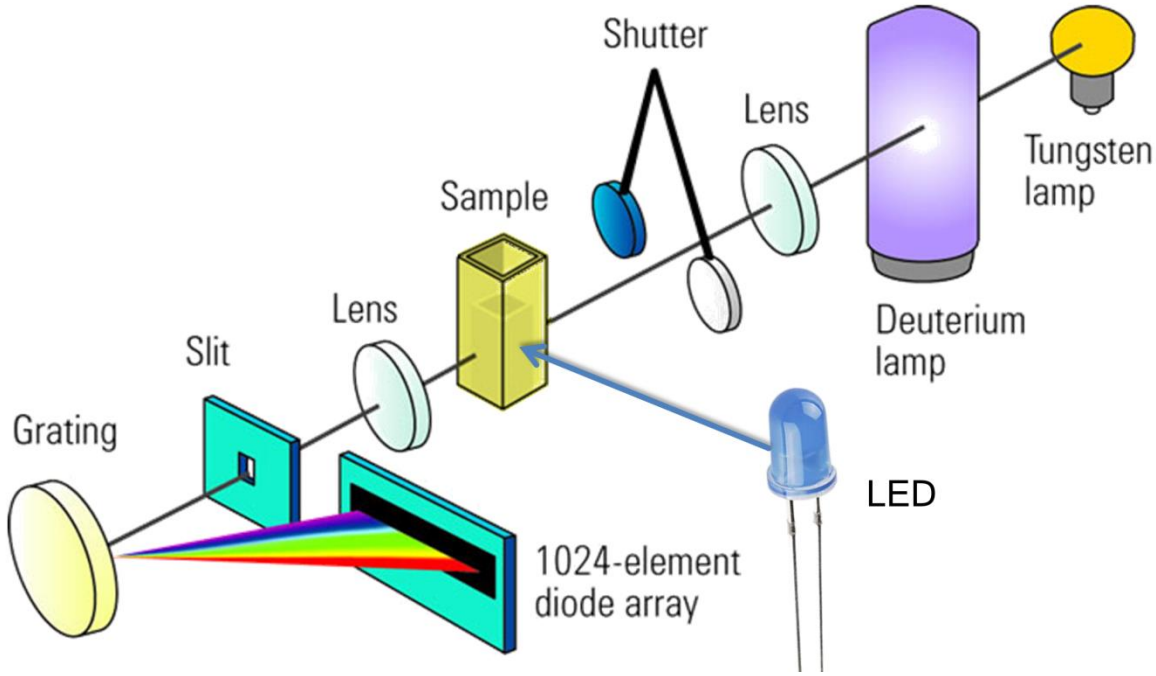

Figure 8: Scheme of the setup for UV-Vis measurement with online irradiation.

Electrochemical studies were carried out under argon atmosphere. The cyclic voltammetry (CV) measurements were performed in acetonitrile (MeCN) containing 0.1 M tetra-n-butylammonium hexafluorophosphate as a conducting salt using ferrocene/ferrocenium (Fc/Fc^+) as an internal standard. A glassy carbon electrode (working electrode), platinum wire counter electrode, and Ag wire quasi-reference electrode were employed. The CV measurements of proflavine aqueous solutions were performed without conducting salt and internal standard. The Ag/AgCl electrode was used as a reference electrode instead of silver wire pseudoreference electrode. Spectroelectrochemical studies were carried out in an optically transparent thin layer electrochemical cell (OTTLE, 0.2 mm optical length). The Pt minigrid working electrode, Pt minigrid reference electrode and silver wire pseudoreference electrode were used.

Photocatalytic reactions were performed with 455 nm LEDs (OSRAM Oslon SSL 80 royal-blue LEDs, λ_{em} = 455 nm (± 15 nm), 3.5 V, 700 mA).
For the reaction with a flow reactor 8 × LED OSRAM Oslon LDH9GP deep blue, 455 nm (Datasheet: http://tinyurl.com/n8vucd5) were used as a light source. The reaction mixture was injected by syringe pump (Landgraf Laborsysteme, Spritzenpumpe LA-100, RS232, Datasheet: http://tinyurl.com/p99nv3m) into a glass flow reactor (Figure 9, LTF factory, 11 × 5.7 cm, 1.7 mL internal volume, 0.3 mL volume of the reactor tubing) previously flushed with nitrogen. The flow reactor was cooled down to 20°C with a custom-made aluminum cooling block placed opposite to LEDs with a mirror to minimize losses of the light.

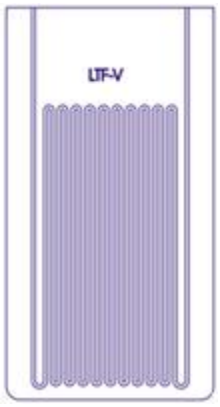

Figure 9: Flow reactor LFT-V.

The quantum yield of the photoreduction was determined using the apparatus previously developed in cooperation with our group.[43] The 3 W 455 nm LED (LXHL-LR3C) was used for irradiation. The calibrated solar cell was used to measure precisely the output power of

the light source. The measured value was in the linear range of the calibration curve. The background light was minimized by working in dark. The photoproduct yield was determined by GC/FID by internal standard method.

The pH measurements were accomplished with WTW pMX 3000 pH meter with glass pH electrode (Metrohm) and temperature sensor (WTW TFK 150).

The laser flash photolysis (LFP) setup was operated in a right-angle arrangement of the pump and probe beams. Laser pulses of ≤ 700 ps duration at 355 nm (170 mJ) were obtained from an Nd:YAG laser and were dispersed over the 4 cm optical path of the quartz cell by a concave cylindrical lens.[44] The absorbance of the sample solutions was adjusted to 0.3 − 0.5 per cm at the wavelength of excitation. A 75 W xenon lamp was used as the source of white probe light. Spectrographic detection (ICCD camera connected to a spectrometer equipped with 300 l/mm gratings blazed at 300 or 500 nm) of the transient absorptions was available. A fresh solution was used for each laser flash to avoid excitation of the photoproducts. Measurements were done at ambient temperature (20 ± 2 °C). All samples were degassed by bubbling with nitrogen directly in the cuvette. All UV-Vis and fluorescence spectra were measured in aqueous solutions unless mentioned otherwise.

General procedure for photocatalytic reductions

The carbonyl compound (0.1 mmol, 1 eq.), triethanolamine (29.8 mg, 0.2 mmol, 2 eq.), proflavine (2.5 mg, 0.01 mmol, 10 mol%), rhodium catalyst (4.7 mg, 0.01 mmol, 10 mol%) were mixed with a small PTFE stirring bar in a 5 mL crimp cap vial. The vial was sealed with a PTFE septum and DMF/water mixture (1:1, v/v, 1.5 mL) was added. The resultant solution was degassed by 3 freeze-pump-thaw cycles and filled with nitrogen atmosphere. The reaction vessel was placed in a cooling block cooled to 20 °C, was irradiated through the plane bottom side by 3W blue LED (λ_{em} = 455 nm) and the reaction conversion was monitored by GC analysis. The samples for GC were taken by a degassed gas-tight Hamilton syringe. After complete conversion an internal standard (*e. g.* ethyl benzoate, 0.5 mL, c = 20 mg/mL) was added to the reaction mixture and the product yield was determined by GC/FID using a calibrated method.

Product yields determination

All photoreduction products were compared with authentic standards either purchased (Sigma Aldrich, Acros) or synthetized according to the published procedures and compared with known spectra. In most cases the mass balance between the substrate and the product determined from the calibration curve corresponded to the conversion.

Irradiation in a flow reactor

Reaction in the flow reactor decreased the irradiation time. The 1 mm flow reactor tubing was irradiated from both sides and therefore all volume of the reaction mixture was irradiated. To keep the system degassed, the flow reactor was first flushed with nitrogen for 10 min and then it was filled with degassed solvent mixture. The degassed reaction mixture was filled into a 5 mL syringe (internal diameter = 13 mm) which was connected to the syringe pump. The reaction mixture was expelled through the tubing to the flow reactor so that the front of the reaction solution was right at the beginning of the irradiated part of the tubing. The syringe pump was set to the flow rate 0.5 mL/h, corresponding to 203 min irradiation time of the reaction mixture (irradiated volume = 1.7 mL). The flow rate was optimized by decreasing the flow rate and measuring the product yield.

General procedure for the preparation of alcohols as standards

The reduction reactions were performed according to known procedures.[45] Sodium borohydride (46 mg, 1.23 mmol, 1.1 eq.) was added to a stirred solution of carbonyl compound (1.12 mmol, 1 eq.) in freshly distilled EtOH (10 mL). The course of the reaction was monitored by TLC (EtOAc:hexane = 1:5) and the reaction was complete after 5 minutes. After stirring for 10 minutes the reaction mixture was concentrated *in vacuo* and the residue dissolved in DCM (30 mL). The organic layer was subsequently washed with ammonium chloride (30 mL, sat. aq.), distilled water (30 mL) and brine (30 mL), the organic extract dried over $MgSO_4$ and concentrated in vacuo to afford the respective alcohol (yield: 57–91%).

1-(4-(Hydroxymethyl)phenyl)ethanone

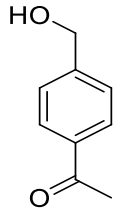

The product was prepared according to the modified general procedure. In order to prevent the double reduction the sodium borohydride was dissolved in EtOH (5 mL) and the substrate solution cooled to 0 °C was titrated by this solution with TLC check after each addition. The reduction was complete after addition of 0.288 eq. (~1.15 reduction equivalents) of $NaBH_4$. The workup followed the general procedure. The crude product was purified by column chromatography (EtOAc:hexane = 1:1) yielding a white crystalline solid. The spectroscopic data match previously reported values.[46]

Yield: 153 mg (57%)

^{1}H-NMR: δ_H (300 MHz, $CDCl_3$): 7.96 (d, J = 8.4 Hz, 2H), 7.46 (d, J = 8.6 Hz, 2H), 4.79 (s, 2H), 2.61 (s, 3H), 1.61 (br. s., 1H).

^{13}C-NMR: δ_C (75 MHz, $CDCl_3$): 198.07, 146.27, 136.31, 128.65, 126.64, 64.60, 26.68.

Methyl 4-(1-hydroxyethyl)benzoate

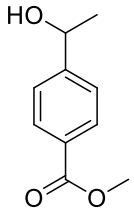

The product was prepared according to the modified general procedure. The reaction in ethanol yielded the transesterification product [ethyl 4-(1-hydroxyethyl)benzoate]. Freshly distilled methanol was used for the reaction yielding colorless oil. The spectroscopic data match previously reported values.[47]

Yield: 164 mg (91%)

^{1}H-NMR: δ_H (300 MHz, $CDCl_3$): 8.02 (d, *J* = 8.4 Hz, 2H), 7.45 (d, *J* = 8.6 Hz, 2H), 4.97 (q, *J* = 6.5 Hz, 1H), 3.93 (s, 3H), 2.31 (s, 1H), 1.52 (d, *J* = 6.5 Hz, 3H).

^{13}C-NMR: δ_C (75 MHz, $CDCl_3$): 167.05, 151.03, 129.84, 129.10, 125.31, 69.93, 52.14, 25.30.

Preparation of [Cp*Rh(bpy)Cl]Cl

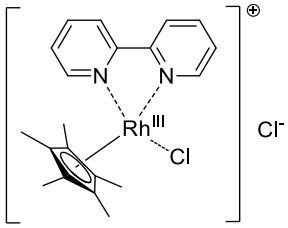

The compound was prepared according to a known procedure.[48] Rhodium dimer $[RhCl_2Cp^*]_2$ (100 mg, 0.162 mmol, 1 eq) was suspended in methanol (4 mL) and 2,2'-bipyridyl (61 mg, 0.388 mmol, 2.4 eq.) was added. The solid rhodium complex dissolved in 5 minutes. The orange-yellow solution was stirred for 20 min at room temperature. The solvent was concentrated to about 2 mL, the product precipitated by adding diethyl ether

(10 mL) while stirring, filtered by a Büchner funnel, washed with diethyl ether (2 × 5 mL) and dried under reduced pressure yielding 150 mg (>99%) of an orange powder.

Yield: 0.150 g (>99%)

Melting point: 180°C, decomposition

^{1}H-NMR: δ_H 9.04 (d, *J* = 8.0 Hz, 2H), 8.84 (d, *J* = 5.6 Hz, 2H), 8.26 (td, *J* = 8.0, 1.5 Hz, 2H), 7.81 (td, *J* = 8.0, 1.5 Hz, 1H), 1.74 (s, 15H).

3.4.2 Control experiments

All control experiments were repeated three times. For each control experiments one component of the reaction system depicted in Scheme 1 was omitted or substituted (Table 3).

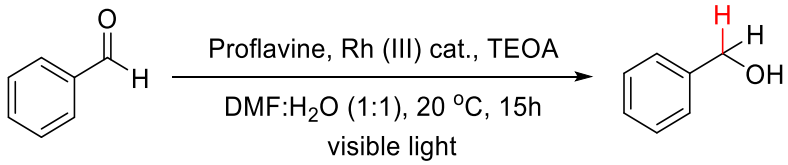

Scheme 1: Typical reaction procedure.

Table 3: Control experiments

Entry	Proflavine (mol%)	Rh_{cat} (mol%)	TEOA (eq.)	Light (455 nm)	Atmosphere	Yield (%)[a]
Control experiments						
1	**10**	**10**	**2**	**Yes**	**N_2**	**97**
2	10	10	-	Yes	N_2	0
3	10	-	2	Yes	N_2	~0
4	-	10	2	Yes	N_2	~0
5	10	10	2	-	N_2	0
6	**10**	**10**	**2**	**Yes**	**Air**	**30**
7	10	-	2	Yes	H_2	0
8	10	10	2	-	H_2	0

[a] GC/FID determined yield with appropriate internal standard.

LED intensity check

The reaction yield of identical reactions shows some variation (±10 %). Having established a reproducible degassing procedure the relative intensities of different LEDs were investigated. Irradiation was accomplished in a cooling block with six positions for gas tight vials (Figure 10).

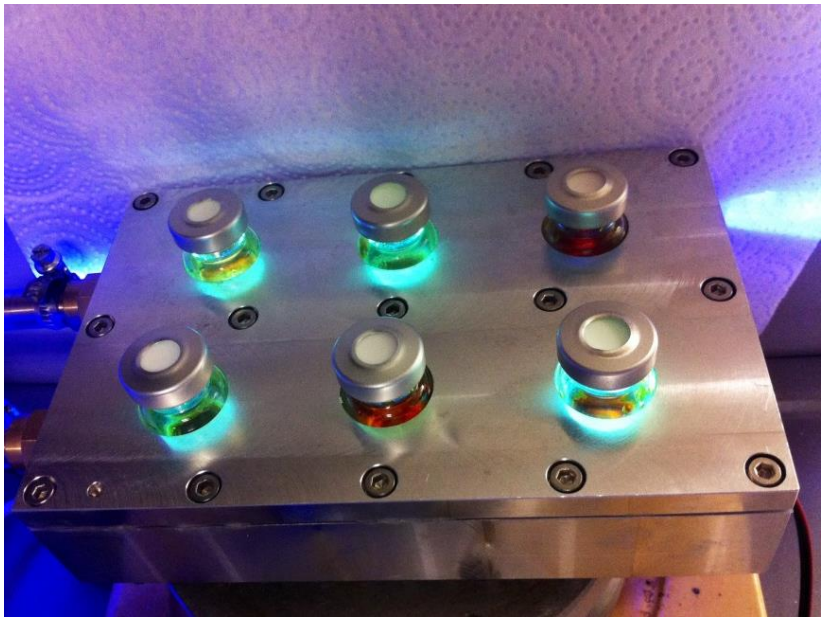

Figure 10: Irradiation setup.

Despite the fact that all LEDs in one cooling block were of the same age and had the same voltage (parallel connection), the intensity of emitted light differed for each position. The results of the test reaction are summarized in Figure 11.

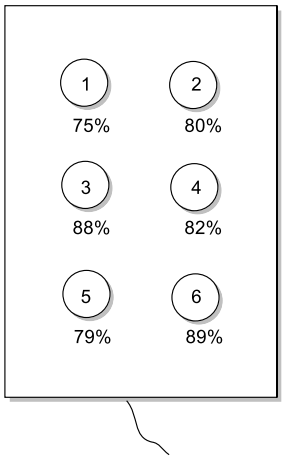

Figure 11: LED intensity test of different positions of the cooling block; the respective yields of benzaldehyde reduction are shown below each position.

3.4.3 Quantum yield determination

The quantum yield of the photocatalytic reduction of benzaldehyde (typical reaction) was determined by a method developed in cooperation with our group.[43] The reaction mixture (3 mL, DMF/water 1:1) of benzaldehyde (c = 5 mM), TEOA (c = 10 mM), rhodium catalyst

(c = 0.5 mM), proflavine hydrochloride (c = 0.5 mM) and internal standard for GC (c = 5 mg/mL) was filled into a fluorescence cuvette with a stirring bar and septum and degassed by bubbling by nitrogen (20 min).

The measurement was accomplished in a dark room to minimize the ambient light. The radiant power of light transmitted by the cuvette with a blank solution was measured (U_{ref} = 96 mV) and the transmitted power ($P_{ref} = U_{ref}/10$ = 9.6 mW) was noted. The cuvette with blank was changed by cuvette with the reaction mixture and the transmitted radiant power (P_{sample} = 0.3 mW) was noted. The transmitted radiant power was monitored during the irradiation and remained constant.

The sample was irradiated for 14 hours to reach 17% conversion (0.277 mg, 2.56×10^{-6} mol; the LED power was significantly lower than in the photocatalytic setup).

The quantum yield was calculated from Equation S1:

$$\Phi = \frac{N_{product}}{N_{ph}} = \frac{N_A * n_{product}}{\frac{E_{light}}{E_{ph}}} = \frac{N_A * n_{product}}{\frac{P_{absorbed} * t}{\frac{h * c}{\lambda}}} = \frac{h * c * N_A * n_{product}}{\lambda * \left(P_{ref} - P_{sample}\right) * t} \quad \text{(S1)}$$

where Φ is quantum yield, $N_{product}$ is the number of molecules created, N_{ph} is the number of photons absorbed, N_A is Avogadro's constant in moles^{-1}, $n_{product}$ is the molar amount of molecules created in moles, E_{light} is the energy of light absorbed in Joules, E_{ph} is the energy of a single photon in Joules, $P_{absorbed}$ is the radiant power absorbed in Watts, t is the irradiation time in sec, h is the Planck's constant in J×s, c is the speed of light in m s^{-1}, λ is the wavelength of irradiation source (455 nm) in meters, P_{ref} is the radiant power transmitted by a blank cuvette in Watts and P_{sample} is the radiant power transmitted by the cuvette with reaction mixture in Watts.

This results in:

$$\Phi = \frac{h * c * N_A * n_{product}}{\lambda * \left(P_{ref} - P_{sample}\right) * t}$$

$$= \frac{6.626 \times 10^{-34}\text{Js} \times 2.998 \times 10^{8}\text{ms}^{-1} \times 6.022 \times 10^{23}\text{mol}^{-1} \times 2.56 \times 10^{-6}\text{mol}}{455 \times 10^{-9}\text{m} \times (9.6 - 0.3) \times 10^{-3}\text{Js}^{-1} \times 50400\text{s}}$$

$$= \frac{3.062 \times 10^{-7}\text{Jm}}{2.133 \times 10^{-4}\text{Jm}} = 1.44 \times 10^{-3} \cong \mathbf{0.14}\ \%$$

From 3 independent measurements the quantum yield was determined to be Φ = (0.14 ± 0.05)%.

General procedure for chemical reductions

The reductions were accomplished according to the known procedure.[49] A mixture of carbonyl compound (0.5 mmol, 1 eq.) and rhodium catalyst (1.15 mg, 2.5 μmol, 0.5 mol%) in formate buffer (2 mL, 2M, pH = 3.50) was degassed in a 5 mL sealed glass vial by bubbling with nitrogen and stirred. The reaction mixture changed color from yellow to deep blue as the rhodium(III) hydride was formed in the system. Formic acid reacts with the catalyst generating gases (H_2, CO_2) and therefore a balloon with nitrogen was attached to the vial.

Aliquots (50 μL of reaction mixture) were taken and extracted by ethyl acetate (1.0 mL) in an Eppendorf tube. The organic extract was measured by GC monitoring the reaction kinetics.

Chemical reductions – results

The results of chemical reductions are summarized in the Table 4. The limiting factor of many organic substrates is the poor solubility/miscibility with the aqueous formate buffer. The reactions with sodium or ammonium formate as a formate ion source did not yield the reduction product.

Table 4: Chemical reductions

Entry	Substrate	Reaction time (min)	Conversion
1	cyclohexane	120	100
2	benzaldehyde	15	100
3	acetophenone	15	40
4	benzaldehyde/acetophenone	15	94/32[a]

[a] conversion of benzaldehyde/acetophenone.

Imine reductions

Analogous to the carbonyl reductions imines were reduced in various solvents (see Table 5) and when noted, thiourea (1 eq.) was used as additive. Imine reductions are shown in Scheme 2. The reduction product 1-amino diphenylmethane was determined by GC-FID by spiking with a purchased authentic sample. The procedure (*e. g.* loading of reagents, degassing procedure) was analogous to carbonyl reductions. Water had to be excluded from the system because otherwise the hydrolysis was a dominant reaction pathway.

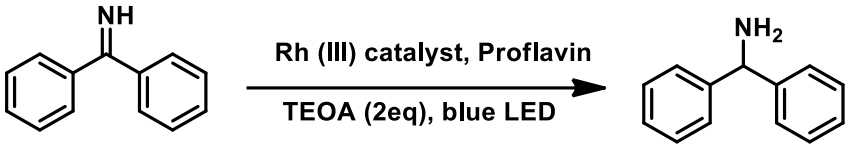

Scheme 2: General scheme of imine reductions.

The results of reductions are summarized in Table 5.

Table 5: Imine reductions

Entry	Reaction conditions	Time (h)	Yield (%)[a]
1	Ph_2C=NH, CH_3CN, 20 °C	15	11
2	Ph_2C=NH, CH_3CN, 20 °C, thiourea	15	87
3	Ph_2C=NH, DMF, 20 °C, thiourea	5.5	63
4	Ph_2C=NH, DMF, 20 °C, thiourea	17	84
5	**Ph_2C=NH, DMSO, 20 °C, thiourea**	**5.5**	**81**
6	Ph_2C=NH, DMSO, 20 °C, thiourea	17	86
7	Ph_2C=NH.HCl, CH_3CN, 20 °C, thiourea	17	47

[a] uncalibrated yield based on GC/FID.

Reduction potential measurements

The reduction potentials were measured by cyclic voltammetry (CV). The half-wave potential of the first reduction peak was taken as the first reduction potential of the compound. The scan-rate was kept at 50mV/s and the average value from tree scans was taken.

The cyclic voltammogram is shown in the Figure 12. The potentials were determined to be E_{red} = –1.16 V vs Ag/AgCl = –0.74 V vs SCE; E_{ox} = +1.20 V vs Ag/AgCl = +1.07 V vs SCE.[q]

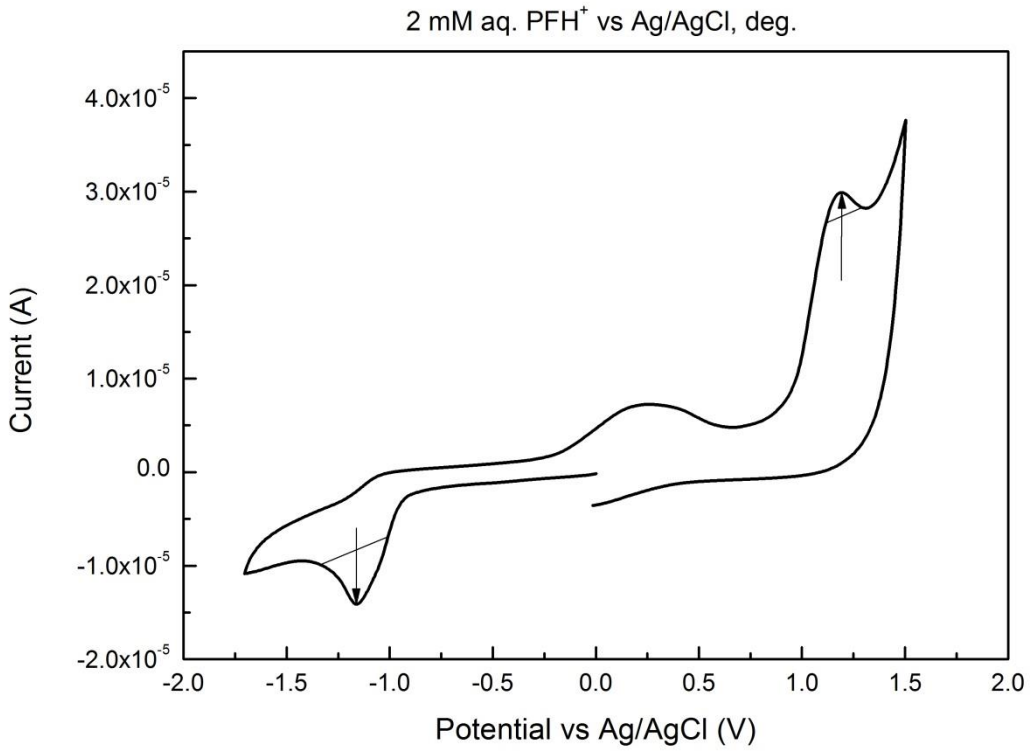

Figure 12: Cyclic voltammogram of proflavine hydrochloride in aqueous solution (c = 2 mM). The reduction peak and oxidation peak are shown by arrows (E_{red}; E_{ox}).

The spectroelectrochemical data of reduction of aqueous solution of proflavine hydrochloride (2 mM, degassed) are shown in Figure 13. The UV-Vis spectra were measured every 100 mV. Both the cyclic voltammetry (irreversible reduction peak) and spectroelectrochemical data (appearance of the new peak at 393 nm) suggest the deprotonation after the reduction.

[q] according to Pavlishchuk, V. V.; Addison, A. W. *Inorg Chim Acta* **2000**, *298*, 97.

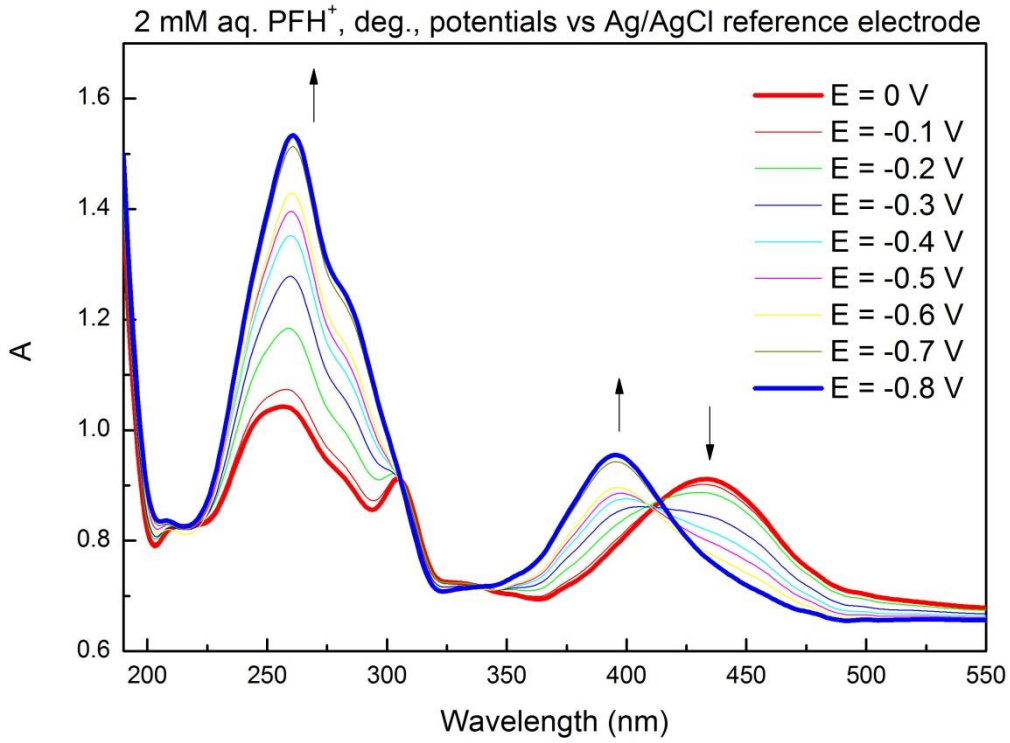

Figure 13: Spectroelectrochemical data of reduction of proflavine hydrochloride.

The CV of a variety of carbonyl compounds was measured in order to make a library of reference data. All benzaldehydes exhibited a reversible reduction peak (E_1) whereas acetophenones showed two reduction peaks, first irreversible (E_1) and second reversible (E_2). When the cyano group was present in the molecule, an additional peak corresponding to the reduction of CN functionality was present in the voltammogram.

Table 6: Reduction potentials (all values are shown in V, the potentials were measured in acetonitrile with BuN_4PF_6 (0.1 mM solution) and ferrocene as an internal standard. The potentials of all reduction peaks are shown. The measured potentials were determined with Fe/Fe^+ oxidation peak as internal standard and recalculated to SCE[r].

No.	Compound	E_1 meas.	E_1 vs SCE	E_2 meas.	E_2 vs SCE	E_3 meas.	E_3 vs SCE
1	Benzaldehyde	–1.91	–1.94[s]				
2	4-MeO-benzaldehyde	–2.30	–2.37				
3	4-MeO-acetophenone	–2.44	–2.48				
4	Benzyl acetone	<–3.0	<–3.1				
5	Acetophenone	–2.36	–2.38[t]				
6	4-F-benzaldehyde	–1.96	–2.03				
7	4-Acetoxy-benzaldehyde	–1.43	–1.47	–2.01	–2.06		
8	4-CN-benzaldehyde	–1.45	–1.59	–2.75	–2.90		
9	4-CN-acetophenone	–1.64	–1.84	–2.20	–2.41	–2.71	–2.92
10	3,4-Dimethoxy-benzaldehyde	–2.11	–2.24				
11	3,4,5-Trimethoxy-benzaldehyde	–1.91	–2.02				
12	Methyl 4-acetylbenzoate	–1.84	–1.84	–2.22	–2.2	–2.70	–2.70
13	4-CF_3 acetophenone	–1.98	–2.11	–2.45	–2.58		

[r] according to Pavlishchuk, V. V.; Addison, A. W. *Inorg Chim Acta* **2000**, *298*, 97.
[s] corresponds to the published value of -1.94 V vs SCE; *Handbook of Photochemistry* 2nd edition, NY, 1993
[t] corresponds to the published value of -2.38 V vs SCE; *Catal. Commun.* **2010**, 11, 1049-1053.

14	Cyclohexyl carbaldehyde	<–3.0	<–3.1				
15	2,2,2-Trifluoro acetophenone	–1.66	–1.65	–2.28	–2.27		
16	2,4-Dimethoxy-benzaldehyde	–2.19	–2.27				
17	Methyl 4-formylbenzoate	–1.76	–1.71				
18	Fluorenone	–1.34	–1.43	–1.87	–1.95		
19	Phenyl acetaldehyde	–3.00	–2.89				
20	3-Phenyl propionaldehyde	<–3.0	<–3.1				
21	Phenylacetone	<–3.0	<–3.1				
22	Cyclohexanone	<–3.0	<–3.1				

The measured reduction potentials were correlated with Hammett's sigma values[u] of the substituents on the aromatic ring. The correlation with the yields at respective reaction times is shown in Figure 14.

[u] C. Hansch and A. Leo, "Substituent Constants for Correlation Analysis in Chemistry and Biology," Wiley-Interscience, NY, 1979.

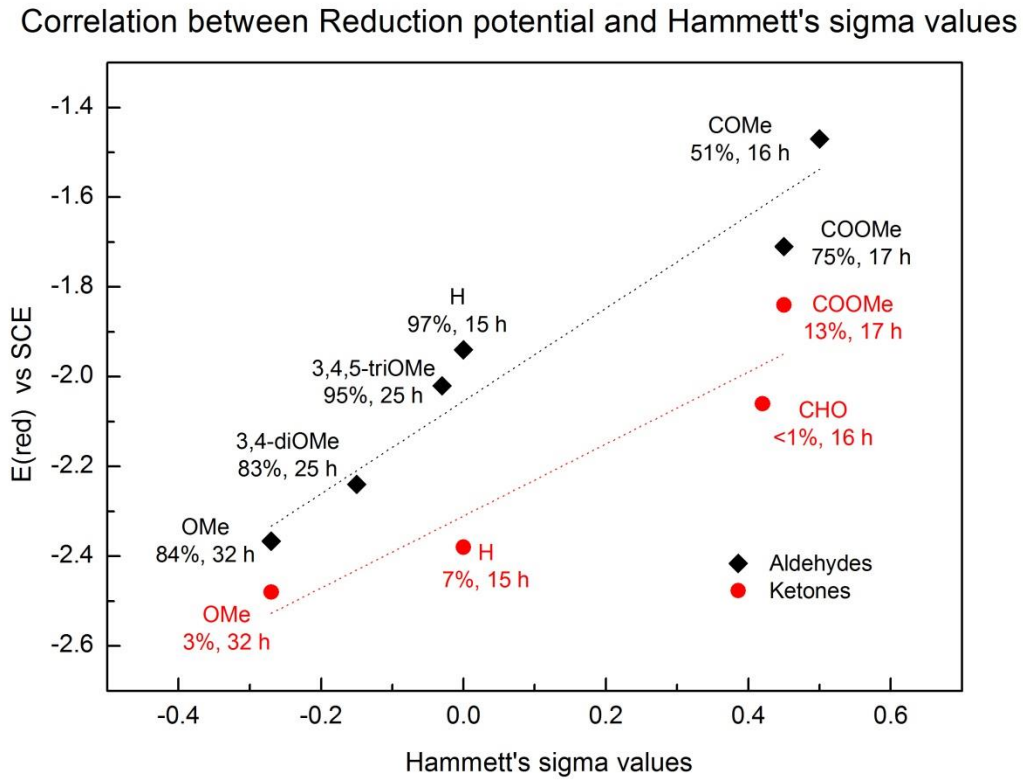

Figure 14: Correlation between reduction potentials and Hammett's sigma value[v] of aromatic aldehydes and acetophenones. The product yield at respective reaction time is shown.

Hydrogen production

The amount of hydrogen generated as a byproduct of the photoreduction was measured by head-space analysis. The detector response was calibrated to be linear dependent on the hydrogen concentration. The typical chromatogram is shown in Figure 15. The results of the hydrogen evolution in photoreduction of benzaldehyde and acetophenone are shown in Figure 16.

[v] C. Hansch and A. Leo, "Substituent Constants for Correlation Analysis in Chemistry and Biology," Wiley-Interscience, NY, 1979.

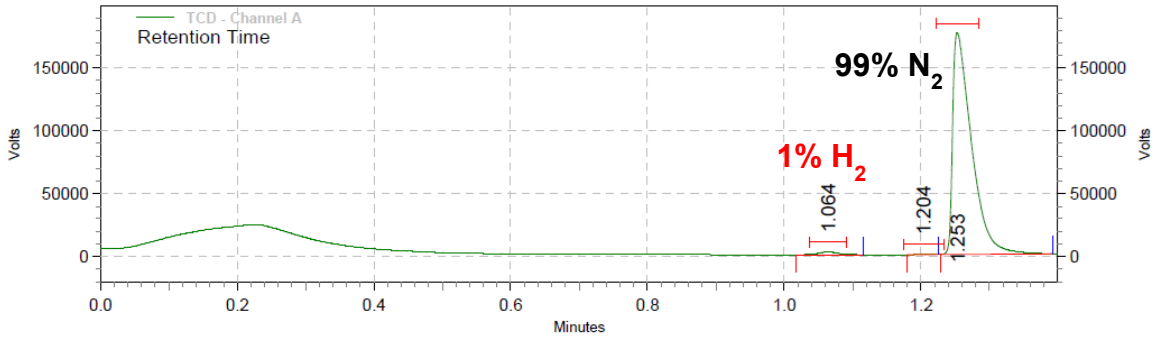

Figure 15: Typical head-space chromatogram; the hydrogen peak (ret. time t_R = 1.064 min) and nitrogen peak (ret. time t_R = 1.253 min) is shown. The peak at 1.204 min corresponds to the residual oxygen introduced at the injection.

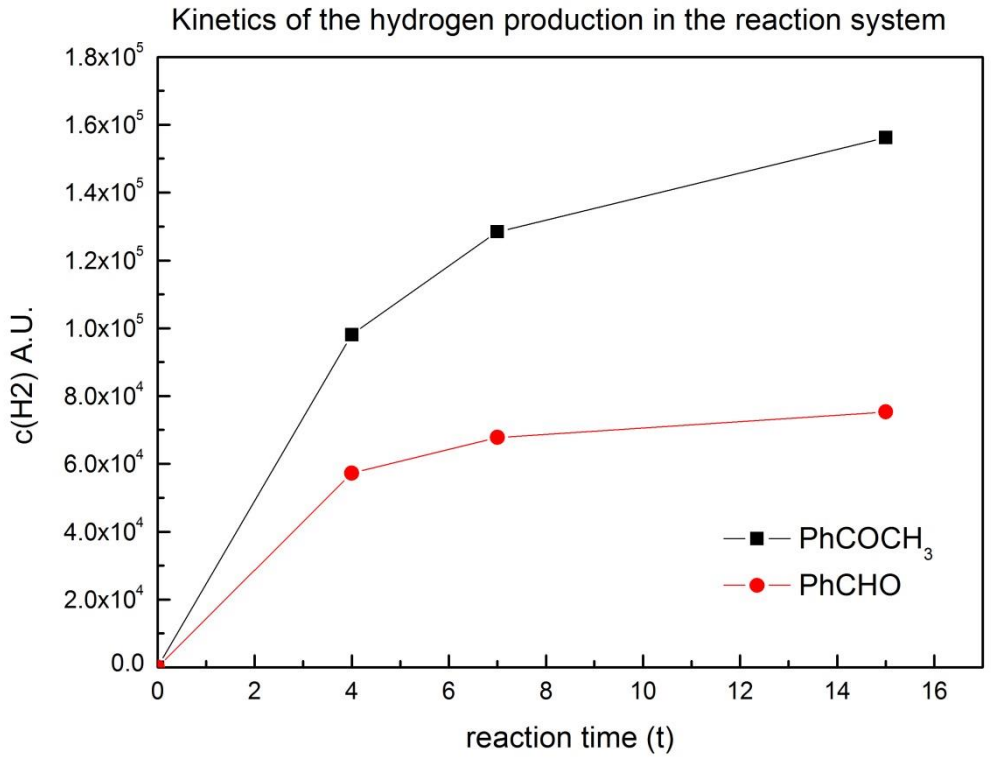

Figure 16: The kinetics of hydrogen production for the reaction with acetophenone (squares, black line) and benzaldehyde (closed circles, red line).

The kinetics of benzaldehyde photoreduction was followed by both GC-FID and Head-space GC. In both cases the result corresponded to the first order decay kinetics shown in Figure 17. The rate constant of benzaldehyde reduction was determined to be ~0.1537 hr^{-1} = 4.27 × 10^{-5} s^{-1}.

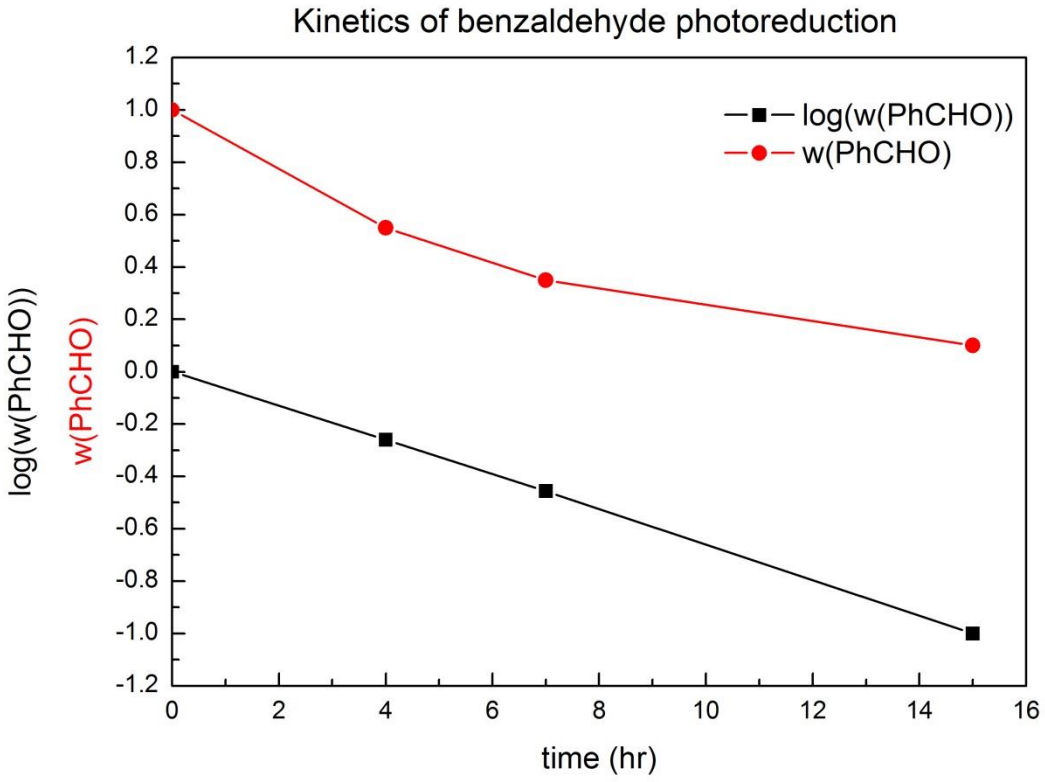

Figure 17: Kinetic evolution of benzaldehyde in photocatalytic reduction.

Rhodium decomposition – reactivity model

The reactivity model of reaction of rhodium hydride with aldehyde and ketone present simultaneously in the reaction mixture was constructed. The general reactivity is shown in Scheme 3.

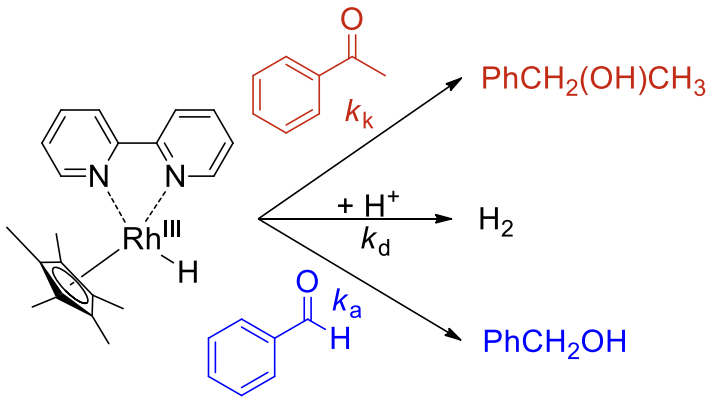

Scheme 3: General reactivity scheme of rhodium hydride with aldehyde and ketone in the reaction mixture.

In case that all reactions in Scheme 3 are of first order (simplified model valid at low conversion), the resultant rate equations are summarized below.

$$\frac{d[\mathrm{RhH}]}{dt} = -(k_a + k_d + k_k)[\mathrm{RhH}]$$

$$[\mathrm{RhH}] = [\mathrm{RhH}]_0 \times e^{-(k_a+k_d+k_k)t}$$

$$\Phi_{ald} = \frac{k_a}{k_a + k_d + k_k}$$

$$\Phi_k = \frac{k_k}{k_a + k_d + k_k}$$

$$\text{selectivity: } \boldsymbol{s} = \frac{\Phi_{ald}}{\Phi_k} = \frac{\frac{k_a}{k_a + k_d + k_k}}{\frac{k_k}{k_a + k_d + k_k}} = \boldsymbol{\frac{k_a}{k_k}}$$

In this case the aldehyde/ketone selectivity is time and conversion independent.

The more realistic model assumes all reductions to be of second order and the decomposition to be of pseudo first order. The rate constants are summarized below.

$$\frac{d[\mathrm{RhH}]}{dt} = -(k_a[\mathrm{RCHO}] + k_d[\mathrm{H^+}] + k_k[\mathrm{RCOR}])[\mathrm{RhH}]$$

$$\Phi_{ald} = \frac{k_a[\mathrm{RCHO}]}{k_a[\mathrm{RCHO}] + k_d[\mathrm{H^+}] + k_k[\mathrm{RCOR}]}$$

$$\Phi_k = \frac{k_k[\mathrm{RCOR}]}{k_a[\mathrm{RCHO}] + k_d[\mathrm{H^+}] + k_k[\mathrm{RCOR}]}$$

$$\text{selectivity: } \boldsymbol{s} = \frac{\Phi_{ald}}{\Phi_k} = \frac{\frac{k_a[\mathrm{RCHO}]}{k_a[\mathrm{RCHO}] + k_d[\mathrm{H^+}] + k_k[\mathrm{RCOR}]}}{\frac{k_k[\mathrm{RCOR}]}{k_a[\mathrm{RCHO}] + k_d[\mathrm{H^+}] + k_k[\mathrm{RCOR}]}} = \boldsymbol{\frac{k_a[\mathrm{RCHO}]}{k_k[\mathrm{RCOR}]}}$$

$$\text{selectivity } t = 0: \boldsymbol{s_0} = \frac{k_a[\text{RCHO}]_0}{k_k[\text{RCOR}]_0} = \frac{\boldsymbol{k_a}}{\boldsymbol{k_k}}$$

The aldehyde/ketone selectivity is time and conversion dependent, it decreases with increasing conversion and is maximal at the beginning of the reaction.

The product development and the aldehyde/ketone selectivity dependence are shown in the Figure 18. Second order kinetic equations and the following constants were used: k_a = 0.15 hr^{-1}; k_k = 0.0025 hr^{-1}. The results after 16 hours (93 % conversion of aldehyde and 4 % of ketone) correspond well with the experimental data. The value k_a = 0.15 hr^{-1} supports the result of head-space analysis (Figure 17).

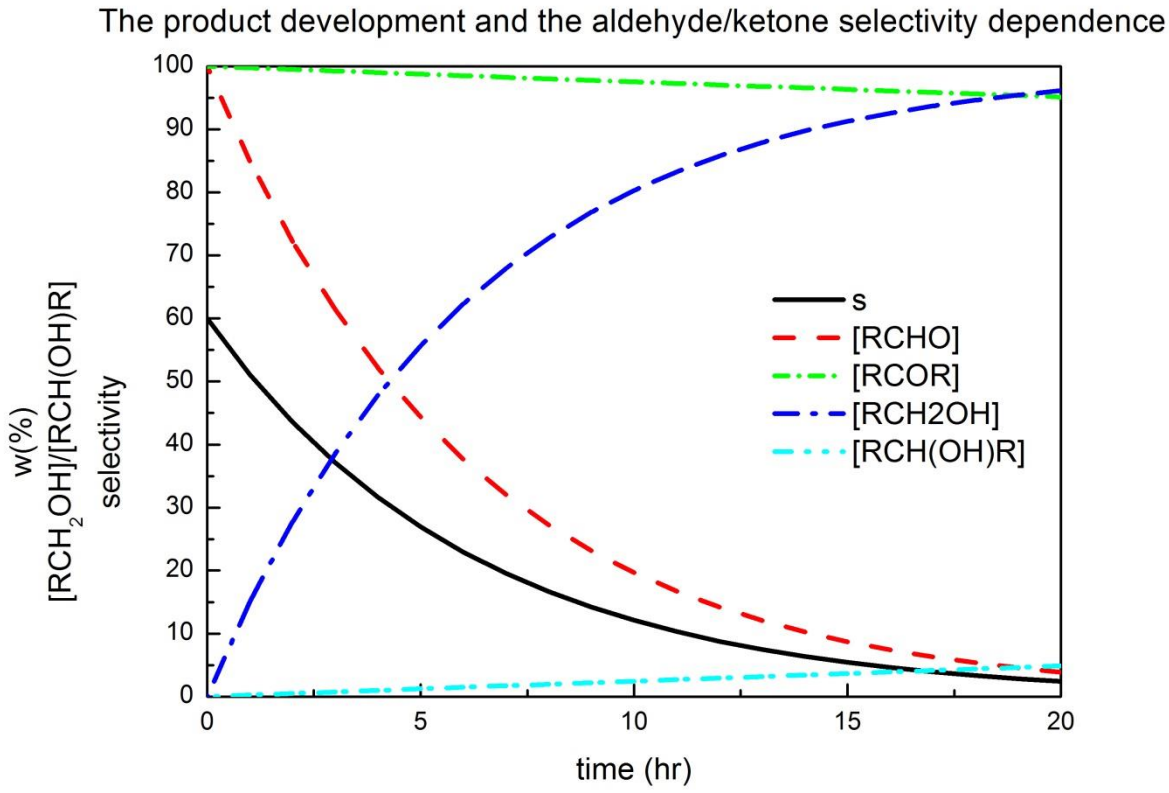

Figure 18: Model of the time dependence of the substrate and product molar ratio (in %; red, blue, green and cyan line) and selectivity (s, solid black line).

Figure 18 shows clearly that the selectivity drops dramatically with conversion and that the absolute selectivity (= 100% vs 0%) at full conversion for substrates reacting by side reactions with a common reagent is not possible.

pKa titration

The p*K*a of proflavine hydrochloride was determined by spectrophotometrical titration. The protonated form has a maximum at 443 nm whereas the neutral form has its maximum at 393 nm. The p*K*a of proflavine hydrochloride was determined to be 9.6 which corresponds to the literature data.[50] The titration profile is depicted in Figure 19. The fitted titration curves are depicted in Figure 20.

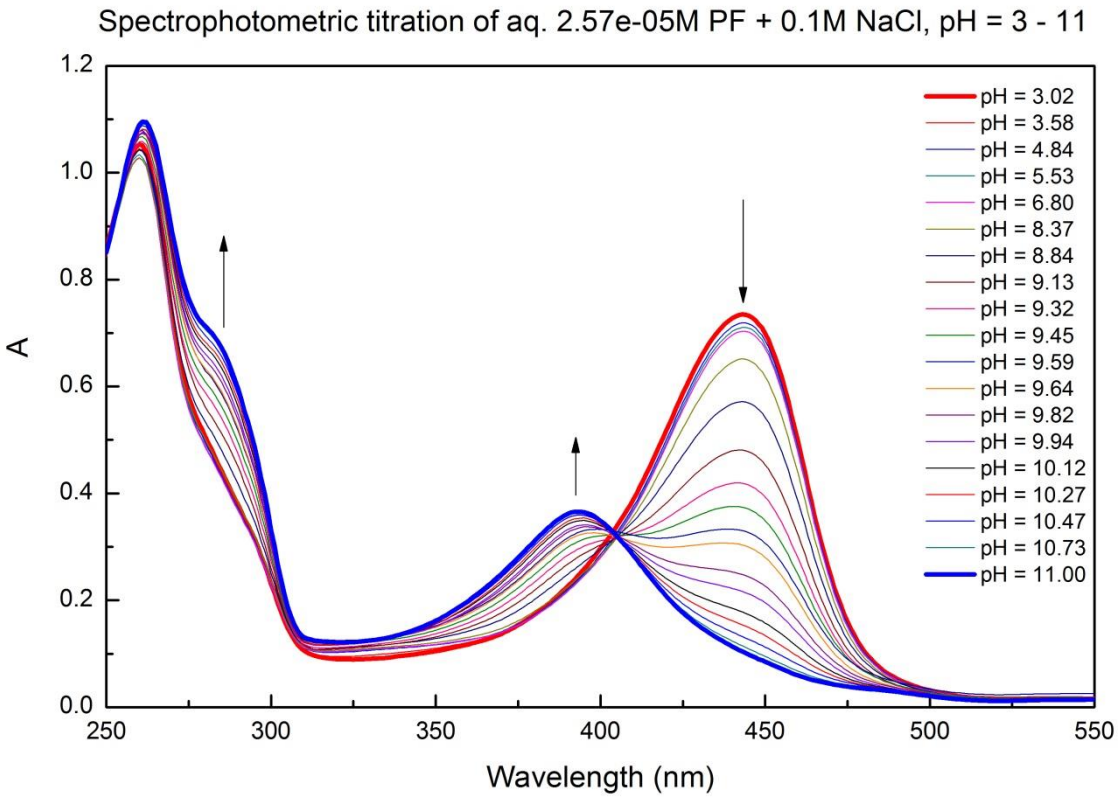

Figure 19: Spectrophotometrical titration of aq. proflavine hydrochloride (c = 2.57 × 10^{-5} M) from pH = 3.0 to pH = 11.0, 0.1 M NaCl was used to keep the ion strength constant.

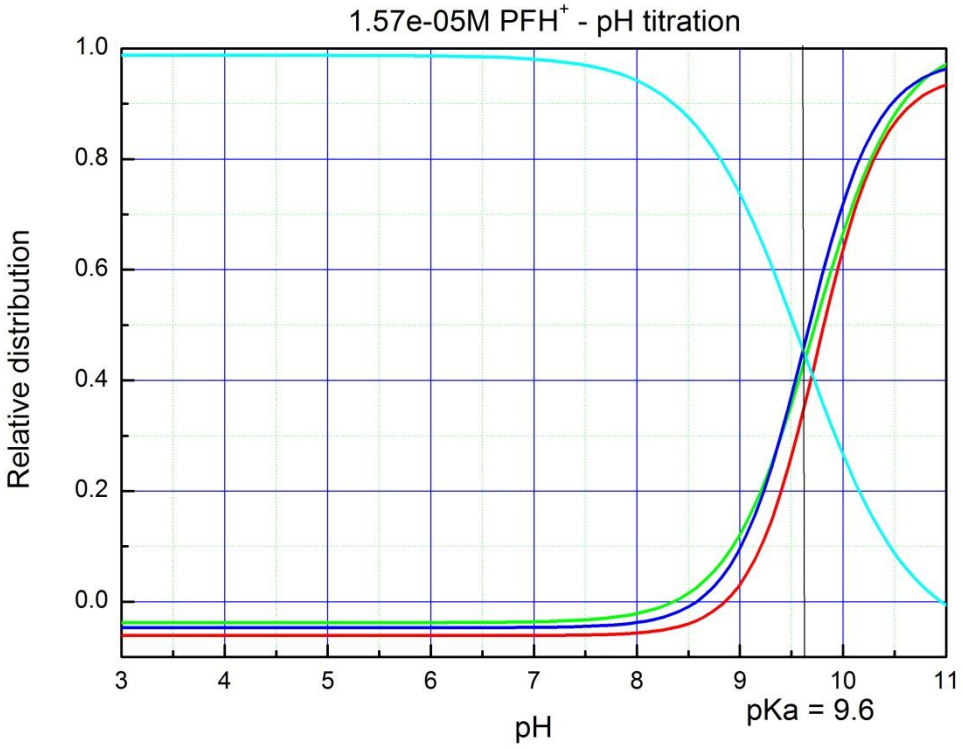

Figure 20: Titration curve of proflavine hydrochloride fitted from spectrophotometric titration, p*K*a is depicted by black vertical line.

Titration of proflavine with TEOA

Proflavine hydrochloride was also titrated by TEOA and UV-Vis spectra were recorded. The same acidobasic behavior was observed as in case of p*K*a titration.

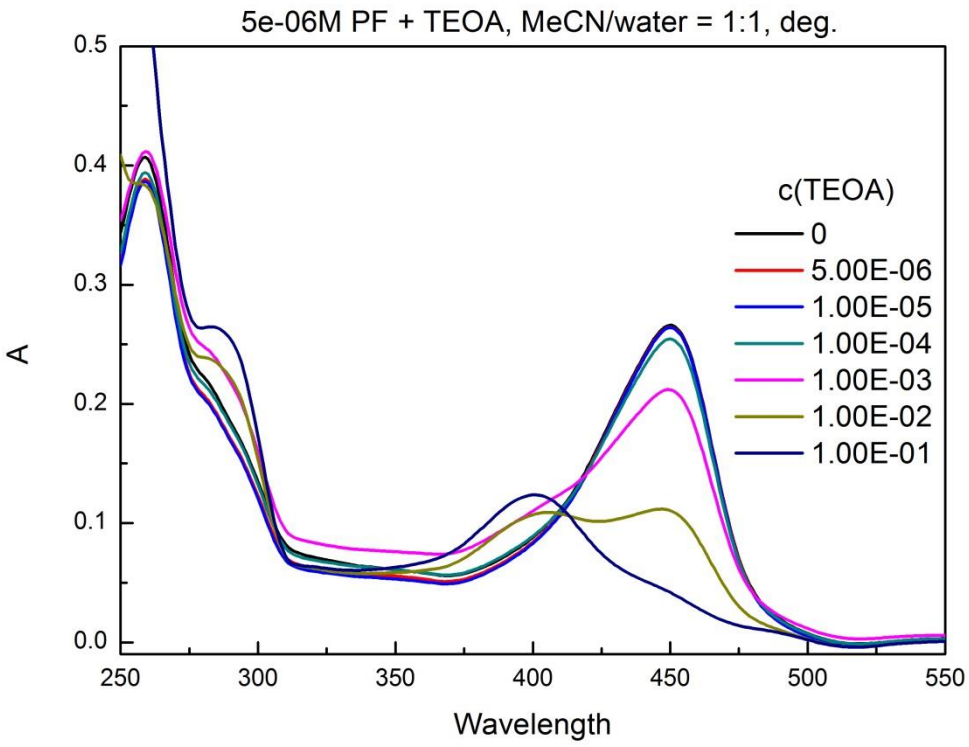

Figure 21: Titration of 5×10^{-6} M proflavine hydrochloride with TEOA in degassed acetonitrile/water 1:1 mixture.

Fluorescence studies

The fluorescence pH titration of proflavine hydrochloride is shown in Figure 22.

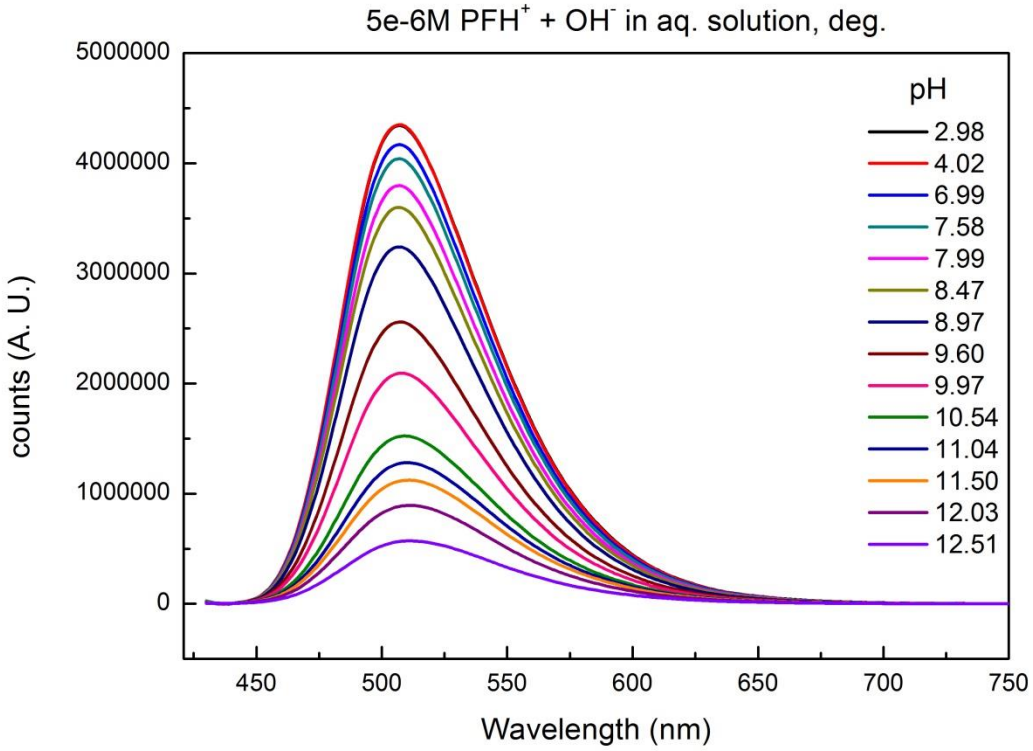

Figure 22: Fluorescence quenching of aq. proflavine hydrochloride (c = 5 × 10^{-6} M) with hydroxide ion (pH = 3 – 12.5).

The titration curve from the fluorescence maximum (λ = 508 nm) is shown in the Figure 23. The p*K*a of proflavine hydrochloride (p*K*a = 9.5) is shown with a vertical line as well as the p*K*a of excited singlet state (p*K*a = 12.5) were determined to be in inflection points of the curve. Both values correspond with the published data.[50][51]

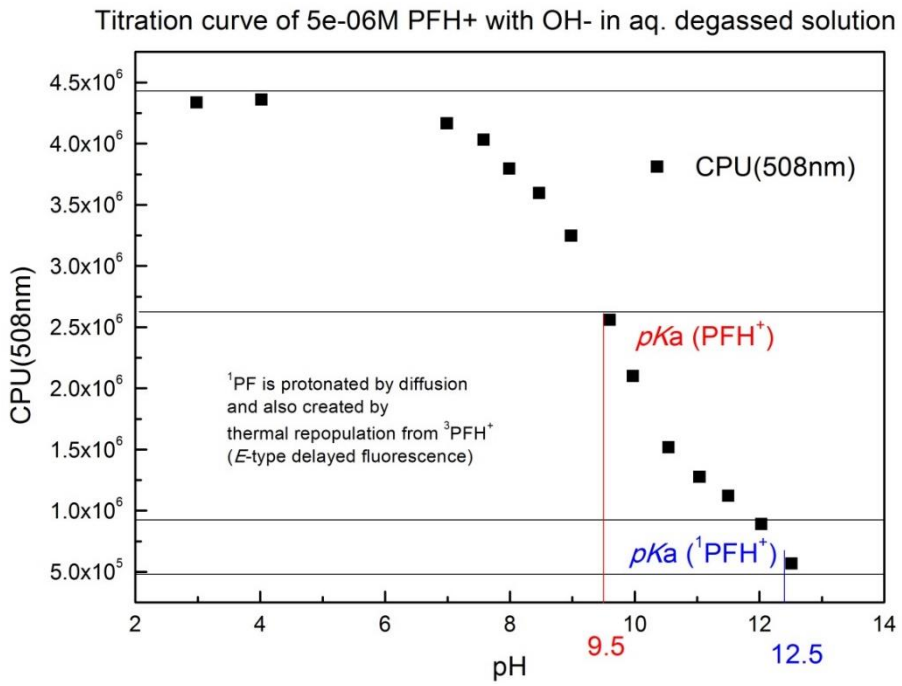

Figure 23: Fluorescence titration of proflavine hydrochloride with p*K*a values depicted.

The fluorescence titration of proflavine hydrochloride with TEOA is shown in Figure 24.

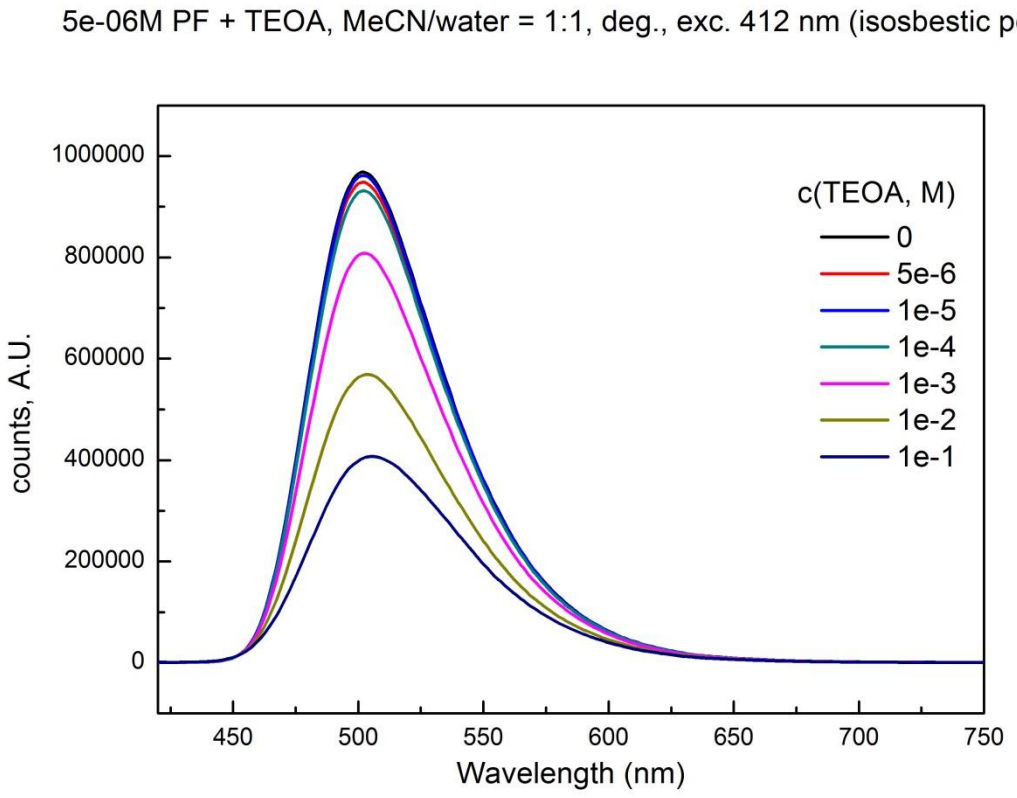

Figure 24: Fluorescence titration of proflavine hydrochloride with TEOA.

The titration curve from the fluorescence maximum (λ = 508 nm) of TEOA and OH^- is shown in the Figure 25. The equation S2 was determined experimentally. The last point of TEOA titration curve deviates from the pH titration because TEOA serves as a buffer with maximal buffer capacity at pH = 9.6 (p*K*a of $TEOAH^+$).

$$pOH = -\log[TEOA] + 2.5 \quad S2$$

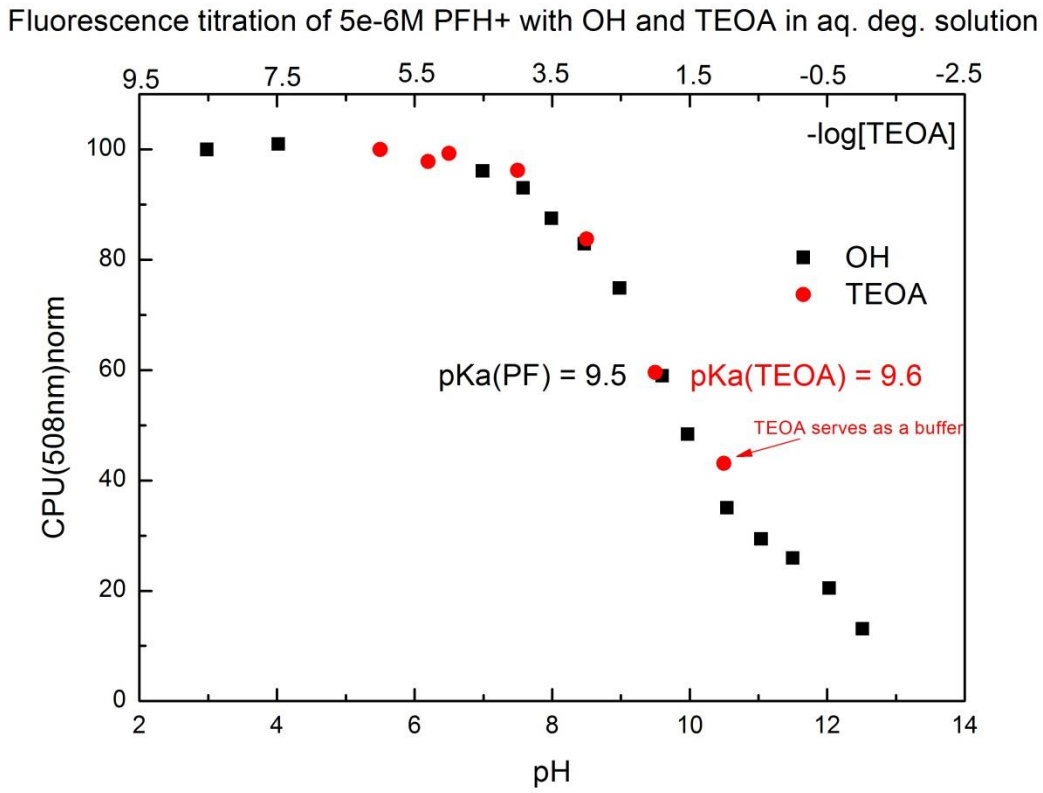

Figure 25: Comparison of titration curves of proflavine hydrochloride with OH^- and TEOA.

From fluorescence titration and TEOA UV-vis titration of proflavine hydrochloride the relative distributions of PF and PFH^+ were calculated according to equations S3 – S5.

$$\chi_{PFH^+} = 1 - \frac{I_{PFH} - I_i}{I_{PFH} - I_{PF}} \quad S3$$

$$A^{450} = \varepsilon^{PF(450)} \cdot \chi_{PF} + \varepsilon^{PFH(450)} \cdot \chi_{PFH} \quad S4$$

$$A^{401} = \varepsilon^{PF(401)} \cdot \chi_{PF} + \varepsilon^{PFH(401)} \cdot \chi_{PFH} \quad S5$$

where χ_{PFH} is the molar distribution of protonated proflavine, χ_{PF} is the molar distribution of neutral proflavine, I_{PFH} is the fluorescence intensity (λ = 508 nm) of fully protonated proflavine, I_{PF} is the fluorescence intensity (λ = 508 nm) of fully deprotonated proflavine, I_i is the fluorescence intensity (λ = 508 nm) of the actual sample, $\varepsilon^{PF(450)}$ is the molar distribution coefficient of the neutral form of proflavine, $\varepsilon^{PF(450)}$ is the molar distribution coefficient of the protonated form of proflavine and A^{450} resp. A^{401} are absorbances at relative wavelengths.

The distribution calculated from the UV-Vis measurements correspond to the ground state acidobasic reaction and the distribution calculated from the fluorescence measurement correspond to the "quenching". The comparison of these two is shown in Figure 26. Since the inflexion point of both curves lies at the same concentration of TEOA, no fluorescence quenching was observed. The partial quench would be observed if the inflexion point calculated from fluorescence would be located at lower concentration TEOA than the one calculated from UV-Vis measurement.

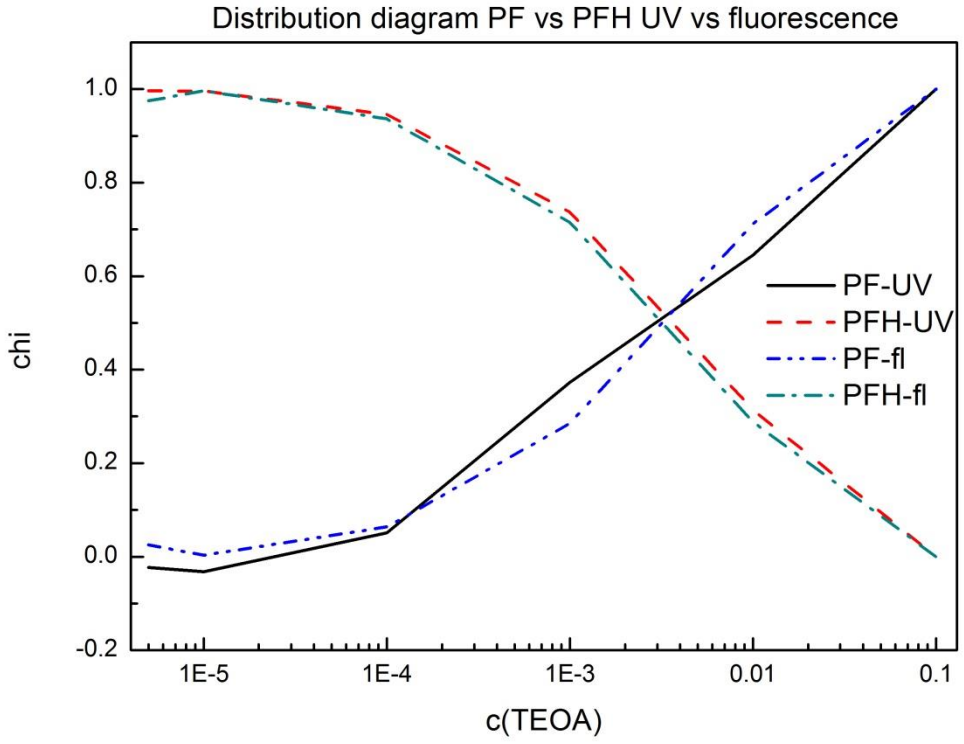

Figure 26: Distribution diagram of relative acidobasic forms of proflavine calculated from UV-Vis and fluorescence measurement.

The Stern-Volmer analysis of fluorescence titration of proflavine hydrochloride either with OH^- or TEOA is shown in Figure 27. Since the points do not lie on a straight line, the quenching is not observed in either case and the decrease of fluorescence is caused by acidobasic equilibrium between strongly fluorescent hydrochloride and weakly fluorescent neutral proflavine.

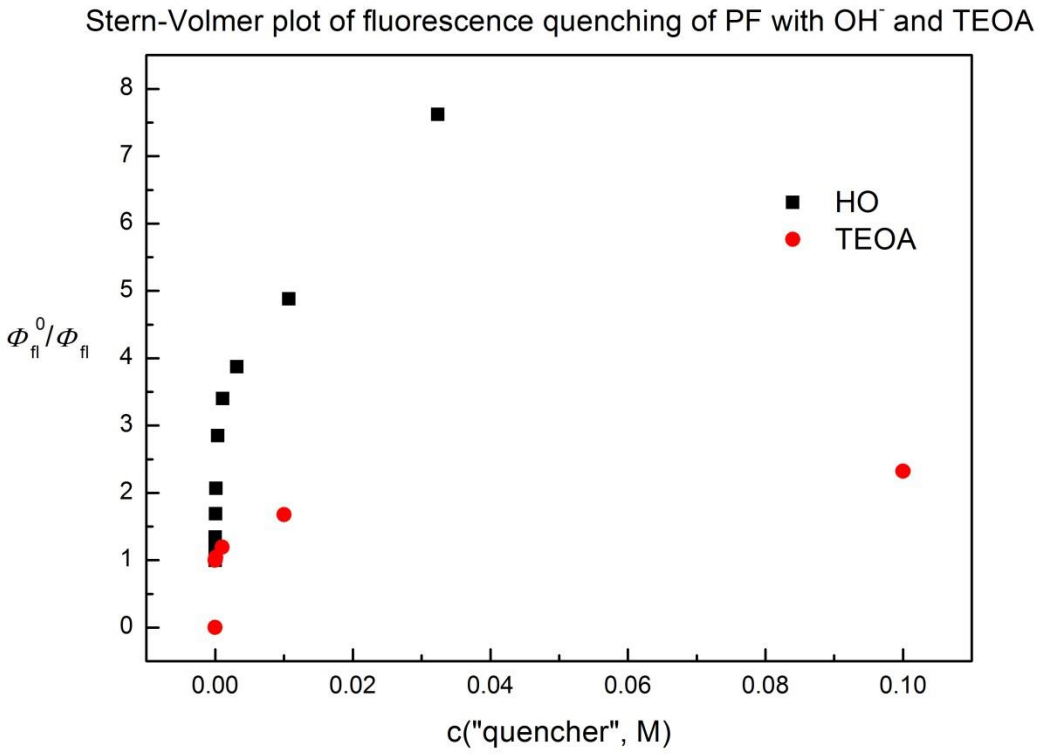

Figure 27: Stern-Volmer plot of fluorescence quenching of proflavine hydrochloride with OH^- and TEOA.

The dependence of fluorescence intensity on the intensity of excitation light was accomplished by varying the intensity of excitation beam and measuring the intensity of emitted fluorescence. The result is shown in Figure 28. The intensity of excitation light was kept low and all excitation light was absorbed by the sample.

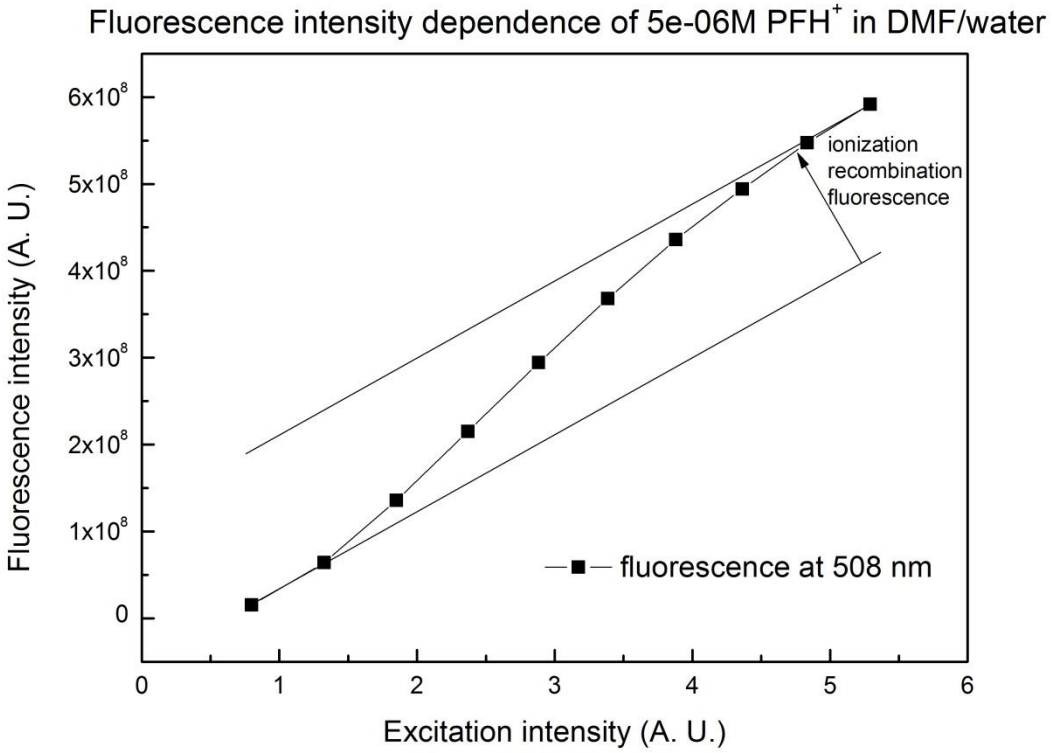

Figure 28: Dependence of fluorescence intensity on the intensity of excitation light.

The quenching of fluorescence of proflavine hydrochloride with rhodium catalyst is shown in Figure 29.

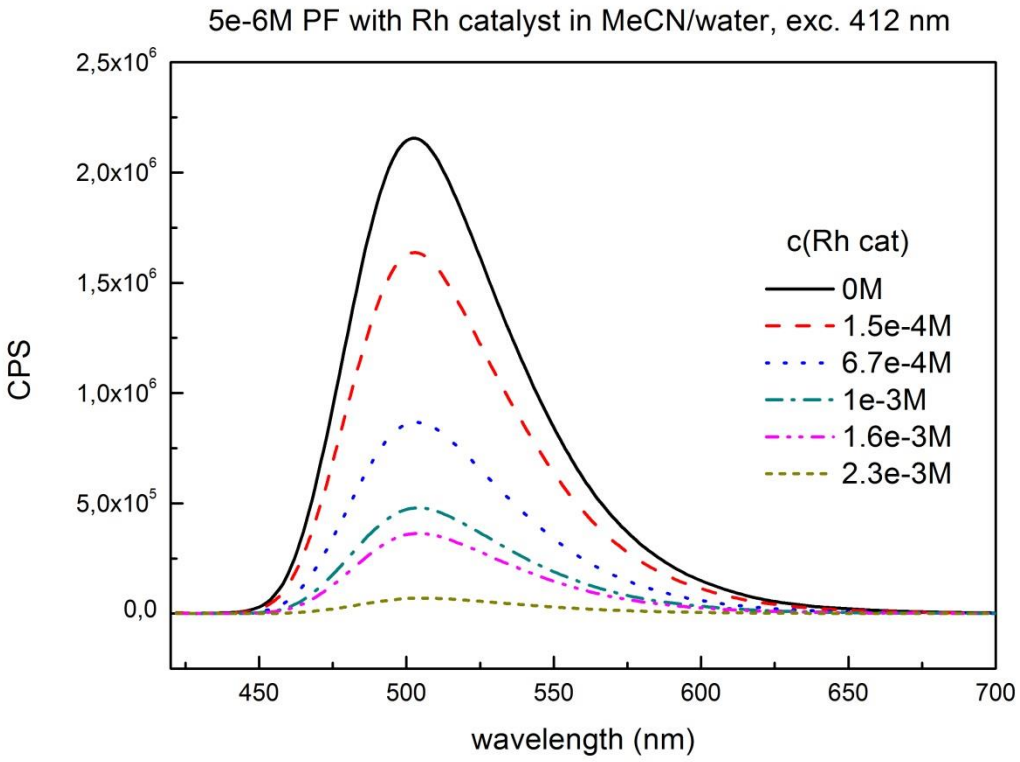

Figure 29: Fluorescence quenching of proflavine hydrochloride by rhodium catalyst.

The Stern-Volmer plot of the rhodium catalyst quenching is shown in Figure 30. The quenching constant was determined to be ~2200 M^{-1}.

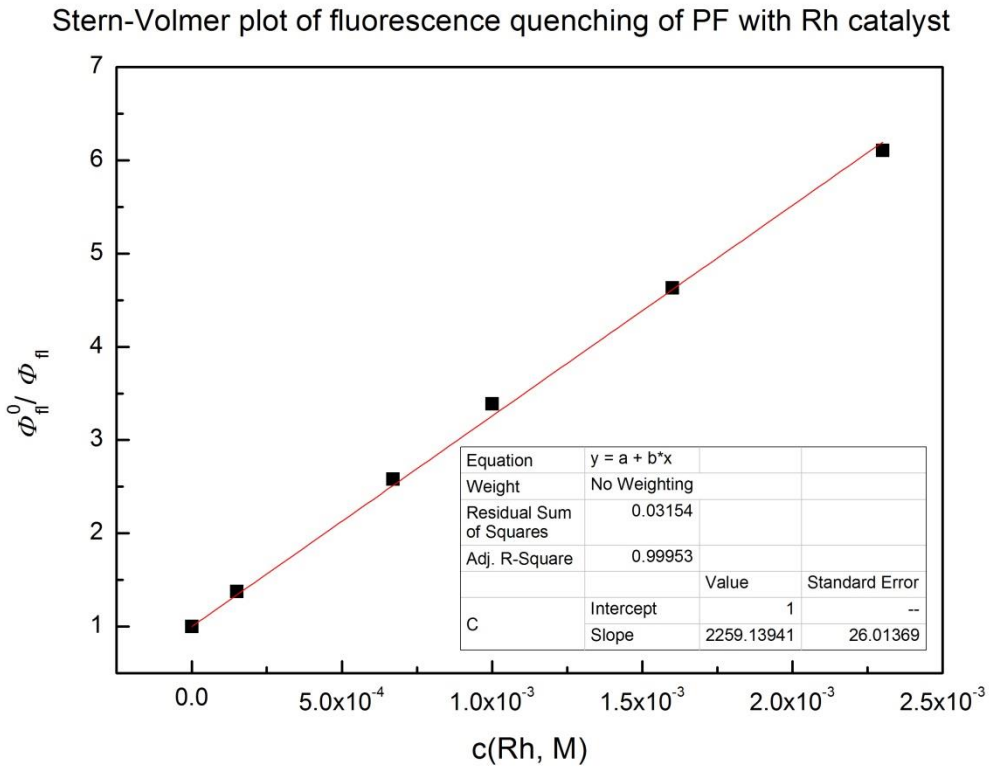

Figure 30: Stern-Volmer plot of fluorescence quenching of proflavine hydrochloride with rhodium catalyst.

Preparation of Rh(III) hydride and its characterization

The Rh(III)–H was prepared analogically to the chemical reduction general procedure. No substrate was added to the reaction mixture and the concentration of rhodium catalyst was 0.2 mM.

The UV-Vis spectra of the parent complex and the Rh^{III} hydride are shown in Figure 31.

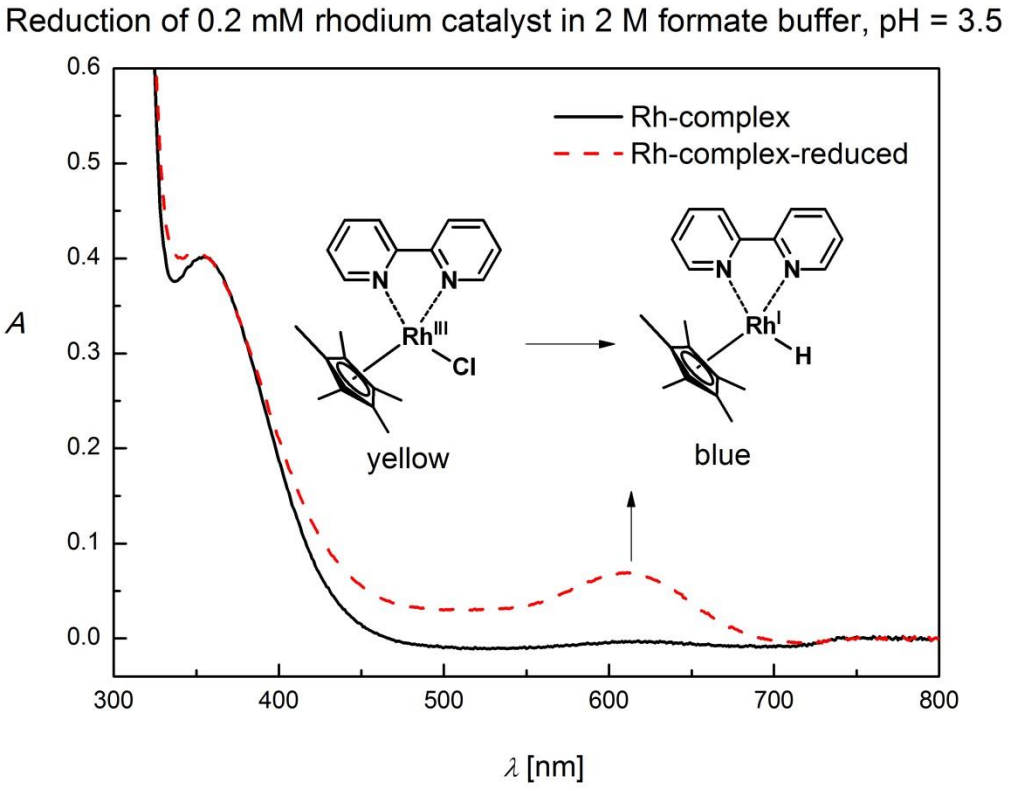

Figure 31: UV-Vis spectra of Rh_{cat} and Rh(III)–H.

The Rh(III)–H was detected in the typical reaction mixture without substrate after 15 hours of irradiation at 455 nm. After the solution was bubbled with oxygen, the Rh^{III} hydride was re-oxidized and the shoulder at 612 nm disappeared. The results are shown in Figure 32.

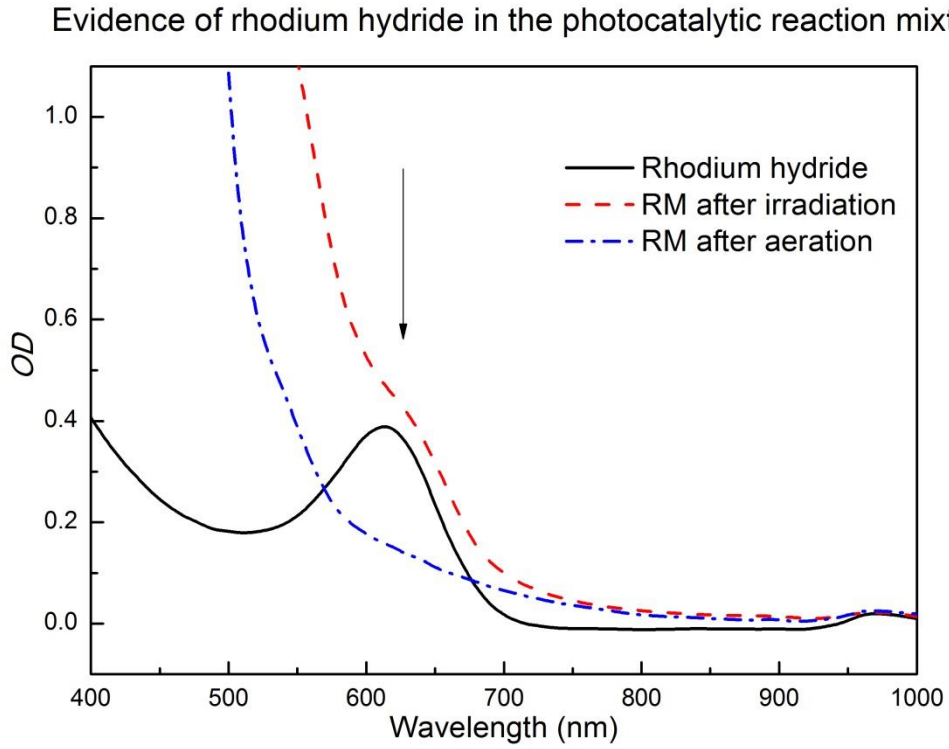

Figure 32: UV-Vis evidence of Rh(III)–H present in the photocatalytic reaction mixture after 15 hours of irradiation at 455 nm.

Irradiation of proflavine

Proflavine is not photostable. The results of the irradiation of proflavine solutions with various components are shown in Figures 33 – 36. The photoproducts TSG249A1 and TSG249A2 were isolated from a typical reaction mixture without substrate and rhodium catalyst. The photoproducts were not fully characterized; only UV-Vis and fluorescence spectra were measured (Figure 37).

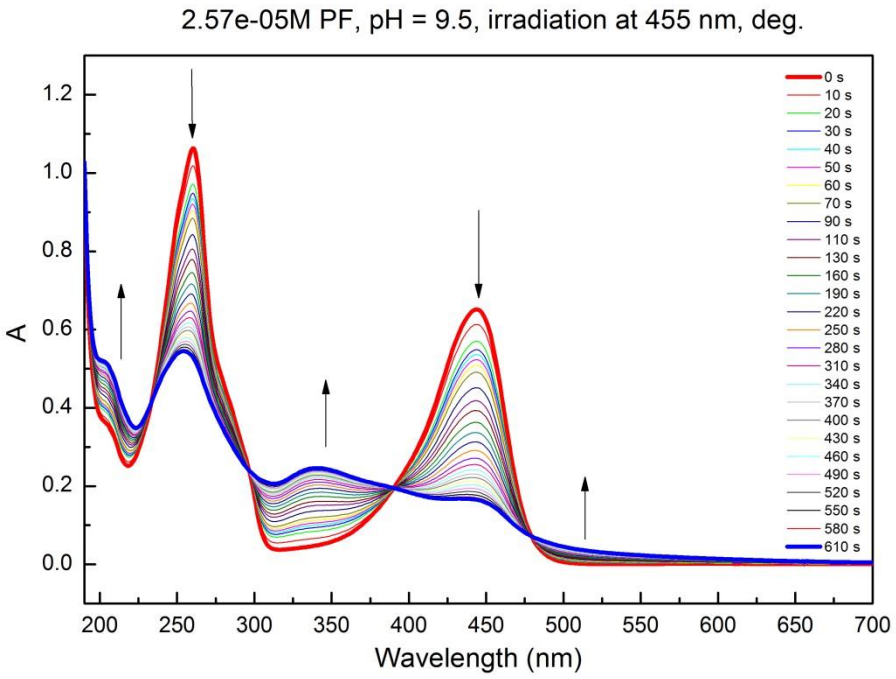

Figure 33: UV-Vis spectra of proflavine hydrochloride (2.57×10^{-5} M) irradiated at 455 nm in 1:1 MeCN/water.

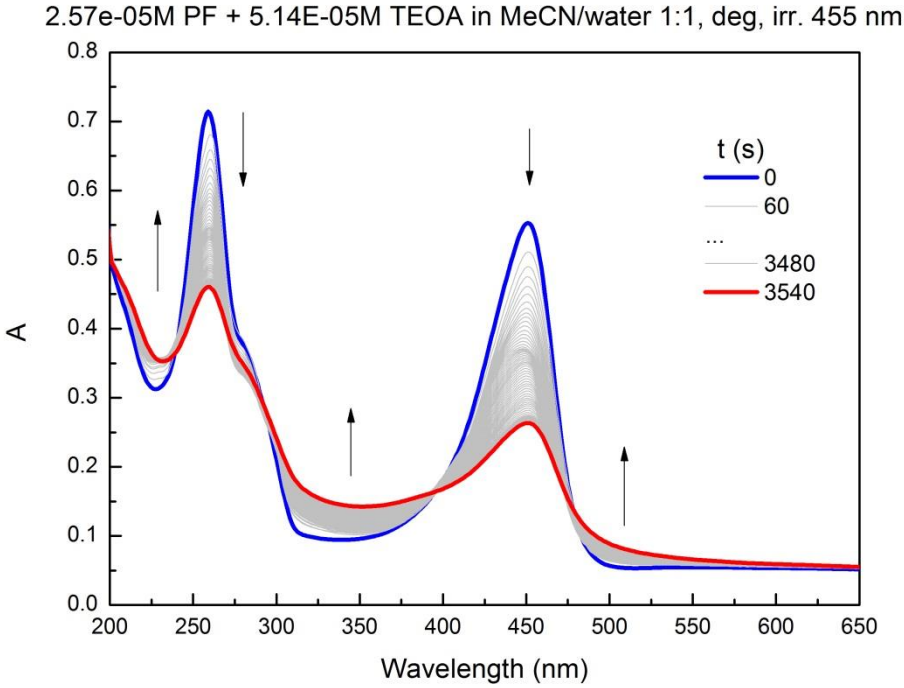

Figure 34: UV-Vis spectra of proflavine hydrochloride (2.57×10^{-5} M) and TEOA (2 eq.) irradiated at 455 nm in 1:1 MeCN/water.

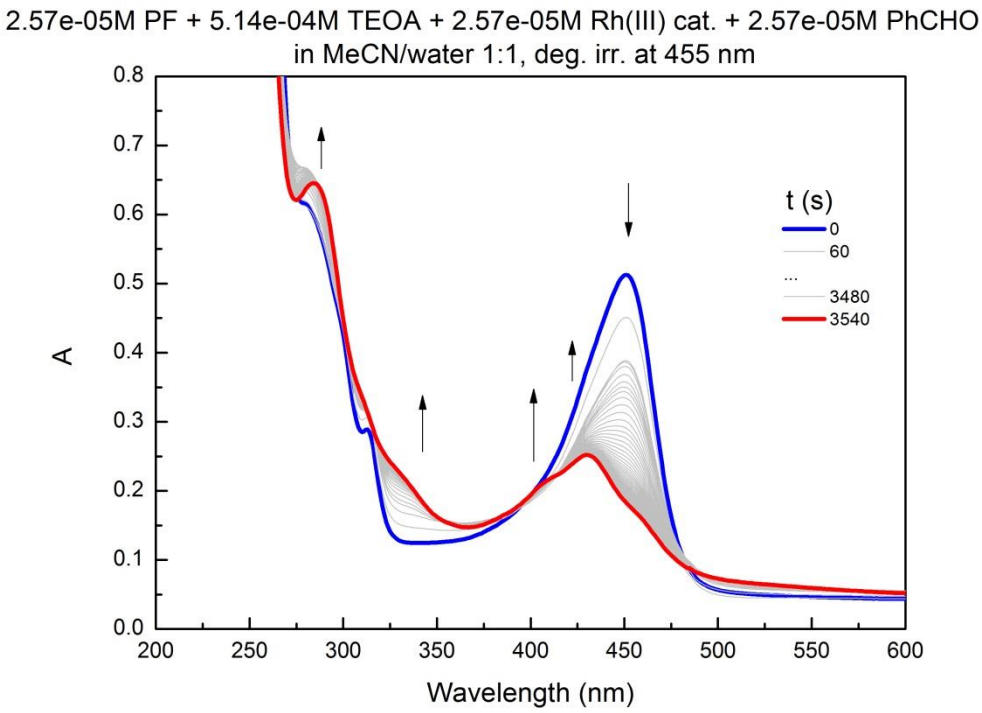

Figure 35: UV-Vis spectra of proflavine hydrochloride (2.57×10^{-5} M), TEOA (2 eq.) and benzaldehyde (2.57×10^{-4} M) irradiated at 455 nm in 1:1 MeCN/water.

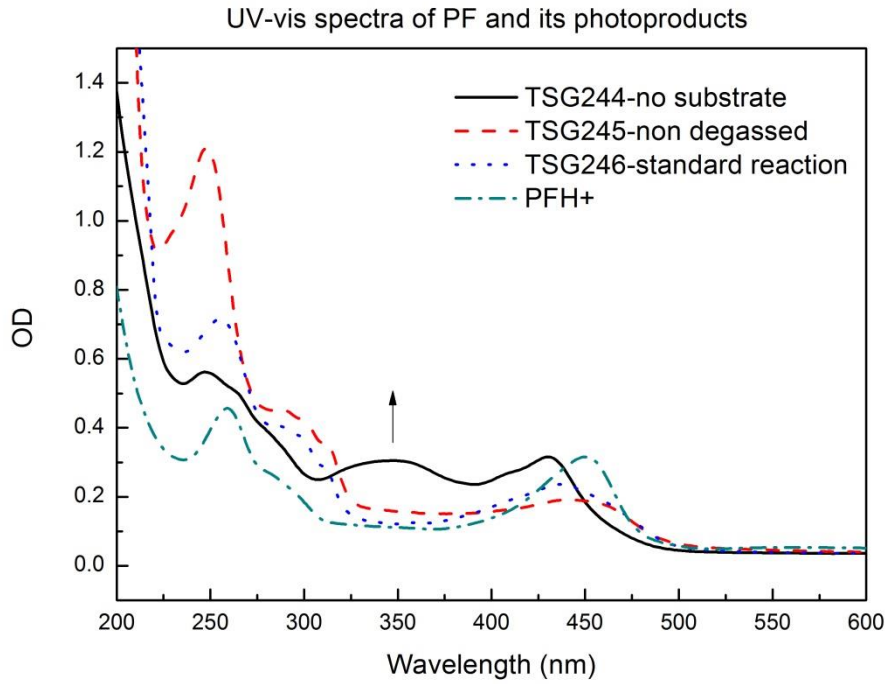

Figure 36: UV-Vis spectra of various photoreactions (the typical reaction mixture without substrate and rhodium catalyst– black line; the non-degassed typical reaction mixture – red line; the typical reaction mixture – blue line, proflavine UV-Vis spectrum – green line).

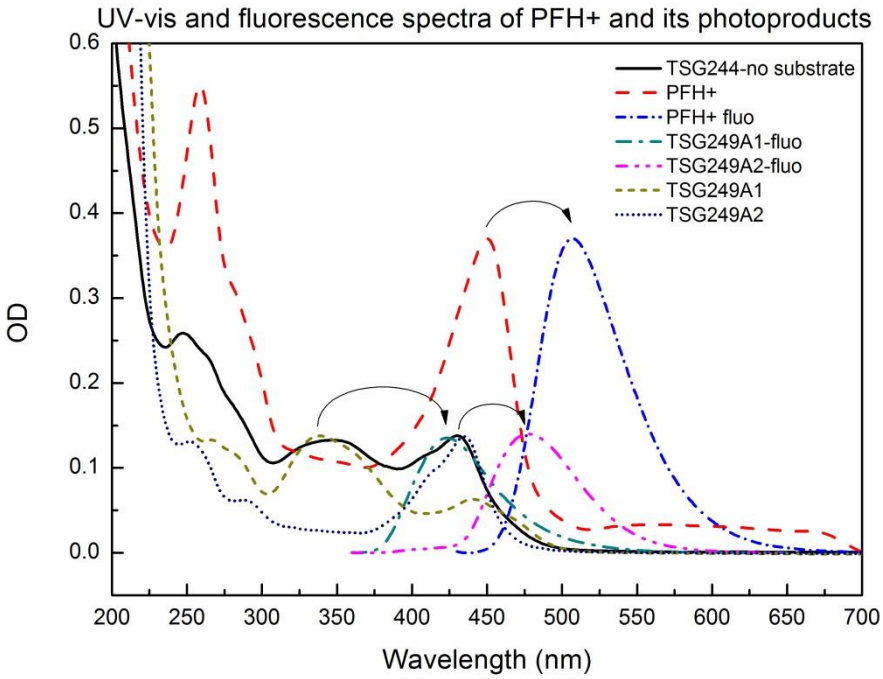

Figure 37: UV-Vis spectra of various proflavine (PFH+) photoproducts (TSG249A1 and TSG249A2) and their fluorescence spectra (PFH+ fluo, TSG249A1-fluo and TSG249A2-fluo) normalized to the height of the absorption peak; the curly arrow indicates the Stokes shift. The black solid line corresponds to the photoproduct of the typical reaction without substrate and rhodium catalyst.

3.4.4 Transient spectroscopy

The transient spectra were measured with time window of 50 ns (= period of signal accumulation). All spectra were smoothed by Savitzky-Golay method (points of window = 100) in program OriginPro 8.

Transient spectra were measured at various times after the flash. The time is depicted in legend in the figures.

The transient spectra of proflavine triplet are depicted in Figure 38. The triplet was identified according to the characteristic absorption peaks at 550, 610 and 670 nm.[52] The estimated lifetime of proflavine triplet is 2 μs.

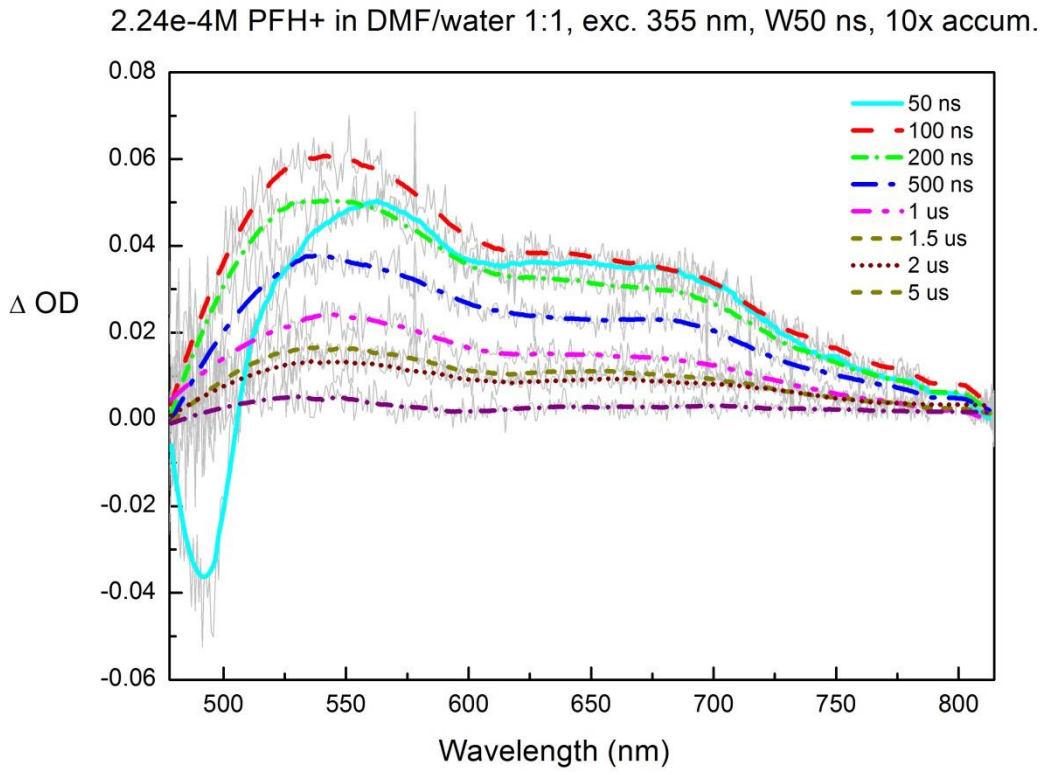

Figure 38: Transient absorption spectra of proflavine hydrochloride in DMF/water 1:1, (*c* = 2.24 × 10^{-4} M) bubbled with nitrogen, excitation wavelength λ_{ex} = 355 nm; time window 50 ns, 10 × accumulated.

The transient spectra of proflavine radical anion are depicted in Figure 39. The radical anion was identified according to the characteristic absorption peak at 530 nm.[31][40] The estimated lifetime of proflavine triplet is 8 μs.

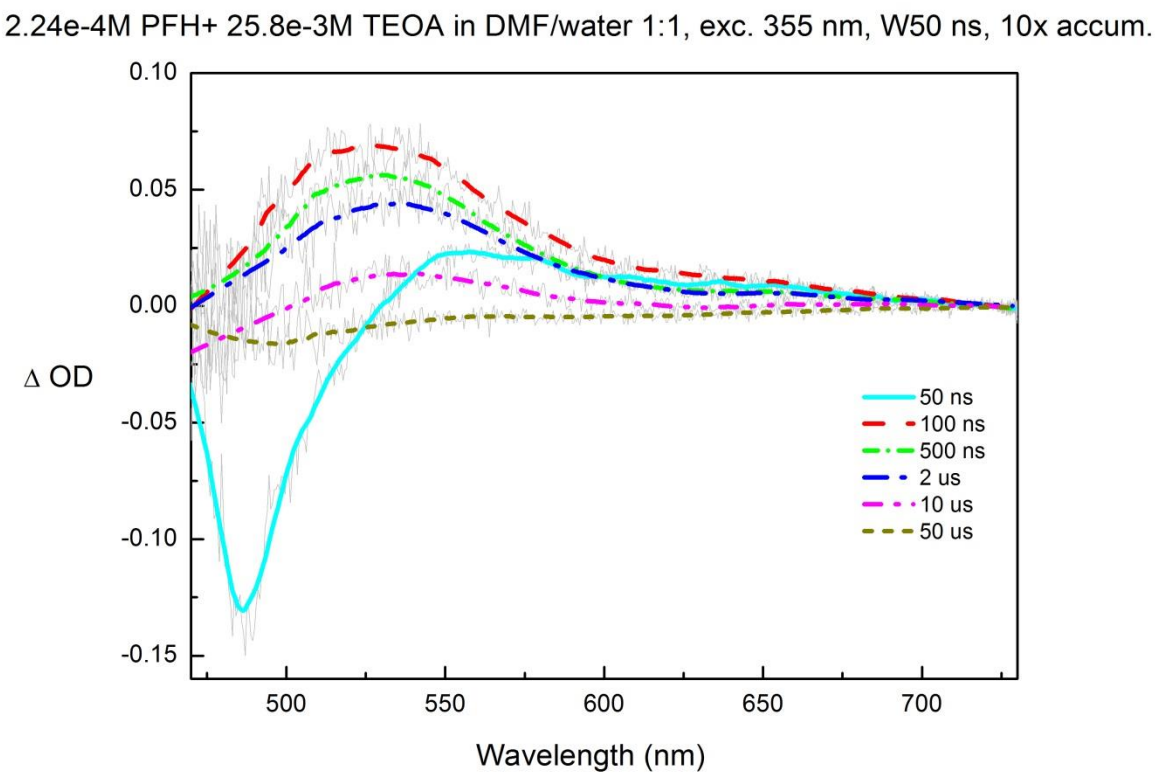

Figure 39: Transient absorption spectra of proflavine hydrochloride (c = 2.24 × 10^{-4} M) and TEOA (c = 25.8 × 10^{-3} M) in DMF/water 1:1, bubbled with nitrogen, excitation wavelength λ_{ex} = 355 nm; time window 50 ns, 10 × accumulated.

The transient spectra of proflavine hydrochloride with rhodium catalyst are depicted in Figure 40. The triplet is still observed but the intensity is lower.

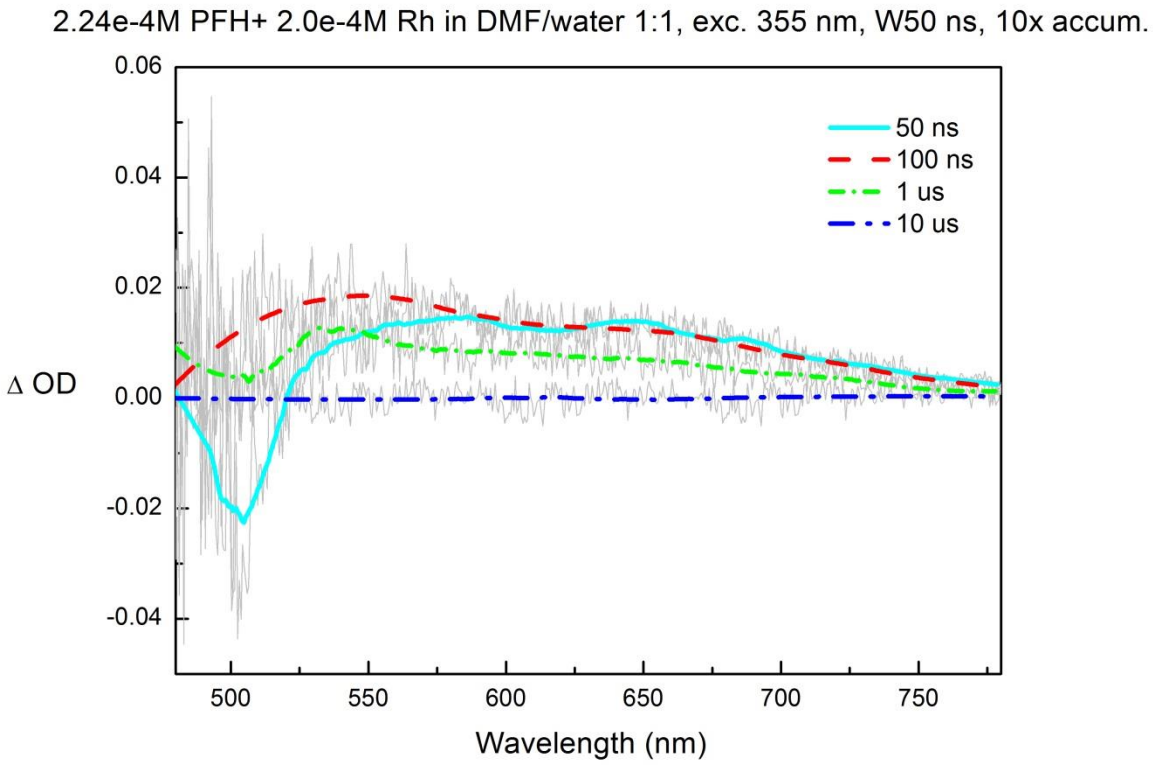

Figure 40: Transient absorption spectra of proflavine hydrochloride (c = 2.24 × 10^{-4} M) and rhodium catalyst (c = 2.0 × 10^{-4} M) in DMF/water 1:1, bubbled with nitrogen, excitation wavelength λ_{ex} = 355 nm; time window 50 ns, 10 × accumulated.

The transient spectra of proflavine hydrochloride with rhodium catalyst and TEOA are depicted in Figure 41. The proflavine radical anion is observed and the lifetime drops.

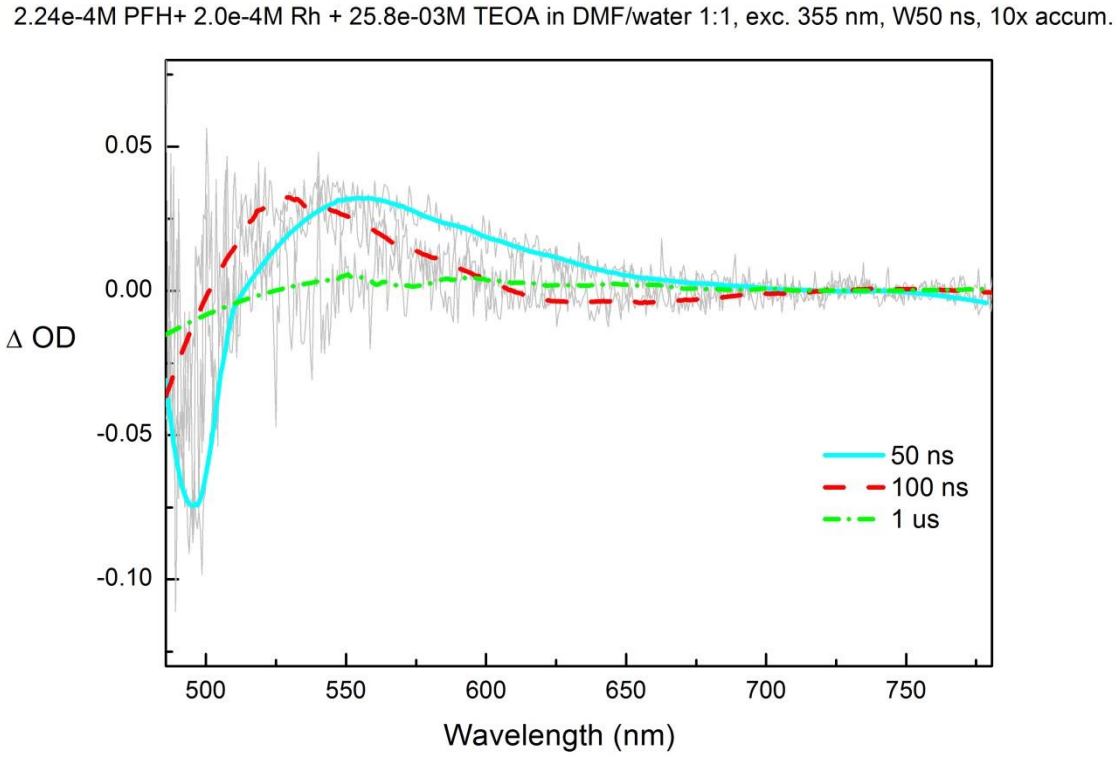

Figure 41: Transient absorption spectra of proflavine hydrochloride (c = 2.24 × 10^{-4} M), rhodium catalyst (c = 2.0 × 10^{-4} M) and TEOA (c = 2.58 × 10^{-2} M) in DMF/water 1:1, bubbled with nitrogen, excitation wavelength λ_{ex} = 355 nm; time window 50 ns, 10 × accumulated.

The transient spectra of rhodium catalyst are depicted in Figure 42.

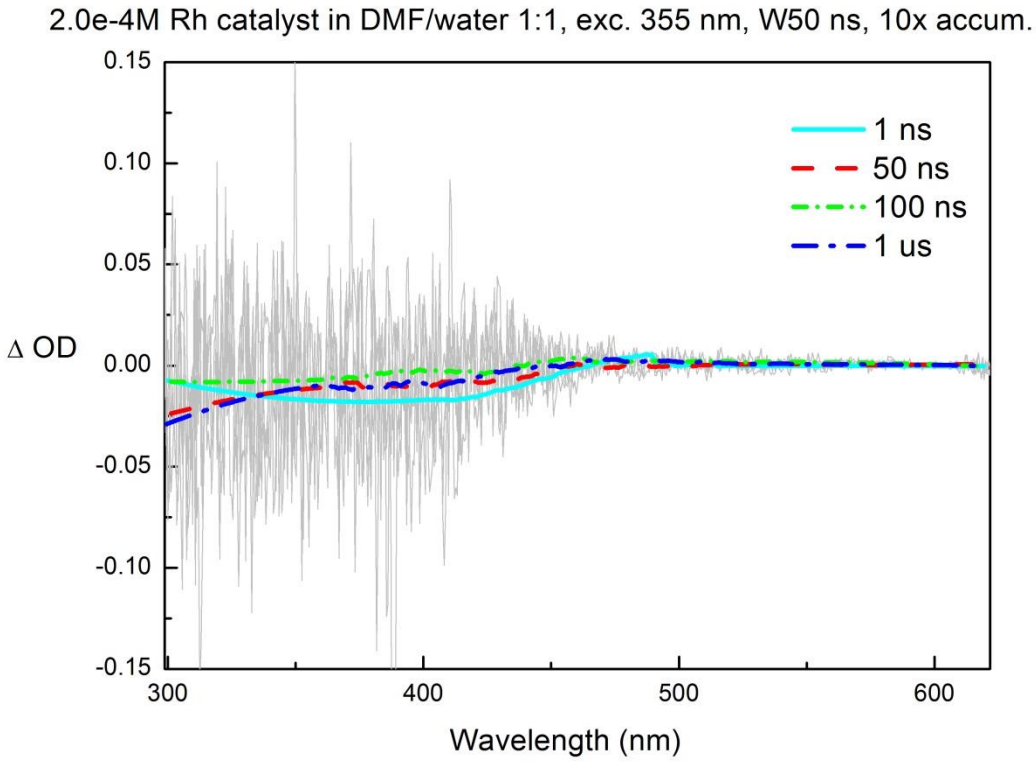

Figure 42: Transient absorption spectra rhodium catalyst (c = 2.0 × 10^{-4} M) in DMF/water 1:1, bubbled with nitrogen, excitation wavelength λ_{ex} = 355 nm; time window 50 ns, 10 × accumulated.

The overlay of the signal of the solution of proflavine hydrochloride and the solution of proflavine hydrochloride and rhodium catalyst at 100 ns after the pulse is shown in Figure 43.

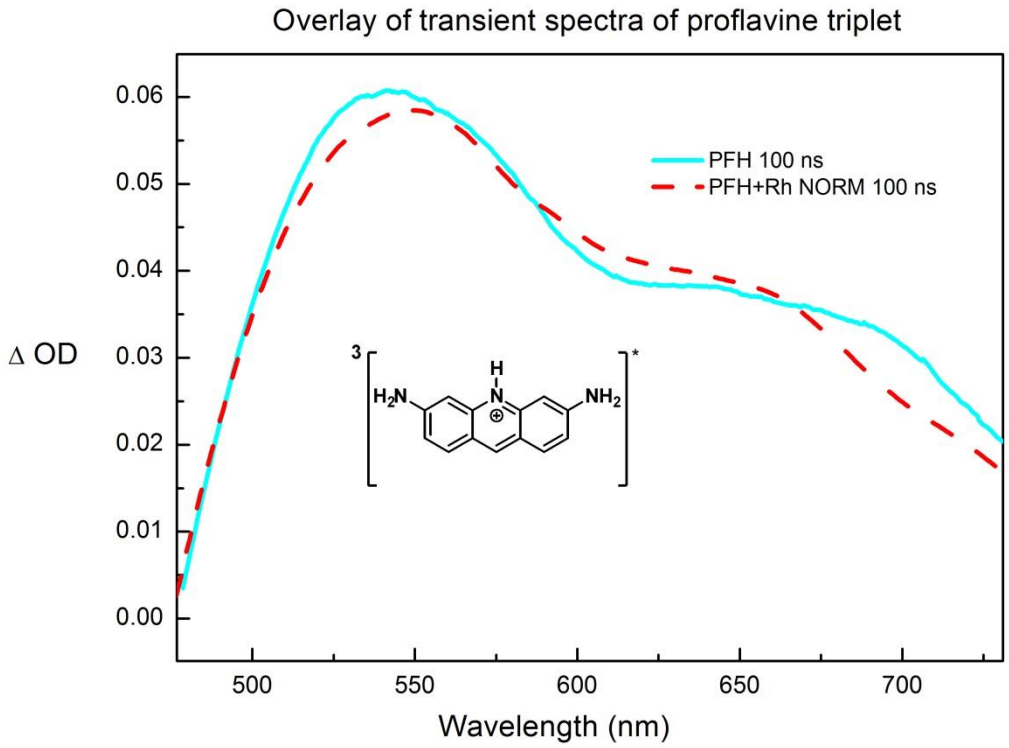

Figure 43: Overlay of transient absorption spectra of proflavine hydrochloride and a mixture of proflavine hydrochloride and rhodium catalyst (normalized) at 100 ns after the pulse.

The overlay of the signal of the solution of proflavine hydrochloride and TEOA and the solution of proflavine hydrochloride, rhodium catalyst and TEOA (normalized) at 100 ns after the pulse is shown in Figure 44.

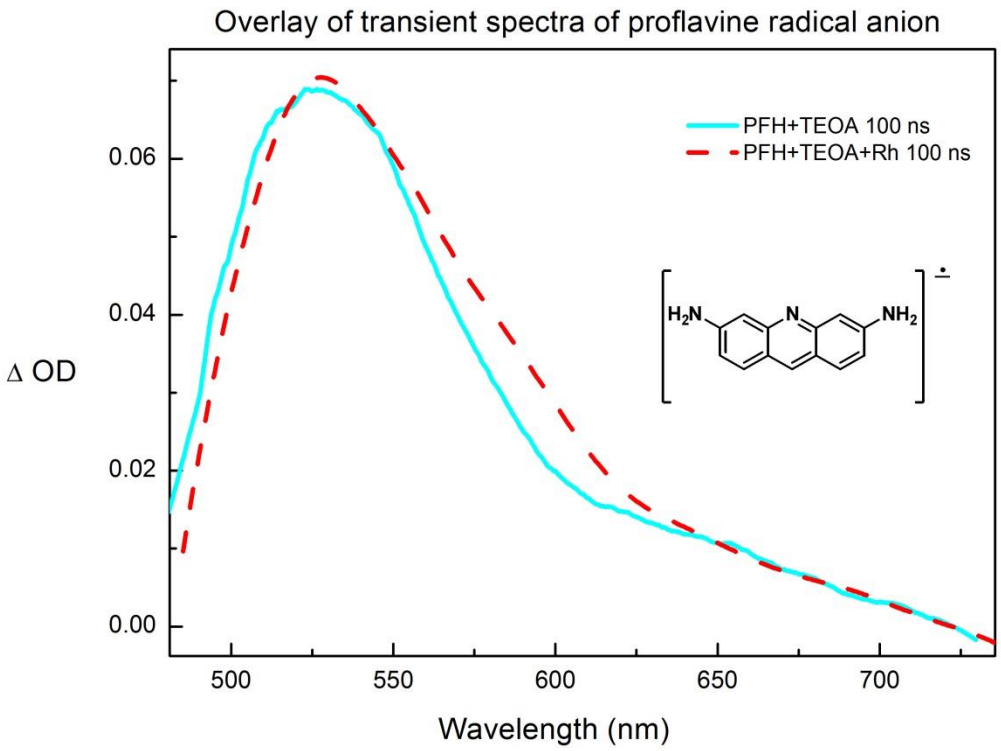

Figure 44: Overlay of transient absorption spectra of proflavine hydrochloride and TEOA and the solution of proflavine hydrochloride, rhodium catalyst and TEOA (normalized) at 100 ns after the pulse.

3.4.5 NMR spectra and others

Figure 45: ^{1}H NMR spectrum of [Cp*Rh(bpy)Cl]Cl.

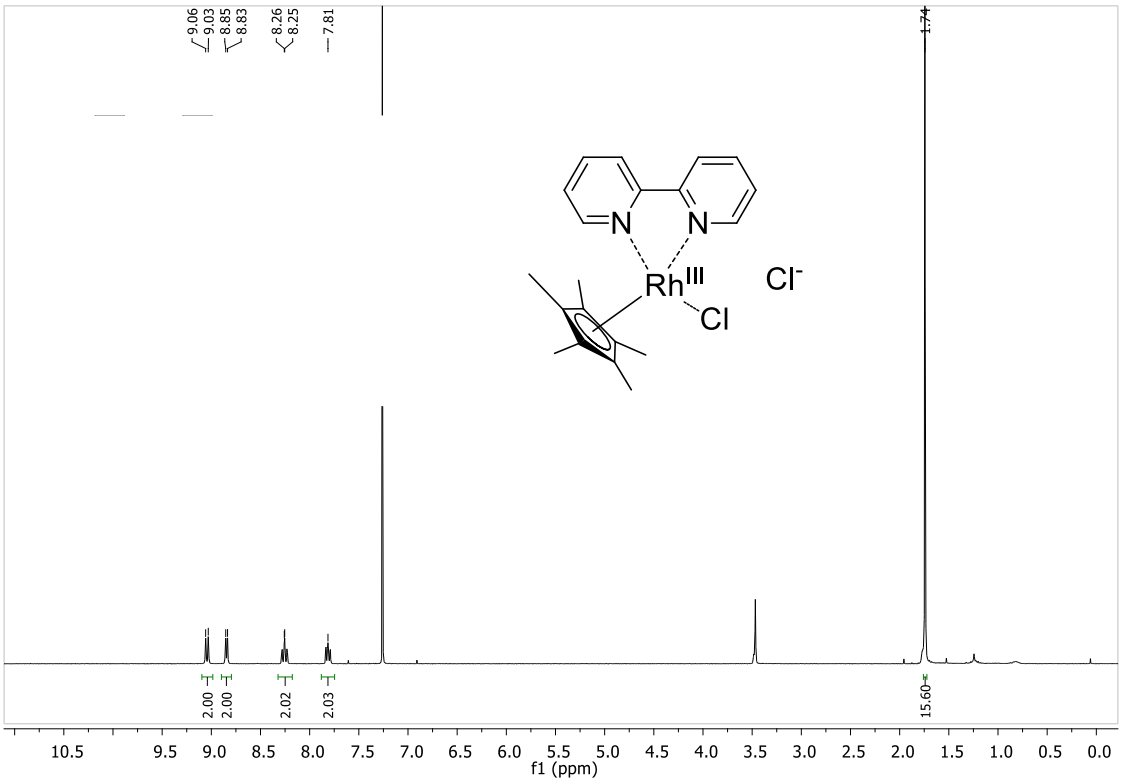

Figure 46: ^{1}H NMR spectrum of 1-(4-(hydroxymethyl)phenyl)ethanone.

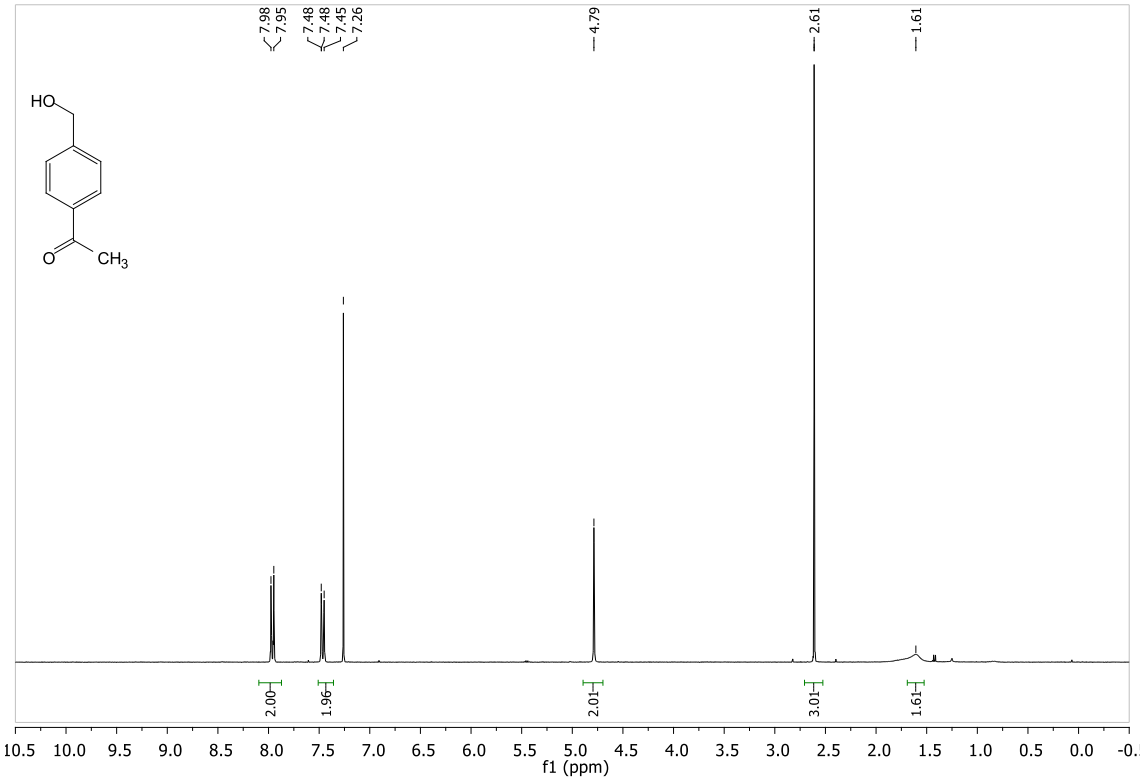

Figure 47: ^{13}C NMR spectrum of 1-(4-(hydroxymethyl)phenyl)ethanone.

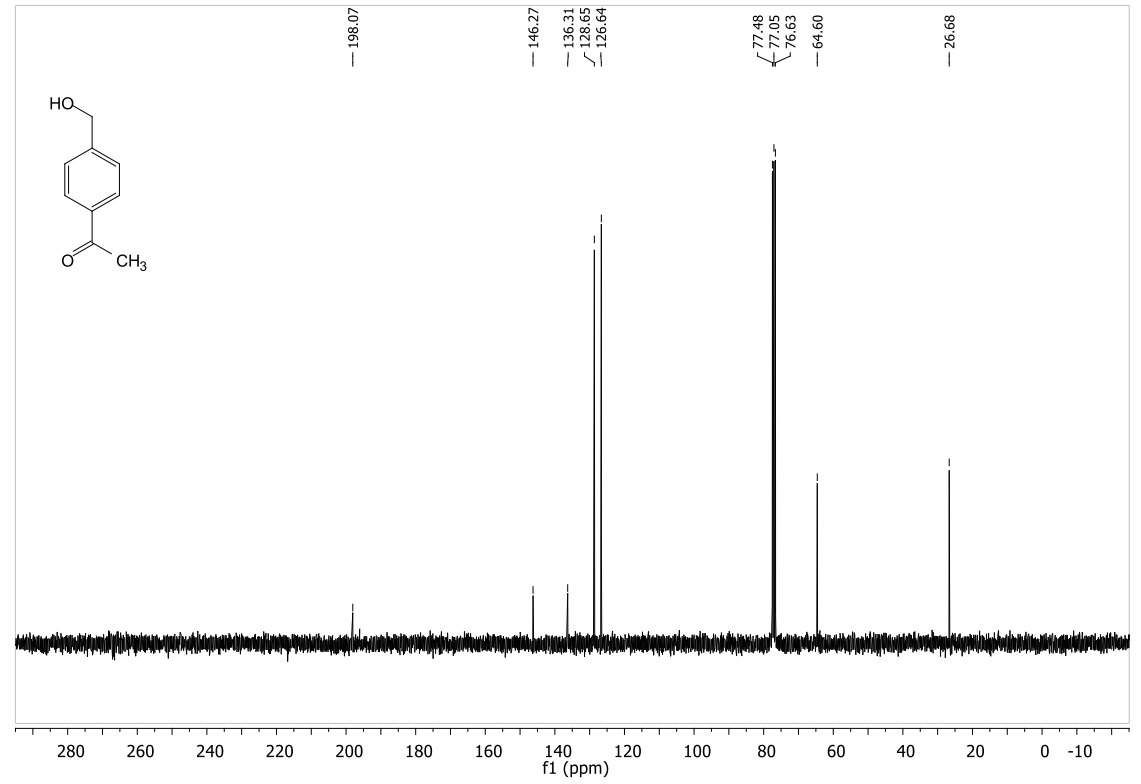

Figure 48: ^{1}H NMR spectrum of methyl 4-(1-hydroxyethyl)benzoate.

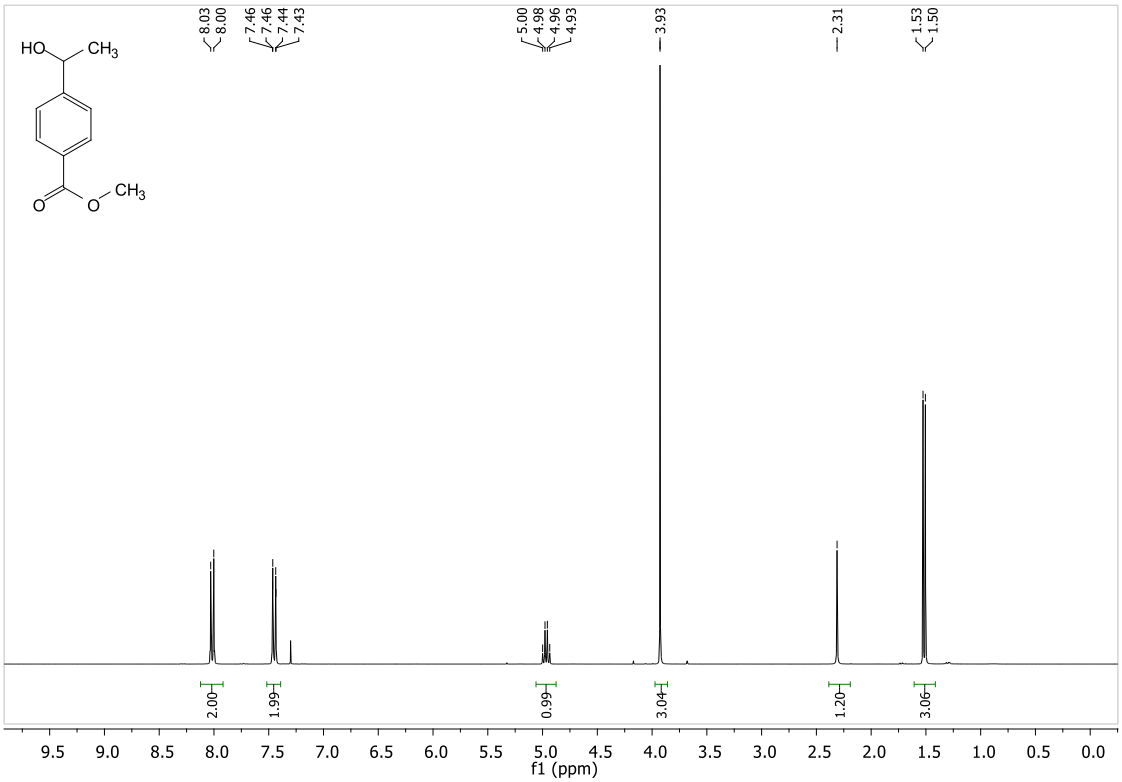

Figure 49: ^{13}C NMR spectrum of methyl 4-(1-hydroxyethyl)benzoate.

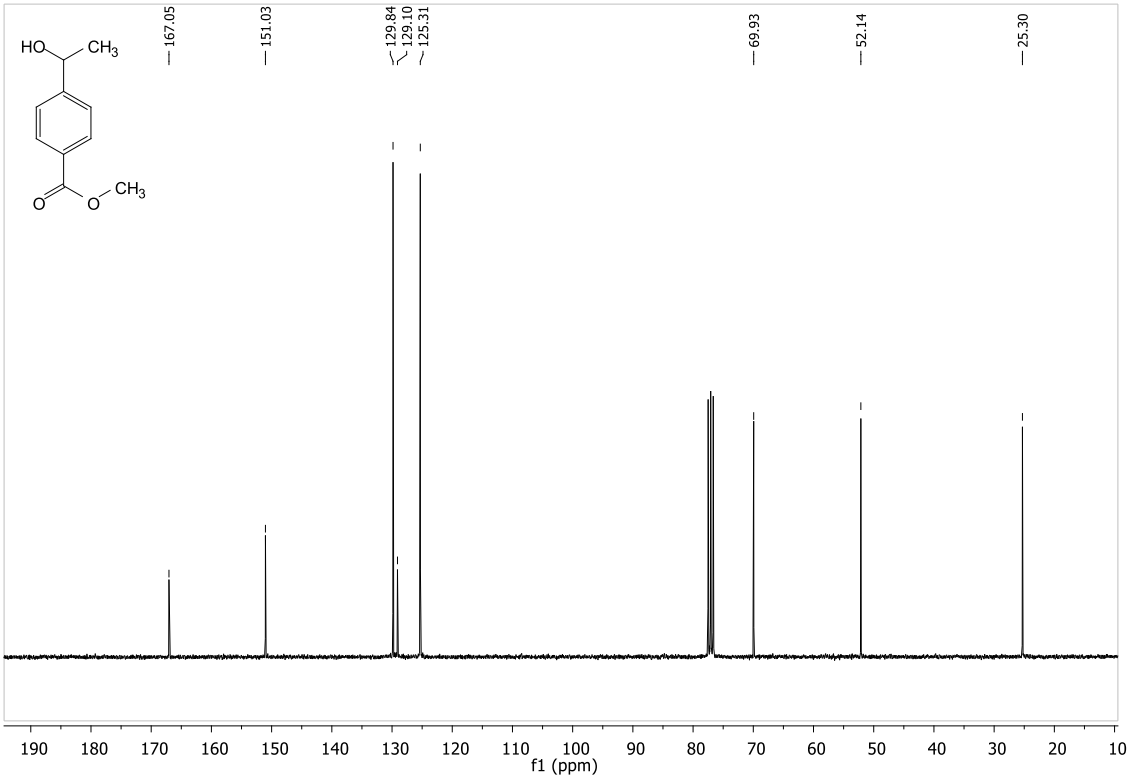

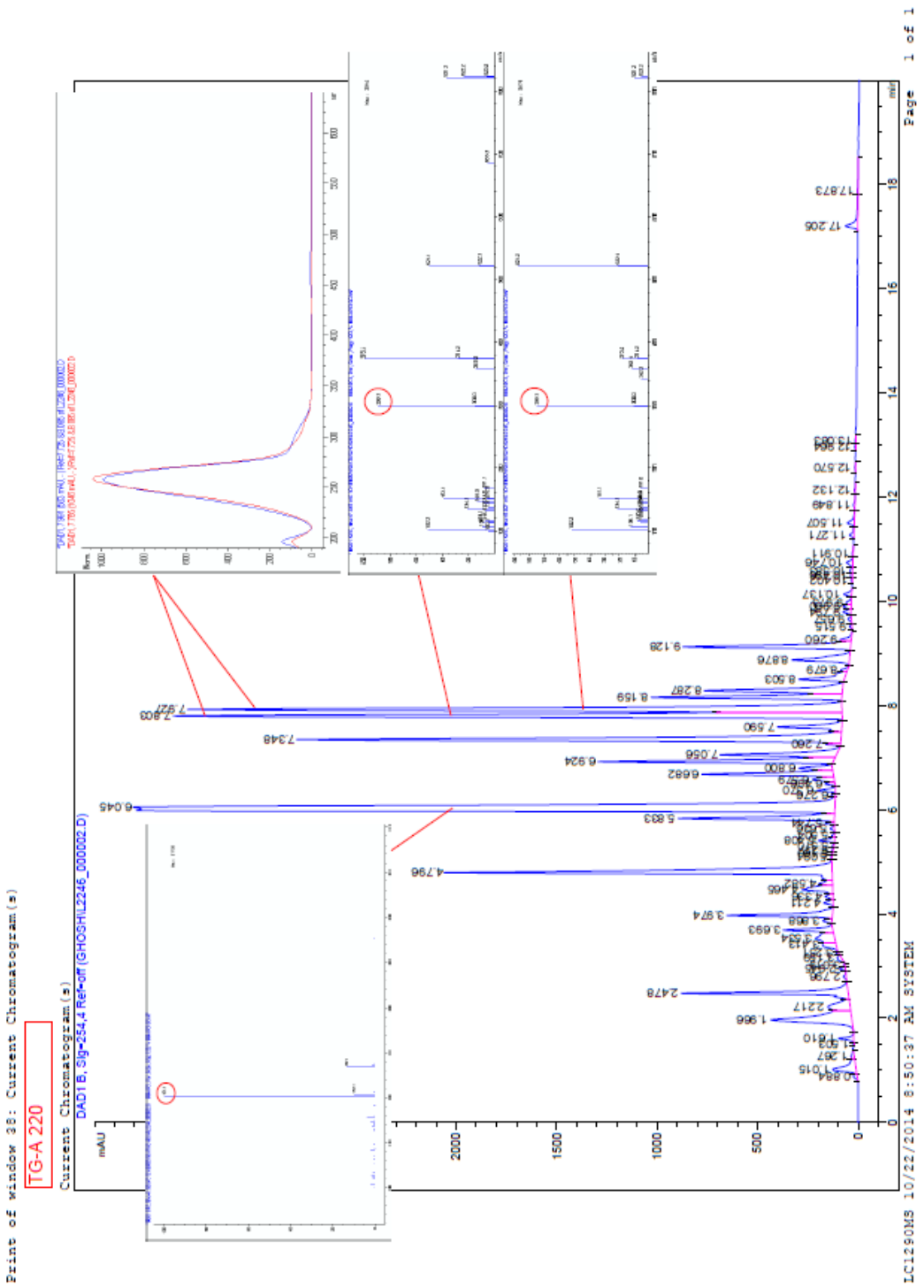

Figure 50: HPLC-MS analysis result for the photochemical reduction of 4-formyl acetophenone; the pinacol products $M+H^+$ (m/z = 299.1; two diastereomers) are indicated.

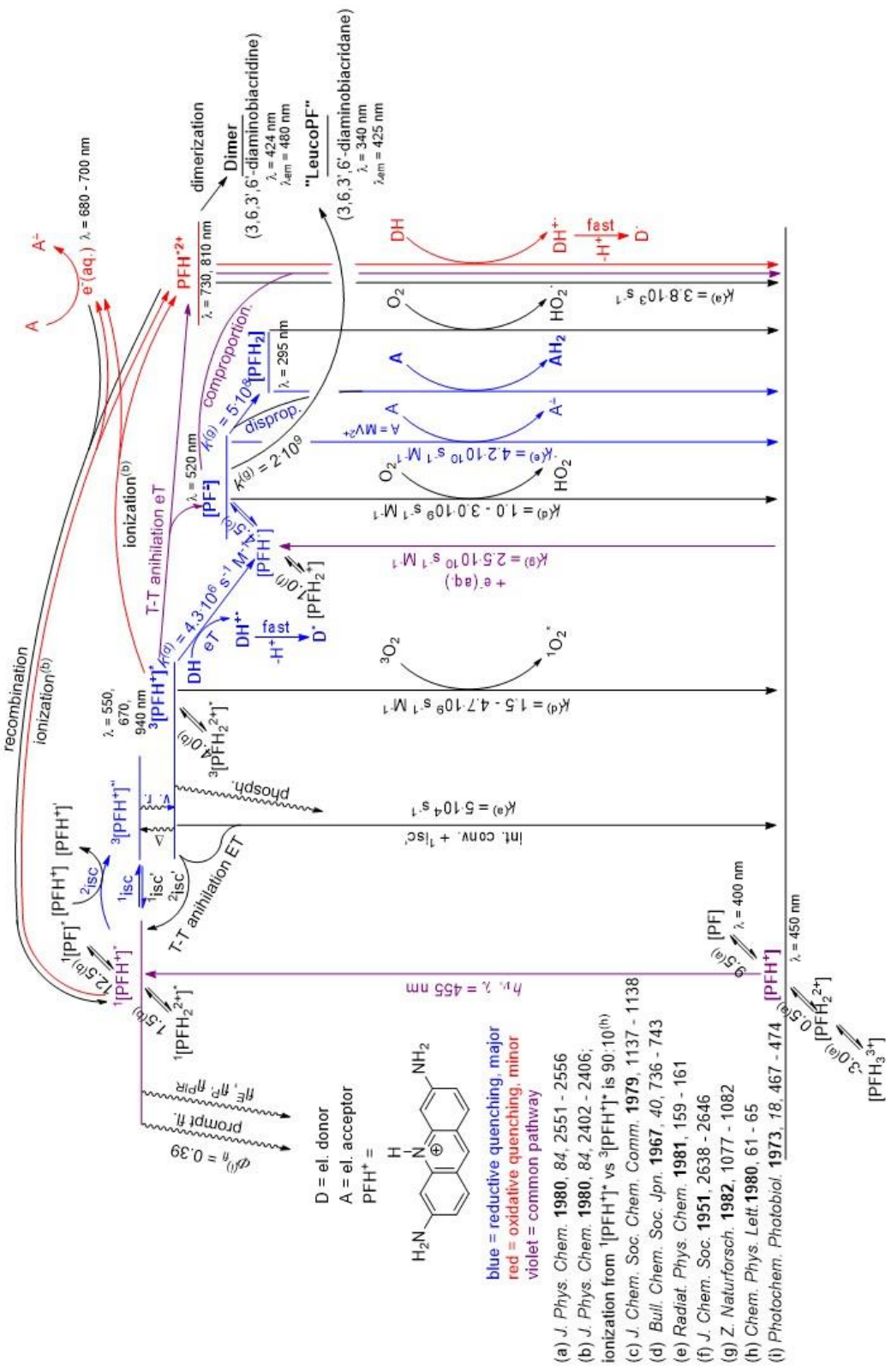

Figure 51: Jabłoński diagram of proflavine catalytic system.

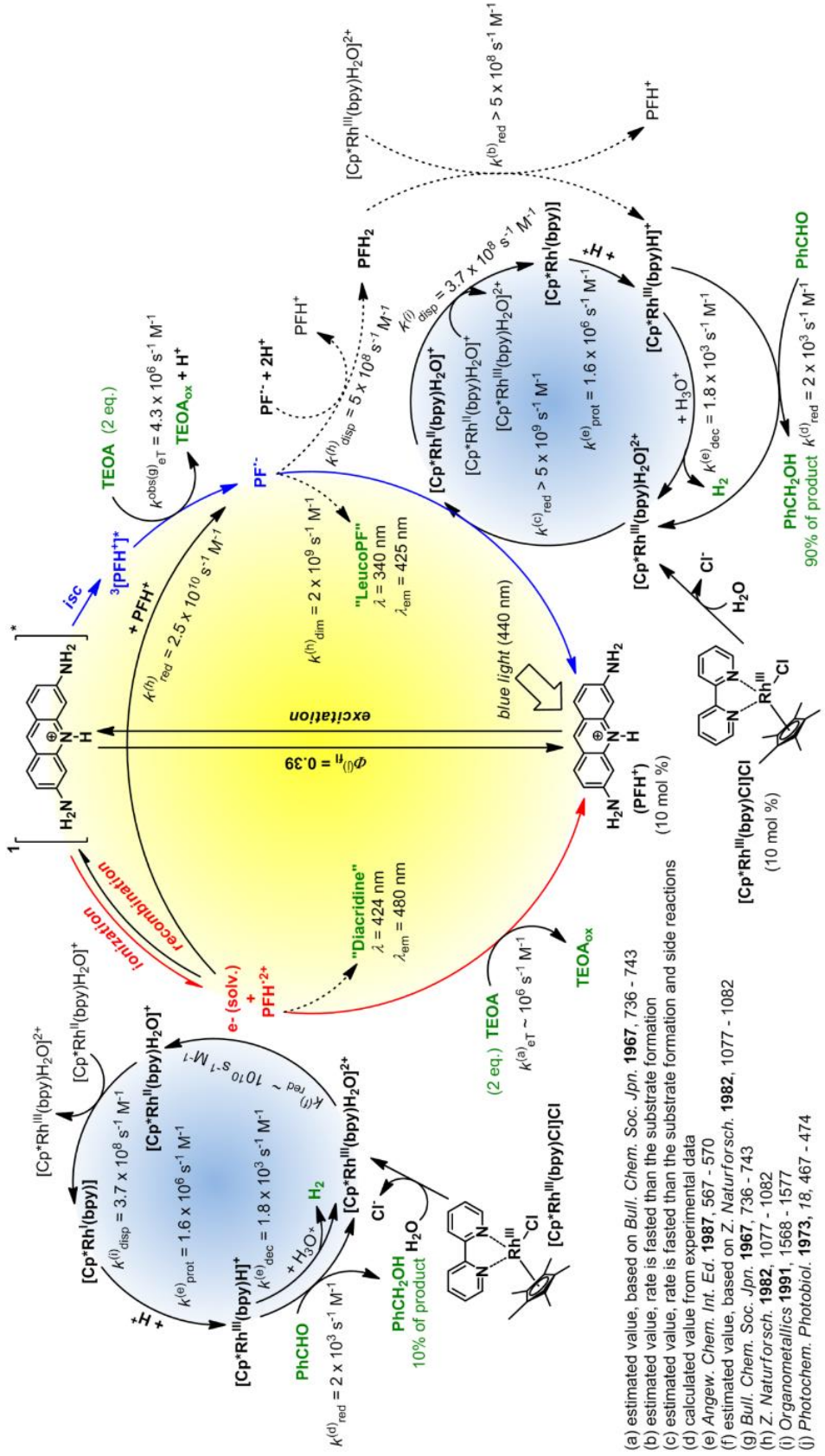

Figure 52: Overall mechanism of proflavine catalytic system

3.5 References

[1] G. A. Tolstikov, V. N. Odinokov, R. I. Galeeva, R. S. Bakeeva, V. R. Akhunova, *Tetrahedron Lett.* **1979**, *20*, 4851-4854.

[2] R. O. Hutchins, D. Kandasamy, *J. Am. Chem. Soc.* **1973**, *95*, 6131-6133.

[3] D. E. Ward, C. K. Rhee, *Synth. Commun.* **1988**, *18*, 1927-1933.

[4] D. E. Ward, C. K. Rhee, *Can. J. Chem.* **1989**, *67*, 1206-1211.

[5] Y. Maki, K. Kikuchi, H. Sugiyama, S. Seto, *Tetrahedron Lett.* **1977**, *18*, 263-264.

[6] C. Adams, *Synth. Commun.* **1984**, *14*, 1349-1353.

[7] B. Zeynizadeh, F. Shirini, *J. Chem. Res.* **2003**, *2003*, 334-339.

[8] K. Tanemura, T. Suzuki, Y. Nishida, K. Satsumabayashi, T. Horaguchi, *Synth. Commun.* **2005**, *35*, 867-872.

[9] S. Chandrasekhar, A. Shrinidhi, *Synth. Commun.* **2014**, *44*, 2051-2056.

[10] D. J. Raber, W. C. Guida, D. C. Shoenberger, *Tetrahedron Lett.* **1981**, *22*, 5107-5110.

[11] G. W. Gribble, D. C. Ferguson, *J. Chem. Soc., Chem. Commun.* **1975**, 535-536.

[12] C. F. Nutaitis, G. W. Gribble, *Tetrahedron Lett.* **1983**, *24*, 4287-4290.

[13] Y. Kuroiwa, S. Matsumura, K. Toshima, *Synlett* **2008**, *2008*, 2523-2525.

[14] C. P. Casey, N. A. Strotman, S. E. Beetner, J. B. Johnson, D. C. Priebe, I. A. Guzei, *Organometallics* **2006**, *25*, 1236-1244.

[15] M. Zhang, W. D. Rouch, R. D. McCulla, *Eur. J. Org. Chem.* **2012**, *2012*, 6187-6196.

[16] D. H. Nam, C. B. Park, *ChemBioChem* **2012**, *13*, 1278-1282.

[17] R. W. Armstrong, N. M. Panzer, *J. Am. Chem. Soc.* **1972**, *94*, 7650-7653.

[18] A. I. Krasna, *Photochem. Photobiol.* **1979**, *29*, 267-276.

[19] M. T. Youinou, R. Ziessel, *J. Organomet. Chem.* **1989**, *363*, 197-208.

[20] F. Hollmann, A. Schmid, E. Steckhan, *Angew. Chem., Int. Edit.* **2001**, *40*, 169-171.

[21] H. C. Lo, O. Buriez, J. B. Kerr, R. H. Fish, *Angew. Chem., Int. Ed.* **1999**, *38*, 1429-1432.

[22] C. Leiva, H. C. Lo, R. H. Fish, *J. Organomet. Chem.* **2010**, *695*, 145-150.

[23] Y. Himeda, N. Onozawa-Komatsuzaki, H. Sugihara, H. Arakawa, K. Kasuga, *J. Mol. Catal. A: Chem.* **2003**, *195*, 95-100.

[24] U. Kölle, M. Grätzel, *Angew. Chem., Int. Ed. Engl.* **1987**, *99*, 572-574.

[25] D. Menche, J. Hassfeld, J. Li, G. Menche, A. Ritter, S. Rudolph, *Org. Lett.* **2006**, *8*, 741-744.

[26] G. R. Haugen, W. H. Melhuish, *Trans. Faraday Soc.* **1964**, *60*, 386.

[27] N. Mataga, Y. Kaifu, M. Koizumi, *Bull. Chem. Soc. Jpn.* **1956**, *29*, 373-379.

[28] C. A. Parker, T. A. Joyce, *Photochem. Photobiol.* **1973**, *18*, 467-474.

[29] W. E. Lee, W. C. Galley, *Biophys. J.* **1988**, *54*, 627-635.

[30] P. Kurz, B. Probst, B. Spingler, R. Alberto, *Eur. J. Inorg. Chem.* **2006**, *2006*, 2966-2974.

[31] M. P. Pileni, M. Gratzel, *J. Phys. Chem.* **1980**, *84*, 2402-2406.

[32] B. Chakraborty, S. Basu, *Chem. Phys. Lett.* **2009**, *477*, 382-387.

[33] E. Steckhan, S. Herrmann, R. Ruppert, E. Dietz, M. Frede, E. Spika, *Organometallics* **1991**, *10*, 1568-1577.

[34] S. H. Lee, D. H. Nam, J. H. Kim, J.-O. Baeg, C. B. Park, *ChemBioChem* **2009**, *10*, 1621-1624.

[35] S. H. Lee, D. H. Nam, C. B. Park, *Adv. Synth. Catal.* **2009**, *351*, 2589-2594.

[36] H. C. Lo, C. Leiva, O. Buriez, J. B. Kerr, M. M. Olmstead, R. H. Fish, *Inorg. Chem.* **2001**, *40*, 6705-6716.

[37] S. Solar, W. Solar, N. Getoff, *Z. Naturforsch.* **1982**, *37a*, 1077-1082.

[38] G. Oster, J. S. Bellin, R. W. Kimball, M. E. Schrader, *J. Am. Chem. Soc.* **1959**, *81*, 5095-5099.

[39] B. H. M. Hussein, M. Goez, Ph.D. Dissertation, Universität Halle-Wittenberg, Germany (Germany), **2005**.

[40] K. Kalyanasundaram, D. Dung, *J. Phys. Chem.* **1980**, *84*, 2551-2556.

[41] H. Lv, W. Guo, K. Wu, Z. Chen, J. Bacsa, D. G. Musaev, Y. V. Geletii, S. M. Lauinger, T. Lian, C. L. Hill, *J. Am. Chem. Soc.* **2014**, *136*, 14015-14018.

[42] S. M. Barrett, C. L. Pitman, A. G. Walden, A. J. M. Miller, *J. Am. Chem. Soc.* **2014**, *136*, 14718-14721.

[43] U. Megerle, R. Lechner, B. Koenig, E. Riedle, *Photochem. Photobiol. Sci.* **2010**, *9*, 1400-1406.

[44] Bonneau, R.; Wirz, J.; Zuberbuhler, A. D. *Pure Appl. Chem.* **1997**, *69*, 979-992.

[45] Ooi, T.; Miura, T.; Itagaki, Y.; Ichikawa, H.; Maruoka, K. *Synthesis* **2002**, *2002*, 279-291.

[46] Chandrasekhar, S.; Shrinidhi, A. *Synth. Commun.* **2014**, *44*, 2051-2056.

[47] Hsu, S.-F.; Plietker, B. *Chem. - Eur. J.* **2014**, *20*, 4242-4245.

[48] Kölle, U.; Grätzel, M. *Angew. Chem., Int. Ed. Engl.* **1987**, *99*, 572-574.

[49] Himeda, Y.; Onozawa-Komatsuzaki, N.; Sugihara, H.; Arakawa, H.; Kasuga, K. *J. Mol. Catal. A: Chem.* **2003**, *195*, 95-100.

[50] Mataga, N.; Kaifu, Y.; Koizumi, M. *Bull. Chem. Soc. Jpn.* **1956**, *29*, 373-379.

[51] Pileni, M. P.; Gratzel, M. *J. Phys. Chem.* **1980**, *84*, 2402-2406.

[52] Kalyanasundaram, K.; Dung, D. *J. Phys. Chem.* **1980**, *84*, 2551-2556.

Chapter 4

4 Photochemical *N*-Formylation of Amines *via* a Reductive Quenching Cycle in the Presence of Air

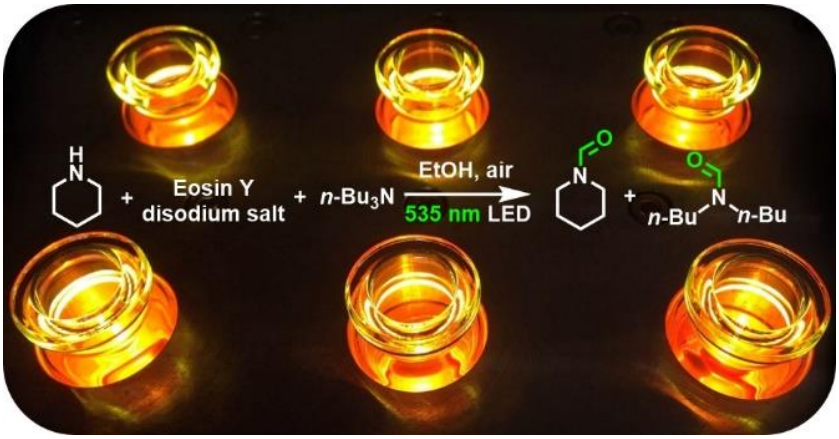

The photochemical *N*-formylation of amines was performed under simple and mild reaction conditions. Amines are common electron donors in reductive photocatalysis, which then typically decompose after donating an electron to the photocatalyst. We have found that these oxidized amines can be utilized to give *N*-formamides in the presence of air without additional formylating agents. The reaction proceeds *via* the *in situ* formation of enamines. Oxygen (air) is necessary for the reaction to occur as it regenerates the photocatalyst forming hydroperoxyl radicals as crucial intermediates involved in the reaction.

This chapter is a manuscript, prepared for submission to a journal:
T. Ghosh, B. König; *manuscript in progress*.

TG performed all the experimental work and wrote the manuscript. BK supervised the project and is corresponding author.

4.1 Introduction

Photoredox catalysis proceeds *via* two possible catalytic cycles: reductive or oxidative quenching pathways.[1] In the reductive quenching cycle, the excited state photocatalyst takes up an electron returning to the ground state in the reduced form. The use of amines as electron donors is very common.[2-10] The amine reductively quenches the photocatalyst forming the radical cation of the amine, which decomposes *via* different irreversible pathways (**Fig. 1**).[11-12] In most cases, amines are used only as sacrificial electron donors and are not further utilized. We thought it will be beneficial if the oxidized amines can be transformed into synthetically useful compounds rather than treating them as waste. We were particularly interested to investigate the fate of the oxidized amines in a reductive photocatalytic cycle in the presence of air. To our surprise, we found out that amines are converted to *N*-formamides in moderate yields without additional formylating agent or any C_1 building block source. The formylation of amines is an important transformation in organic, medicinal and biological chemistry,[13-14] as *N*-formamides are useful intermediates for the synthesis of biologically active molecules.[15-18] Formamides are used as Lewis bases, which can catalyze reactions such as the allylation[19-20] and hydrosilylation[21] of carbonyl compounds. More importantly, formamides are utilized as reagents in Vilsmeier formylation reactions[22] and they have been employed in the synthesis of isocyanides and formamidines.[23]

A variety of methods are available for the formation of *N*-formamides, but they typically require high temperatures at reflux conditions[24] or strong bases[25] in the presence of different formylating reagent or C_1 building blocks *e.g.* CO,[25-26] CO_2,[27-28] DMF,[24]29] chloroform,[30] methanol,[31-32] formaldehyde/paraformaldehyde,[33-36] formic acid[37-38] and its derivatives. Most of these methods involve either moisture sensitive, toxic or expensive reagents.

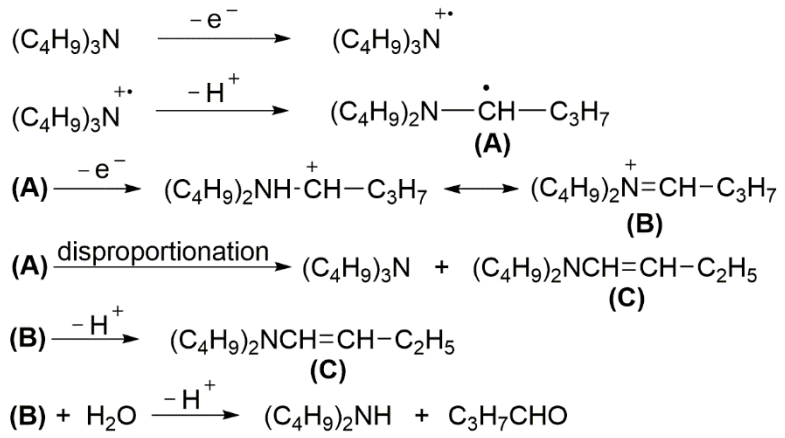

Fig. 1: Decomposition products observed in the oxidation of tributylamine.[39]

Herein, we report the photochemical oxidation of amines yielding *N*-formamides under mild reaction conditions without additional formylation agents. In 1970, the electrochemical oxidation of amines to amides was reported, which used elemental oxygen.[39] In 1976, Mann *et. al.* showed[40] the electrochemical oxidation of tropane and nortropane giving *N*-formamide as one of the products. In 2014, Wang *et. al.* reported[41] the photochemical transformation of enamines to *N*-formamides by singlet oxygen. We suggest that under our reaction conditions the reaction proceeds *via* an enamine intermediate, but singlet oxygen is unlikely be involved. In the presence of different singlet oxygen quenchers[42-44] (*e.g.*, 1,4-diazabicyclo[2.2.2]octane (DABCO), 1,3-diphenylisobenzofuran or 9,10-diphenylanthracene) the reaction still occurs at the same rate with similar yields excluding the singlet oxygen participation. Tertiary amines are better electron donors than secondary amines, because of their less positive reduction potentials.[45] Therefore they form radical cations easily reducing the catalyst to the corresponding radical anion. The radical anion of the catalyst is oxidized by molecular oxygen, which acts as the sacrificial electron acceptor yielding a superoxide radical anion (**Fig. 2**). The superoxide radical anions can be utilized in combination with other reagents to produce valuable compounds.[46] We have used photochemically generated superoxide radical anions to form *N*-formamides from amines.

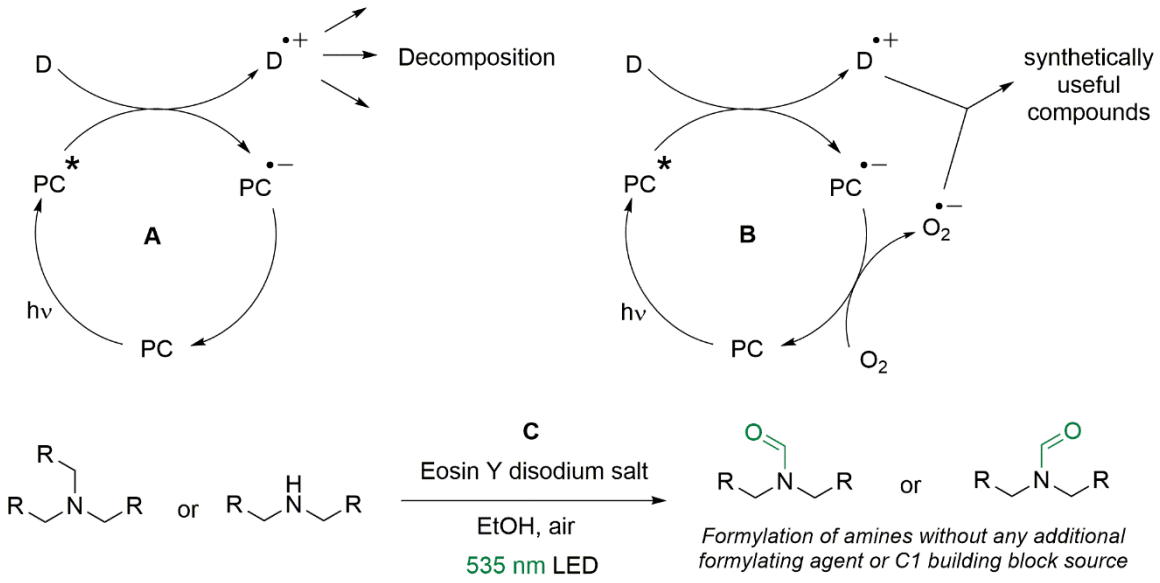

Fig. 2: (A) A typical reductive quenching cycle where radical cations of amines decompose after oxidation; (B) This work: the radical cation of amines is used in synthesis; (C) Photochemical *N*-formylation of amines without additional formylating agent.

4.2 Results and discussion

4.2.1 Synthetic investigations

The reaction conditions were optimized using piperidine as a substrate. The selected results are summarized in Table 1. The yields were determined by GC/FID with an appropriate internal standard after 8 hours of irradiation at 535 nm. Initially, the reactions were performed in DMF, where 1-formylpiperidine (**1a**) was formed as a product (Table 1, entry 1), but the addition of a tertiary amine (*n*-Bu_3N) to the reaction mixture increased the product yield (Table 1, entry 2). It was thought that the formyl group of DMF is being transferred to the amine, but solvents, which do not contain a formyl group give the same product (Table 1, entry 3-5). Changing the tertiary amine from *n*-Bu_3N to DIPEA did not increase the yield (Table 1, entry 6). Increasing the amount of *n*-Bu_3N from 1 to 2 equiv. resulted in a higher reaction yield (Table 1, entry 7), but increasing the catalyst loading (from 5 to 10 mol%) and more *n*-Bu_3N (3 equiv.) did not change the yield significantly (Table 1, entries 8 and 9).

Table 1: Optimization of reaction conditions

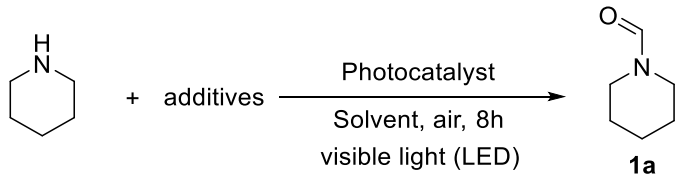

Entry	Photocatalyst (PC)	PC (mol%)	Additives	Additives (equiv.)	Solvent	Yield of **1a** (%)*
1	Eosin Y disodium salt	5	-	-	DMF	11
2	Eosin Y disodium salt	5	*n*-Bu_3N	1	DMF	41
3	Eosin Y disodium salt	5	*n*-Bu_3N	1	EtOH	48
4	Eosin Y disodium salt	5	*n*-Bu_3N	1	MeOH	43
5	Eosin Y disodium salt	5	*n*-Bu_3N	1	DCM	35
6	Eosin Y disodium salt	5	DIPEA	1	EtOH	42
7	**Eosin Y disodium salt**	**5**	***n*-Bu_3N**	**2**	**EtOH**	**68**
8	Eosin Y disodium salt	10	*n*-Bu_3N	1	EtOH	68
9	Eosin Y disodium salt	5	*n*-Bu_3N	3	EtOH	70
10	Eosin Y disodium salt	5	-	-	EtOH	16
11	Eosin Y disodium salt	5	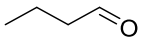	2	EtOH	32
12	Eosin Y	5	*n*-Bu_3N	2	EtOH	61
13	Eosin B	5	*n*-Bu_3N	2	EtOH	31
14	Fluorescein	5	*n*-Bu_3N	2	EtOH	41
15	Rose Bengal	5	*n*-Bu_3N	2	EtOH	64
16	Erythrosin B	5	*n*-Bu_3N	2	EtOH	65
17	PDI	5	*n*-Bu_3N	2	EtOH	54
18	Rh-6G	5	*n*-Bu_3N	2	MeOH	17
19	$Ru(bpy)_3Cl_2.6H_2O$	5	*n*-Bu_3N	2	EtOH	40

*****GC/FID determined yield of 1-formylpiperidine with appropriate internal standard.

Different photocatalysts were screened (Table 1, entry 12-19) for the reaction with Eosin Y disodium salt providing the best results (Table 1, entry 7). The control experiments (summarized in Table 2) show that light and photocatalyst are both essential for the reaction to occur. Oxygen is also necessary for the reaction to proceed (Table 2, entry 6). Tributylamine was used to accelerate the reaction and was transformed to *N,N*-dibutylformamide (**2b**) after losing a butyl group. Reactions without any additives in ethanol gave 16% of the formylated product of piperidine, but the addition of butyraldehyde doubled the reaction yield (Table 1, entry 10-11). The role of *n*-Bu_3N or butyraldehyde as an accelerator for the formylation of secondary amines is discussed in detail in the mechanistic part.

Mainly secondary and tertiary amines were tested as substrates in our catalytic system (**Scheme 1**).‡ For the formylation of secondary amines, a tertiary amine (*n*-Bu_3N) was added, where both of the amines were transformed to the respective formylated products. However, for the formylation of tertiary amines no additives were required. Two equivalents of *n*-Bu_3N were used for the formylation of secondary amines converting 32% of *n*-Bu_3N into *N,N*-dibutylformamide (**2b**) with a small amount of *n*-Bu_3N left unreacted after 8 hours of irradiation

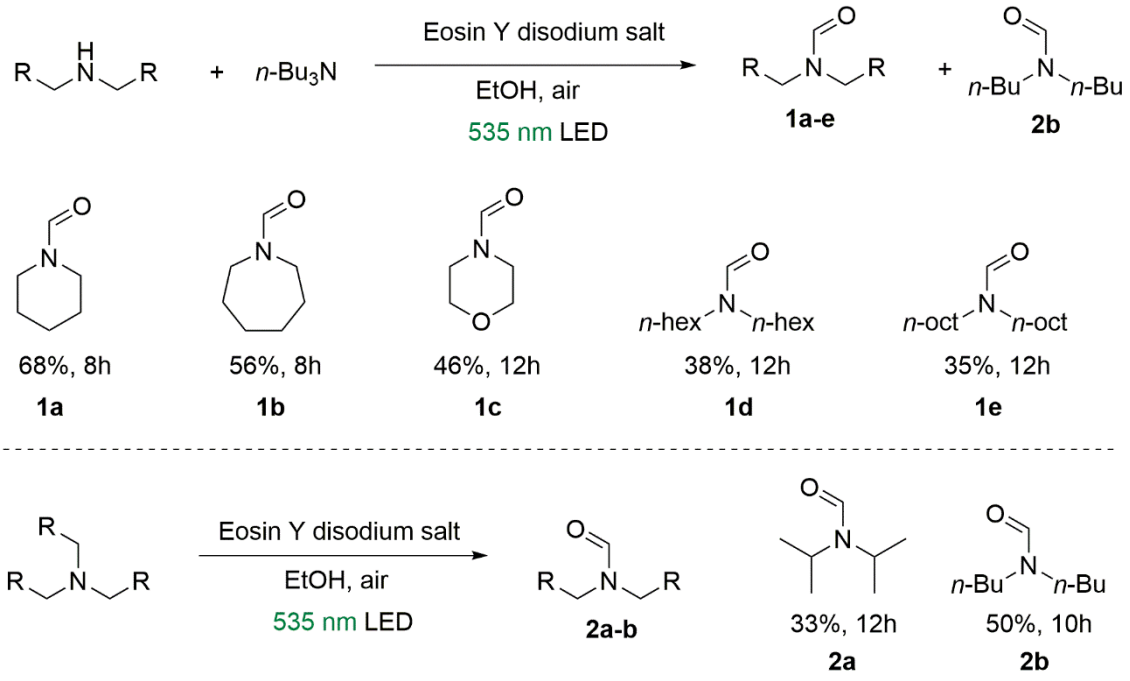

Scheme 1: Substrate scope for the formylation of amines (GC/FID determined yields with appropriate internal standard).

4.2.2 Mechanistic investigations

Tertiary amines are easier oxidized than secondary amines,[45] therefore they can reductively quench the excited state of the photocatalyst more easily than the secondary amines. After reductive quenching, the radical anion of the catalyst is reoxidized by molecular oxygen. The reported reaction does not work if we use another electron acceptor (*e.g.* nitrobenzene) for the regeneration of the catalyst (Table 2, entry 7), which indicates the role of oxygen in the reaction to proceed. The solvent is not acting as a formyl group source as we have screened different solvents and the expected product is formed in almost every solvent. We believe that the formylation of tertiary amines proceeds through an imine intermediate, which transforms into an enamine *in situ*. Previous reports show[41] that enamines can be transformed to *N*-formamides in the presence of singlet oxygen. It has also been shown that the addition of DABCO (effective quencher of singlet oxygen) to the reaction mixture stops the product formation. In our reaction, we have deliberately added different singlet oxygen quenchers (*e.g.* DABCO or 1,3-diphenylisobenzofuran or 9,10-diphenylanthracene), but the reaction proceeds giving similar product yields, which shows that singlet oxygen might not be involved in the reaction mechanism. After accepting an electron from the radical anion of the catalyst, molecular oxygen may form superoxide radical anions, which give hydroperoxyl radicals after abstracting a proton from the solvent. This hydroperoxyl radical reacts with the enamine in a stepwise mechanism to give *N*-formamide.[46] In the case of tertiary amines, it is reported[39] that after oxidation and loss of a proton a radical is obtained (**Fig. 1**, **(A)**), which may disproportionate to an enamine or deprotonation of the iminium ion leads to the enamine. The formation of formamide from secondary amines follows a slightly different pathway: the enamine is generated first, which then reacts with the hydroperoxyl radical in a stepwise mechanism similar to tertiary amines. Secondary amines are not very efficient quenchers for the photocatalyst and therefore form smaller amounts of superoxide radical anion. The addition of a tertiary amine accelerates the formylation of secondary amines, because it produces more of the superoxide radical anion. The side product of the oxidation of *n*-Bu_3N is butyraldehyde, which reacts with secondary amines to enamines. Table 1, entry 10 and 11, show that the addition of butyraldehyde doubled the reaction yield, indicating that butyraldehyde is essential to increase the reaction yield. We suggest that butyraldehyde reacts with the secondary amine to form an enamine, which gives rise to *N*-formamide *via* a stepwise mechanism. Piperidine forms formamide more easily than morpholine as piperidine (pK_a =

11.22) is more basic than morpholine (pK_a = 8.36)[47] (**Scheme 1**, **1a** vs **1c**). The lower yield for the formylation of DIPEA is due to the fact that most of the DIPEA decomposes after oxidation to diisopropylamine and acetaldehyde. Acetaldehyde, being a very volatile compound evaporates from the open reaction vial very easily. So, diisopropylamine does not react, due to the absence of any aldehyde to form an enamine. To prove the mechanistic proposal further, we have used the intermediate, **1f** as starting material, which converts into **1a** after the photoreaction. Aliphatic enamines are not very stable compounds; they decompose quite fast if left in open atmosphere. The moderate yields of the formylated products can be the result of the decomposition of the *in situ* generated enamines in the presence of air. Based on our mechanistic experiments we propose the overall catalytic mechanism depicted in the **Fig. 3**.

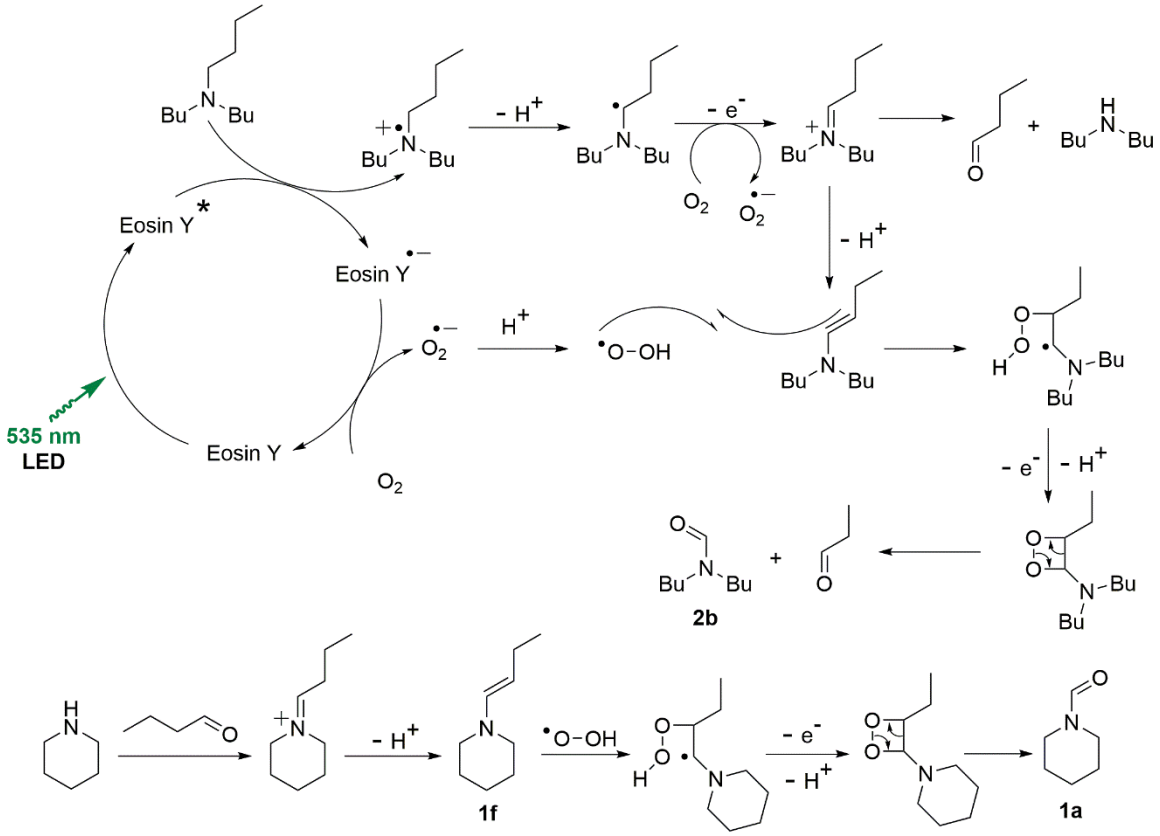

Fig. 3: Proposed catalytic mechanism.

4.3 Conclusion

In summary, we have used by-products of photochemically oxidized amines to form *N*-formamides without additional formylating agent. Different amines can be transformed into their corresponding *N*-formamides with moderate yields. Oxygen is necessary for the regeneration of the catalyst as well as for the formylation of the amines. Consistent with all observations, we propose that the reaction proceeds *via* enamine intermediates, which then react with hydroperoxyl radicals, formed *in situ* from superoxide radical anions giving *N*-formamides. The reaction does not require the participation of singlet oxygen as the reaction proceeds well in the presence of singlet oxygen quenchers.

4.4 Experimental section

4.4.1 Materials and methods

Eosin Y disodium salt (≥ 85% dye content, catalogue number 115935-25G) was purchased from Merck Millipore. All other commercially available reagents and solvents were purchased and used without further purification. Compound **1f** was prepared according to the literature procedure.[1]

Thin-layer chromatography was performed using silica gel plates 60 F254: Visualization was accomplished with appropriate stain (basic $KMnO_4$).

Standard flash chromatography was performed on an Isolera™ Spektra Systems automated with high performance flash purification system using silica gel of particle size 40−63 μm. Macherey-Nagel silica gel 60 M (230-440 mesh) was used for column chromatography.

^{1}H and ^{13}C NMR spectra were recorded on Bruker Avance spectrometers (400 MHz and 101 MHz) in $CDCl_3$ solution with internal solvent signal as reference (7.26 and 77.0, respectively). Proton NMR data are reported as follows: chemical shift (ppm), multiplicity (s = singlet, d = doublet, t = triplet, q = quartet, dd = doublet of doublets, ddd = doublet of doublets of doublets, td = triplet of doublets, m = multiplet, br. s. = broad singlet), coupling constants (Hz) and numbers of proton. Data for ^{13}C NMR are reported in terms of chemical shift and no special nomenclature is used for equivalent carbons.

Gas chromatography (GC) and gas chromatography coupled to low resolution mass spectrometry (GC-MS) analyses were performed using a capillary column (length: 30 m;

diam. 0.25 mm; film: 0.25 µm) using He gas as carrier. GC was equipped with a FID detector. GC-MS was performed on 5975 MSD single quadruple detector. Formylated products were identified by comparing with authentic samples (GC/FID). Quantification of the *N*-formylated products was performed by GC/FID analysis using internal standard.

UV–Vis analyses were performed with Varian Cary 50 UV/Vis spectrophotometer and Agilent 8453 UV-Vis Spectrometer. For UV measurements 10 mm Hellma fluorescence quartz cuvette (117.100F-QS) was used.

Photocatalytic reactions were performed with 535 nm LEDs (OSRAM Oslon SSL 80 green LEDs, λ_{em} = 535 nm (± 15 nm), 3.5 V, 700 mA).

4.4.2 General procedure for the formylation of amines

The amine (0.05 mmol, 1 eq.) was placed in a 5 mL vial equipped with a small PTFE stirring bar and then 2 mL solution of Eosin Y disodium salt in ethanol (0.0025 mmol, 5 mol%) was added immediately to avoid any evaporation of the amine. Then tributylamine (0.1 mmol, 2 eq.) was added (only for the formylation of secondary/primary amines, not for the formylation of tertiary amines) to the reaction mixture and the reaction vial was placed in a cooling block maintaining 23 °C in open atmosphere. The reaction mixture was stirred and irradiated through the plane bottom of the vials by 3W blue LED (λ_{em} = 535 nm) and the reaction conversion was monitored by GC analysis. After complete conversion an internal standard (4-*tert*-butylcyclohexanone, 0.5 mL, *c* = 15 mg/mL) was added to the reaction mixture and the product yield was determined by GC/FID using a calibrated method.

4.4.3 Control Experiments

All control experiments were repeated three times. For each control experiments one component of the reaction system depicted in Scheme 2 was omitted or substituted (Table 2).

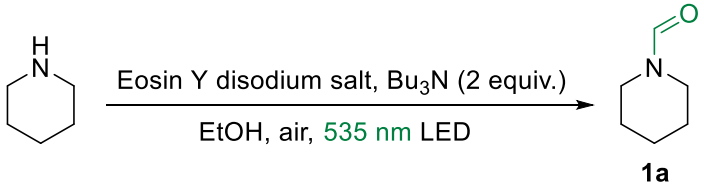

Scheme 2: Typical reaction procedure.

Table 2: Control experiments

Entry	Photocatalyst (mol%)	*n*-Bu_3N (equiv.)	Light (535 nm)	Reaction condition	Time (h)	Yield of **1a** (%)*
1	**5**	**2**	**yes**	**EtOH, air**	**8**	**68**
2	5	2	-	EtOH, air	12	<1
3	-	2	yes	EtOH, air	12	0
4	5	-	yes	EtOH, air	12	0
5	-	2	yes	EtOH, air	12	0
6	5	2	yes	EtOH, N_2	12	0
7	5	2	yes	EtOH, $PhNO_2$, N_2	12	0

[a] GC/FID determined yield with appropriate internal standard.

Photochemical reaction setup for the *N*-formylation of amines

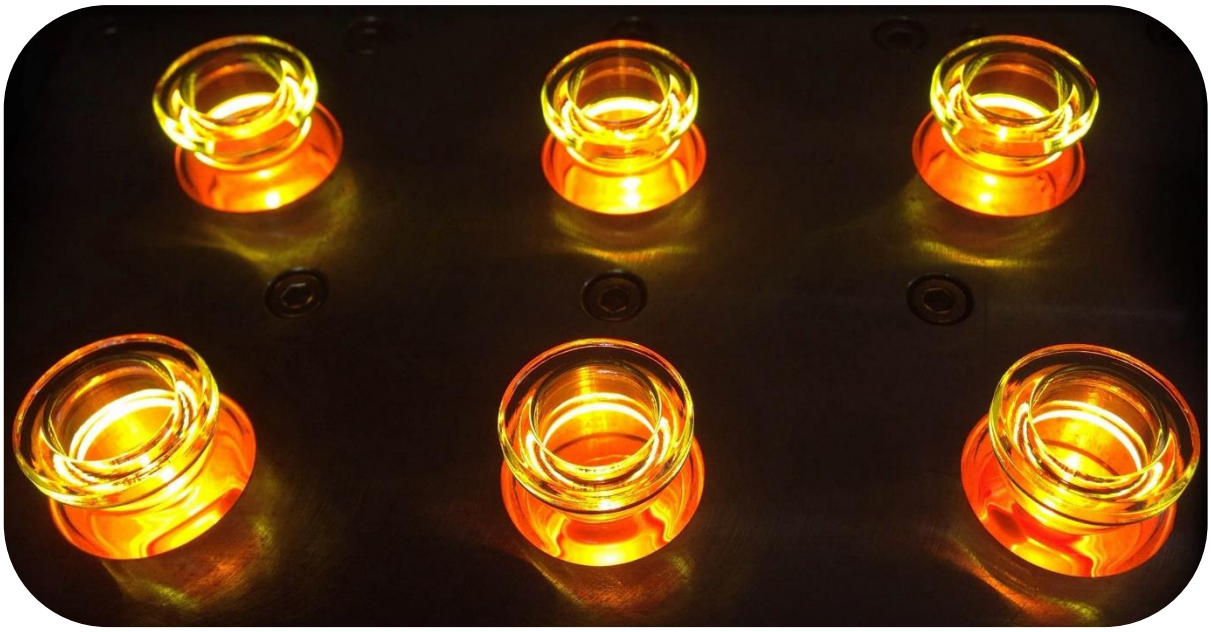

Fig. 4: Irradiation setup.

4.4.4 GC calibration curves

GC was calibrated using a four-point calibration; all calibrations were performed using 4-*tert*-butylcyclohexanone as an internal standard. The GC oven temperature program was adjusted to an initial temperature of 40 °C kept for 3 minutes, the temperature was increased at a rate of 15 °C/min over a period of 16 minutes until it reached 280 °C, then it was kept for 5 minutes at that temperature. Finally, the GC oven was heated at a rate of 25 °C/min till the final temperature (300 °C) was reached and kept for 5 minutes.

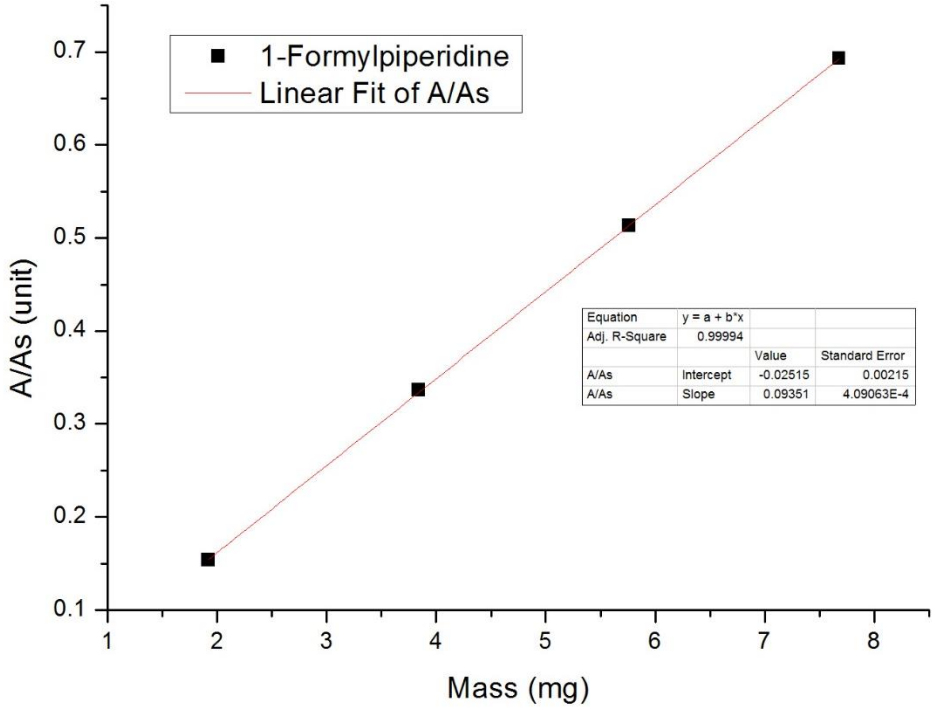

Fig. 5: Calibration curve for 1-formylpiperidine (**1a**).

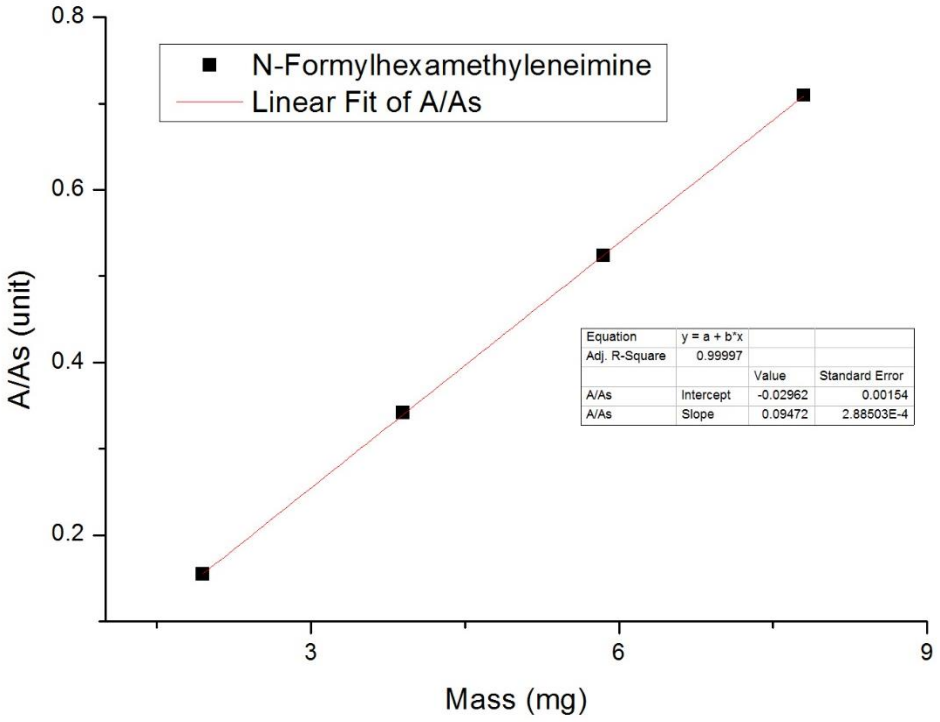

Fig. 6: Calibration curve for *N*-formylhexamethyleneimine (**1b**).

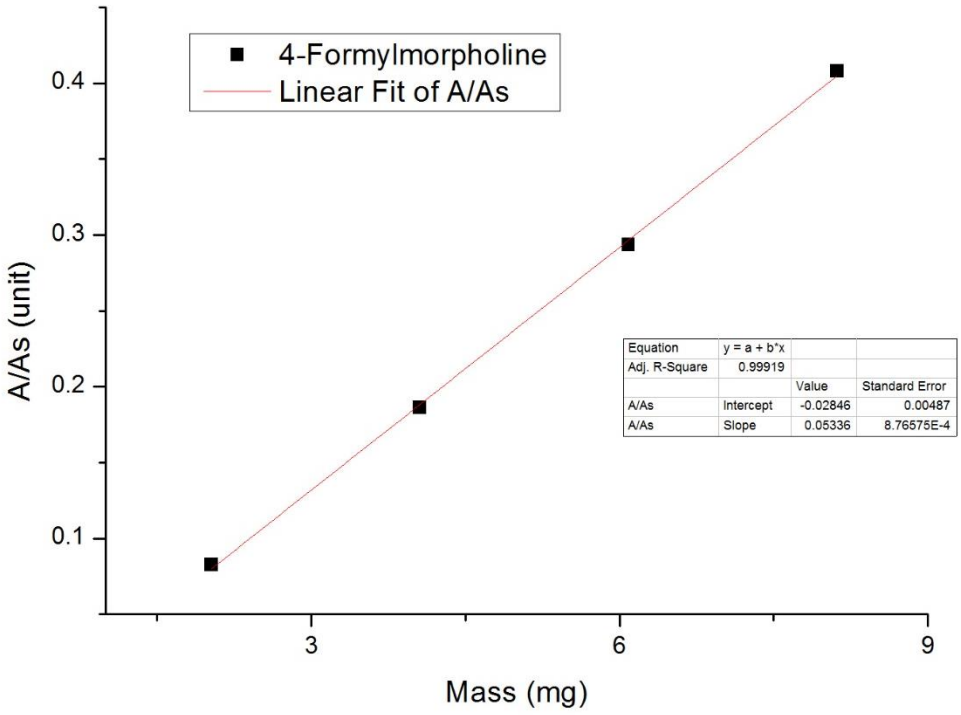

Fig. 7: Calibration curve for 4-formylmorpholine (**1c**).

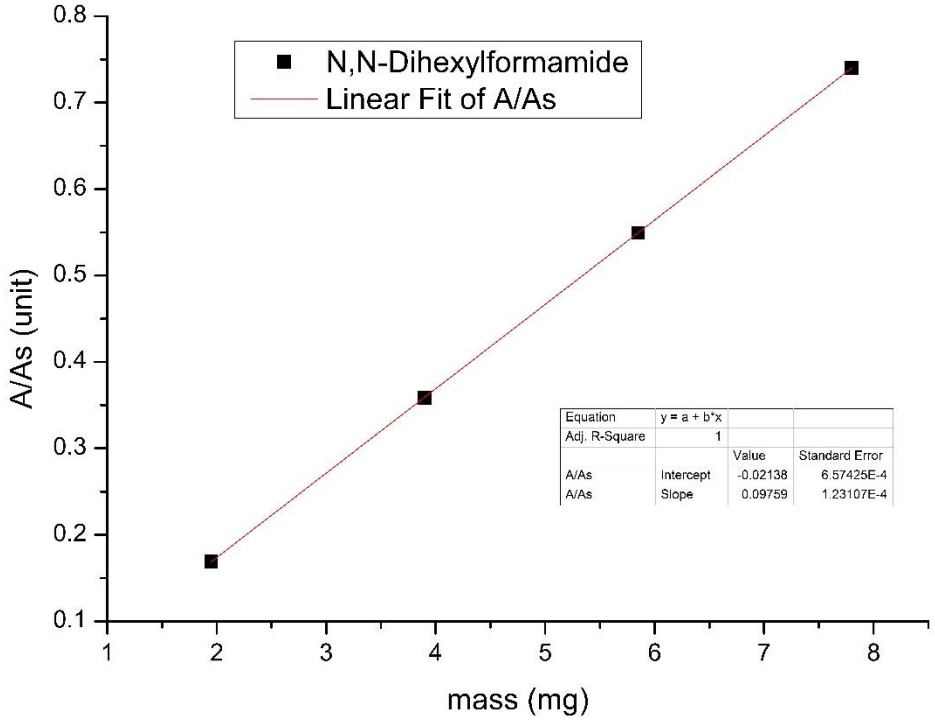

Fig. 8: Calibration curve for *N*,*N*-dihexylformamide (**1d**).

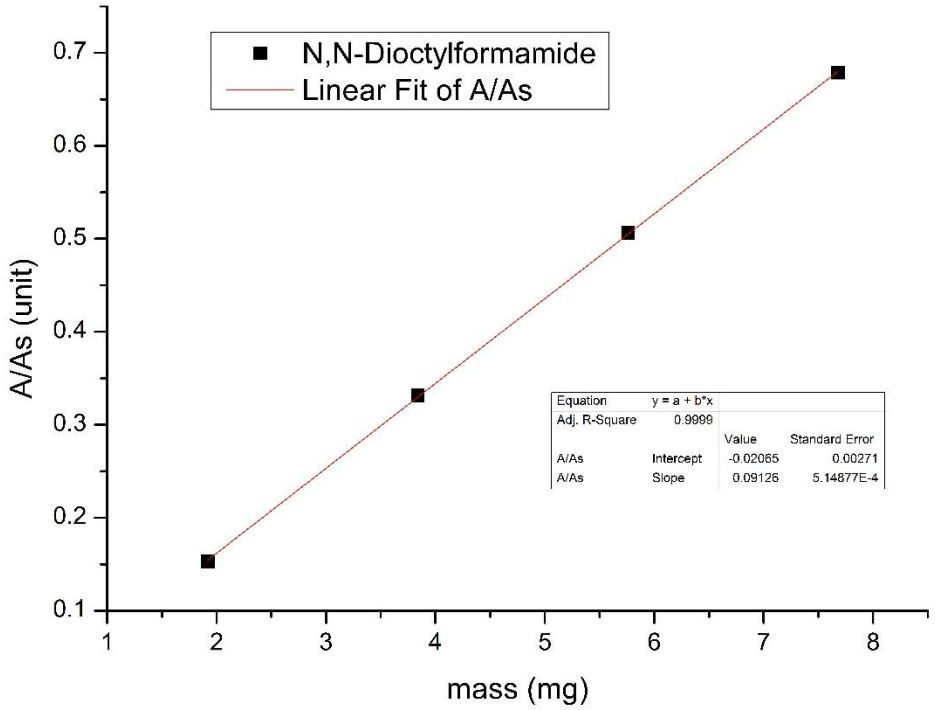

Fig. 9: Calibration curve for *N*,*N*-dioctylformamide (**1e**).

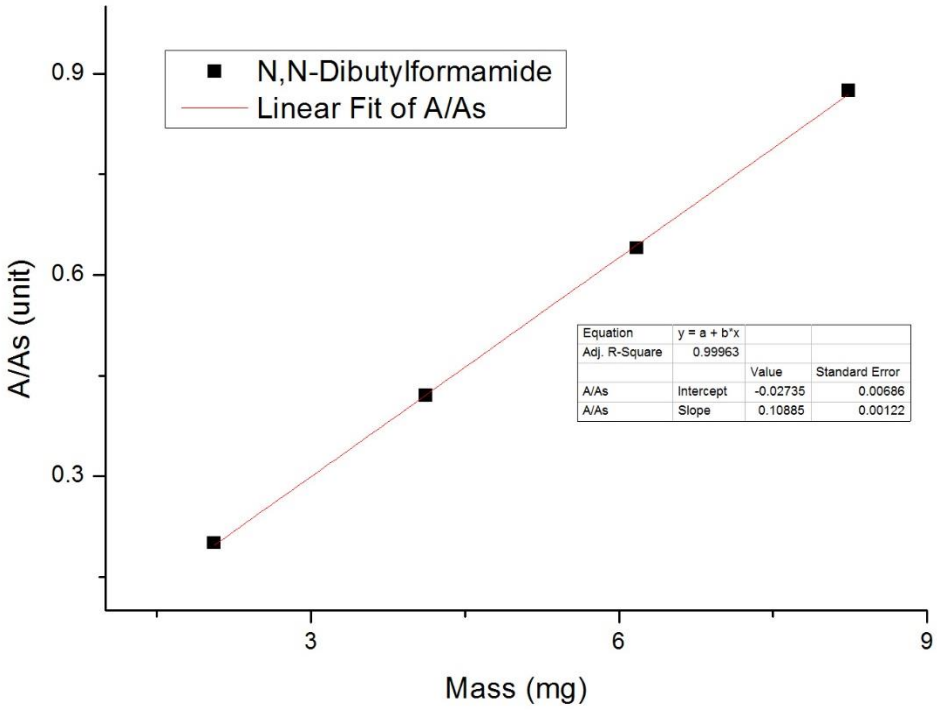

Fig. 10: Calibration curve for *N*,*N*-dibutylformamide (**2b**).

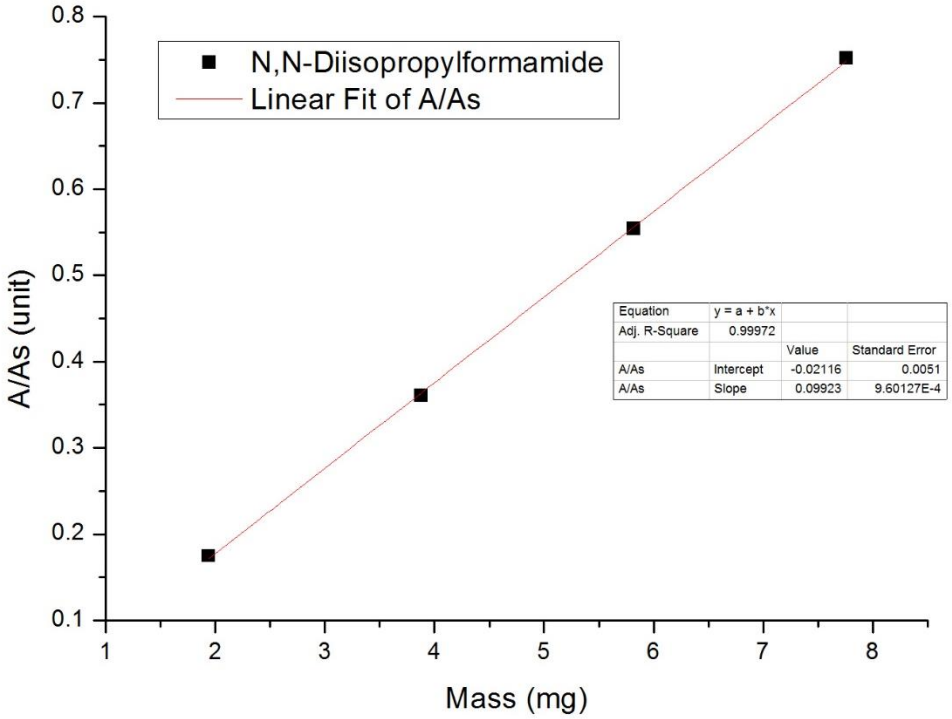

Fig. 11: Calibration curve for *N*,*N*-diisopropylformamide (**2a**).

4.4.5 Recovering the catalyst for further reactions

Eosin Y disodium salt was used 5 mol% with respect to the amine, 70% of which can be recovered after the reaction and can be used for further reaction. The formylation of piperidine gives 68% of the formylated product using 5 mol% of Eosin Y disodium salt. Using the recovered amount of photocatalyst from one reaction, the next reaction was performed using piperidine as a substrate, which gave 60% of the formylated product. The UV-Vis spectra confirmed that the recovered photocatalyst is identical to the original one.

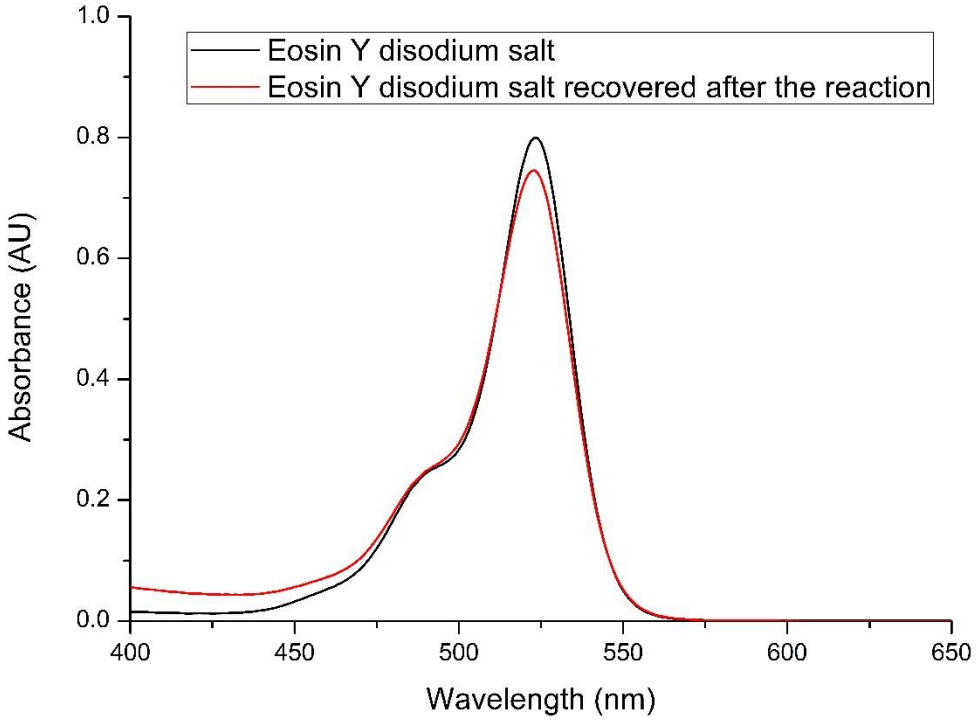

Fig. 12: Comparison of the UV-Vis spectra of Eosin Y disodium salt and the recovered Eosin Y disodium salt after the reaction.

4.4.6 Characterization of isolated *N*-formamides

Piperidine-1-carbaldehyde (**1a**):[2]

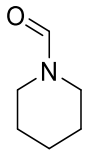

The compound was prepared according to the general procedure for the formylation of secondary/primary amines. The product was obtained by column chromatography (hexane/EtOAc, 1:1) as a colorless liquid in a yield of 54%.

^{1}H NMR (400 MHz, $CDCl_3$) δ = 7.98 (s, 1H), 3.54 – 3.36 (m, 2H), 3.36 – 3.21 (m, 2H), 1.73 – 1.60 (m, 2H), 1.60 – 1.44 (m, 4H).

^{13}C NMR (101 MHz, $CDCl_3$) δ = 160.87, 46.93, 40.71, 26.58, 25.09, 24.70.

HRMS: calculated for M^+ $C_6H_{11}NO^+$ 113.0835; found 113.0835.

N,*N*-Dihexylformamide (**1d**):[2]

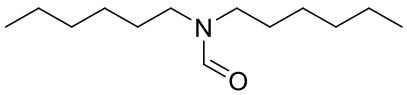

The compound was prepared according to the general procedure for the formylation of amines. The product was obtained by column chromatography (hexane/diethyl ether, 2:3) as a colorless liquid in a yield of 28%.

^{1}H NMR (300 MHz, $CDCl_3$) δ = 8.04 (s, 1H), 3.36 – 3.23 (m, 2H), 3.19 (t, *J*=7.1, 2H), 1.59 – 1.45 (m, 4H), 1.36 – 1.21 (m, 12H), 0.93 – 0.83 (m, 6H).

^{13}C NMR (75 MHz, $CDCl_3$) δ = 161.81, 46.65, 41.30, 30.50, 30.35, 27.55, 26.20, 25.58, 25.11, 21.54, 21.51, 13.00, 12.97.

HRMS: calculated for M^+ $C_6H_{11}NO^+$ 213.2087; found 213.2088.

N,*N*-Dioctylformamide (**1e**):[3]

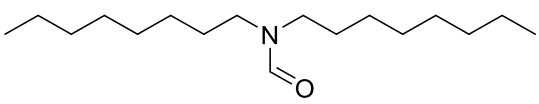

The compound was prepared according to the general procedure for the formylation of amines. The product was obtained by column chromatography (hexane/diethyl ether, 2:3) as a colorless liquid in a yield of 26%.

^{1}H NMR (400 MHz, $CDCl_3$) δ = 8.05 (s, 1H), 3.34 – 3.24 (m, 2H), 3.20 (t, *J*=7.2, 2H), 1.59 – 1.44 (m, 4H), 1.35 – 1.20 (m, 20H), 0.91 – 0.84 (m, 6H).

^{13}C NMR (101 MHz, $CDCl_3$) δ = 162.94, 47.80, 42.44, 31.79, 31.75, 29.31, 29.22, 29.17, 28.65, 27.29, 26.96, 26.49, 22.64, 22.63, 14.09, 14.08.

HRMS: calculated for M^+ $C_6H_{11}NO^+$ 269.2713; found 269.2703.

4.4.7 ^{1}H and ^{13}C NMR spectra of the isolated *N*-formamides

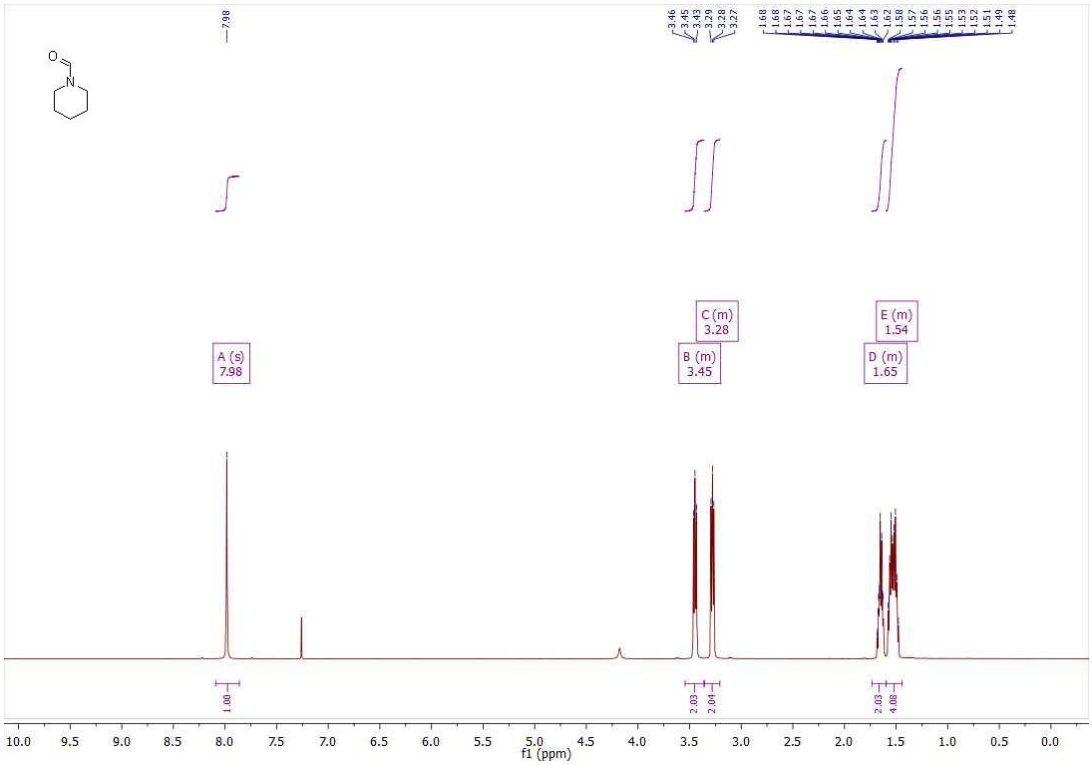

Fig. 13: ^{1}H spectrum of piperidine-1-carbaldehyde (**1a**).

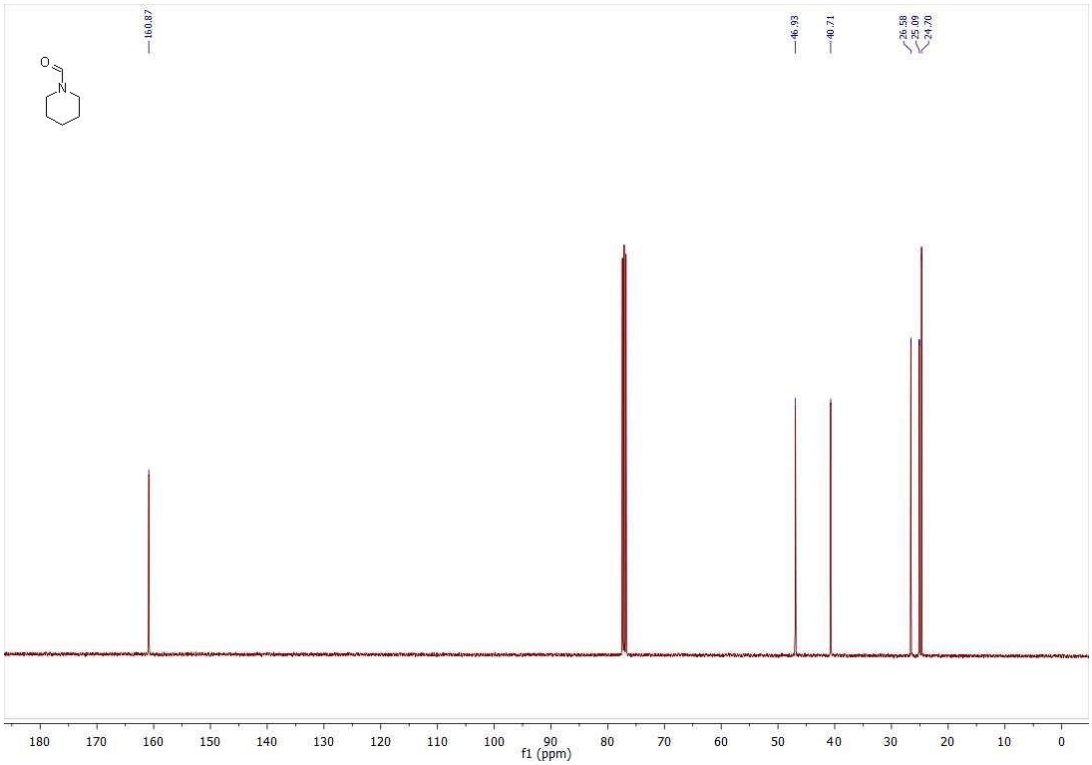

Fig. 14: ^{13}C spectrum of piperidine-1-carbaldehyde (**1a**).

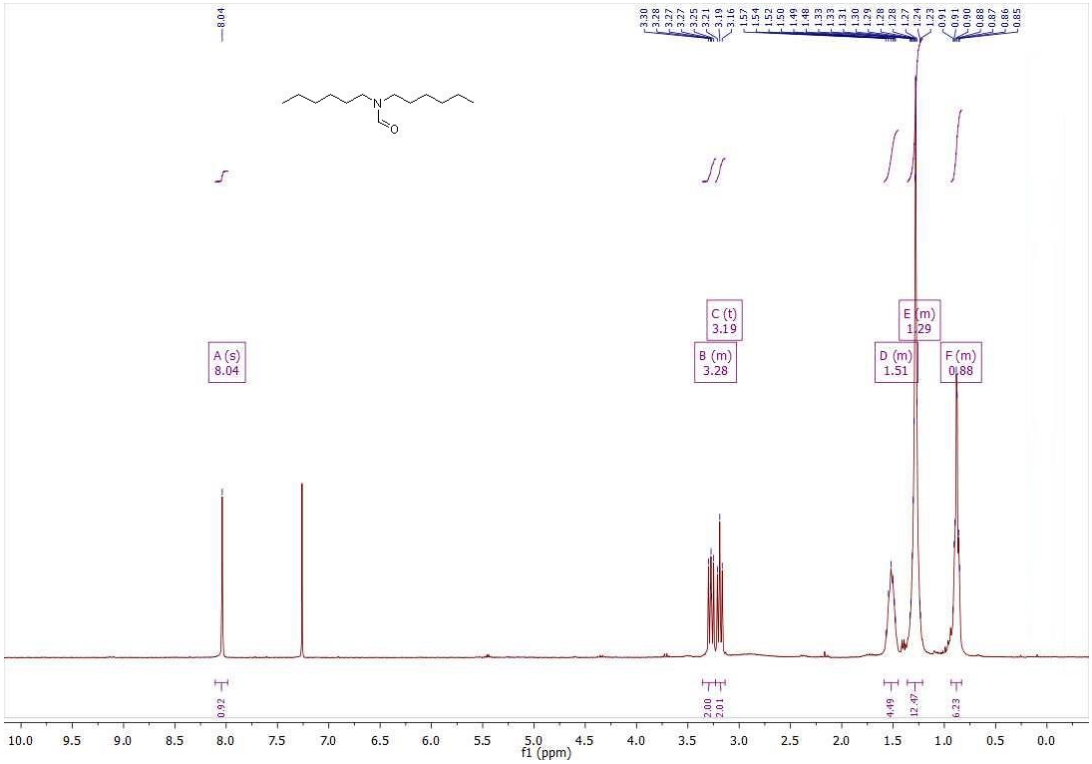

Fig. 15: ^{1}H spectrum of *N*,*N*-dihexylformamide (**1d**).

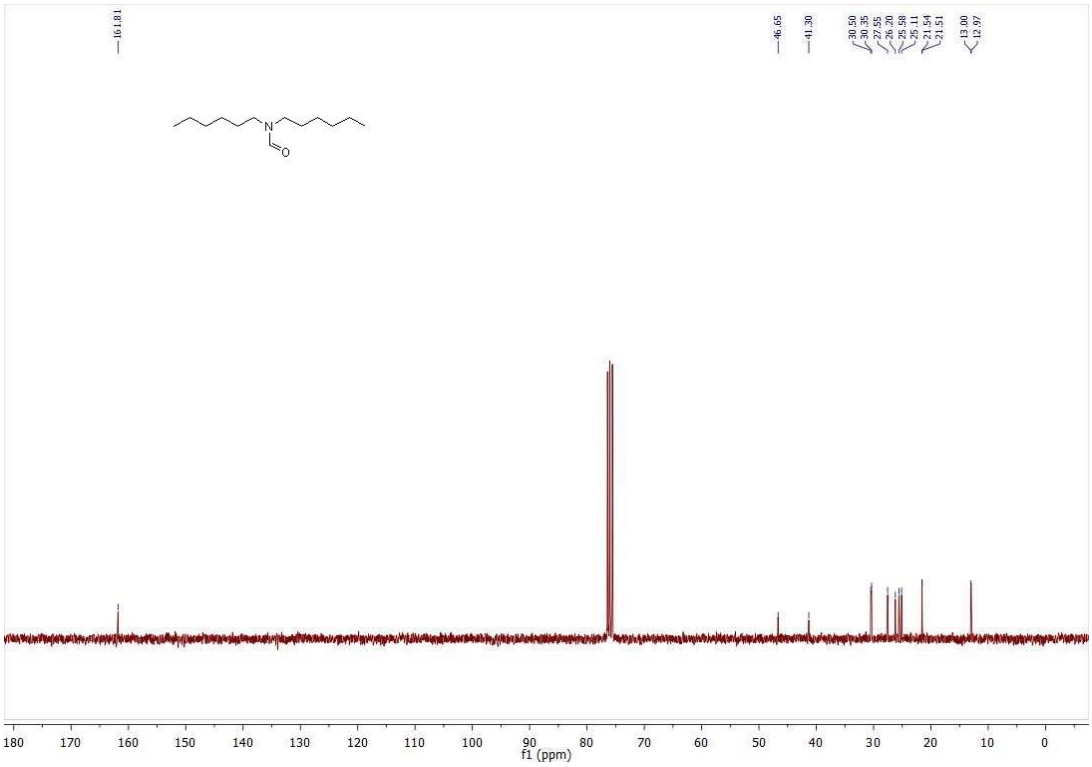

Fig. 16: ^{13}C spectrum of *N*,*N*-dihexylformamide (**1d**).

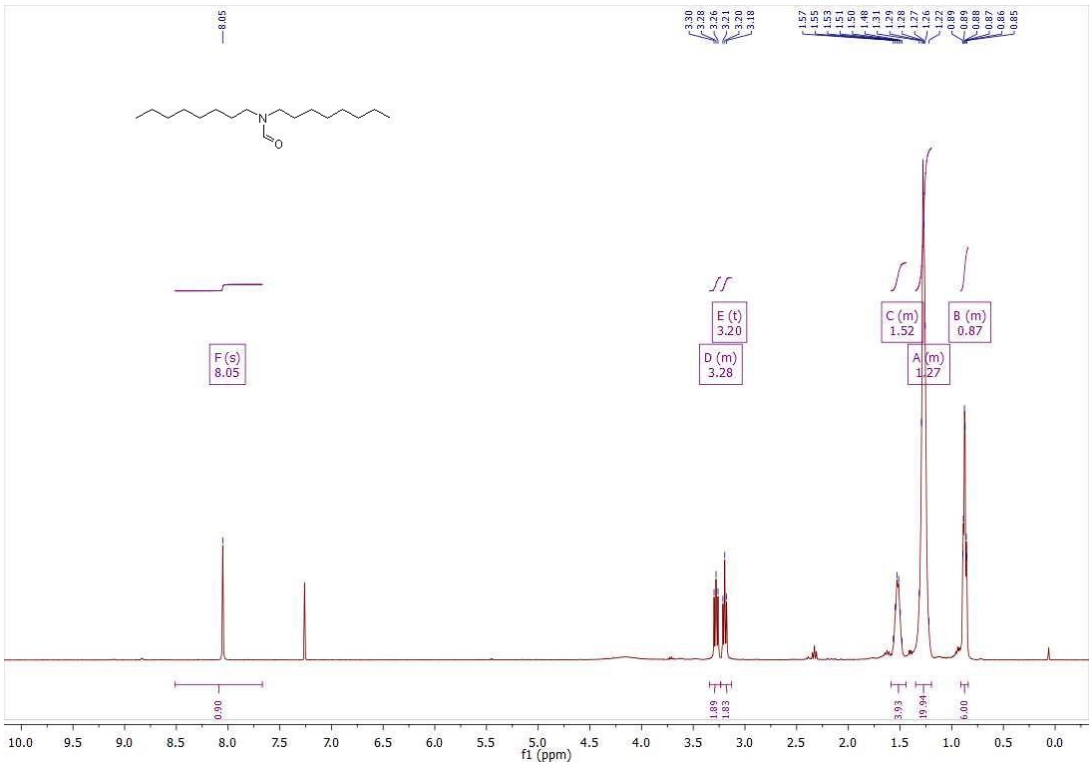

Fig. 17: ^{1}H spectrum of *N*,*N*-dioctylformamide (**1e**).

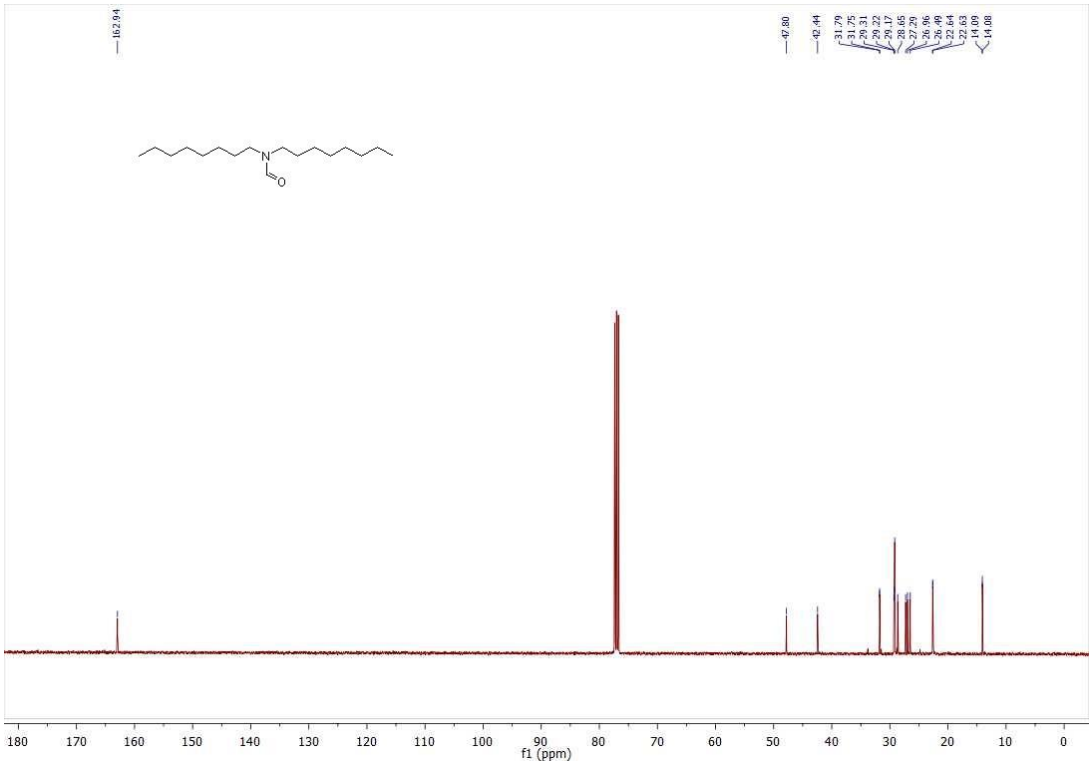

Fig. 18: ^{13}C spectrum of *N*,*N*-dioctylformamide (**1e**).

4.5 References and Notes

‡ Primary amines can also be formylated but with a very low yield (17% yield in case of octylamine to *N*-octylformamide), because they are much less basic compared to secondary or tertiary amines.

[1] C. K. Prier, D. A. Rankic, D. W. MacMillan, *Chem. Rev.* **2013**, *113*, 5322-5363.

[2] J. Hu, J. Wang, T. H. Nguyen, N. Zheng, *Beilstein J Org Chem* **2013**, *9*, 1977-2001.

[3] J. D. Nguyen, E. M. D'Amato, J. M. Narayanam, C. R. Stephenson, *Nat Chem* **2012**, *4*, 854-859.

[4] T. Ghosh, T. Slanina, B. König, *Chem. Sci.* **2015**, *6*, 2027-2034.

[5] I. Ghosh, T. Ghosh, J. I. Bardagi, B. König, *Science* **2014**, *346*, 725-728.

[6] S. Fukuzumi, S. Mochizuki, T. Tanaka, *J. Phys. Chem.* **1990**, *94*, 722-726.

[7] J. M. R. Narayanam, J. W. Tucker, C. R. J. Stephenson, *J. Am. Chem. Soc.* **2009**, *131*, 8756-8757.

[8] J.-M. Kern, J.-P. Sauvage, *J. Chem. Soc., Chem. Commun.* **1987**, 546-548.

[9] A. G. Condie, J. C. González-Gómez, C. R. J. Stephenson, *J. Am. Chem. Soc.* **2010**, *132*, 1464-1465.

[10] R. S. Andrews, J. J. Becker, M. R. Gagné, *Org. Lett.* **2011**, *13*, 2406-2409.

[11] K. S. Schanze, L. Y. C. Lee, C. Giannotti, D. G. Whitten, *J. Am. Chem. Soc.* **1986**, *108*, 2646-2655.

[12] L. Y. C. Lee, X. Ci, C. Giannotti, D. G. Whitten, *J. Am. Chem. Soc.* **1986**, *108*, 175-177.

[13] G. A. Olah, L. Ohannesian, M. Arvanaghi, *Chem. Rev.* **1987**, *87*, 671-686.

[14] C. L. Allen, J. M. J. Williams, *Chem. Soc. Rev.* **2011**, *40*, 3405-3415.

[15] A. Jackson, O. Meth-Cohn, *J. Chem. Soc., Chem. Commun.* **1995**, 1319-1319.

[16] A. Kakehi, S. Ito, S. Hayashi, T. Fujii, *Bull. Chem. Soc. Jpn.* **1995**, *68*, 3573-3580.

[17] B.-C. Chen, M. S. Bednarz, R. Zhao, J. E. Sundeen, P. Chen, Z. Shen, A. P. Skoumbourdis, J. C. Barrish, *Tetrahedron Lett.* **2000**, *41*, 5453-5456.

[18] K. Czifrák, V. Gyóllai, K. E. Kövér, L. Somsák, *Carbohydr. Res.* **2011**, *346*, 2104-2112.

[19] S. Kobayashi, K. Nishio, *J. Org. Chem.* **1994**, *59*, 6620-6628.

[20] K. Iseki, S. Mizuno, Y. Kuroki, Y. Kobayashi, *Tetrahedron* **1999**, *55*, 977-988.

[21] S. Kobayashi, M. Yasuda, I. Hachiya, *Chem. Lett.* **1996**, *25*, 407-408.

[22] I. M. Downie, M. J. Earle, H. Heaney, K. F. Shuhaibar, *Tetrahedron* **1993**, *49*, 4015-4034.

[23] Y. Han, L. Cai, *Tetrahedron Lett.* **1997**, *38*, 5423-5426.

[24] D.-S. Yang, H.-B. Jeon, *Bull. Korean Chem. Soc.* **2010**, *31*, 1424-1426.

[25] W. Li, X.-F. Wu, *Chem. Eur. J.* **2015**, *21*, 14943-14948.

[26] J. J. Byerley, G. L. Rempel, N. Takebe, B. R. James, *J. Chem. Soc. D* **1971**, 1482-1483.

[27] Y. Wang, J. Zhang, J. Liu, C. Zhang, Z. Zhang, J. Xu, S. Xu, F. Wang, F. Wang, *ChemSusChem* **2015**, *8*, 2066-2072.

[28] T. V. Q. Nguyen, W.-J. Yoo, S. Kobayashi, *Angew. Chem. Int. Ed.* **2015**, *54*, 9209-9212.

[29] Y. Wang, F. Wang, C. Zhang, J. Zhang, M. Li, J. Xu, *Chem. Commun.* **2014**, *50*, 2438-2441.

[30] L. A. Shastri, S. L. Shastri, C. D. Bathula, M. Basanagouda, M. V. Kulkarni, *Synth. Commun.* **2011**, *41*, 476-484.

[31] S. Tanaka, T. Minato, E. Ito, M. Hara, Y. Kim, Y. Yamamoto, N. Asao, *Chem. Eur. J.* **2013**, *19*, 11832-11836.

[32] N. Ortega, C. Richter, F. Glorius, *Org. Lett.* **2013**, *15*, 1776-1779.

[33] G.-L. Li, K. K.-Y. Kung, M.-K. Wong, *Chem. Commun.* **2012**, *48*, 4112-4114.

[34] Z. Ke, Y. Zhang, X. Cui, F. Shi, *Green Chem.* **2016**, *18*, 808-816.

[35] N. Shah, E. Gravel, D. V. Jawale, E. Doris, I. N. N. Namboothiri, *ChemCatChem* **2014**, *6*, 2201-2205.

[36] P. Preedasuriyachai, H. Kitahara, W. Chavasiri, H. Sakurai, *Chem. Lett.* **2010**, *39*, 1174-1176.

[37] B. A. Aleiwi, K. Mitachi, M. Kurosu, *Tetrahedron Lett.* **2013**, *54*, 2077-2081.

[38] S. Rostamnia, Z. Karimi, *Inorg. Chim. Acta* **2015**, *428*, 133-137.

[39] C. K. Mann, K. K. Barnes, *"Electrochemical Reactions in Nonaqueous Systems"*, Marcel Dekker, New York, N.Y., **1970**.

[40] B. L. Laube, M. R. Asirvatham, C. K. Mann, *J. Org. Chem.* **1977**, *42*, 670-674.

[41] D. Wang, J. Li, S. Cai, J. Chen, Y. Zhao, *Synlett* **2014**, *25*, 1626-1628.

[42] C. Ouannes, T. Wilson, *J. Am. Chem. Soc.* **1968**, *90*, 6527-6528.

[43] R. H. Young, R. L. Martin, *J. Am. Chem. Soc.* **1972**, *94*, 5183-5185.

[44] H. H. Wasserman, J. R. Scheffer, J. L. Cooper, *J. Am. Chem. Soc.* **1972**, *94*, 4991-4996.

[45] M. Masui, H. Sayo, Y. Tsuda, *J. Chem. Soc. B* **1968**, 973-976.

[46] S. Park, W. H. Jeon, W. S. Yong, P. H. Lee, *Org. Lett.* **2015**, *17*, 5060-5063.

[47] H. K. Hall, *J. Am. Chem. Soc.* **1957**, *79*, 5441-5444.

Chapter 5

5 Attempts Towards Achieving Extremely High Reduction Potentials in Photoredox Catalysis

5.1 Introduction

In the past decades, visible light induced photoredox catalysis has emerged into a useful method for organic synthesis.[1-5] In most cases single photon excitation of dye molecules[1] were used for the photocatalytic conversion of more reactive molecules, which includes electron-poor arenes, such as diazonium[2] or iodonium salts,[6-7] or in a few cases aryl iodides[8-9] with weakly bound leaving groups, due to the limitation of reduction potentials of typical visible light photocatalysts. Recently, we have developed a novel concept in photochemistry, consecutive photo-induced electron transfer (conPET),[10] to overcome this limitation and introduce aryl halides including aryl chlorides for potential aryl radical precursor in photoredox catalysis. However, having said that, this conPET processes are limited to mainly aryl halides with electron withdrawing substituents.[11] Reduction of aryl halides with electron donating substituents or chlorobenzene is difficult to perform due to their high negative reduction potentials (*e.g.* measured reduction potential of chlorobenzene = – 3.11 V vs SCE in MeCN). To achieve such high reduction potential remains a largely elusive and unmet research goal in photoredox catalysis.

Riboflavin and its derivatives are yellow compounds absorbing in the blue region and widely used in photocatalysis especially for oxidation,[12-14] but the reductive flavin photocatalysis is still little investigated.[15-16] Riboflavin tetraacetate (**RFTA**) can be photochemically reduced by electron donors (e.g. tertiary amines, electron rich aromatic alcohols)[17-19] to **RFTAH$_2$** very easily, but regeneration of **RFTA** works only with molecular oxygen, attempts to react the reduced flavin with electron acceptors other than dioxygen were not successful. From calculations it is estimated that the excited state of the fully reduced flavin has a very high reduction potential (– 2.6 V vs SCE).[20-21] Therefore, our next aim was to utilize this high reduction power of excited fully reduced flavin in photocatalysis. In nature, there is an evidence of the excited reduced flavin moiety giving one electron to the thymine dimer in the enzyme Photolyase.[22-23] Photolyase is an enzyme that catalyzes photo-repair of thymine dimers in UV-damaged DNA by electron transfer reaction. There is a direct electron transfer from the excited flavin cofactor to the dimer and back electron transfer from the reduced thymine. Achieving this high reduction potential in photoredox catalysis can solve a long desired research goal.

In our recently developed conPET processes we have used non-substituted (in the bay region) perylene diimide (**PDI**) as the photocatalyst.[10] **PDI** as a photocatalyst we can reach only up to approx. –2.1 V vs SCE *via* conPET using the excited state of the **PDI** radical anion. Using the current conPET photocatalyst (PDI or Rhodamine-6G), reduction of aryl halides with electron donating groups or chlorobenzene are mostly out of reach [*e.g.* $E^0(PhCl/PhCl^{\bullet-})$ = –3.11 V vs SCE]. In this regard, we were investigating new photocatalysts, which can potentially be used in conPET processes and which will have a higher excited state reduction potential of the radical anion. The **PDI** radical anion has an absorption maximum at 702 nm. If we substitute the core positions of **PDI**, the photophysical properties changes dramatically, especially the reduction potentials.[24] The ground state reduction potential is increased if we introduce some electron donating groups at the bay region of **PDI**, but at the same time the absorption maximum of the radical anion is red shifted beyond the visible region. In this aspect, it is worth to mention that naphthalene diimides (**NDIs**) have similar photophysical properties like **PDIs**.[25] **NDIs** possess similar or in most of the cases higher ground state reduction potentials than that of **PDIs**.[26]vs[27] **NDIs** with electron donating substituent in the core position have absorption maxima of the radical anion in the visible region unlike **PDIs**.[28]

5.2 Results and discussion

5.2.1 Oxidation of RFTAH$_2$ to RFTA without dioxygen

RFTA has been widely used for the photochemical oxidation of several organic compounds.[12-14]29] Synthetic reduction of organic compounds has not been well explored yet by flavin photocatalysis. In oxidative flavin photocatalysis, molecular oxygen reacts with the reduced flavin to form H_2O_2 after accepting two protons and two electrons and regenerate **RFTA** in the oxidized form. We wanted to use different two electron acceptors (substrates and mediators) to replace oxygen and overcome the current limit of electron transfer from reduced flavin (**Fig.1**).

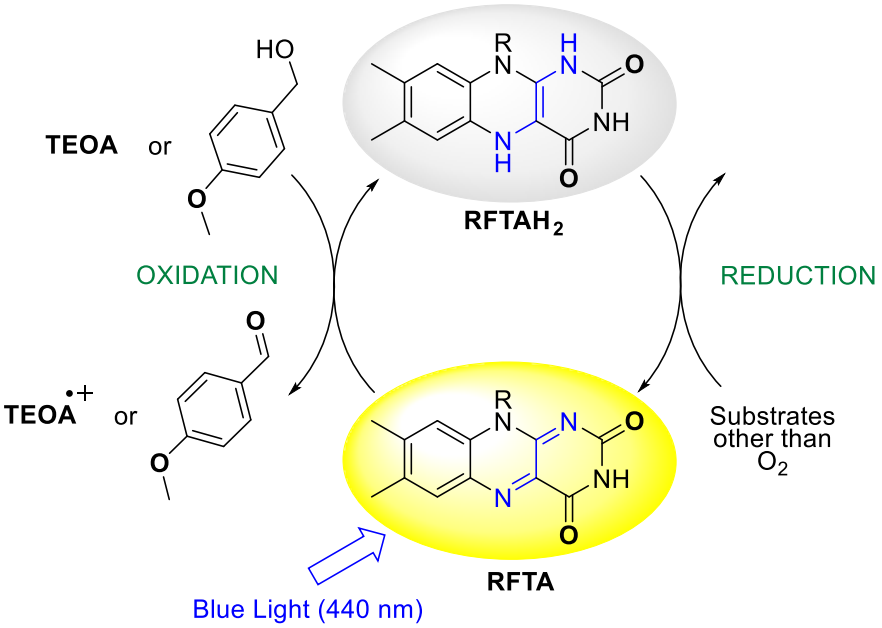

Fig. 1: Attempts to react $RFTAH_2$ with electron acceptor other than dioxygen.

Different substrates were tested to oxidize **RFTAH2** in the absence of oxygen. In most of the cases the substrates stay unreacted and in few cases only trace amounts of product was detected in GC-MS (**Scheme 1**). In 2014, Corma *et. al.* proposed a photobiocatalytic reduction system[30] where flavin was used as a mediator and the reducing equivalents are transferred to the active site of the oxidoreductase, which finally reduces Ketoisophorone to (R)-Levodione. After photochemical reduction of **RFTA** to **RFTAH2** by triethanolamine (**TEOA**), we used Ketoisophorone instead of dioxygen to regenerate **RFTA**. To our surprise, we found out 61% (uncalibrated GC yield) of Ketoisophorone (**1i**) has converted to Levodione (**2i**). Therefore, we tried similar substrates to react the reduced form of RFTA, but it seems that Ketoisophorone (**1i**) was the only special case where the reduction works. Attempts to react with different mediators were not successful either.

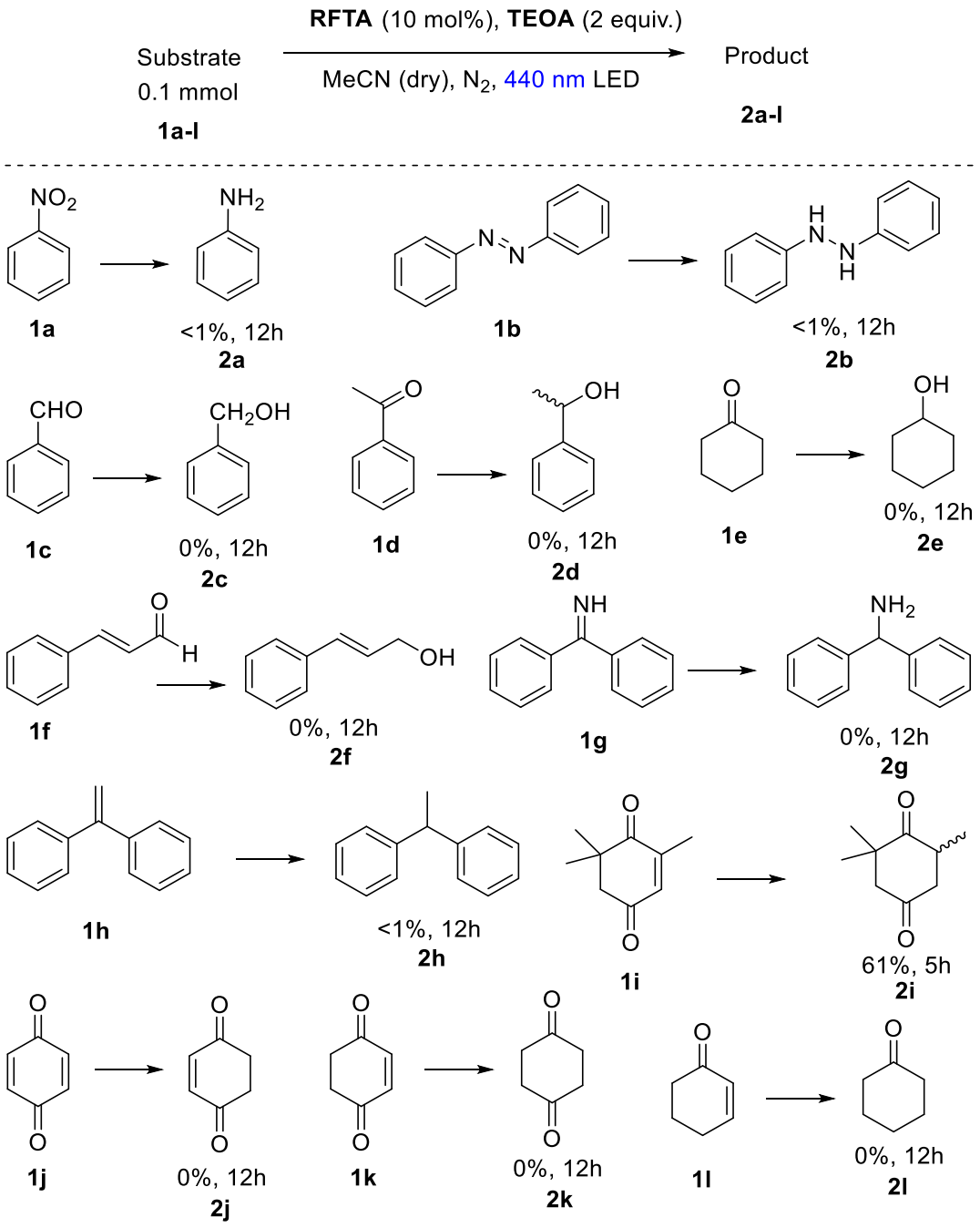

Mediators which were used instead of dioxygen:

[Cp*Rh(III)(bpy)Cl]Cl, Benzoquinone, Co(IV) complexes and Fe(III) complexes.

Yields: uncalibrated GC conversion

Scheme 1: Substrates or mediators which were screened to reduce by $RFTAH_2$ in inert atmosphere (N_2).

5.2.2 Reduction with the excited reduced flavin

As mentioned before, the excited fully reduced flavin has a very high reduction potential.[20-21] Just like in nature, where this high reduction power is being used in photolyase enzymes, we wanted to mimic the strategy in the laboratory for the synthetic reduction of organic compounds (**Fig. 2**).

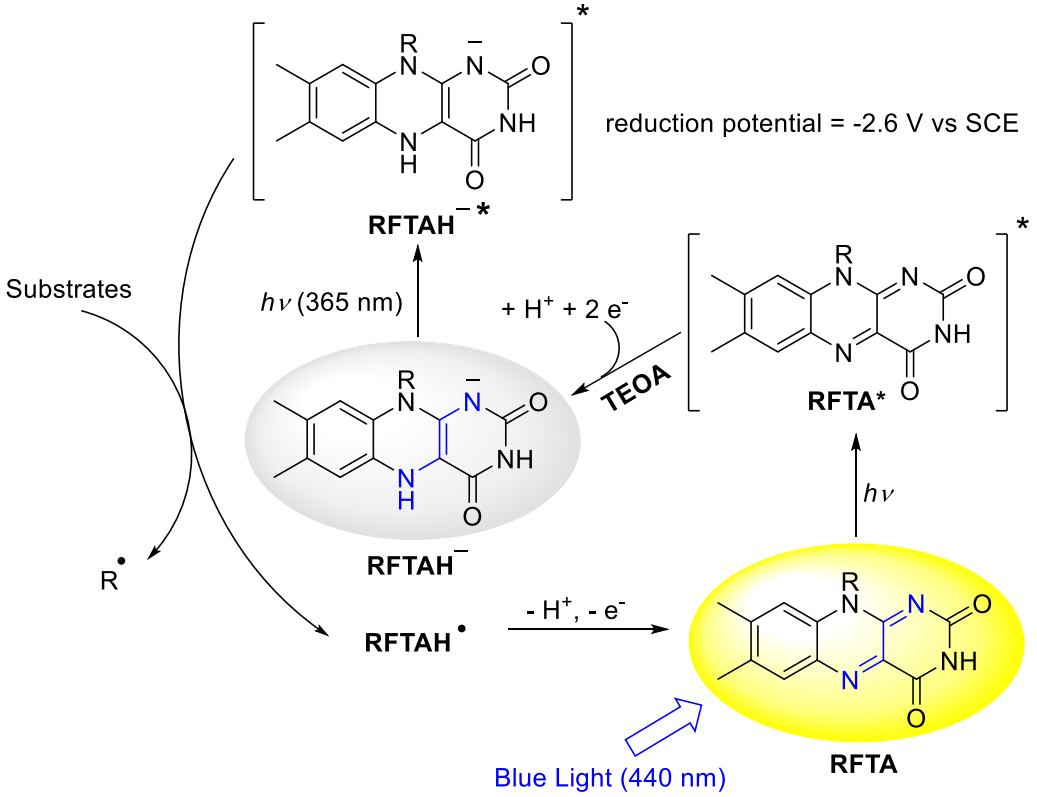

Fig. 2: Attempts to use high reduction power of excited reduced flavin for synthetic reductions.

Flavin can be photochemically reduced by benzyl alcohols or by tertiary amines efficiently.[17-19] In the case of benzyl alcohols **RFTA** is reduced to its fully reduced form (**RFTAH$_2$**), but when amines (*e.g.* **TEOA**) are used as electron donors, we believe the reduced flavin stays in its deprotonated form (**RFTAH$^-$**), because the amine deprotonates the fully reduced flavin. Reduced flavin can be monitored by UV-Vis spectroscopy and it has a broad absorption maximum around 365 nm **(Fig.3)**. So, for the photo-reduction of RFTA we used 455 nm LED. To excite the reduced flavin we used 365 nm UV light. The results are summarized in **Scheme 2**.

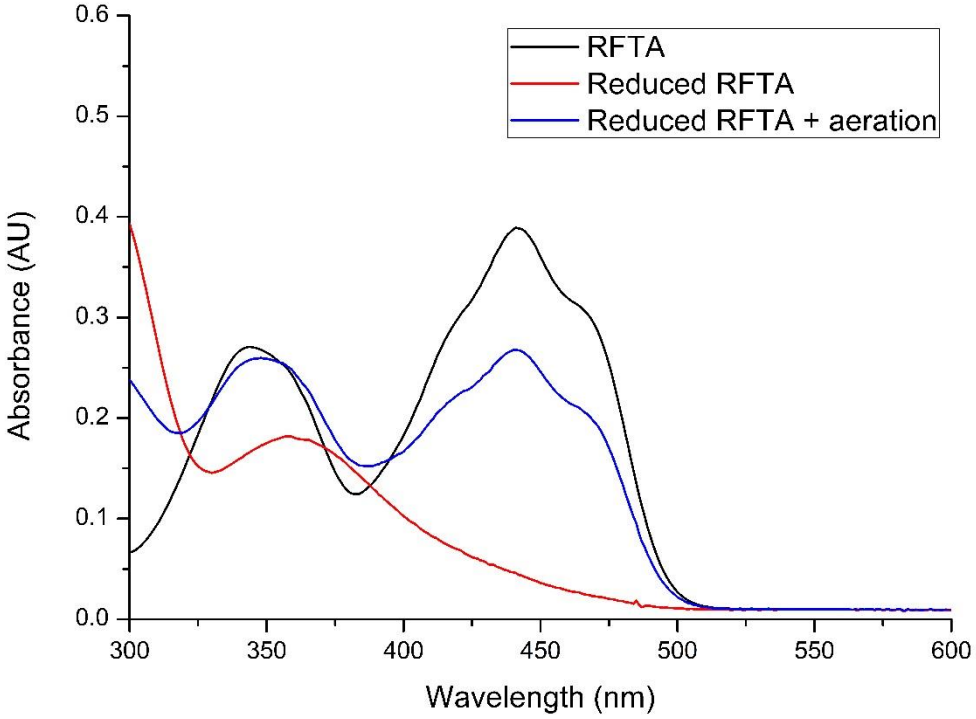

Fig. 3: Photochemical generation of reduced flavin (TEOA as the electron donor, 45 seconds irradiation with 440 nm LED) and reoxidation of reduced flavin after 45 seconds in air.

We have tested both one and two electron reduction systems with the excited reduced flavin catalytic system (**Scheme 2**). In the case of substrates **3c** and **3d** (**Scheme 2A**), small amounts of arylated products (**5c** and **5d** respectively) with furan were detected by GC-MS (Table 1, entries 3 and 4). A control experiment without **RFTA** also showed product formation, as some amount of the carbon-halogen bonds break in the presence of the UV light (365 nm). It is noteworthy to mention that the reduction product was always less than that of the arylated product and the remaining starting material stays unreacted. Many more similar substrates were tested (one electron reduction system), but none of those gave acceptable product yields. We also tried [2+2] cycloadditions with our catalytic system (**Scheme 2A**), but it did not show any product formation. In the case of two electron reduction using the excited reduced flavin, only **1a**, **1b** and **1g** showed product (**2a**, **2b** and **2g** respectively) formation, while other systems did not give any product (**Scheme 2B**).

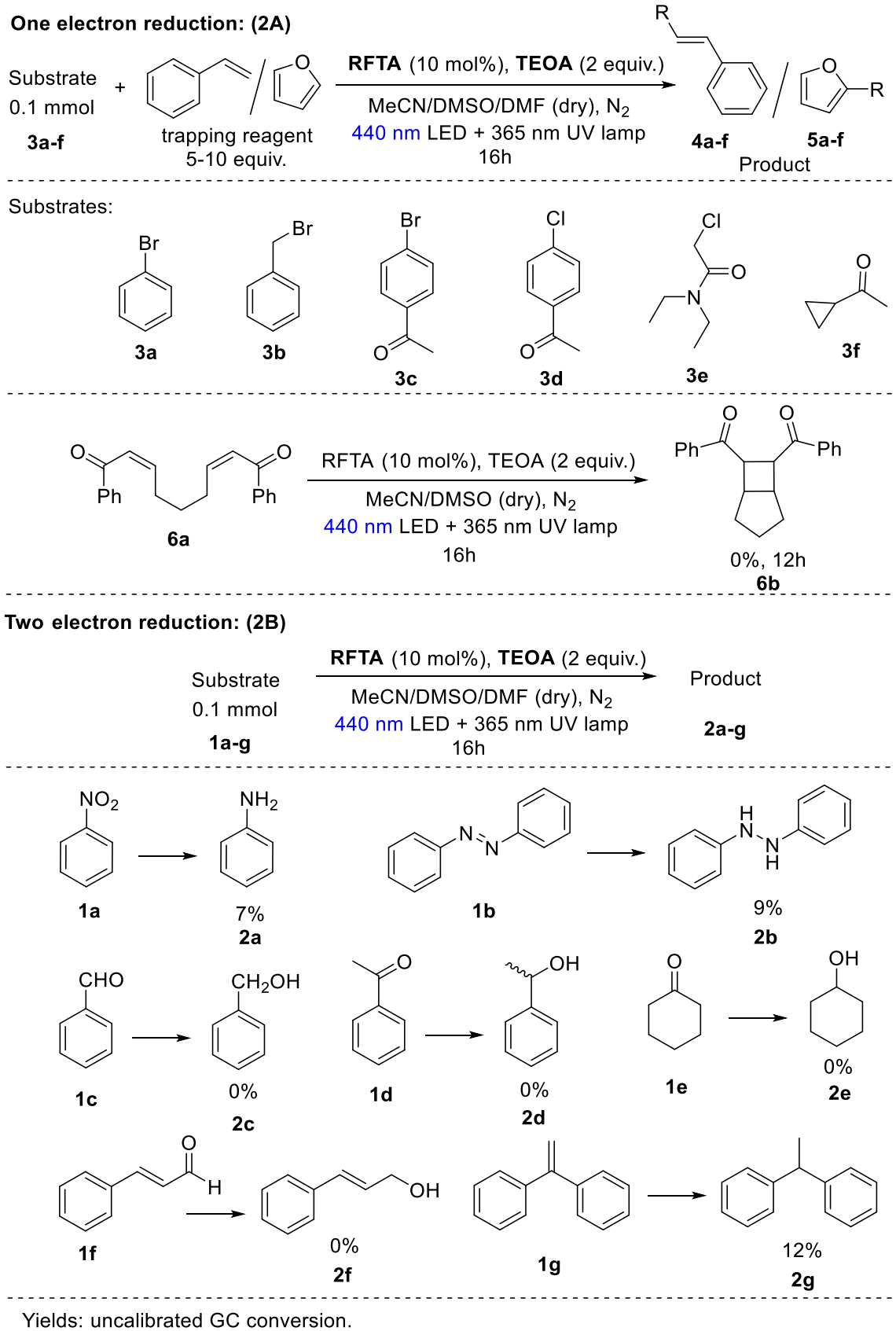

Scheme 2: Substrates used for the reduction with excited reduced flavin.

Table 1: Addition to heteroarenes or double bonds with one electron reduction systems (in the **Scheme 2A**)

Entry	Substrate	Product	Reaction yield with **RFTA** (%)[§]	Reaction yield without **RFTA** (%)[§]
1	**3a**	**4a**	0	0
		5a	0	0
2	**3b**	**4b**	0	0
		5b	0	0
3	**3c**	**4c**	0	0
		5c	14	8
4	**3d**	**4d**	0	0
		5d	9	4
5	**3e**	**4e**	0	0
		5e	14	8
6	**3f**	**4f**	0	0
		5f	0	0

[§] Uncalibrated GC conversion.

5.2.3 Synthesis of substituted NDIs with high negative reduction potential in the excited states

NDI$_{2\text{-}4}$ possess high ground state reduction potentials[28] and forms very stable radical anions[31] in inert atmosphere, which can be excited again with visible light. Most of the radical anions of **NDIs** do not show florescence, therefore it is difficult to calculate the exact excited state reduction potential, but an estimation (see experimental part) shows it may reach a reduction potential of approx. – 3.0 V vs SCE or more, which will be sufficient to reduce most the organic substrates. Therefore, it can be an alternative to the excited reduced flavin. The main problem with these catalysts is their low solubility in polar aprotic solvents such as DMSO, DMF or MeCN. They are very well soluble in DCM, but the photoreduction of aryl halides does not work properly in DCM. Mixtures of DCM/DMF improve the situation, but with a still slow reaction rate.

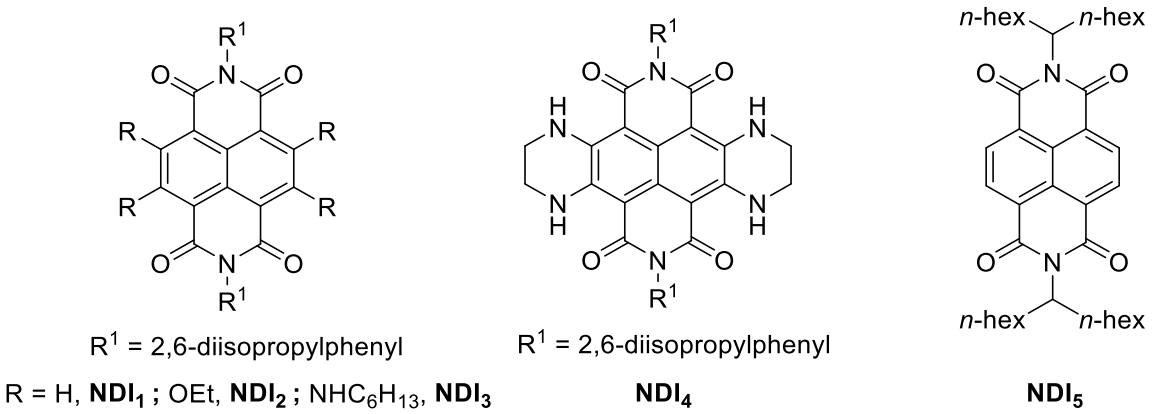

Figure 4: ConPET potent **NDIs** which possess high ground state reduction potentials (see experimental part).

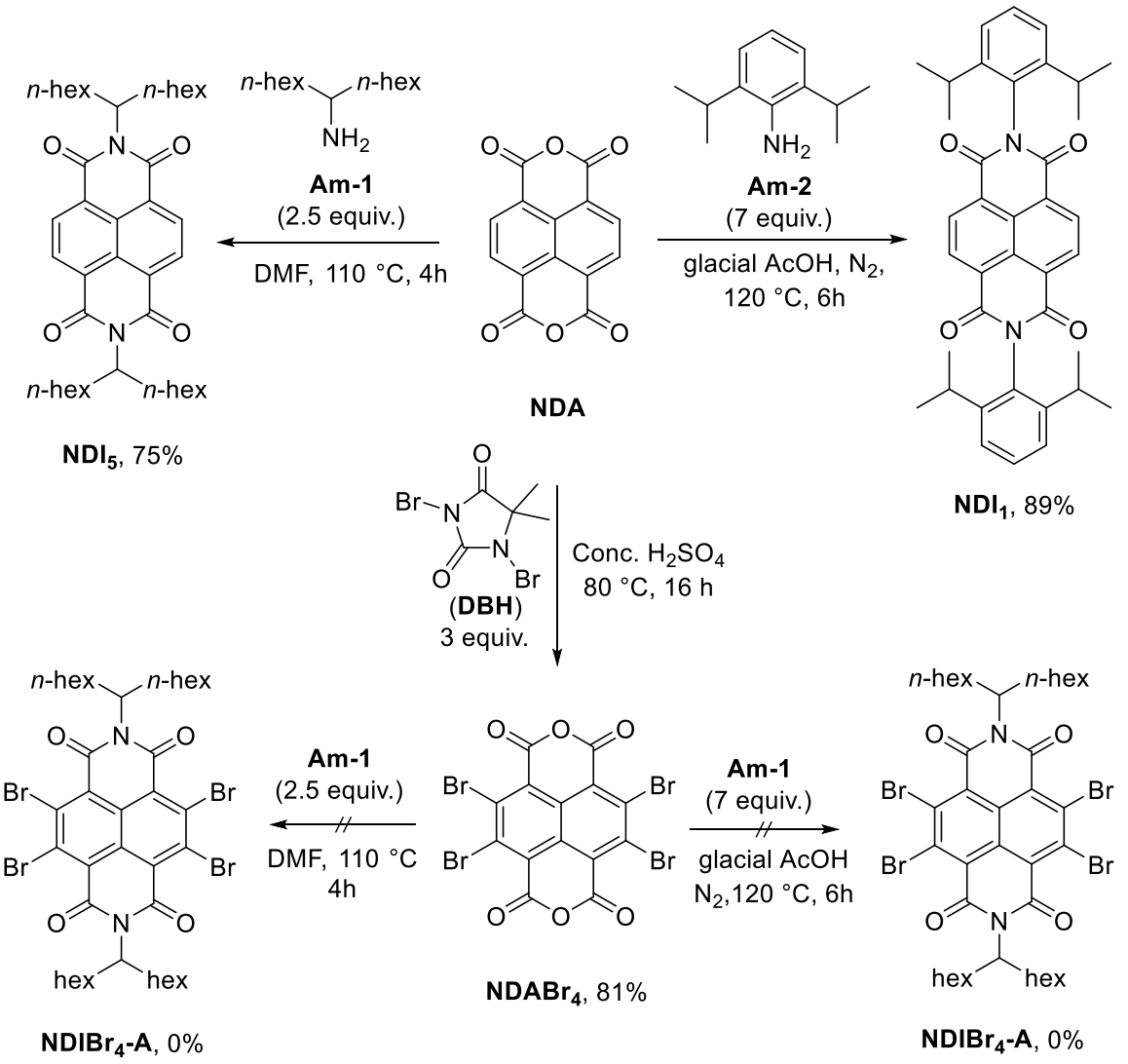

Scheme 3: Synthetic strategy for the preparation of **NDI_1**, **NDI_5**, **$NDABr_4$** and **$NDIBr_4$-A**.

The diimide substitution for the non-core-substituted **NDIs** does not change the UV-Vis spectral properties or the ground state reduction potentials significantly.[25] These properties change dramatically when the core positions of the **NDIs** are substituted.[32-33] **NDI_1** and **NDI_5** have similar UV-Vis spectra both for the neutral and the radical anion forms. The neutral form has an absorption maximum at 382 nm and for the radical anion it is 474 nm (see experimental part, **Fig. 6**). We have used 400 nm LED for the excitation of the neutral form and 455 nm LED for the excitation of the radical anion. However, combination of 380 nm and 475 nm LED might work better. **NDI_1** and **NDI_5** were synthesized according to **Scheme 3** following literature procedures.[28][34] Attempts to synthesize **$NDIBr_4$-A** from **$NDABr_4$** using both procedures were not successful. **$NDABr_4$** was synthesized from **NDA** using 1,3-dibromo-5,5-dimethylhydantoin (**DBH**).[35]

Table 2: Photoreduction with **NDI_1** as a conPET photocatalyst in comparison to **PDI**

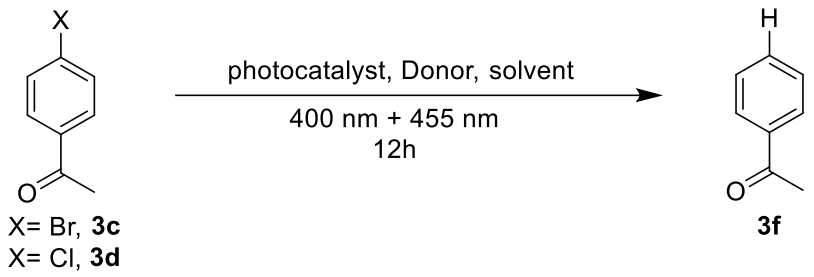

Entry	Catalyst	Substrate	Solvent	Light (nm)	Donor (equiv.)	Yield of **3f** (%)
1	**NDI_1**	**3c**	Dry DCM	(400+455)	Et_3N (8)	~3
2	**NDI_1**	**3c**	Dry DMF	(400+455)	Et_3N (8)	<1
3	**NDI_1**	**3c**	Dry DMSO	(400+455)	Et_3N (8)	~0
4	**NDI_1**	**3c**	DCM/DMF (1:1)	(400+455)	Et_3N (8)	54
5	**NDI_1**	**3c**	DCM/DMF (1:1)	(400+455)	DIPEA (8)	66
6	**NDI_1**	**3c**	DCM/DMF (1:5)	(400+455)	DIPEA (8)	91
7	**NDI_1**	**3c**	DCM/DMF (1:5)	(400+455)	DIPEA (4)	81
8	-	**3c**	DCM/DMF (1:5)	(400+455)	DIPEA (8)	19
9	**PDI**	**3c**	DCM/DMF (1:5)	455	Et_3N (8)	79
10	**NDI_1**	**3d**	DCM/DMF (1:5)	(400+455)	Et_3N (8)	30*

§ Calibrated GC yields with appropriate internal standard; *yield after 72h.

NDI_1 is not well soluble in DMF, therefore DCM was added to increase the solubility. **NDI_1** and **PDI** work at a similar rate for the reduction of 4-bromoacetophenone (**3c**) in (1:5) DCM/DMF (**Table 2**). From entry 8, it is evident that there is a background reaction for the reduction of **3c**. When we moved to 4-chloroacetophenone (**3d**), there is no background reaction, but the photoreduction rate drops even further (Table 2, entry 10). As the above mentioned **NDIs** were very poorly soluble we wanted to synthesize **NDIs** with branched alkyl chains (**$NDIBr_4$-A**) for better solubility and then introduce different electron donating substituents in the core of **$NDIBr_4$-A**. **NDI_5** is well soluble in DMF/DMSO and was used as a conPET photocatalyst, which is able to reduce aryl bromides for C-H arylation reactions. So, if we can substitute the bay region of **NDI_5** it should also be well soluble and more importantly should possess very high reduction potential in the ground state like **$NDI_{2\text{-}4}$**. This may lead to highly reducting excited radical anions.

In 2013, Govindaraju *et. al.* reported[35] that the reaction of **$NDABr_2$** to **$NDIBr_2$** proceeds *via* one step with good yield, but the reaction from **$NDABr_4$** to **$NDIBr_4$-B** forms a ring-opened side product, which is the major product. After refluxing the side product in toluene in the presence of PBr_3 the desired ring-closed product can be obtained in good yield (**Scheme 4**). So, it was thought that the previously performed reactions for the formation of **$NDIBr_4$-A** was not successful, because it always formed the ring-opened side product. However, we found using these two step procedure, the reaction from **$NDABr_4$** to **$NDIBr_4$-B** works out well only in case of *n*-octylamine as the coupling partner, not with the branched alkyl amine (*e.g.* 1-hexylheptylamine, **Am-1**). We have also followed the synthetic route from **$NDABr_2$** to **$NDIBr_2$-B** for the synthesis of **$NDIBr_2$-A**, but we were unable to achieve the expected product. **$NDABr_2$** was synthesized from **NDA** using tribromoisocyanuric acid (**TBCA**) by selective bromination (**Scheme 4B**) using a literature known procedure.[36]

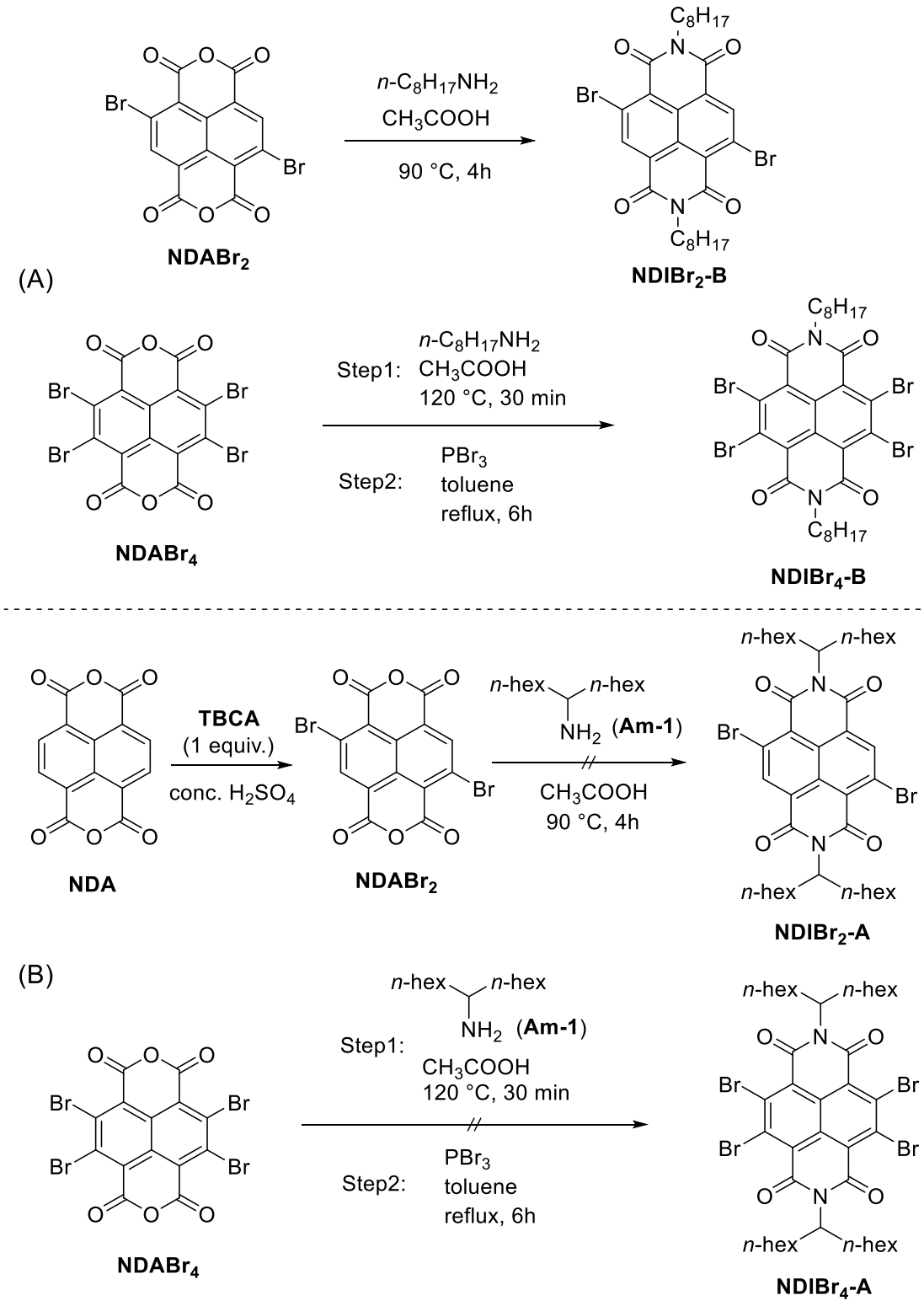

Scheme 4: (A) Reported synthetic route of **NDIBr$_2$-B** and **NDIBr$_4$-B**; (B) Attempted synthesis of **NDIBr$_2$-A** and **NDIBr$_4$-A** using the same strategy.

5.3 Conclusion

A reduction reaction with RFTA was successful in only one case other than molecular oxygen; Ketoisophorone (**1i**) was converted to Levodione (**2i**) with reduced **RFTA**. Although it is known that reduced **RFTA** in the excited state is a very powerful reducing agent, utilizing this power for synthetic reductions seems to be very challenging and has to be investigated further. The addition of a base can be useful for the deprotonation (**RFTAH**$^-$) of the fully reduced flavin (**RFTAH$_2$**), which may facilitate the photocatalytic cycle. Initial studies were performed for the syntheses of **NDIs** as potential photocatalysts for conPET processes, which can exceed the current conPET limit. Unfortunately, **NDIs** shows low solubility in polar aprotic solvents, which were attempted to be improved using branched alkyl amines for the diimide formation. However, the synthesis of these **NDIs** remained challenging and has to be investigated further.

5.4 Experimental section

5.4.1 Materials and methods

All commercially available compounds and solvents were purchased and used without further purification unless otherwise stated. **RFTA** was prepared according to the literature procedure.[37] **NDA** was purchased from Sigma Aldrich and was used for the preparation of **NDIs** and brominated **NDAs** and **NDIs**. Spectroscopic grade MeCN, DMF and DMSO were dried with molecular sieves according to the reported procedure.[38]

Thin-layer chromatography was performed using silica gel plates 60 F254: Visualization was accomplished with short wavelength UV light (254 nm). Standard flash chromatography was performed on an Isolera™ Spektra Systems automated with high performance flash purification system using silica gel of particle size 40−63 μm or a reverse column (specification: Biotage SNAP KP-C18-HS-12g). Preparative high-pressure liquid chromatography (HPLC) was performed using a C18 reverse column and water/acetonitrile mixtures with a UV detector.

^{1}H and ^{13}C NMR spectra were recorded on Bruker Avance spectrometers (300 MHz and 75 MHz or 400 MHz and 101 MHz) in $CDCl_3$ and DMSO-d_6 solution with internal solvent signal as reference (7.26 and 77.0, 2.50 and 39.4 respectively). Proton NMR data are

reported as follows: chemical shift (ppm), multiplicity (s = singlet, d = doublet, t = triplet, q = quartet, quint = quintet, sext = sextet, hept = heptet, dd = doublet of doublets, ddd = doublet of doublets of doublets, td = triplet of doublets, qd = quartet of doublets, m = multiplet, br. s. = broad singlet), coupling constants (Hz) and numbers of protons. Data for ^{13}C NMR are reported in terms of chemical shift and no special nomenclature is used for equivalent carbons.

High resolution mass spectra (HRMS) were obtained from the central analytic mass spectrometry facilities of the Faculty of Chemistry and Pharmacy, Regensburg University and are reported according to the IUPAC recommendations 2013. Gas chromatography (GC) and gas chromatography coupled to low resolution mass spectrometry (GC–MS) analysis were performed using a capillary column (length: 30 m; diam. 0.25 mm; film: 0.25 µ) using He gas as carrier. GC was equipped with an FID detector. GC–MS was performed on 5975 MSD single quadruple detector. Reduction products were identified by comparing with authentic samples (GC/FID and GC–MS). Detection of reduction products was performed by GC/FID analysis UV–Vis analyses were performed with Varian Cary 50 UV/Vis spectrophotometer and Agilent 8453 UV-Vis Spectrometer. The UV-Vis measurements with online irradiation were performed (**Fig. 3**) on a self-made apparatus[39] using a fluorescence cuvette in a fluorescence cuvette holder, LED (Cree-XP, royal blue, 455 nm) placed perpendicular to the optical pathway of the Agilent 8453 UV-Vis Spectrometer. The whole system was stirred with a small magnetic PTFE stirring bar by a magnetic stirrer placed above the cuvette. Photocatalytic reactions with RFTA were performed with 440 nm LEDs and 365 nm one-spot UV lamp; photoreaction with **NDIs** were performed with 455 nm LEDs and 400 nm LEDs from OSRAM.

5.4.2 General photoreaction procedure

General procedure for the reduction reaction with $RFTAH_2$ (Scheme 1)

The starting material (0.1 mmol, 1 equiv.), triethanolamine (**TEOA**, 0.2 mmol, 2 equiv.), **RFTA** (0.01 mmol, 10 mol%) were taken in a 5 mL crimp cap vial equipped with a small PTFE stirring bar. The vial was sealed with a PTFE septum and dry MeCN/ (1:1) MeCN/H_2O was added under N_2 atmosphere. The reaction mixture was degassed by 3 freeze-pump-thaw cycles and filled with nitrogen gas. The reaction vessel was placed in a cooling block cooled to 25 °C, was irradiated through the plane bottom side by 3W blue

LED (λ_{em} = 440 nm) and the reaction conversion was monitored by GC analysis and GC-MS.

General procedure for the reduction reaction with excited reduced RFTA (Scheme 2 and Table 1)

The starting material (0.1 mmol, 1 equiv.), **TEOA** (0.2 mmol, 2 equiv.), **RFTA** (0.01 mmol, 10 mol%) and trapping reagent (if stated; 5-10 equiv.) were placed in a 5 mL crimp cap vial equipped with a small PTFE stirring bar. The vial was sealed with a PTFE septum and dry MeCN/ DMF/ DMSO was added under N_2 atmosphere. The reaction mixture was degassed by 3 freeze-pump-thaw cycles and filled with nitrogen gas. The reaction vessel was placed in a cooling block cooled to 25 °C, was irradiated through the bottom side by 3W blue LED (λ_{em} = 440 nm) and from the side by 365 nm high power UV lamp. The reaction conversion was monitored by GC analysis and GC-MS.

General procedure for the photo-reduction of aryl halides with NDIs (Table 2)

The aryl halide (0.1 mmol, 1 equiv.), trimethylamine or *N*,*N*-diisopropylethylamine (**TEA** or **DIPEA**; 2-8 equiv.), **NDI_1** or **NDI_5** (0.01 mmol, 10 mol%) and the trapping reagent (only for C-H arylation; 5-10 equiv.) were mixed in a 5 mL crimp cap vial equipped with a small PTFE stirring bar. The vial was sealed with a PTFE septum and dry MeCN/ DMF/ DMSO was added under N_2 atmosphere. The resulting mixture was degassed (× 2) *via* a syringe needle and filled with nitrogen gas. The reaction vessel was placed in a cooling block cooled to 25 °C, was irradiated through the bottom side of the vial by 3W blue LED (λ_{em} = 455 nm). The reaction conversion was monitored by GC analysis and GC-MS.

5.4.3 Syntheses of compounds

Synthesis of riboflavin tetraacetate (RFTA)[37]

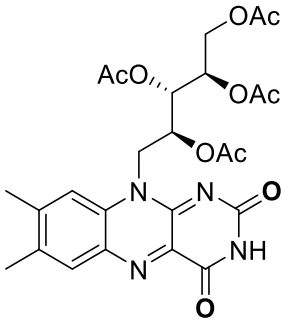

The reaction was carried out following a literature known procedure.[37]
To a (1:1) mixture of glacial acetic acid (200 mL) and acetic anhydride (200 mL), riboflavin (5.0 g, 13.3 mmol) was added. 1 mL of HClO4 was added dropwise while stirring and the colour of the solution turned greenish-yellow. The reaction mixture was stirred for 30 min at 40 C, then cooled in an ice bath. Then, the reaction mixture was diluted with 400 mL of cold water and extracted with chloroform (3 x 200 mL). The combined organic phase was extracted and washed with water and brine. The solution was dried over Na_2SO_4 and evaporated to dryness. After recrystallisation from ethanol, compound RFTA (5.4 g, 75%) was obtained as a yellow colored crystalline solid.
^{1}H NMR (400 MHz, $CDCl_3$) δ = 8.48 (s, 1H), 8.03 (s, 1H), 7.56 (s, 1H), 5.67 (d, *J*=9.0, 1H), 5.53 – 5.34 (m, 2H), 4.90 (s, 1H), 4.43 (dd, *J*=12.3, 2.9, 1H), 4.24 (dd, *J*=12.3, 5.7, 1H), 2.56 (s, 3H), 2.44 (d, *J*=0.9, 3H), 2.28 (s, 3H), 2.21 (s, 3H), 2.07 (s, 3H), 1.76 (s, 3H).

^{13}C NMR (101 MHz, $CDCl_3$) δ = 170.64, 170.31, 169.90, 169.76, 159.28, 154.37, 151.99, 148.17, 137.05, 136.05, 134.67, 133.01, 131.25, 115.54, 70.50, 69.46, 69.03, 61.90, 45.07, 21.50, 21.07, 20.83, 20.72, 20.36, 19.49.

Synthesis of N,N‘-Bis-(2‘,6‘-diisopropylphenyl)-1,4,5,8-naphthalene tetracarboxylic diimide (NDI_1)[28]40]

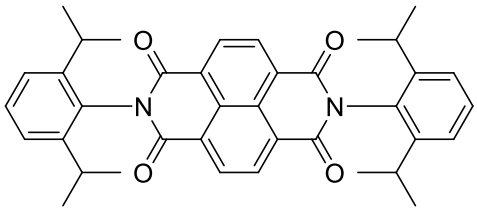

To a mixture of **NDA** (2.0 g, 7.46 mmol) and glacial acetic acid (109 mL) 2,6-diisopropylaniline (9.85 mL, 52.2 mmol) was added and the suspension was stirred for 6 h at 120 °C under N_2 atmosphare. After cooling down to room temperature water (50 mL) was poured into the reddish-brown solution and the mixture was neutralized with a saturated solution of $NaHCO_3$. The compound was extracted with chloroform (4 x 60 mL) and $MgSO_4$ was added to the combined organic phases. The solvent was evaporated and the product was dried in high vacuum. White solid was purified by flash chromatography (DCM/petroleum ether = 1:1). Yield: 3.9 g, 89%.

^{1}H NMR (300 MHz, $CDCl_3$) δ = 8.89 (s, 4H), 7.53 (dd, *J*=8.3, 7.2, 2H), 7.37 (d, *J*=7.7, 4H), 2.71 (hept, *J*=6.8, 4H), 1.17 (d, *J*=6.9, 24H).

^{13}C NMR (75 MHz, $CDCl_3$) δ = 162.95, 145.50, 131.61, 130.02, 129.98, 127.68, 126.90, 124.26, 29.32, 23.99.

Synthesis of N,N’-Bis-1-hexylheptylnaphthalenetetracarboxylic-1,4,5,8-biscarboximide(NDI_5)[34]

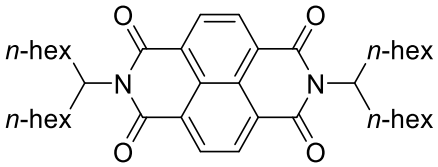

NDA (500 mg, 1.9 mmol) and 1-hexylheptylamine (0.93 g, 4.7 mmol) were suspended in DMF (17 mL), and the resulting mixture was stirred at 110 °C for 4 h until complete dissolution of all components). The reaction mixture was cooled to room temperature and then quenched by the addition of hydrochloric acid (2 N, 33 mL), extracted with chloroform (3 x 40 mL), dried over $MgSO_4$. The organic phase was evaporated and purified by column

chromatography (DCM/petroleum ether = 1:1). An orange, slowly crystalizing viscous oil was obtained in 75% yield (880 mg).

^{1}H NMR (300 MHz, $CDCl_3$) δ = 8.88 – 8.58 (m, 4H), 5.34 – 4.99 (m, 2H), 2.33 – 2.08 (m, 4H), 1.95 – 1.73 (m, 4H), 1.35 – 1.11 (m, 32H), 0.87 – 0.77 (m, 12H).

^{13}C NMR (75 MHz, $CDCl_3$) δ = 164.19, 163.00, 131.39, 130.61, 126.80, 55.17, 32.29, 31.73, 29.16, 26.86, 22.56, 14.05.

Synthesis of 2,3,6,7-tetrabromo-1,4,5,8-naphthalenetetracarboxylic dianhydride ($NDABr_4$)[35]

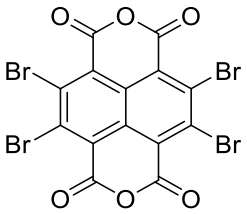

In a 100 mL single-necked RB flask, NDA (2.68 g, 10 mmol) was added in concentrated sulfuric acid (50 mL) at room temperature. Then, DBH (8.8 g, 30.8 mmol) was added in portions and the flask was tightly closed with a glass stopper. The resulting brown suspension was stirred at room temperature for 4 h and then the mixture was heated at 80 °C for 12 h. The mixture was poured into ice to precipitate the solid. The precipitated solid was filtered and washed with water and methanol. Finally, it was dried in a desiccator over KOH to obtain **$NDABr_4$** as yellow solid (4.7 g, 81%). The obtained yellow solid was used in next steps without further purification.

Synthesis of tribromoisocyanuric acid (TBCA)[41]

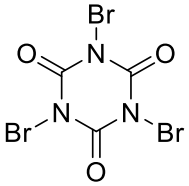

Cyanuric acid (12.5 mmol), NaOH (37.5 mmol), Na_2CO_3 (18.75 mmol) and KBr (37.5 mmol) was added in 180 mL of H_2O and cooled in an ice bath while stirring. A solution of Oxone (37.5 mmol) in H_2O (150 mL) was added dropwise. A white solid precipitates during

the addition of oxone forming a dense suspension, which was stirred for 24 h. The product is isolated by vacuum filtration and washed with cold H_2O. The white solid (**TBCA**)was then dried over P_2O_5 in a desiccator yielding 85% of pure TBCA.

Synthesis of 2,6-dibromo-1,4,5,8-naphthalenetetracarboxylic dianhydride ($NDABr_2$)[36]

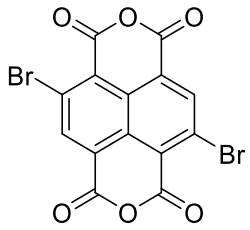

In a 50 mL single necked RB flask **NDA** (10 mmol) was added in 25 mL of concentrated H_2SO_4 at room temperature. The suspension was stirred for 5 min and then **TBCA** (1.0 equiv.) was added in portions for 1 h while stirring. The resulting solution was further stirred for 12 hours at room temperature. The reaction mixture was then poured into crushed ice to precipitate the solid. Then the solid substance was washed with water and methanol, and finally dried in desiccator over KOH. The obtained light yellow solid (**$NDABr_2$**) was used in next steps without further purification.

Synthesis of 1-hexylheptylamine (Am-1)[42]

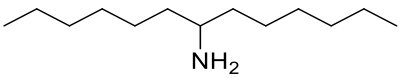

Dihexyl ketone (2.5 g, 12.6 mmol), NH_4OAc (10 g, 129 mmol) and $NaBH_3CN$ (0.56 g, 8.9 mmol) were dissolved in 40 ml methanol and stirred at room temperature for 56 h. The reaction was quenched by slow addition of 2 mL of concentrated HCl . The solution was then concentrated with a rotary evaporator. The solid obtained was dispersed in 250 mL of water and adjusted to pH=10 with KOH. The obtained latex solution was extracted by $CHCl_3$ (2 x 150 mL). After evaporating the organic phase, a pale yellow oil (**Am-1**) was obtained in 92% yield (2.3 g).

^{1}H NMR (300 MHz, $CCDCl_3$) δ = 2.76 – 2.58 (m, 1H), 1.43 – 1.14 (m, 20H), 0.86 (h, *J*=3.2, 2.8, 6H).

^{13}C NMR (75 MHz, $CDCl_3$) δ = 51.26, 38.03, 31.89, 29.50, 26.15, 22.66, 14.11.

Calculation of approx. reduction potentials for NDI radical anions in the excited state[43]

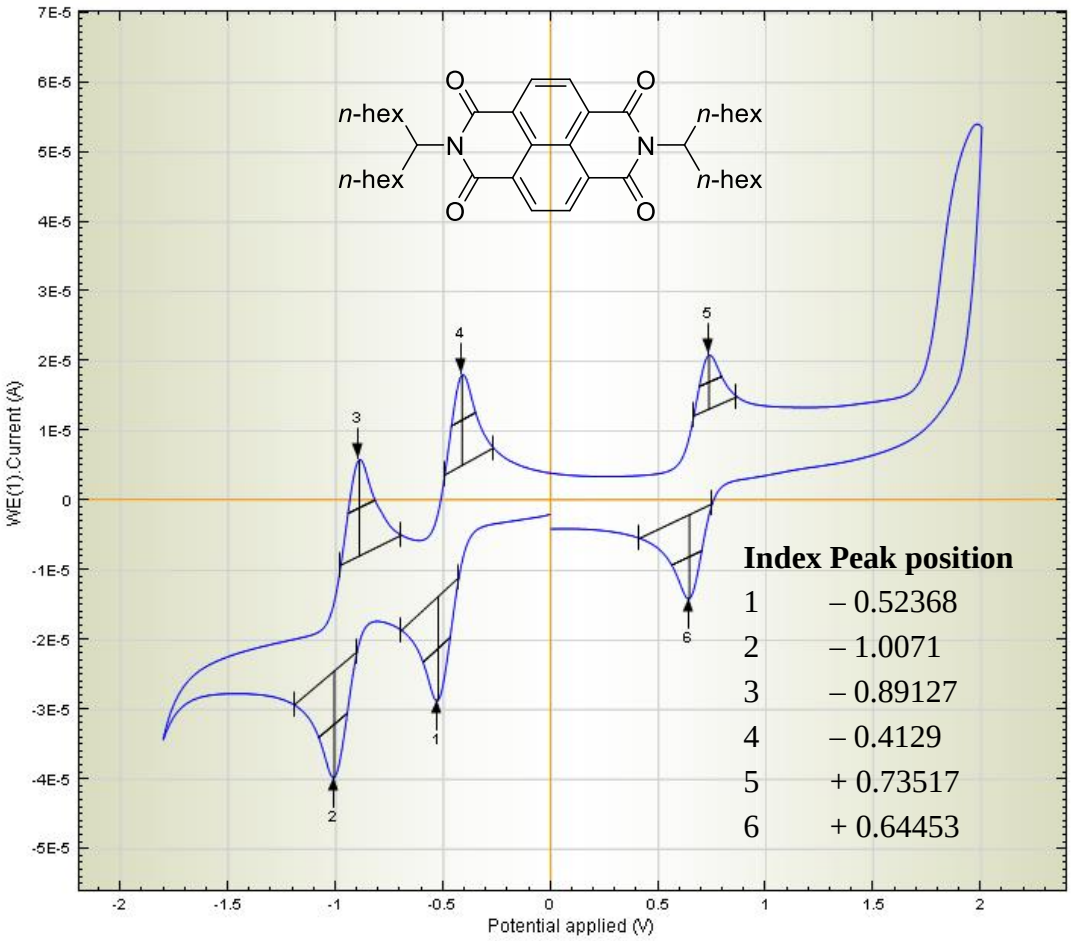

Fig 4: Cyclic voltammogram for **NDI_5** in DCM against FC/FC^+ electrode. Peak positions 5 and 6 correspond to FC/FC^+, peak positions 1 and 4 correspond to **NDI_5**/**$NDI_5^{\bullet-}$** and peak positions 2 and 3 correspond to **$NDI_5^{\bullet-}$**/**NDI_5^{2-}**.

Calculation of ground state reduction potential of **NDI_5**:

$$E^0(\mathbf{NDI_5}/\mathbf{NDI_5^{\bullet-}}) = -[(0.52368 + 0.4129)/2 + (0.73517 + 0.64453)/2]\ \text{V vs } FC/FC^+$$
$$= -1.158\ \text{V vs } FC/FC^+$$
$$= (-0.778 + 0.38)\ \text{V vs SCE}$$
$$= -0.778\ \text{V vs SCE}$$

Similarly, $E^0(\mathbf{NDI_5^{\bullet-}}/\mathbf{NDI_5^{2-}}) = -1.259$ V vs SCE

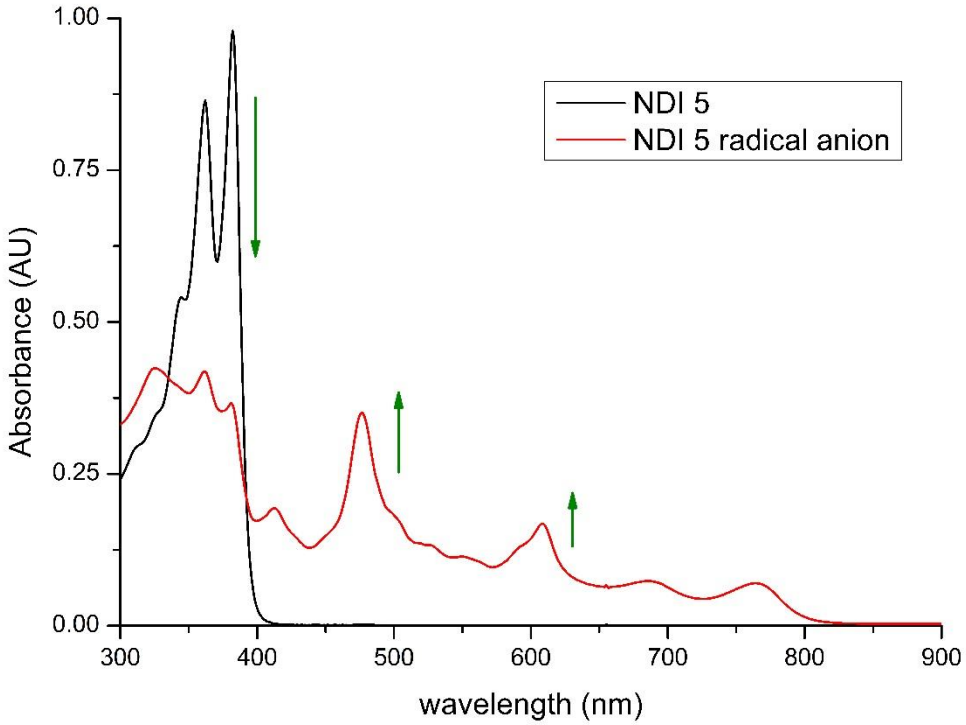

Fig 5: UV-Vis absorption spectrum of **NDI$_5$** (black) and the radical anion of **NDI$_5$** (red).

The radical anion of **NDI$_5$** has intense visible and near-infrared (NIR) absorption bands at > 450 nm. The most characteristic and prominent band is at 474 nm (**Fig. 5**) which is very common for Non-core-substituted **NDIs** irrespective of the imide substituents (*e.g.* butyl, octyl, branched alkyl chain, 2,6-diisopropylphenyl, 2,5-di-*tert*-butylphenyl).[31][44] The diimide substituents for the non-core-substituted **NDIs** mainly affect the solubility in polar aprotic solvents (e.g. MeCN, DMF, DMSO) and do not affect the ground state reduction potential or the UV-Vis spectral properties significantly. Most of the radical anions of **NDIs** do not show fluorescence, therefore it is hard to evaluate the crossover point between the absorption spectra and the fluorescence spectra; leaving an uncertainty in calculating the E_{00} (0-0 transition, energy gap between the zeroth vibrational levels of the ground and excited states) value. If we excite the **NDI$_5$** at 474 nm and if we calculate the E_{00} transition energy at around 600 nm, we get a value *c.a.* 2.1 eV.

So, the approx. excited state reduction potential of **NDI$_5$** radical anion, E^0(**NDI$_5$**/**NDI$_5^{\bullet -*}$**) = [E^0(**NDI$_5$**/**NDI$_5^{\bullet -}$**) – E_{00}] = (– 0.778 – 2.1) V vs SCE = – 2.88 V vs SCE

NDI$_2$, **NDI$_3$** and **NDI$_4$** have higher ground state reduction potentials [E^0(NDI/NDI$^{\bullet -}$) = – 0.9 V, – 1.31 V and – 1.47 V vs SCE respectively; E^0_{red} vs FC/FC$^+$ + 0.38 V = E^0_{red} vs SCE][28] in comparison to – 0.778 V of **NDI$_5$**. Therefore, core substituted (electron donating substituents) **NDIs** has the potential to go beyond – 3.0 V in their excited state of radical anions.

5.4.4 ^{1}H and ^{13}C NMR spectra of few synthesized compounds

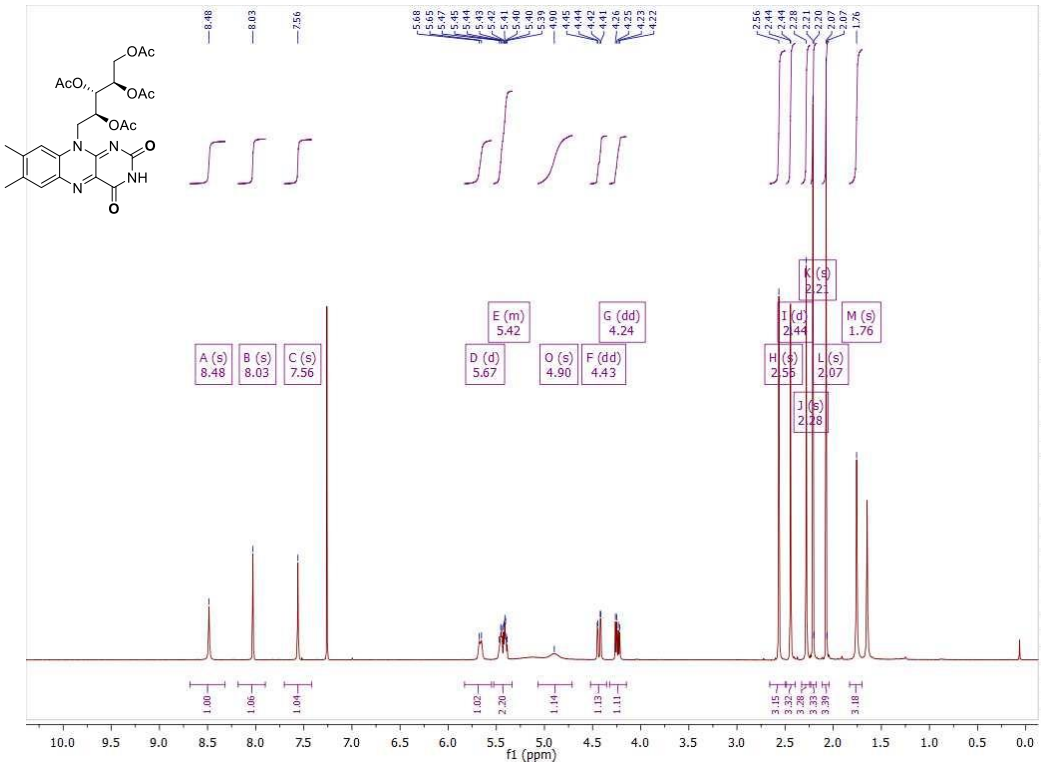

Fig. 6: ^{1}H spectrum of **RFTA**.

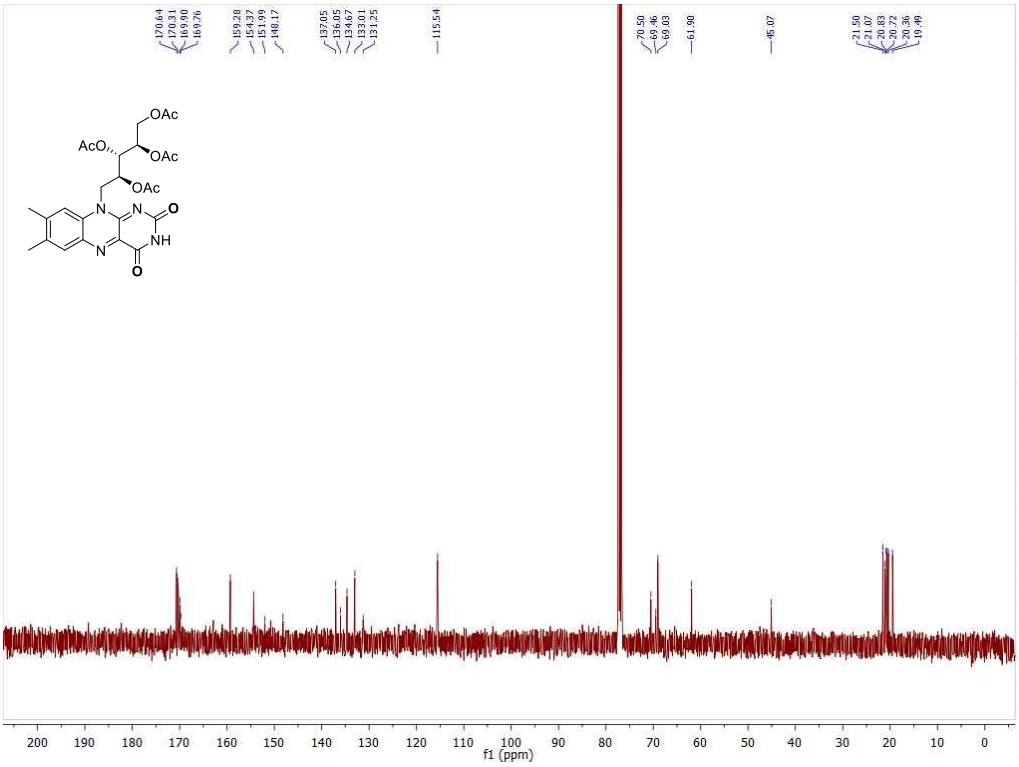

Fig. 7: ^{13}C spectrum of **RFTA**.

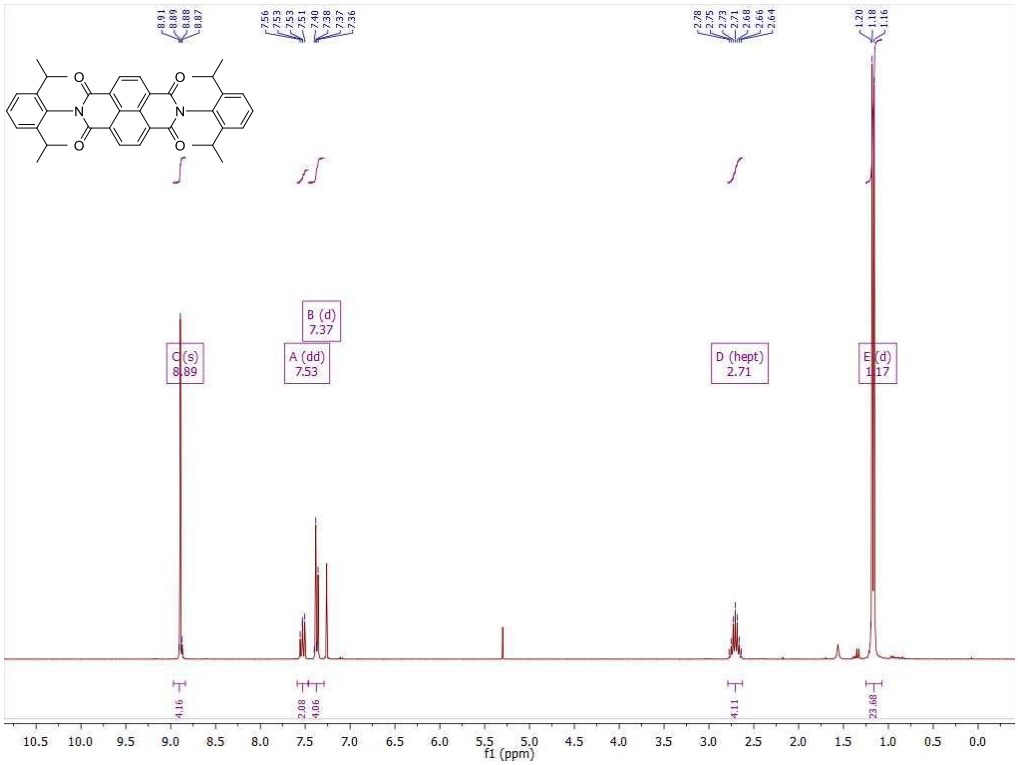

Fig. 8: ^{1}H spectrum of **NDI_1**.

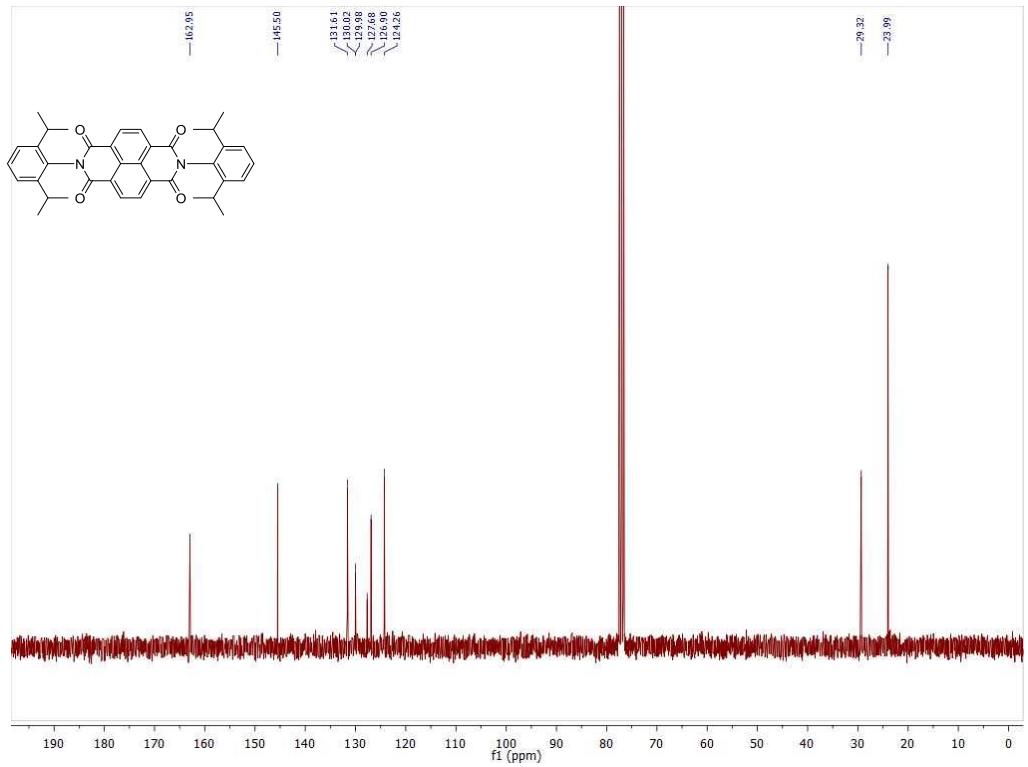

Fig. 9: ^{13}C spectrum of **NDI_1**.

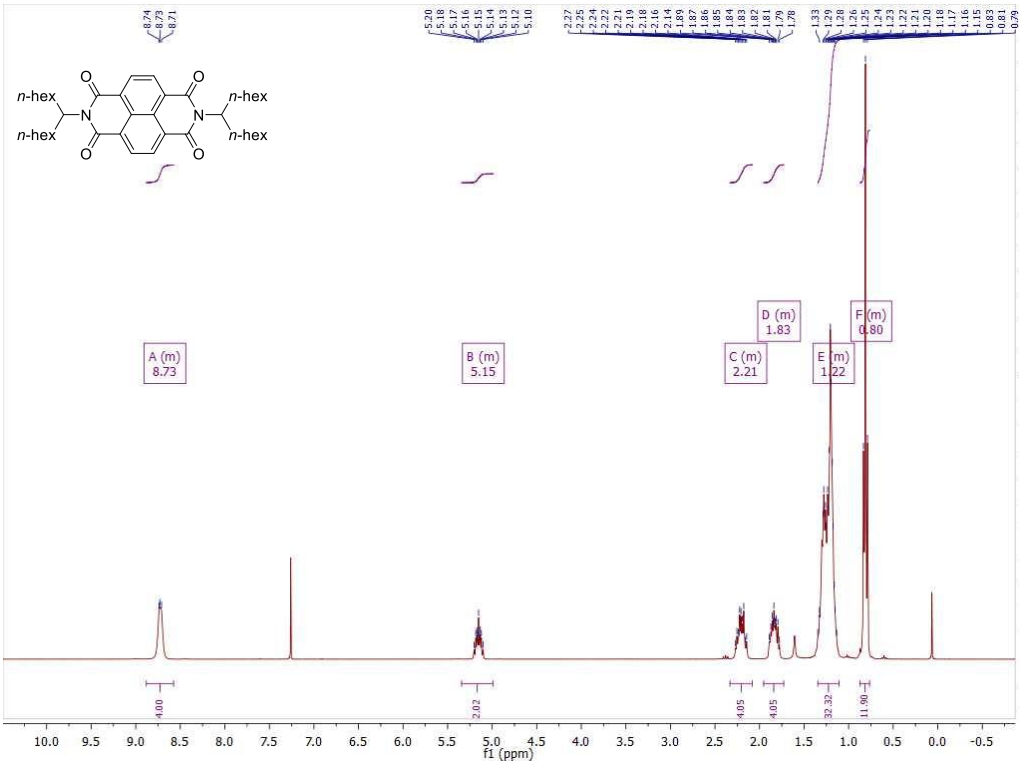

Fig. 10: ^{1}H spectrum of **NDI_5**.

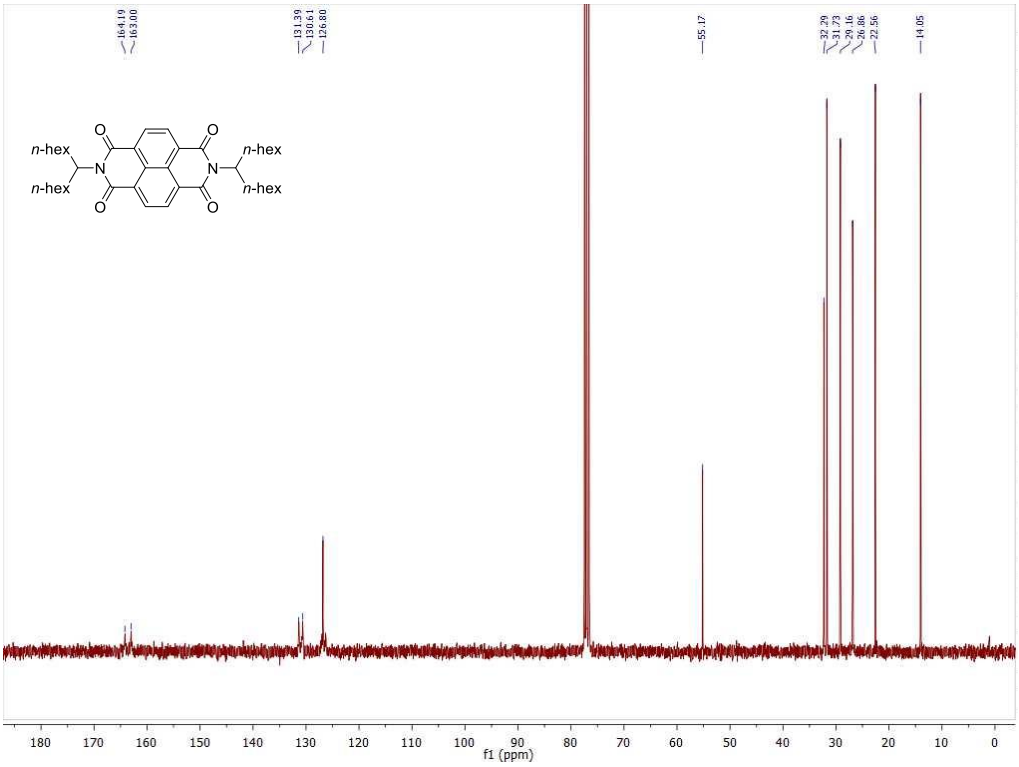

Fig. 11: ^{13}C spectrum of **NDI$_5$**.

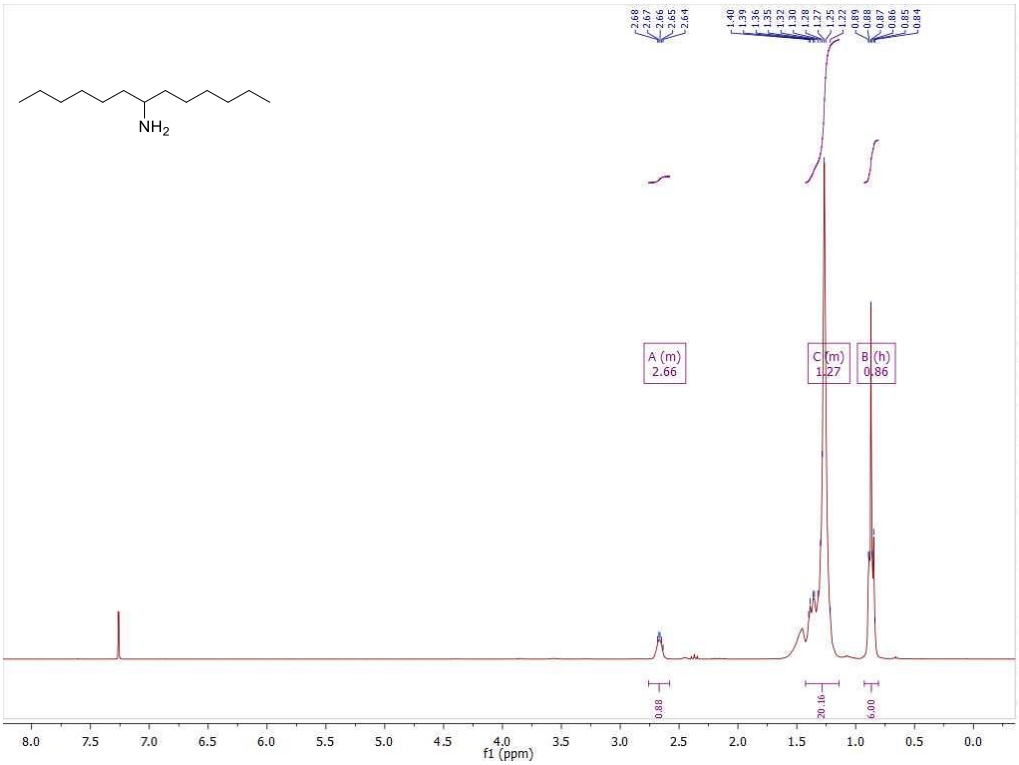

Fig. 12: ^{1}H spectrum of 1-hexylheptylamine (**Am-1**).

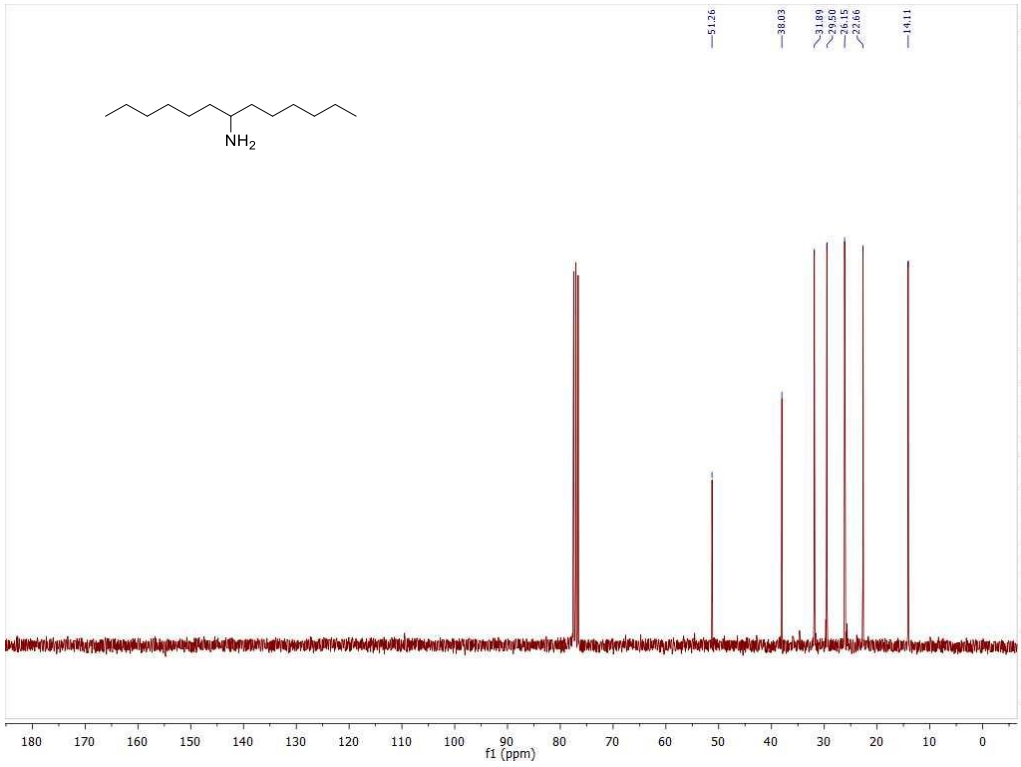

Fig. S13: ^{13}C spectrum of 1-hexylheptylamine (**Am-1**).

5.5 References

[1] C. K. Prier, D. A. Rankic, D. W. MacMillan, *Chem. Rev.* **2013**, *113*, 5322-5363.

[2] D. P. Hari, B. König, *Angew. Chem. Int. Ed.* **2013**, *52*, 4734-4743.

[3] N. A. Romero, D. A. Nicewicz, *Chem. Rev.* **2016**, DOI: 10.1021/acs.chemrev.1026b00057.

[4] S. Fukuzumi, K. Ohkubo, *Org. Biomol. Chem.* **2014**, *12*, 6059-6071.

[5] M. D. Kärkäs, J. A. Porco, C. R. J. Stephenson, *Chem. Rev.* **2016**, DOI: 10.1021/acs.chemrev.1025b00760.

[6] A. Baralle, L. Fensterbank, J.-P. Goddard, C. Ollivier, *Chem. Eur. J.* **2013**, *19*, 10809-10813.

[7] M. Tobisu, T. Furukawa, N. Chatani, *Chem. Lett.* **2013**, *42*, 1203-1205.

[8] J. D. Nguyen, E. M. D'Amato, J. M. R. Narayanam, C. R. J. Stephenson, *Nat. Chem.* **2012**, *4*, 854-859.

[9] H. Kim, C. Lee, *Angew. Chem. Int. Ed.* **2012**, *51*, 12303-12306.

[10] I. Ghosh, T. Ghosh, J. I. Bardagi, B. König, *Science* **2014**, *346*, 725-728.

[11] I. Ghosh, B. König, *Angew. Chem. Int. Ed.* **2016**, *55*, 7676-7679.

[12] R. Lechner, S. Kummel, B. Konig, *Photochem. Photobiol. Sci.* **2010**, *9*, 1367-1377.

[13] H. Schmaderer, P. Hilgers, R. Lechner, B. König, *Adv. Synth. Catal.* **2009**, *351*, 163-174.

[14] R. Lechner, B. König, *Synthesis* **2010**, *2010*, 1712-1718.

[15] T. Hering, B. Mühldorf, R. Wolf, B. König, *Angew. Chem. Int. Ed.* **2016**, *55*, 5342-5345.

[16] B. Mühldorf, R. Wolf, *Angew. Chem. Int. Ed.* **2016**, *55*, 427-430.

[17] E. Amouyal, *Sol. Energy Mater. Sol. Cells* **1995**, *38*, 249-276.

[18] P. F. Heelis, *Chem. Soc. Rev.* **1982**, *11*, 15-39.

[19] U. Megerle, M. Wenninger, R.-J. Kutta, R. Lechner, B. Konig, B. Dick, E. Riedle, *Phys. Chem. Chem. Phys.* **2011**, *13*, 8869-8880.

[20] S. R. Yeh, D. E. Falvey, *J. Am. Chem. Soc.* **1992**, *114*, 7313-7314.

[21] R. F. Anderson, *Biochim. Biophys. Acta, Bioenerg.* **1983**, *722*, 158-162.

[22] Z. Liu, C. Tan, X. Guo, Y.-T. Kao, J. Li, L. Wang, A. Sancar, D. Zhong, *PNAS* **2011**, *108*, 14831-14836.

[23] S. Weber, *Biochim. Biophys. Acta, Bioenerg.* **2005**, *1707*, 1-23.

[24] C.-W. Chang, H.-Y. Tsai, K.-Y. Chen, *Materials* **2014**, *7*, 5488-5506.

[25] D. Gosztola, M. P. Niemczyk, W. Svec, A. S. Lukas, M. R. Wasielewski, *J. Phys. Chem. A* **2000**, *104*, 6545-6551.

[26] C. Thalacker, C. Röger, F. Würthner, *J. Org. Chem.* **2006**, *71*, 8098-8105.

[27] M. J. Ahrens, M. J. Tauber, M. R. Wasielewski, *J. Org. Chem.* **2006**, *71*, 2107-2114.

[28] C. Röger, F. Würthner, *J. Org. Chem.* **2007**, *72*, 8070-8075.

[29] S. Fukuzumi, S. Kuroda, T. Tanaka, *J. Am. Chem. Soc.* **1985**, *107*, 3020-3027.

[30] M. Mifsud, S. Gargiulo, S. Iborra, I. W. C. E. Arends, F. Hollmann, A. Corma, *Nat Commun* **2014**, *5*, 3145, DOI: 3110.1038/ncomms4145.

[31] S. V. Bhosale, C. H. Jani, S. J. Langford, *Chem. Soc. Rev.* **2008**, *37*, 331-342.

[32] N. Sakai, J. Mareda, E. Vauthey, S. Matile, *Chem. Commun.* **2010**, *46*, 4225-4237.

[33] S.-L. Suraru, F. Würthner, *Angew. Chem. Int. Ed.* **2014**, *53*, 7428-7448.

[34] H. Langhals, S. Kinzel, *J. Org. Chem.* **2010**, *75*, 7781-7784.

[35] M. Sasikumar, Y. V. Suseela, T. Govindaraju, *Asian J. Org. Chem.* **2013**, *2*, 779-785.

[36] Y. V. Suseela, M. Sasikumar, T. Govindaraju, *Tetrahedron Lett.* **2013**, *54*, 6314-6318.

[37] A. Barthel, L. Trieschmann, D. Ströhl, R. Kluge, G. Böhm, R. Csuk, *Arch. Pharm.* **2009**, *342*, 445-452.

[38] D. B. G. Williams, M. Lawton, *J. Org. Chem.* **2010**, *75*, 8351-8354.

[39] T. Ghosh, T. Slanina, B. König, *Chem. Sci.* **2015**, *6*, 2027-2034.

[40] G. Rauch, S. Hoger, *Chem. Commun.* **2014**, *50*, 5659-5661.

[41] L. S. de Almeida, P. M. Esteves, M. C. S. de Mattos, *Synlett* **2006**, *2006*, 1515-1518.

[42] Y. Che, A. Datar, K. Balakrishnan, L. Zang, *J. Am. Chem. Soc.* **2007**, *129*, 7234-7235.

[43] G. J. Kavarnos, *"Fundamentals of Photoinduced Electron Transfer"*, VCH Publishers, Inc., **1993**.

[44] A. Viehbeck, M. J. Goldberg, C. A. Kovac, *J. Electrochem. Soc.* **1990**, *137*, 1460-1466.

6 Summary

This thesis reports new methods using the reductive quenching cycle in photoredox catalysis for organic synthesis, including C-H arylation of pyrroles and double bonds, chemoselective aldehyde reduction and *N*-formylation.

In Chapter 1, we depict a few important tools on the basis of redox potentials for the photo-induced electron transfer between the photocatalyst and the electron donor/acceptor. We also describe the initial ideas behind the developed projects.

In Chapter 2, a novel concept, consecutive photo-induced electron transfer (conPET) is introduced to overcome the limitations of visible light photocatalysis for the reduction of less reactive aryl halides. The scope of aryl radical precursors was extended to aryl chlorides, which was beyond the limit of normal photocatalytic cycles. Perylene diimide (PDI) was used as the conPET photocatalyst, which after excitation to PDI^{*} takes up an electron from a suitable electron donor (*e.g.* Et_3N) and forms the radical anion in the ground state ($PDI^{\bullet -}$). Upon excitation this stable $PDI^{\bullet}$ gains enough redox power to transfer an electron to aryl halides (Ar-X) and regenerate the PDI in the ground state. This photogenerated radical anion ($Ar\text{-}X^{\bullet -}$) then fragments to form an aryl radical ($Ar^{\bullet}$). This aryl radical is either trapped by heteroarenes or double bonds to give C-H arylated products or accepts a hydrogen atom either from the solvent or from the oxidized amine to give the reduction product.

In Chapter 3, we summarize the findings examining the previously reported Rhodium-Proflavine (Rh_{cat}-PF) system for synthetic reduction reactions. With this system, the chemoselective photoreduction of aldehydes was performed with a broad substrate scope *via* slow *in situ* generation of Rh(III)–H, which kinetically distinguishes between aldehydes and ketones. The photoreduction proceeds *via* two different pathways. The major pathway which is highly oxygen sensitive is the photo-induced electron transfer from triethanolamine to the proflavine triplet state and the subsequent reduction of Rh_{cat} leading to Rh(III)–H. The other pathway, which is dependent on light intensity is the oxidative quenching of the PF singlet state by Rh_{cat} which occurs dominantly in non-degassed systems. The light intensity clearly influences the reaction mechanism and the product yields.

In Chapter 4, we show that the by-products from photochemically oxidized amines can be utilized for further transformations. We have successfully transformed byproducts of oxidized amines to *N*-formamides without adding any formylating agent under simple and mild reaction conditions. Oxygen is essential for the reaction to proceed as it helps to regenerate the photocatalyst to its ground state and forms a superoxide radical anion, which is a vital intermediate for the reaction. The photoreaction is assumed to proceed *via* the *in situ* formation of an enamine intermediate reacting with a hydroperoxyl radical, which is formed after proton abstraction by the superoxide radical anion.

In Chapter 5, we summarize some attempts to achieve very high reduction potentials *via* photoredox catalysis. Since conPET processes with PDI as a photocatalyst are limited to mainly aryl halides with electron withdrawing groups, we wanted to broaden the scope by developing a photocatalytic system, which can go beyond. Potential photocatalysts, which were considered for this unmet goal are riboflavin tetraacetate (RFTA) and naphthalene diimides (NDIs) as theoretically both of them possess a high reduction potential in their excited reduced form. Initial studies were performed for synthesizing potential NDIs for conPET processes and reduction reactions with reduced RFTA or excited reduced RFTA, but they remain challenging and can potentially be explored prospectively.

7 Zusammenfassung

Diese Arbeit beschäftigt sich mit der Entwicklung neuer Synthesemethoden auf dem Gebiet der Photoredoxkatalyse. Hierbei wurde der angeregte Photokatalysator reduktiv gelöscht (gequencht), um verschiedene organische Reaktionen wie die C-H –Arylierung von Pyrrol Derivaten und Alkenen, die chemoselektive Reduktion von Aldehyden sowie eine *N*-Formylierung photokatalytisch zu ermöglichen.

Im ersten Kapitel werden wichtige, theoretische Grundlagen zur Berechnung von Redoxpotentialen im angeregten Zustand sowie zu photoinduziertem Elektronentransfer dargelegt. Zudem werden die grundlegenden Konzepte der einzelnen Projekte erläutert.

Im zweiten Kapitel wird ein neuartiges Konzept, der konsekutive photoinduzierte Elektronentransfer (conPET) vorgestellt, welches die Reduktion von bisher photokatalytisch nicht zugänglichen Arylhalogeniden ermöglicht. Die Substratbreite reduzierbarer Arylhalogenide konnte so auf Arylchloride ausgeweitet werden, eine Substanzklasse, die außerhalb der Reichweite des klassischen Ein-Photonen-Zyklus lag. Als Photokatalysator im conPET Prozess wurde der organische Farbstoff Perylendiimid (PDI) eingesetzt. PDI kann nach Anregung durch sichtbares Licht ein Elektron von einem geeigneten Elektronendonor aufnehmen (*z.B.* Et_3N) und bildet so ein Radikalanion im Grundzustand ($PDI^{\bullet-}$). Dieses stabile Radikalanion ($PDI^{\bullet-}$) besitzt nach einer weiteren Anregung durch sichtbares Licht genug Reduktionskraft, um ein Elektron auf ein Arylhalogenid (Ar-X) zu übertragen, wodurch PDI selbst in seinem Grundzustand regeneriert wird. Das photokatalytisch erzeugte Radikalanion des Arylhalogenids ($Ar\text{-}X^{\bullet-}$) fragmentiert zu einem Arylradikal ($Ar^{\bullet}$), welches entweder durch Heteroarene oder Alkene abgefangen werden kann und so C-H –arylierte Produkte erzeugen kann. Andererseits kann auch ein H-Atom vom Lösungsmittel oder dem oxidierten Amin abstrahiert werden und somit das Reduktionsprodukt gebildet werden.

In Kapitel 3 haben wir das literaturbekannte Rhodium-Proflavin (Rh_{cat}-PF) System auf synthetisch nutzbare Reduktionen angewandt. Dabei konnte die chemoselektive Photoreduktion von Aldehyden durch die langsame *in situ* Erzeugung von Rh(III)–H realisiert werden. Das System weist eine hohe Substratbreite auf und ermöglicht die kinetische Differenzierung zwischen Aldehyden und Ketonen. Die beschriebene

Photoreduktion verläuft über zwei verschiedene Reaktionswege. Der dominierende Reaktionsweg ist stark sauerstoffempfindlich und läuft über einen photoinduzierten Elektronentransfer von Triethanolamin auf den Triplett-Zustand des Proflavins, wodurch im folgenden Rh_{cat} zu Rh(III)–H umgesetzt wird. Der zweite Reaktionsweg ist abhängig von der Lichtintensität und tritt vorwiegend auf, wenn die Reaktion an Luft durchgeführt wird. Der wichtigste Schritt bei diesem Reaktionsweg ist das oxidative Löschen (Quenchen) des Singulett-Zustandes von PF durch Rh_{cat}. Es konnte ein deutlicher Einfluss der Lichtintensität auf die Ausbeute der Reaktion sowie den Mechanismus festgestellt werden.

Im vierten Kapitel beschreiben wir, dass die bei der photochemischen Oxidation von Aminen auftretenden Nebenprodukte für weitere Umsetzungen genutzt werden können. Die Nebenprodukte der Aminoxidation wurden unter milden Reaktionsbedingungen und ohne die Zugabe eines Formylierungsreagenzes zu *N*-Formamiden umgesetzt. Sauerstoff ist für die Reaktion von zentraler Bedeutung, da er zur Regenerierung des Photokatalysators beiträgt und dabei ein Superoxidanion ausbildet, welches ein wichtiges Intermediat für die Reaktion darstellt. Der postulierte Mechanismus verläuft über die *in situ* Bildung einer Enamin Zwischenstufe, welche mit einem durch Protonierung des Superoxidanions entstandenen Hydroperoxyl-Radikal reagiert.

Kapitel 5 beschäftigt sich mit der Erzeugung von stark reduzierenden Spezies mittels Photoredoxkatalyse. Die Anwendung des conPET Prozesses mit PDI als Photokatalysator ist größtenteils beschränkt auf Arylhalogenide mit elektronenziehenden Substituenten. Ziel war es ein System zu entwickeln, welches es erlaubt auch schwerer zu reduzierende Arylhalogenide zu erreichen. Potentielle Photokatalysatoren, die auf ihre Anwendbarkeit für ein solches Katalysatorsystem untersucht wurden sind Riboflavintetraacetat (RFTA) und Naphthalindiimide (NDIs), da theoretisch beide ein ausreichend hohes Reduktionspotential im angeregten Zustand ihrer reduzierten Form besitzen. Erste Schritte zur Synthese potentieller NDIs und von Reduktionen mit reduziertem RFTA im Grund- oder angeregtem Zustand wurden unternommen. Dies stellt jedoch noch immer eine Herausforderung dar und muss zukünftig weiter untersucht werden.

8 Abbreviations

Å	Ångström
Ar	aryl
AU	arbitrary unit
Bpy	2,2'-bipyridine
°C	degree Celsius
$CDCl_3$	deuterated chloroform
ConPET	consecutive photo-induced electron transfer
CV	cyclic voltammetry
DCM	dichloromethane
DIPEA	*N*,*N*-diisopropylethylamine
DMF	dimethyl formamide
DMSO	dimethyl sulfoxide
DMSO-d_6	deuterated dimethyl sulfoxide
EtOAc	ethylacetate
EI	electron impact (MS)
Equiv.	equivalents
ESI	electron spray ionization (MS)
EtOH	ethanol
Et	ethyl
eV	electron volts
Fc	ferrocene
Fc^+	ferrocenium
FID	flame ionization detector
GC	gas chromatography
h	hour (s)
HRMS	high resolution mass spectrometry
IC	internal conversion
ISC	inter system crossing
LED	light emitting diode
M	molar
m-	meta
Me	methyl
MeCN	acetonitrile
MeOH	methanol
mg	milligram
MHz	mega hertz
min	minutes

mL	milliliter
mm	millimeter
mmol	millimole
mol%	mole percent
MS	mass spectroscopy
NDI	naphthalene diimide
n-Bu	*n*-butyl
n-hex	*n*-hexyl
nm	nanometer
NMR	nuclear magnetic resonance
n-oct	*n*-octyl
o-	*ortho*-
OAc	acetate
OD	optical density
OTf	triflate
p-	*para*
PC	photocatalyst
PDI	perylene diimide
PE	petroleum ether
PF	proflavine
Ph	phenyl
Ppm	parts per million
RFTA	riboflavin tetraacetate
Rh_{cat}	[Cp*Rh(III)(bpy)Cl]Cl
rt	room temperature
secs	seconds
SCE	saturated calomel electrode
SET	single electron transfer
tert-Bu	*tert*-butyl
TEA	trimethylamine
TEMPO	(2,2,6,6-Tetramethylpiperidin-1-yl)oxyl
TEOA	triethanolamine
THF	tetrahydrofuran
TLC	thin layer chromatography
TMS	trimethylsilyl
UV	ultraviolet
V	volt
Vis	visible
W	watt
X	arbitrary anion

9 Acknowledgements

Firstly, I would like to express my deep and sincere gratitude to my research supervisor Prof. Dr. Burkhard König for giving me the opportunity to explore my scientific research career. His supervision, knowledge and vast experience has inspired me at every stage of my doctoral studies. Moreover, his useful suggestions, enthusiastic comments, constant encouragement and freedom has helped me to grow as an independent organic chemist.

I am very much thankful to Prof. Dr. David Díaz Díaz and Prof. Dr. Arno Pfitzner for being the doctoral committee members and referring my thesis. I also like to thank PD Dr. Sabine Amslinger for being chair person in my Ph.D. defense.

I deeply acknowledge Prof. Dr. S. Sankararaman, Department of Organic Chemistry (IITM, India) for giving me an opportunity to carry out my first research career in his laboratory during my M.Sc. studies.

I would like to thank Dr. Rudi Vasold and Simone Strauß for the GC and GC-MS measurements, Ernst Lautenschlager for all kind of technical help, Susanne Schulze and Britta Badziura for ordering the chemicals and Regina Hoheisel for CV measurements.

My special thanks go to all my project partners for their excellent support, useful critiques and fruitful discussions; especially Dr. Javier Bardagi and Dr. Tomáš Slanina from whom I learned a lot about different instrument techniques. I do not want to forget my fellow students who also contributed to this thesis during their research internships; Christopher, Mustafa, Kerstin, Swarupa, Kamil and Patrik. Thank you!

I convey my thanks to all past and present members of ‘AK König’ for keeping friendly atmosphere inside and outside the lab, especially Anna, Amrita, Nadja, Caro, Willi, Karin, Anuushka, Thea, Simone, Daniel, Qiu, Durga, Mischko, Tonda, Melli, Somnath, Ani, Swarupa, Steffi, Thomas, Tomáš, Eli, Javier, Andi M., Alex, Martin, Johana, Leyre, Rizwan, Troppi, Malte, Andi Mü., Andi G., Daniel P, Dino, Anna B, Flo and few others…who made the last years so special for me during Ph.D. parties, international evenings, cake and coffee on birthdays, barbecue events, movie nights etc.

My awesome lab mates Caro and Willi…it was a pleasure to share the lab (32.1.23) with both of you for the last years; I will miss you both. Thank you for being there for me in good and bad times. Besides, I will really miss our 'special' discussions. ;-)

Thank you so much Amrita, Swarupa, Somnath, Suva, Santanu, Uttam, Santosh, Sureshan, Datta, Rajendra, Durga, Maloy, Asik for the wonderful cooking time together or playing cricket together in Regensburg. My heartiest thanks go to Amrita, Swarupa and Somnath for supporting me so much during writing my thesis and for being good friends.

Special thanks to Sven, Wolfgang, Regina and Max for helping me always whenever I needed any kind of help; like painting apartment, transporting big things by car, for getting 'Polizeiliches Führungszeugnis', drinking beer together, staying at their places etc. and more importantly for being good friends.

During my stay in Regensburg I learned more Bayerisch than Hochdeutsch, thank you so much Wolfgang, Sven, Rudi, Willi, Caro, Max, Regina for teaching me the most important words in Bayerisch.

For the thorough proofreading of parts of my thesis and valuable suggestions I would like to thank Dr. Somnath Das and Regina Hoheisel. Thea, Regina and Willi, thank you so much for translating the summary in German.

I am very much grateful to Deutsche Forschungsgemeinschaft (GRK 1626) for the financial support during my doctoral research.

Finally, and most importantly, I pay my due respect and sincere regards to my parents whose love, support, blessing and believe are always with me for the accomplishments that I had so far in my life. I would like to thank my brother and other family members for their love and encouragements; only words are difficult to explain what I owe them. *Thank you so much!*

Last but not the least; to anyone who has supported me on this journey, I would like to thank you as well. There have been too many names and faces that have passed through my life and all of you have helped me to grow just not as a chemist but also as a good person.

Thank you *Danke Schön* *ধন্যবাদ.*

10 Curriculum Vitae

Tamal Ghosh
Ph.D. student
Institute of Organic Chemistry
University of Regensburg
D- 93053 Regensburg, Germany
Phone: +49-941-943-4567
Mobile: +49-17635295094
E-mail: tamal.ghosh@chemie.uni-regensburg.de

Personal Information

Date of birth: August 30, 1989
Nationality: Indian
Marital status: Unmarried

Education

Ph.D. student in Chemical Photocatalysis, 09/2012- present
University of Regensburg (Regensburg, Germany)
Advisor: Prof. Dr. Burkhard König

M.Sc. in Chemistry, 08/2010- 07/2012
Indian Institute of Technology Madras (Chennai, India)
Advisor: Prof. Dr. S. Sankararaman
M.Sc. thesis title: Studies on donor-acceptor complexes of pyrene derivatives & Reactivity of 4,5,9,10-tetraketo pyrene with 1,2-diamines.

B.Sc. in Chemistry (First Class with honors), 07/2007- 06/2010
Ramakrishna Mission Vidyamandira, Belur Math (University of Calcutta, Kolkata, India)

Research Experience

University of Regensburg, 09/2012- present
Institute of Organic Chemistry; Advisor: Prof. Dr. Burkhard König
Photochemistry and Synthesis:

- Involved in the development of a novel concept in photochemistry called "Consecutive PET" or "conPET" for the reduction of less reactive aryl halides.
- Used less reactive chemical bonds in metal-free organic synthesis using "ConPET".
- Achieved chemoselectivity of aldehydes over ketones using a well-known Rhodium (III)-Proflavine system which was used for enzyme cofactor regeneration.

- Involved in the detailed mechanistic investigation of Rhodium (III)-Proflavine system for synthetic reduction.
- Contributed to prove the mechanism of C-H amidation reaction of heteroarenes with benoyl azide under visible light irradiation.
- Measured 'Quantum Yield' of several reactions with a setup which was previously developed in cooperation with our group.
- Measured Cyclic Voltammetry, UV-Vis spectra, Emission spectra of several compounds, different photocatalysts and synthesized dyes.
- Worked on flavin chemistry, mainly with the reduced form of flavin and its excited state.
- Involved in synthesizing different dye molecules with high reduction potential which can potentially be used for photoredox calalysis and also worked with flavinium salts.
- Utilized photochemically oxidized amine by-products for further chemistry.

Indian Institute of Technology Madras, 08/2010- 07/2012
Department of Chemistry; Advisor: Prof. Dr. S. Sankararaman

- Investigated charge-transfer complexes of pyrene derivatives and was able to get crystals of those complexes.
- Prepared pyrene based azaacenes which are useful for electron transporting materials for thin film transistors.

Skills

Instrumental techniques and synthetic skills:

- Strong background and extensive experience with the analytical techniques: NMR, HPLC, IR, LCMS, GC-MS, Elemental analysis and Cyclic voltammetry.
- Hands on experience with various purification techniques: Column chromatography, TLC, GC and preparative HPLC.
- Fluorescence spectrometer (Perkin Elmer, Cary Eclipse, Edinburgh Instruments), UV spectrophotometer (JASCO, Cary), polarimeter, calorimeter, potentiometer, pH meter, boiling/ melting point apparatus etc.
- Well trained in handling the air/moisture sensitive reagents and Organometallic reactions.
- Able to perform reactions ranging from milligram scale to preparative scale and from low temperature (–78 °C) to high temperature (300 °C).

Software skills:

Publishing:

- MS Office (Word, Powerpoint and Excel), EndNote, Adobe Illustrator, Adobe Photoshop.

Scientific:

- ChemDraw, Scifinder, Origin, CorelDRAW, Spartan, Mercury software for crystal structure visualization, web of knowledge and software related to above-mentioned instruments.

Languages:

- English, German (A2), Hindi, Bengali (mother tongue).

Teaching experience

- Supervised two undergraduate and six graduate students during their research internships at the University of Regensburg.

Scholarships and Awards

- Selected for the oral communications (23 out of 150 was selected) at the 19th European Symposium of Organic Chemistry (ESOC), Lisbon, July **2015**.
- Also, selected (among the seven) from more than 100 posters to give a talk at 'Physical Organic Chemistry, Gordon Research Conference', NH, USA, June **2015**.
- Awarded **iPUR** scholarship from the University of Regensburg, Germany.
- Member of the Gesellschaft Deutscher Chemiker (**GDCh**) since **2015**.
- Scholarship of the "**GRK 1626**, Chemical Photocatalysis (**2012-present**)".
- Qualified Graduate Aptitude Test in Engineering (GATE) (for Ph.D. in India) – **2012**.
- Awarded the "Merit scholarship" by Indian Institute of Technology Madras – (**2010-2012)**.
- Secured **1st** rank in an all India level entrance examination for the Integrated Ph.D. program 2010, in Chemical Sciences conducted by **JNCASR**, India.
- Qualified in the entrance test for the Integrated Ph.D program in chemistry conducted by the Indian Institute of Science (IISc) in 2010.
- Secured 91st rank in an all India level entrance examination, Joint Admission test for Masters (JAM), conducted by Indian Institute of Technology (IIT) – **2010**.
- Awarded Gold Medal at Ramakrishna Mission Vidyamandira college for securing **First Class** Bachelor's degree (Honors) in chemistry from the University of Calcutta in **2010**.

Research Publications

1) I. Ghosh,† **T. Ghosh**,† J. I. Bardagi and B. König, "Reduction of aryl halides by consecutive visible light-induced electron transfer processes", ***Science,* 2014, *346,* 725-728.** (†: These authors contributed equally to this work).
2) E. Brachet, **T. Ghosh**, I. Ghosh and B. König, "Visible light C–H amidation of heteroarenes with benzoyl azides", ***Chem. Sci.,* 2015, 6, 987-992**.

3) **T. Ghosh**,† T. Slanina† and B. König, "Visible light photocatalytic reduction of aldehydes by Rh(III)–H: a detailed mechanistic study", ***Chem. Sci.*, 2015, 6, 2027-2034.** (†: These authors contributed equally to this work).
4) L. N. Mataranga-Popa, I. Torje, **T. Ghosh**, M. J. Leitl, A. Späth, M. L. Novianti, R. D. Webster and B. König, "Synthesis and electronic properties of π–extended flivins", ***Org. Biomol. Chem.*, 2015, 13, 10198-10204**.
5) **T. Ghosh** and B. König, "Photochemical *N*-formylation of amines *via* a reductive quenching cycle in the presence of air", ***manuscript in preparation*, 2016**.

Attended Conferences and Meetings

Posters:

- T. Ghosh, I. Ghosh, J. I. Bardagi and B. König, "Reduction of aryl halides by consecutive visible light-induced electron transfer processes", 'Physical Organic Chemistry, Gordon Research Conference', Holderness, NH, USA, June **2015**.
- T. Ghosh, I. Ghosh, J. I. Bardagi and B. König, "Reduction of aryl halides by consecutive visible light-induced electron transfer processes", DocDays2015, University of Graz, Austria, April **2015**.
- T. Ghosh, T. Slanina and B. König, "Chemoselective Photoreduction of Aldehydes over non-activated Ketones by slowly in situ generated Rh(III) hydride", 24th Lecture Conference of the GDCH on Photochemistry, Köln, Germany, September **2014**.
- Presented a poster on "B1: Flavin Photocatalysis", Review colloquium of GRK 1626-Chemical Photocatalysis, University of Regensburg, Germany, January **2014**.

Oral presentations:

- T. Ghosh, I. Ghosh, J. I. Bardagi and B. König, "Reduction of aryl halides by consecutive visible light-induced electron transfer processes", '19th European Symposium of Organic Chemistry (ESOC)', Lisbon, July **2015**.
- T. Ghosh, I. Ghosh, J. I. Bardagi and B. König, "Reduction of aryl halides by consecutive visible light-induced electron transfer processes", 'Physical Organic Chemistry, Gordon Research Conference', Holderness, NH, USA, June **2015**.
- T. Ghosh, J. I. Bardagi, I. Ghosh and B. König, "Metal-free photoredox catalysis employing two consecutive PET under visible light irradiation", INDIGO conference, Regensburg, Germany, October **2013**.

References

1) Prof. Dr. Burkhard König
Institut of Organic Chemistry
University of Regensburg
D-93053 Regensburg, Germany
E-mail: burkhard.koenig@ur.de
Phone: (+49) 941 943 4575.

2) Prof. Dr. S. Sankararaman
Department of Chemistry
IIT Madras
Chennai 600036, India
E-mail: sanka@iitm.ac.in
Phone: (+91) 44 2257 4210.